

O₂-Oxidations Catalyzed by *Trans*-Dioxoporphyrinato Ruthenium(VI) Species

by

**Stephen Yau Sang Cheng
B.Sc., University of British Columbia, 1992**

**A THESIS SUBMITTED IN PARTIAL FULFILLMENT OF
THE REQUIREMENTS FOR THE DEGREE OF
DOCTOR OF PHILOSOPHY**

in

**THE FACULTY OF GRADUATE STUDIES
(Department of Chemistry)**

We accept this thesis as conforming
to the required standard.

THE UNIVERSITY OF BRITISH COLUMBIA

July 1996

© Stephen Y. S. Cheng, 1996.

In presenting this thesis in partial fulfilment of the requirements for an advanced degree at the University of British Columbia, I agree that the Library shall make it freely available for reference and study. I further agree that permission for extensive copying of this thesis for scholarly purposes may be granted by the head of my department or by his or her representatives. It is understood that copying or publication of this thesis for financial gain shall not be allowed without my written permission.

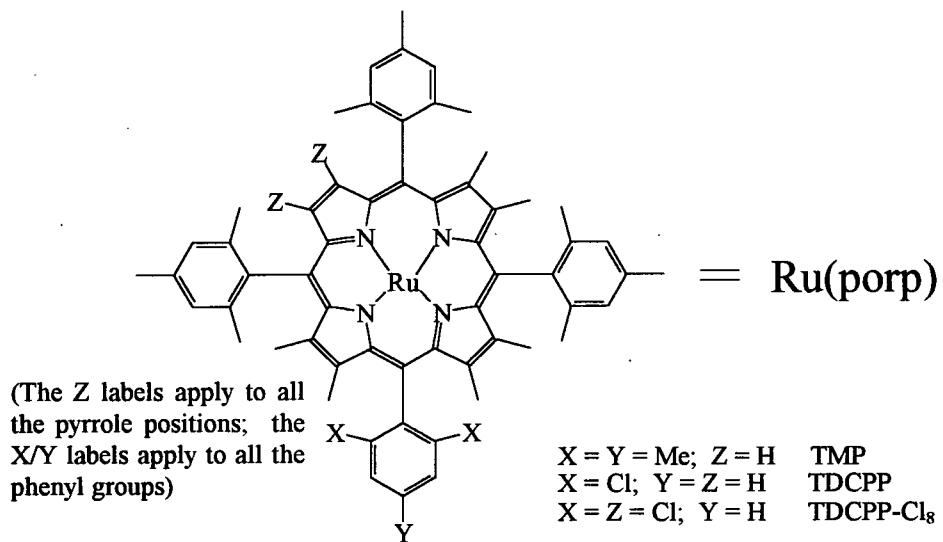
Department of CHEMISTRY

The University of British Columbia
Vancouver, Canada

Date Sept 4, 96

Abstract

Some *trans*-Ru^{VI}(porp)(O)₂ complexes [porp = TMP (**1**), TDCPP (**2**), TDCPP-Cl₈ (**3**)] were synthesized and used to oxidize, both stoichiometrically and (in the presence of air/O₂) catalytically, a variety of organic compounds in benzene under relatively mild conditions.



The kinetic data (measured by stopped-flow) for the stoichiometric oxidation of EAr₃ substrates (E = P, As, Sb) by (**1**) to give initially Ru^{IV}(TMP)(O)(OEAr₃) suggest that the O-atom transfer mechanism, governed by a k₁ second-order rate constant, involves electrophilic attack of a Ru=O moiety on the lone-pair of electrons on the E-atom. For a series of P(*p*-X-C₆H₄)₃ substrates, the k₁ values do not give a linear Hammett plot ($\log \frac{k_X}{k_H}$ vs. σ); however, the plot of ΔH^\ddagger versus σ is linear, and shows that a more electron-releasing para substituent gives a more favourable, lower value ΔH^\ddagger . The ΔS^\ddagger values correlate linearly with the molecular masses of the phosphines, with bulkier substrates giving rise to more favourable, less negative ΔS^\ddagger values, an indication that the O-atom

transfers are strongly vibrationally coupled. In subsequent stages of the mechanism, the OEAR₃ ligand dissociates from the Ru(IV) intermediate to form Ru^{IV}(TMP)(O), which then disproportionates to (**1**) and Ru^{II}(TMP), and excess EAr₃ reacts with the latter to form Ru^{II}(TMP)(EAr₃) species. Under 1 atm air or O₂, the oxidation of EAr₃ substrates becomes catalytic; approximately 1 turnover h⁻¹ is obtained for the oxidation of PPh₃ at ambient conditions.

The oxidative dehydrogenation of ⁱPrOH by (**1**) follows the indicated stoichiometry: (**1**) + 3 ⁱPrOH → Ru^{IV}(TMP)(OⁱPr)₂ + acetone + 2 H₂O

The Ru(IV) product was characterized crystallographically. Species (**1**) can also oxidize other primary or secondary alcohols (e.g. benzyl alcohol, 1-PrOH, 1,3-dichloro-2-propanol, 1-phenylethanol, etc.) to the corresponding aldehydes or ketones. The activation parameters for the stoichiometric oxidation of ⁱPrOH and benzyl alcohol are: ΔH[‡] = 45 ± 7 and 65 ± 11 kJ mol⁻¹, and ΔS = -167 ± 10 and -70 ± 20 J mol⁻¹ K⁻¹, respectively. A small kinetic isotope effect of k_H/k_D ~ 1.9 observed for the stoichiometric oxidation of ⁱPrOH at 18 °C is attributed to cleavage of the alcohol α-C-H bond in the rate-determining step.

Exposure of Ru^{IV}(TMP)(OⁱPr)₂ to moist air in benzene solution regenerates (**1**), and thus the catalytic O₂-oxidation of ⁱPrOH becomes viable. Complexes (**1**), (**2**) and (**3**) are all active catalysts for the aerobic, selective oxidation of alcohols to aldehydes or ketones at room temperature or 50 °C under 1 atm air. The activities of the catalysts followed the order (**1**) > (**3**) >> (**2**) for the oxidation of benzyl alcohol to benzaldehyde: in a 2-phase benzene/3.0 M aq. KOH system, (**1**) gave 2000 turnovers in 13 d at 50°C,

and (**3**) gave 1200 turnovers in 15 d. While (**1**) was not very efficient in oxidizing 1-phenylethanol to acetophenone, giving only a few turnovers before being deactivated, (**3**) produced 140 turnovers in 60 h under the same 2-phase conditions.

Complex (**3**) does not effectively catalyze the oxidation of alkenes and alkanes in benzene under 1 atm O₂ at 50 °C; however, at 35 - 90 °C under 1 atm O₂, (**3**) (at low concentrations of ~10⁻⁵ M, but not at 10⁻³ M) does catalyze the oxidation of neat cyclohexene, *cis*-cyclooctene and methylcyclohexane via free-radical pathways. Hydroperoxides are present in the reaction solutions, and the addition of the radical inhibitor BHT (2,6-diterbutyl-4-methylphenol) stops the oxidations. Approximately 60000 turnovers were realized in 26 h (and after 55 h, 120000 turnovers, 80% total conversion) for the oxidation of cyclooctene, and the reaction was > 80% selective for epoxide formation; cyclohexene yielded only ~ 3 % epoxide, the main products being cyclohexene-2-ol and cyclohexene-2-one. The oxidation of methylcyclohexane yielded mainly 1-methylcyclohexanol and 2-, 3- and 4-methylcyclohexanones, with smaller amounts of the corresponding 2-, 3- and 4-methylcyclohexanols.

The reaction of HOAc' acids (CF₃COOH and CHCl₂COOH) with (**1**) yields paramagnetic Ru^{IV}(TMP)(OAc')₂ species. For the bis(CF₃COO) complex, a μ_{eff} value of 2.5 μ_{B} is consistent with a Ru(IV) S = 1 spin state, and the linear dependence of the ¹H-chemical shifts of the TMP ligand with inverse temperature shows that a single spin state exists from -60 to +25 °C .

The reaction of phenol with (**1**) studied in preliminary work earlier in this laboratory was shown to give the following products: a paramagnetic, S = 1 Ru(IV)-TMP

species, 0.5 equivalents of *p*-benzoquinone and 1.3 equivalents of H₂O. The Ru(IV) product was proposed to be Ru^{IV}(TMP)(*p*-OC₆H₄OH)₂; however, the data from the present thesis work favour the formulation as Ru^{IV}(TMP)(OC₆H₅)₂, while *p*-hydroquinone is formed via O-atom insertion at the para position of the phenol. Species (1) oxidizes the *p*-hydroquinone formed to give *p*-benzoquinone (and presumably H₂O); the oxidation of *p*-hydroquinone itself is demonstrated in separate experiments (without phenol) to be catalytic, and under 1 atm O₂ at ~20 °C, ~ 200 turnovers are obtained after 22 h. The O₂-oxidation of *N,N*-dimethylaniline to *p*-hydroxy-*N,N*-dimethylaniline by (1) in wet benzene is also catalytic, but less than 10 total turnovers are achieved at 50 °C under 1 atm air.

Table of Contents		Page
Abstract		ii
Table of Contents		vi
List of Figures		xii
List of Tables		xix
List of Abbreviations		xxi
Acknowledgements		xxiv
Chapter 1	Ruthenium Complexes as Oxidants for Organic Compounds	1
1	Introduction	2
1.1	Using O ₂ as a Terminal Oxidant: Nature's Cytochrome P-450	2
	1.1.1 Metalloporphyrins as P-450 Models	7
1.2	Ruthenium(VIII) Complexes	9
1.3	Ruthenium(VII) Complexes	11
1.4	Ruthenium(VI) Complexes	12
	1.4.1 Ruthenium(VI) Porphyrin Complexes	12
	1.4.2 Ruthenium(VI) Non-Porphyrin Complexes	18
1.5	Ruthenium(V) Complexes	21
1.6	Ruthenium(IV) Complexes	22
1.7	Ruthenium(III) Complexes	26
1.8	Ruthenium(II) Complexes	27
1.9	Aims and Scope of this Thesis	29

References for Chapter 1	32
Chapter 2	
Experimental Methods	37
2.1 Materials	38
2.1.1 Gases	38
2.1.2 Solvents and Reagents	38
2.2 Instrumentation and General Experimental Procedures	40
2.2.1 UV-Visible Spectroscopy	40
2.2.2 Stopped-flow Kinetic Studies	41
2.2.3 Infrared Spectrophotometer	43
2.2.4 FT-NMR Instruments	43
2.2.5 Gas Chromatography Experiments	44
2.2.6 Elemental Analyses, X-ray Crystallography and Mass Spectral Analyses	46
2.3 Techniques	46
2.4 Synthesis and Characterization of Starting Compounds	46
References for Chapter 2	55
Chapter 3	
Mechanism of Aerobic Oxidation of EAr₃ (E = P, As, Sb)	56
3.1 Introduction	57
3.1.1 Aims of Phosphine Oxidation in Current Work	58
3.2 Sample Preparation and Data Analysis	59
3.2.1 Sample Preparation	59
3.2.1 Data Analysis	61

3.3	Overview of the Mechanism of Tertiaryarylphosphine Oxidation	63
	3.3.1 O-atom Transfer	68
	3.3.2 Disproportionation of Ru ^{IV} (TMP)(O)	81
3.4	Ru ^{II} (TMP)(L) Species and Catalytic Aerobic Oxidation of Phosphines	95
	3.4.1 Ru ^{II} (TMP)(L) Species	95
	3.4.2 Catalytic Aerobic Oxidation of Phosphines	99
3.5	Conclusions	109
	References for Chapter 3	110
Chapter 4	Catalytic Aerobic Oxidation of Alcohols and Alkanes	112
4.1	Introduction	113
	4.1.1 Scope of Alcohol Oxidations in Current Work	114
4.2	Sample Preparation and Data Analysis	114
	4.2.1 Sample Preparation	114
	4.2.2 Data Acquisition and Analysis	117
4.3	Stoichiometric Oxidation of Alcohols by Oxoruthenium Species	120
	4.3.1 Bis(alkoxo)porphyrinatoruthenium(IV) Species	120
	4.3.2 Mechanism of Alcohol Oxidation by Ru ^{VI} (TMP)(O) ₂	129
	4.3.3 Aerobic Oxidations of Alcohols to Aldehydes and Ketones	141
4.4	Aerobic Oxidation of Tertiary Alkanes Catalyzed by Ru ^{VI} (porp)(O) ₂ Species	151

4.5	Conclusions	154
	References for Chapter 4	155
Chapter 5	Reactivities of Ru(TDCPP-Cl₈) Species	157
5.1	Introduction	158
	5.1.1 Ru-Perhalogenated Porphyrins: Aims and Scope	159
5.2	Sample Preparation and Data Analysis	160
	5.2.1 Sample Preparation in Catalysis Studies	160
	5.2.2 Preparation of <i>trans</i> -Ru ^{VII} (TDCPP-Cl ₈)(O) ₂	163
	5.2.3 Data Acquisition and Analysis	166
5.3	Catalytic Aerobic Oxidation of Alcohols	167
5.4	Oxidation of Alkenes	171
5.5	Oxidation of Alkanes	177
5.6	Conclusions	185
	References for Chapter 5	187
Chapter 6	Preliminary Work: Reactions of Ru^{VII}(TMP)(O)₂ with HX acids and Oxidation of Phenol and <i>N,N</i>-Dimethylaniline	189
6.1	Introduction	190
6.2	Experimental: Sample Preparation and Data Analysis	191
6.3	Ru ^{IV} (TMP)(X) ₂ Species	197
6.4	Oxidation of Phenol by Ru ^{VII} (TMP)(O) ₂	210
	6.4.1 Oxidation of Phenol	210
	6.4.2 Kinetic Studies	220

6.5	Oxidation of <i>N,N</i> -Dimethylaniline by Ru ^{VI} (TMP)(O) ₂	225
6.6	Conclusions	233
	References for Chapter 6	235
Chapter 7	Conclusion and Recommendations for Future Work	236
7.1	General Conclusions	237
7.2	Recommendations for Future Work	239
Appendix A	Kinetic Data for the Oxidation of EAr₃	241
Appendix B	Mathematical Derivation for the Equation Reflecting the Observed 1st-Order Absorbance-Time Changes in the Oxidation of PPh₃ by Ru^{VI}(TMP)(O)₂	257
Appendix C	Oxidation of Alcohols and Alkanes: Kinetic and Catalysis Data	259
Appendix D	Supplementary Data for the Crystallographic Structures of Ru^{IV}(TMP)(OR)₂ Complexes	276
	D.1 Ru ^{IV} (TMP)(O <i>i</i> Pr) ₂	276
	D.2 Ru ^{IV} (TMP)(OCH(CH ₂ Cl) ₂) ₂	284
Appendix E	Catalytic Oxidation of Alcohols, Alkenes and Alkanes by Ru(TDCPP-Cl₈) Species: Catalysis Data	293
E.1	Oxidation of Benzyl Alcohol at 50 °C Under 1 atm air.	293
E.2	Oxidation of Alkenes under 1 Atm O ₂	294
E.3	Oxidation of Alkanes	295
E.4	GCMS Data for the Cyclohexene Oxidation	296
E.5	GCMS Data for the Cyclooctene Oxidation	300
E.6	GCMS Data for the Methylcyclohexane Oxidation	304
Appendix F	Kinetic Data for the Oxidation of Phenol by Ru^{VI}(TMP)(O)₂	310

List of Figures

Figure		Page
1.1	Molecular orbital (MO) diagram for O ₂ in its ground state	4
1.2	Illustration of Fe-Protoporphyrin-IX in Cytochrome P-450	5
1.3	Mechanism of Cytochrome P-450 oxidation	6
1.4	Structures of dianions of some free base porphyrins	8
1.5	Various O ₂ -oxidations catalyzed by Ru ^{VI} (TMP)(O) ₂	13
1.6	Schematic representation of a chiral Ru ^{VI} (por*)(O) ₂ species	15
1.7	Illustration of several macrocyclic tetraaza and dioxadiazole ligands	19
1.8	Schematic representations of two Ru-oxo polypyridyl complexes	23
1.9	Catalytic cycle of a triple component ruthenium(II)-/quinone/cobalt system for the aerobic oxidation of alcohols	30
2.1	Diagram of the sample handling unit of the Applied Photophysics stopped-flow spectrophotometer	42
3.1	Mechanism of oxidation of P(<i>p</i> -X-C ₆ H ₄) ₃ , AsPh ₃ and SbPh ₃ by Ru ^{VI} (TMP)(O) ₂	65
3.2	Room temperature UV-visible/time traces for the oxidation of PPh ₃ by Ru ^{VI} (TMP)(O) ₂ in benzene in the presence of O=PPh ₃	67
3.3	Plot of k _{obs} versus [PPh ₃] for the initial O-atom transfer to PPh ₃ from Ru ^{VI} (TMP)(O) ₂	71
3.4	Eyring Plots for the determination of ΔH _i [‡] and ΔS _i [‡] of the initial O-atom transfer reaction	72
3.5	Hammett plot for log $\frac{k_X}{k_H}$ values for the k ₁ step at 20 °C	75

3.6	Modified Hammett plot, ΔH_1^\ddagger versus σ , for the initial O-atom transfer reaction for $P(p\text{-}X\text{-}C_6H_4)_3$ systems	77
3.7	Plot of molecular mass of $P(p\text{-}X\text{-}C_6H_4)_3$ and related substrates versus ΔS_2^\ddagger	78
3.8	Plot of $[PPh_3]$ versus k_{obs} (slower 2nd reaction) at various concentrations of $O=PPh_3$ in benzene at 20 °C	82
3.9a	Plot of $\frac{1}{k_{obs}}$ versus $\frac{[O=PPh_3]}{[PPh_3]}$ at 20 °C (slower 2nd reaction)	84
3.9b	Plot of $\frac{1}{k_{obs}}$ versus $\frac{[OPPh_3]}{[P(p\text{-}OMe\text{-}C_6H_4)_3]}$ for the kinetic data of the Soret shift from 430 to 412 nm (slower 2nd reaction)	85
3.9c	Plot of $\frac{1}{k_{obs}}$ versus $\frac{[OPPh_3]}{[P(p\text{-}Me\text{-}C_6H_4)_3]}$ for the kinetic data of the Soret shift from 430 to 412 nm (slower 2nd reaction)	85
3.9d	Plot of $\frac{1}{k_{obs}}$ versus $\frac{[OPPh_3]}{[P(p\text{-}F\text{-}C_6H_4)_3]}$ for the kinetic data of the Soret shift from 430 to 412 nm (slower 2nd reaction)	86
3.9e	Plot of $\frac{1}{k_{obs}}$ versus $\frac{[OPPh_3]}{[P(p\text{-}Cl\text{-}C_6H_4)_3]}$ for the kinetic data of the Soret shift from 430 to 412 nm (slower 2nd reaction)	86
3.9f	Plot of $\frac{1}{k_{obs}}$ versus $\frac{[OPPh_3]}{[P(p\text{-}CF_3\text{-}C_6H_4)_3]}$ for the kinetic data of the Soret shift from 430 to 412 nm (slower 2nd reaction)	87
3.10	Plot of k_{obs} versus $[PPh_3]$ for the kinetic data of the Soret shift from 430 to 412 nm at 20.5 °C (slower 2nd reaction)	88
3.11	Plots of $\frac{[PPh_3]}{k_{obs}}$ versus $[PPh_3]$ for slower 2nd reaction	89
3.12	Eyring plots derived from the temperature dependence data for the slower 2nd reaction for the PPh_3 system	90
3.13	Room temperature $^1\text{H-NMR}$ (200 MHz) spectra of $Ru^{II}(\text{TMP})(PPh_3)$ in benzene- d_6	97

3.14	Variable-temperature ^1H and $^{31}\text{P}\{^1\text{H}\}$ -NMR (300 MHz) spectra of $\text{Ru}^{\text{II}}(\text{TMP})(\text{PPh}_3)$ in toluene- d_8	98
3.15	^1H -NMR (300 MHz) spectrum of $\text{Ru}^{\text{II}}(\text{TMP})(\text{AsPh}_3)$ in benzene- d_6 exposed to air for ~ 2 min at 25°C	102
3.16a	Catalytic oxidation of PPh_3 in the presence of $\text{Ru}^{\text{VI}}(\text{TMP})(\text{O})_2$ under 1 atm air or O_2 in benzene- d_6 at 24°C	105
3.16b	Catalytic oxidation of $\text{P}(p\text{-F-C}_6\text{H}_4)_3$ in the presence of $\text{Ru}^{\text{VI}}(\text{TMP})(\text{O})_2$ under 1 atm air or O_2 in benzene- d_6 at 24°C	106
3.16c	Catalytic oxidation of $\text{P}(p\text{-OMe-C}_6\text{H}_4)_3$ in the presence of $\text{Ru}^{\text{VI}}(\text{TMP})(\text{O})_2$ under 1 atm O_2 in benzene- d_6 at 24°C	107
3.16d	Catalytic oxidation of $\text{P}(p\text{-Cl-C}_6\text{H}_4)_3$ in the presence of $\text{Ru}^{\text{VI}}(\text{TMP})(\text{O})_2$ under 1 atm O_2 in benzene- d_6 at 24°C	108
4.1	The kinetics of the stoichiometric oxidation of $^i\text{PrOH}$ by $\text{Ru}^{\text{VI}}(\text{TMP})(\text{O})_2$ in benzene- d_6 under 1 atm Ar at 18.2°C followed by ^1H -NMR spectroscopy (300 MHz)	118
4.2	Room temperature ^1H -NMR (300 MHz) spectra of $\text{Ru}^{\text{IV}}(\text{TMP})(\text{O}^i\text{Pr})_2$ in benzene- d_6 with and without the presence excess $^i\text{PrOH}$	122
4.3	ORTEP diagram of $\text{Ru}^{\text{IV}}(\text{TMP})(\text{O}^i\text{Pr})_2$	124
4.4	ORTEP diagram of $\text{Ru}^{\text{IV}}(\text{TMP})(\text{OCH}(\text{CH}_2\text{Cl})_2)_2$	125
4.5	Pseudo-1st-order rate constant, k_{obs} , as a function of excess $^i\text{PrOH}$ concentration in benzene- d_6 under 1 atm Ar at 18.2°C	131
4.6	Pseudo-1st-order rate constant, k_{obs} , as a function of [benzyl alcohol] at various temperatures in benzene- d_6 under 1 atm Ar	132
4.7	Eyring plots for the stoichiometric oxidation of $^i\text{PrOH}$ by $\text{Ru}^{\text{VI}}(\text{TMP})(\text{O})_2$ under 1 atm Ar in benzene- d_6	139
4.8	Eyring plots for the stoichiometric oxidation of benzyl alcohol by $\text{Ru}^{\text{VI}}(\text{TMP})(\text{O})_2$ under 1 atm Ar in benzene- d_6	140
4.9	Mechanism of alkene epoxidation catalyzed by $\text{Ru}^{\text{VI}}(\text{TMP})(\text{O})_2$	145

4.10	Plot of daily turnovers versus [benzyl alcohol] for the aerobic oxidation of benzyl alcohol catalyzed by Ru ^{VI} (TMP)(O) ₂ at 50 °C in benzene	149
4.11	Plot of total turnovers versus time for the aerobic oxidation of benzyl alcohol catalyzed by Ru ^{VI} (TMP)(O) ₂ at 50 °C	150
4.12	Plots of total turnovers versus time for the aerobic oxidations of Ph ₃ CH and adamantane catalyzed by Ru ^{VI} (porp)(O) ₂ species at 24 °C in benzene	153
5.1	Experimental setup for the oxidations of neat cyclohexene, cyclooctene and methylcyclohexane under 1 atm O ₂	162
5.2	Mass spectrum (EI) of Ru ^{IV} (TDCPP-Cl ₈)(Cl) ₂	165
5.3	Progress of the aerobic oxidation of benzyl alcohol to benzaldehyde catalyzed by Ru ^{VI} (TDCPP-Cl ₈)(O) ₂ in benzene at 50 °C	168
5.4	Progress of the aerobic oxidation of <i>R,S</i> -1-phenylethanol to acetophenone catalyzed by Ru ^{VI} (TDCPP-Cl ₈)(O) ₂ in benzene at 50 °C	169
5.5	Diagram illustrating a radical-chain mechanism proposed for the autoxidation of alkenes	174
5.6	Progress of the O ₂ -oxidation of neat cyclooctene under 1 atm O ₂ at 93 °C catalyzed by Ru ^{VI} (TDCPP-Cl ₈)(O) ₂	176
5.7	Diagram showing a radical-chain mechanism for the O ₂ -oxidation of alkanes via peroxide decomposition catalyzed by Fe-porphyrin species	178
5.8	Aerobic oxidation of Ph ₃ CH to Ph ₃ COH catalyzed by Ru ^{VI} (TDCPP-Cl ₈)(O) ₂ in benzene at 24 °C	185
6.1	Mass spectrum of Ru ^{IV} (TMP)(CF ₃ COO) ₂ (FAB ionization in a 3-nitrobenzylalcohol matrix)	194
6.2	UV-visible spectra recorded on monitoring the reaction of Ru ^{IV} (TMP)(O) ₂ with phenol in benzene under 1 atm O ₂ to form Ru ^{IV} (TMP)(OC ₆ H ₅) ₂	195

6.3	Mass spectra of solid residue isolated from the reaction of Ru ^{VI} (TMP)(O) ₂ with <i>N,N</i> -dimethylaniline in benzene- <i>d</i> ₆ under 1 atm air	196
6.4	UV-visible spectra of Ru ^{VI} (TMP)(O) ₂ in benzene at 25 °C acquired after the addition of CF ₃ COOH and CHCl ₂ COOH	198
6.5	¹ H-NMR (300 MHz) spectrum of Ru ^{IV} (TMP)(CF ₃ COO) ₂ in toluene- <i>d</i> ₈ at -57.1 °C under air	201
6.6	¹ H-NMR (300 MHz) spectrum of Ru ^{IV} (TMP)(CHCl ₂ COO) ₂ in toluene- <i>d</i> ₈ at 17.3 °C <i>in vacuo</i>	202
6.7	Inverse temperature plot, ¹ H-chemical shifts (300 MHz) versus T ⁻¹ , for Ru ^{IV} (TMP)(CF ₃ COO) ₂ in toluene- <i>d</i> ₈	204
6.8	Inverse temperature plot, ¹ H-chemical shifts (300 MHz) versus T ⁻¹ , for Ru ^{IV} (TMP)(CHCl ₂ COO) ₂ in toluene- <i>d</i> ₈	205
6.9	Infrared spectra of free CF ₃ COOH and Ru ^{IV} (TMP)(CF ₃ COO) ₂ obtained as Nujol mulls in KBr plates	207
6.10	Infrared spectra of free CHCl ₂ COOH and Ru ^{IV} (TMP)(CHCl ₂ COO) ₂ obtained as Nujol mulls in KBr plates	208
6.11	Mass spectrum (EI ionization) of Ru ^{IV} (TMP)(OC ₆ H ₅) ₂	212
6.12	¹ H-NMR spectrum (400 MHz, C ₆ D ₆) for the metathesis reaction of Ru ^{IV} (TMP)('OPr) ₂ with <i>p</i> -hydroquinone under Ar	213
6.13	¹ H-NMR spectrum (200 MHz) acquired after 2 min for the reaction between Ru ^{VI} (TMP)(O) ₂ and <i>p</i> -hydroquinone (1:2) in benzene- <i>d</i> ₆ under 1 atm air	216
6.14	Illustration showing the proposed phenol oxidation mechanism based on the reversible interconversion of Ru ^{IV} (TMP)(O) to Ru ^{IV} (TMP)(OH) ₂ and phenol metathesis reactions	218
6.15	Plots of k _{obs} versus [phenol] (0.1 - 1 M) for the oxidation of phenol by Ru ^{VI} (TMP)(O) ₂ in benzene under 1 atm air at various temperatures	221

6.16	Plot of k_{obs} versus [phenol] (0.01 - 0.1 M) for the oxidation of phenol by Ru ^{VI} (TMP)(O) ₂ in benzene at 20 °C under 1 atm air	221
6.17	Log(k_{obs}) versus log[phenol] plot for the oxidation of phenol at various temperatures	223
6.18	Arrhenius plot, ln(A) versus T ⁻¹ , for the parameter A for the reaction between Ru ^{VI} (TMP)(O) ₂ and phenol	224
6.19	Illustration of the proposed scheme for the oxidation of N,N-dimethylaniline catalyzed by Ru ^{VI} (TMP)(O) ₂ under 1 atm air	226
6.20	¹ H-NMR (200 MHz) spectra for the reaction “Ru ^{VI} (TMP)(O) ₂ + 4 N,N-dimethylaniline” in benzene- <i>d</i> ₆ at 25 °C under 1 atm air	228
6.21	¹ H-NMR (200 MHz) spectra monitoring the reaction “Ru ^{VI} (TMP)(O) ₂ + 10 N,N-dimethylaniline” in benzene- <i>d</i> ₆ at 25 °C under 1 atm Ar	229
A.1	Absorbance-time traces monitored at 422 nm by stopped-flow spectrophotometry for the reaction of Ru ^{VI} (TMP)(O) ₂ with PPh ₃	241
A.2	Semilog and Guggenheim plots for [PPh ₃] = 4.05 x 10 ⁻³ M trace in Figure A.1	241
A.3	Absorbance-time traces monitored at 430 nm by stopped-flow spectrophotometry for the loss of the intermediate Ru ^{VI} (TMP)(O)(O=PPh ₃)	242
A.4	Semilog and Guggenheim plots for [PPh ₃] = 3.83 x 10 ⁻³ M, [O=PPh ₃] = 3.93 X 10 ⁻³ M trace in Figure A.3	242
A.5	Absorbance-time traces monitored at 412 nm by stopped-flow spectrophotometry for the appearance of the product Ru ^{II} (TMP)(PPh ₃)	243
A.6	Semilog and Guggenheim plots for [PPh ₃] = 3.83 x 10 ⁻³ M, [O=PPh ₃] = 3.93 X 10 ⁻³ M trace in Figure A.5	243
D.1	ORTEP plot of Ru ^{IV} (TMP)(O <i>i</i> Pr) ₂ (sideway view) along the porphyrin plane	276

D.1.2	Stereoview of Ru ^{IV} (TMP)(O <i>i</i> Pr) ₂	276
D.2.1	PLUTO plot showing the partial structure of Ru ^{IV} (TMP)(OCH(CH ₂ Cl) ₂) ₂	284
D.2.2	Stereoview of Ru ^{IV} (TMP)(OCH(CH ₂ Cl) ₂) ₂	285
E.4.1	GC trace for the run in Table E.2.2 for the oxidation of neat cyclohexene	296
E.4.2	Low resolution mass spectra (EI) for the various products from the cyclohexene oxidation	297
E.5.1	GC trace for the run in Table E.2.1 for the oxidation of neat <i>cis</i> -cyclooctene	300
E.5.2	Low resolution mass spectra (EI) for the various products from the cyclooctene oxidation	301
E.5.3	Known fragmentation patterns for cyclooctene oxide and <i>cis</i> -7-oxabicyclo[4.3.0]-nonane	303
E.6.1	GC trace for the run in Table E.3.1 for the oxidation of neat methylcyclohexane	304
E.6.2	Low resolution mass spectra (EI) for the various products from the methylcyclohexane oxidation	305
G.1	GC trace of the benzene solution of Ru ^{VI} (TMP)(O) ₂ with added <i>N,N</i> -dimethylaniline used for GCMS analysis	313
G.2	Mass spectrum of analyte at 2:23 in the GC trace in Figure G.1	314
G.3	Mass spectrum of analyte at 4:15 in the GC trace in Figure G.1	314

List of Tables	Page
2.1 Optimum conditions of GC runs used throughout this thesis work for the separation of mixtures of compounds	45
3.1 Second-order rate constants, k_1 , for the initial O-atom transfer from $\text{Ru}^{\text{VI}}(\text{TMP})(\text{O})_2$ to various phosphines, AsPh_3 and SbPh_3 substrates in benzene	70
3.2 Activation parameters, ΔH_1^\ddagger and ΔS_1^\ddagger , for the initial O-atom transfer from $\text{Ru}^{\text{VI}}(\text{TMP})(\text{O})_2$ to $\text{P}(p\text{-X-C}_6\text{H}_4)_3$, AsPh_3 and SbPh_3 substrates.	73
3.3 Values of j_2 , dissociation of OPPh_3 from $\text{Ru}^{\text{IV}}(\text{TMP})(\text{O})(\text{OPPh}_3)$	89
3.4 Values of $\frac{k_2}{k_2 k_4 K_3^{1/2}}$ obtained from the kinetic data for the spectral change of the Soret maximum from 430 to 412 nm	93
3.5 ^1H and $^{31}\text{P}\{^1\text{H}\}$ -NMR data for various $\text{Ru}^{\text{II}}(\text{TMP})(\text{L})$ species	100
3.6 Total turnovers for various phosphines catalytically oxidized in benzene- d_6 at 24 °C under 1 atm O_2 in the presence of $\text{Ru}^{\text{VI}}(\text{TMP})(\text{O})_2$	104
4.1 ^1H -NMR data for <i>trans</i> - $\text{Ru}^{\text{IV}}(\text{TMP})(\text{OR})_2$ species	127
4.2 Selected pseudo-1st-order rate constants, k_{obs} , for the stoichiometric oxidation of $^i\text{PrOH}$ to acetone by $\text{Ru}^{\text{VI}}(\text{TMP})(\text{O})_2$ in benzene- d_6	134
4.3 2nd-order rate constants, k_2 , for the stoichiometric oxidations of $^i\text{PrOH}$ and benzyl alcohol in benzene- d_6 by $\text{Ru}^{\text{VI}}(\text{TMP})(\text{O})_2$	138
4.4 Catalytic activity of $\text{Ru}^{\text{VI}}(\text{porp})(\text{O})_2$ [porp=TMP or TDCPP] towards O_2 -oxidation of $^i\text{PrOH}$ and benzyl alcohol in benzene	148
5.1 Oxidation of neat alkenes catalyzed in the presence of $\text{Ru}^{\text{II}}(\text{TDCPP-Cl}_8)(\text{CO})$ or $\text{Ru}^{\text{VI}}(\text{TDCPP-Cl}_8)(\text{O})_2$ under 1 atm O_2	173

5.2	Oxidation of methylcyclohexane in the presence of $\text{Ru}^{\text{II}}(\text{TDCPP-Cl}_8)(\text{CO})$ or $\text{Ru}^{\text{VI}}(\text{TDCPP-Cl}_8)(\text{O})_2$ under 1 atm O_2	180
6.1	IR absorption frequencies for some Ru-porphyrin complexes in the 1000 cm^{-1} region	200
6.2	Observed variable temperature $^1\text{H-NMR}$ chemical shifts for some $\text{Ru}^{\text{IV}}(\text{TMP})(\text{X})_2$ species	206
6.3	Values for the parameter A for the oxidation of phenol by $\text{Ru}^{\text{VI}}(\text{TMP})(\text{O})_2$ derived from the expression $k_{\text{obs}} = A \cdot [\text{phenol}]^{3/2}$	223
6.4	Oxidation of <i>N,N</i> -dimethylaniline catalyzed by $\text{Ru}^{\text{VI}}(\text{TMP})(\text{O})_2$ under 1 atm air in benzene	232

List of Abbreviations

[X]	concentration of species X
A or Abs	absorbance
Å	angstrom unit (10^{-10} m)
ABN	azobis(2-methylpropionitrile); common radical initiator
Ar	aryl group (or argon)
BHT	2,6-ditertbutyl-4-methylphenol
bpy	2,2'-bipyridine
dcbpy	6,6'-dichloro-2,2'-bipyridine
d	day (unit of time)
ϵ	extinction coefficient in UV-visible spectra
EI	electron impact
exp(x)	natural base e raised to the power of x
FAB	fast atom bombardment
FID	flame ionization detector
FT	Fourier Transform
GC	gas chromatography
GCMS	tandem gas chromatography-mass spectrometry
h	Planck's constant, 6.626×10^{-34} J s (or hour)
H ₂ TDCPP	<i>meso</i> -tetra(2,6-dichlorophenyl)porphyrin
H ₂ TMP	<i>meso</i> -tetramesitylporphyrin
Int	area of integration in ¹ H-NMR spectrum
K	Kelvin
k _n	kinetic rate constant for nth elementary step
k _b	Boltzman's constant, 1.38×10^{-23} J K ⁻¹
k _H /k _D	kinetic isotope effect
k _{obs}	pseudo-first order rate constant
ln	natural logarithm
log	base ten logarithm

M	molarity
m	multiplet, as used in the description of NMR resonances
M⁺	parent ion (mass spectrometry)
<i>m</i>-CPBA	<i>meta</i> -chloroperbenzoic acid
<i>m</i>-H <i>m'</i>-H	<i>meta</i> -proton
M.W.	molecular weight
μ_B	Bohr Magneton
μ_{eff}	effective magnetic susceptibility
mg	milligram
MO	molecular orbital
(m)mol	(milli)mole
v	infrared frequency
nm	nanometer
<i>o</i>-Me	<i>ortho</i> -Methyl group
OEP	dianion of 2,3,7,8,12,13,17,18-octaethylporphyrin
π^*	antibonding π -molecular orbital
P-450	cytochrome P-450 enzyme system
<i>p</i>-H	<i>para</i> -proton
<i>p</i>-Me	<i>para</i> -Methyl group
Ph	phenyl group
ppm	parts per million
q_{vib}	vibrational partition function
R	alkyl group (or Ideal gas constant)
<i>Ru</i>	ruthenium porphyrin
σ	Hammett factor
s	second (unit of time)
S	spin quantum number
t	triplet, as in the description of NMR resonances
% T	percent transmittance, as used in IR spectroscopy
T	temperature

TDCPP	dianion of <i>meso</i> -tetra(2,6-dichlorophenyl)porphyrin
TDCPP-Cl ₈	dianion of <i>meso</i> -tetra(2,6-dichlorophenyl)- β -octachloroporphyrin
terpy	terpyridine
THF	tetrahydrofuran
TLC	thin layer chromatography
TMP	dianion of <i>meso</i> -tetramesitylporphyrin
TMS	tetramethylsilane
TPFPP	dianion of <i>meso</i> -tetra(pentafluorophenyl)porphyrin
TPFPP-Cl ₈	dianion of <i>meso</i> -tetra(pentafluorophenyl)- β -octachloroporphyrin
TPP	dianion of <i>meso</i> -tetr phenylporphyrin
TRIZMA® HCl	tris(hydroxymethyl)aminomethane hydrochloride (Sigma Chemicals)
UBC	University of British Columbia
VT	variable temperature
W	Watt
X _n	mole fraction of nth species

Acknowledgments

This is perhaps the most difficult section to write; perhaps I am not used to committing myself in writing. Clearly, thesis writing is not possible without readily available resources. I have to say that UBC and NSERC have treated me well in the last four years in the form of a scholarship. Without some luck, my work would not have gone as smoothly as it had in the last few years; success is 100% hard work, but luck is the catalyst.

To acknowledge specific names would do injustice to those I do not mention. Everyone around me has contributed to this thesis, either through his/her spiritual support or helpful comments/suggestions. (Those who deserve to have a bigger share of my thanks will find it in some other form!)...If this page does not make any sense, probably it is because BRJ has not edited this page (and I am quite happy that there is ONE page in this thesis that did not undergo any editing); nonetheless, this thesis appears that much more presentable than it was when it was first completed is due in no small part to my supervisor...

THANKS !!!

Chapter 1

Ruthenium Complexes as Oxidants for Organic Compounds

1 Introduction

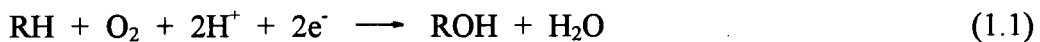
The oxidation of organic functional groups plays an important role in the synthesis of organic compounds in the laboratory and industry.¹ Classical stoichiometric oxidants, such as permanganate and dichromate, used for oxidizing organics are disfavoured because of growing environmental concerns over the disposal of such ecologically harmful metal wastes.² High-valent oxoruthenium complexes are competent oxidants, the classic example being RuO₄, which found its place in laboratory syntheses in the 1950s.³ (RuO₄ is not implied to be environmentally benign.) In this chapter, advances in the last few years pertaining to the development of the oxidation chemistry of ruthenium complexes will be discussed, with particular focus on, but not limited to, alkane hydroxylations. The subject is vast, and this is by no means a complete review; there are several recent reviews on oxoruthenium complexes.⁴ The work in the present thesis, which pertains to the catalytic oxidations effected by ruthenium porphyrin species, will be incorporated in the discussion of such recent work where appropriate. Some of the material in this thesis has been published⁵ or presented in conference proceedings.⁶

1.1 Using O₂ as a Terminal Oxidant: Nature's Cytochrome P-450

The ideal oxidant satisfies the following criteria: i) economically affordable; ii) naturally abundant; iii) produces clean reaction by-products; iv) high reactivity and v) high selectivity under relatively mild conditions. Usually, only some of these conditions can be satisfied at the expense of others. In recent years, the use of molecular oxygen as an alternative to currently used oxidants has led to intense research.⁷ Already, O₂ satisfies

the first three criteria out of the five (O_2 from air would be more inexpensive than pure O_2); however, O_2 exists in a paramagnetic triplet ground state (see Figure 1.1), and thus the reaction of O_2 with diamagnetic organic molecules is invariably slowed down in overcoming this spin-forbidden barrier. If any reaction with O_2 proceeds, it usually operates via a radical (paramagnetic) pathway. Free-radical reactions are usually undesired as they give to little regio- and enantio-selectivity.

Strong oxidants such as RuO_4 , OsO_4 and MnO_4^- are high-valent, diamagnetic oxometal species capable of oxidizing a variety of organic substrates.^{1,8} The active centre in the ubiquitous cytochrome P-450 enzyme (from now on referred to as P-450), found in abundance in the mammalian liver, as well as among many other living organisms, is believed to oxidize substrates via a high-valent oxoiron porphyrin intermediate (see Figures 1.2 and 1.3).⁹ This Fe=O moiety is generated by the reductive activation of O_2 (Eq. 1.1), in which one O-atom is reduced to H_2O , while the other O-atom is used for oxidation (Figure 1.3).



Nature's P-450 system perhaps represents the optimal conditions for the oxidation of organic substrates. The mechanism of the O-atom transfer with a P-450 oxidation is generally accepted to occur via the "*oxygen rebound mechanism*", depicted in Figure 1.3.^{9,10} The hydrophobic hydrocarbon substrate occupies a binding site in the protein cavity adjacent to the iron centre¹¹ and is oxidized as the iron is activated to a high valence. In hydrocarbon hydroxylation a hydrogen atom is thought to be abstracted, and the OH group bound to the Fe-centre is then transferred to, and recombines with, the

hydrocarbon fragment (R^+) before it leaves the protein cavity, hence *oxygen rebound*.

Perhaps a synthetic metalloporphyrin system mimicking the active centre in P-450 may become practical, hence affording the use of O_2 (with appropriate reductants) as a clean and inexpensive oxidant without the need of the protein in a natural enzyme.

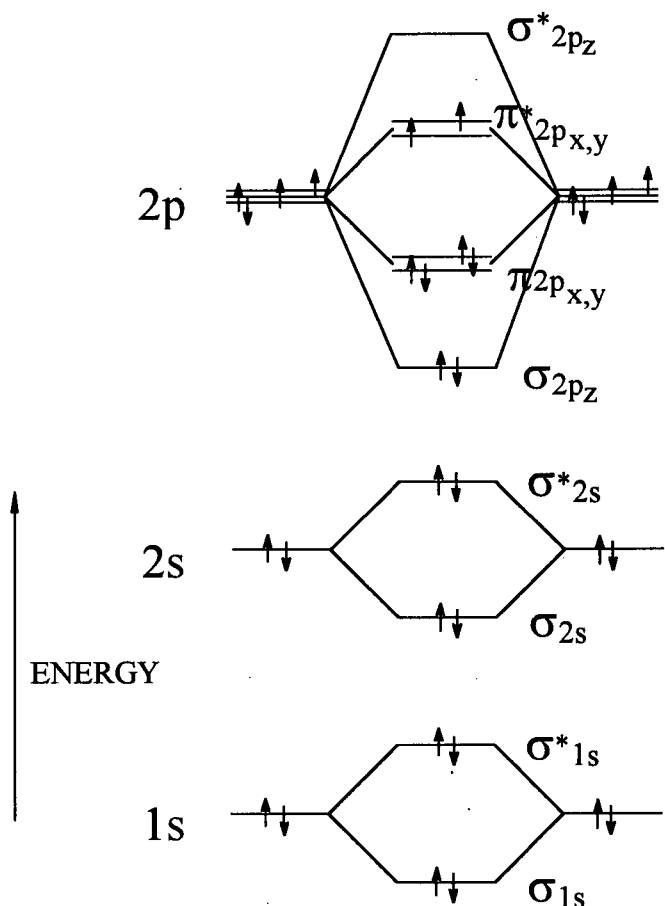
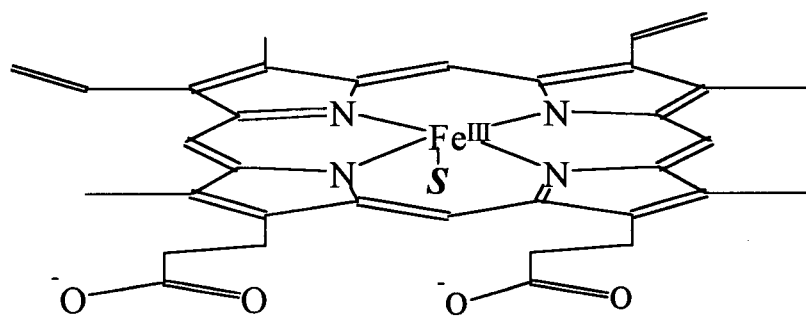


Figure 1.1 Molecular orbital (MO) diagram for O_2 in its ground state. Note that the energy levels are not drawn to scale, and the diagram shows only the relative energies of the orbitals. The ground state electronic configuration is a ${}^3\Sigma$ state. Two unpaired electrons occupy the highest occupied molecular orbitals (HOMO), a pair of degenerate π^* -antibonding orbitals.



S = thiolate RS^- from the cysteine residue of
cytochrome P-450 protein

Figure 1.2 The active centre of cytochrome P-450 enzymes is an iron protoporphyrin-IX moiety. The 5th coordination site is occupied by a sulfur-bound thiolate from a cysteine amino acid residue of the P-450 protein.

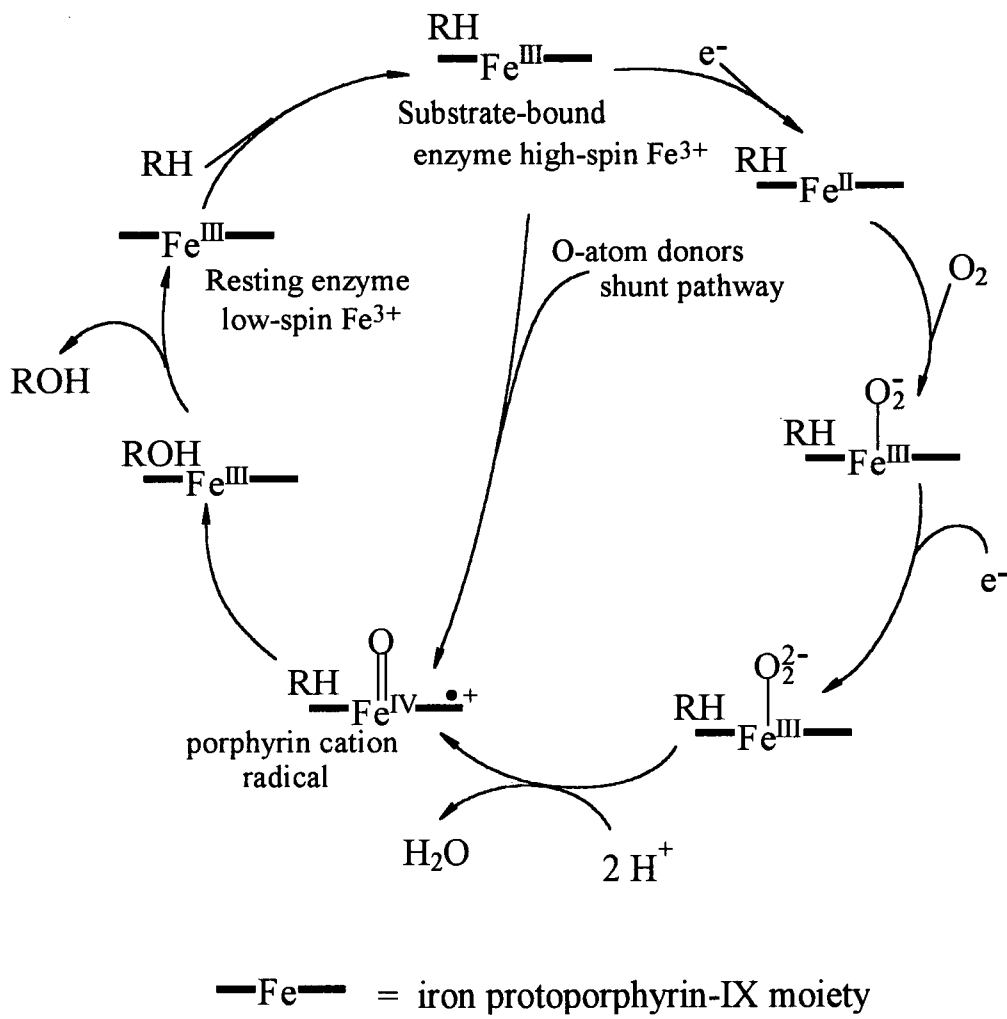


Figure 1.3 Mechanism of the catalytic cycle of the cytochrome P-450 enzyme. The oxidizing species is written as an oxoiron(IV) porphyrin radical-cation species, which is favoured in model studies.^{9,10} Two equivalents of reductant are not required if an O-atom donor is used; this bypasses the full P-450 cycle and proceeds via what is known as the *shunt pathway*.

1.1.1 Metalloporphyrins as P-450 Models

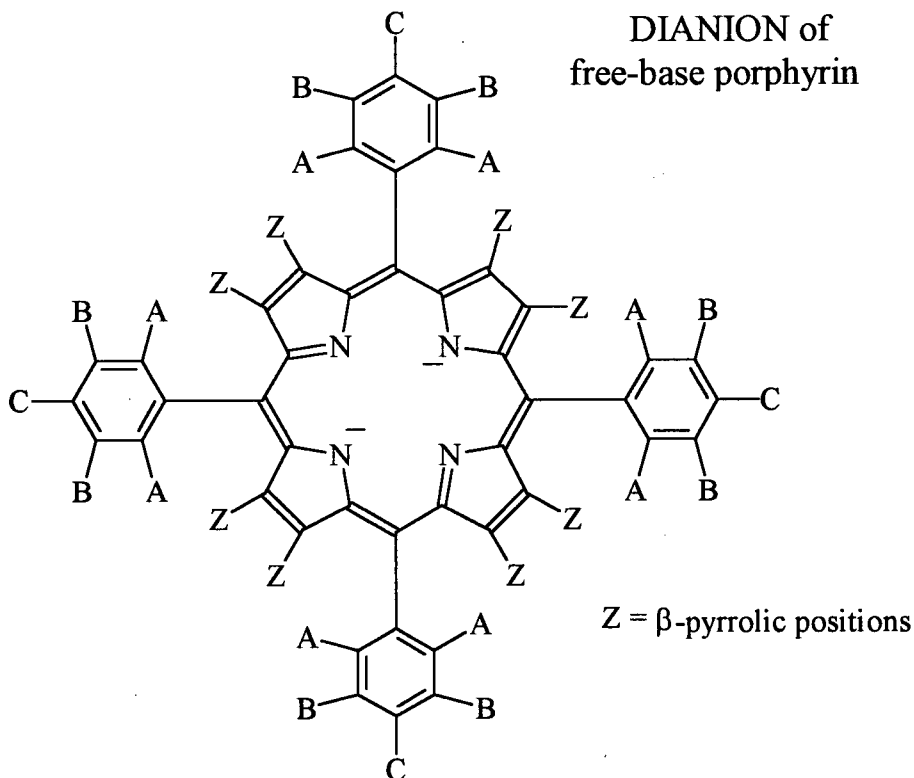
Generally, synthetic porphyrins fall into three classes or generations when it comes to the description of metalloporphyrin oxidation catalysts (see Figure 1.4).¹² The first generation metalloporphyrin catalysts are TPP[‡] derivatives (OEP[†] derivatives also have been used). Such porphyrins are susceptible to destruction under the oxidizing conditions that exist in the reaction medium, or to deactivation to the thermodynamically more stable μ -oxo-dinuclear species;¹³ however, the steric bulk present in TMP[§] prevents the formation of μ -oxo-diruthenium species, and a derived monomeric *trans*-Ru^{VII}(TMP)(O)₂ species exhibits a rich array of oxidation chemistry (see Section 1.4.1). The second generation metalloporphyrin catalysts, with the addition of halogens on the *meso*-phenyl group for improved stability, are improvements over the first-generation type, and the steric bulk of the 2- and 6- chloro groups of TDCPP[§] also prevents the formation of μ -oxo-dinuclear ruthenium species. To go one step further, the third generation metalloporphyrins have the β -pyrrolic positions halogenated as well. One can envision the steric repulsion amongst the halogens, especially at the β -pyrrole positions, and the porphyrin adopts a saddle-shaped conformation to relieve such stress. Crystallographic analyses on some such metalloporphyrins show that they adopt saddle-shaped structures;¹⁴ these results are complemented by theoretical studies which favour a non-planar conformation for such highly halogenated metalloporphyrins.¹⁵

[‡] TPP = dianion of *meso*-tetraphenylporphyrin (see Figure 1.4).

[†] OEP = dianion of 2,3,7,8,12,13,17,18-octaethylporphyrin.

[§] TMP = dianion of *meso*-tetramesitylporphyrin (see Figure 1.4).

[§] TDCPP = dianion of *meso*-tetra(2,6-dichlorophenyl)porphyrin (see Figure 1.4).



1 st Generation Porphyrins	2nd Generation Porphyrins	3rd Generation Porphyrins
A, B, C, Z = H (TPP) <u>meso-TetraphenylPorphyrin</u>	B,C,Z = H; A = Cl (TDCPP) <u>meso-Tetra(2,6-DiChlorophenyl)Porphyrin</u>	B,C = H; A,Z = Cl (TDCPP-Cl ₈)
A, C = Me; B, Z = H (TMP) <u>meso-TetraMesitylPorphyrin</u>	A,B,C = F; Z = H (TPFPP) <u>meso-Tetra(PentaFluorophenyl)-Porphyrin</u>	A,B,C = F; Z = Cl (TPFPP-Cl ₈) A,B,C = F; Z = F (TPFPP-F ₈) A,B,C = F; Z = Br (TPFPP-Br ₈)

Figure 1.4. Abbreviations and names of some dianions of free-base porphyrins that are based on the tetraphenylporphyrin family mentioned in this chapter and the rest of this thesis. A systematic nomenclature has been developed for porphyrins, but the above abbreviations (or ones similar to those used by other authors) are more convenient.

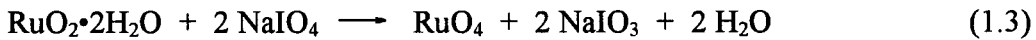
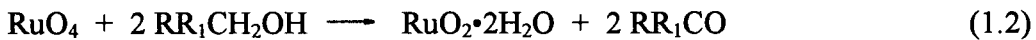
Experimentally, the extensive halogenation appears to increase the stability, and above all the reactivity of the metalloporphyrin catalysts.¹⁶

Ruthenium, periodically analogous with iron, was a natural choice in the extension of iron porphyrin chemistry. The active species carrying out the P-450 oxidation is generally accepted to be an extremely unstable and reactive, high-valent oxoiron moiety.^{9,10} By switching to ruthenium, it was hoped the chemistry could be “slowed down” to allow for mechanistic studies.^{2,13} Also, the wide range of oxidation states available, as high as 8+, makes ruthenium a potentially powerful oxidant (see Sections 1.2 to 1.8). To date, a number of oxidations carried out by ruthenium porphyrins has been discovered and investigated (examples from References 2,5,6,7,22-25,27-30,32,34,38,51,53,55,59 are discussed in the following sections) but the oxidation chemistry of ruthenium non-porphyrin species is also very rich (examples from References 3,4,17-20,39-50,52,57,61).

1.2 Ruthenium(VIII) Complexes

The highest attainable oxidation state for ruthenium is +8. The most well-known and perhaps the only well-defined ruthenium(VIII) complex is RuO₄.^{1,3} The potential of RuO₄ as a laboratory reagent for organic synthesis was not realized until the 1950s,³ even though the compound had been discovered early in the turn of the century. In the laboratory, RuO₄ finds wide use in the oxidation of secondary alcohols to ketones,^{1,3,4,17} but the oxidation of primary alcohols almost always over-oxidizes the aldehyde product to the carboxylic acid, diminishing the value of this reagent in this respect. Perhaps RuO₄ is

of greater importance in the field of carbohydrate chemistry, where the selective oxidation of the hydroxyl groups in carbohydrates to carbonyl groups without oxidizing the other protected groups is possible.¹ Lee and Van den Engh performed mechanistic studies on the stoichiometric oxidation of alcohols by RuO₄,¹⁷ and found that two different rate-limiting steps govern the overall rate of the reaction at different pH ranges. At very high acidities, carbenium-ion formation was rate-determining, but at lower acidities (1 to 6 M perchloric acid) hydride abstraction was the slow step. The stoichiometric alcohol oxidation by RuO₄ is represented in Eq. 1.2, and the process can be made catalytic if the tetraoxide is regenerated (Eq. 1.3).



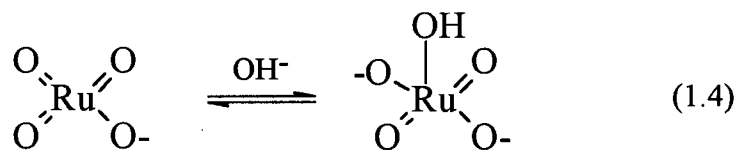
Hence, instead of using the tetraoxide stoichiometrically, in the presence of excess oxidizing agents such as hypochlorite or periodate, RuO₄ can be regenerated catalytically, a definite advantage over using a large, stoichiometric amount of the tetraoxide. RuO₄ can also be formed from lower-valent ruthenium species, such as RuCl₃•nH₂O.¹⁸

More recently, RuO₄ generated *in situ* has been used in the hydroxylation of saturated hydrocarbons.¹⁸ The stoichiometric oxidation of *cis* and *trans*-pinane with a RuCl₃ / NaIO₄ / (CCl₄ / CH₃CN / H₂O) system showed some interesting mechanistic insights. In summary, the bond-breaking in the saturated hydrocarbons was observed mainly to occur at tertiary C-H bonds and was proposed to occur via a two-electron hydride transfer pathway. Of greater interest is that the analysis of the numerous products

from the oxidation of the pinanes by the *in situ* RuO₄ indicated that an unprecedented methyl (1°) C-H cleavage occurred.

1.3 Ruthenium(VII) Complexes

The perruthenate ion, RuO₄⁻, is the only well-defined oxoruthenium(VII) complex. Lee and Congson have also carried out some mechanistic studies on the oxidation of alcohols by RuO₄⁻,¹⁹ and invoked a free-radical mechanism, as the oxidation of cyclobutanol cleaved the C-C bond and yielded mainly butanoic acid rather than cyclobutanone. More recently, the same group investigated the oxygen-atom transfer properties of the perruthenate ion to sulfides;²⁰ here, the active oxidizing species was proposed to be a five-coordinate oxoruthenium(VII) species formed by coordination sphere expansion (Eq. 1.4).



The oxidation of the thioether substrate was proposed to occur via either direct O-atom transfer or attack of the S lone pair on an empty π^* -orbital of Ru=O, followed by the release of the S=O moiety. Both mechanisms have been considered for other O-atom transfer reactions,^{21,29} however, kinetic and mechanistic data are generally lacking in ruthenium oxidation chemistry, and the O-atom chemistry is not fully understood.

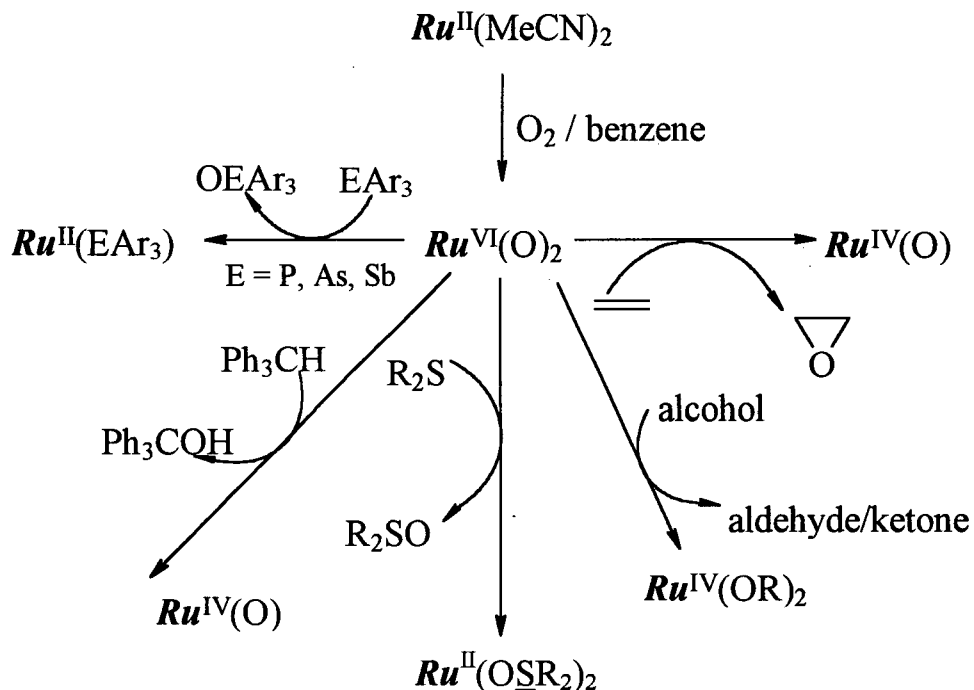
1.4 Ruthenium(VI) Complexes

Many oxoruthenium(VI) complexes are competent oxidation reagents or catalysts. Examples from both non-porphyrin and porphyrin work are numerous, with the latter emerging in recent years. These complexes contain high-valent ruthenium-oxo moieties capable of oxygen-atom transfer or C-H bond cleavage.

1.4.1 Ruthenium(VI) Porphyrin Complexes

The first dioxoporphyrinato ruthenium(VI) complex, *trans*-Ru^{VI}(TMP)(O)₂, was discovered independently by Grove's group²² and this group at UBC.²³ The Ru^{VI}(TMP)(O)₂ complex can be formed by the *meta*-chloroperbenzoic acid (*m*-CPBA) oxidation of Ru^{II}(TMP)(CO), or by the aerobic oxidation of Ru^{II}(TMP)(L)₂ (L = MeCN,²⁴ THF,²⁵ N₂ or vacant²⁶). More recently, Ru^{VI}(TMP)(O)₂ was reported to be generated by oxidizing Ru^{II}(TMP)(THF)₂ with N₂O.²⁷ The use of TMP as a ligand, with its methyl substituents on the 2- and 6- positions on the *meso*-phenyl groups, prevents dimerization of the porphyrin complex to μ -oxo-dinuclear ruthenium(IV) species, which are generally regarded as catalytically inactive, thermodynamic sinks.^{2b,13} The use of TMP for catalytic systems was thus an improvement over the use of unhindered Ru(TPP) species.

The Ru^{VI}(TMP)(O)₂ complex is a versatile, stoichiometric and O₂-catalytic oxidant (see Figure 1.5).^{2b} Both of the oxygen atoms in Ru^{VI}(TMP)(O)₂ can be used for the oxidation of substrates, hence this shows that the dioxo species exhibits genuine dioxygenase-type activity. Under air or O₂ at mild conditions, the following oxidations catalyzed by Ru^{IV}(TMP)(O)₂ take place: alkenes^{25,28c} or steroids^{28a,b} to corresponding



$\text{Ru} = \text{Ru}(\text{TMP})$ unit

Figure 1.5. Various oxidations carried out by $\text{Ru}^{\text{VI}}(\text{TMP})(\text{O})_2$ in benzene or toluene; the processes become catalytic in the presence of excess substrate under 1 atm air or O_2 . The intermediates and/or products, where indicated, are identified based on spectroscopic or structural evidence. Higher temperatures usually speed up the rate of catalysis; however, the porphyrin decomposes faster under such conditions than at room temperature.

epoxides, thioethers to sulfoxides,²⁹ tertiaryarylphosphines,^{5b,6a,24,†} AsPh₃^{5b,6a,†} and SbPh₃^{5b,6a,†} to the corresponding oxides, alcohols to aldehydes or ketones,^{5a,6a,†} and the tertiary alkane Ph₃CH to Ph₃COH.[†] Stoichiometrically, Ru^{VI}(TMP)(O)₂ hydroxylates activated mono-substituted aromatic rings, such as phenol^{29a,b} and *N,N*-dimethylaniline to *p*-hydroquinone and *p*-hydroxy-*N,N*-dimethylaniline, respectively.[†] Prior to this thesis work, mechanistic details and a kinetic database were generally lacking on the Ru^{VI}(TMP)(O)₂ oxidation chemistry, and the present work has sought to study such systems in more detail, as well as to develop catalytic O₂-oxidation systems based on the dioxo complex.

Recently, a catalytic system based on Ru^{VI}(TMP)(O)₂ using pyridine-*N*-oxide was developed,³⁰ with remarkable activity towards the hydroxylation of secondary and tertiary alkanes. For adamantane, up to 14000 turnovers (giving primarily 1-adamantanol) were realized at ambient conditions. Water inhibited the catalytic activity of the system; however, trace anhydrous acid (HCl or HBr) enhanced the rates of catalysis. Treatment of a benzene solution of Ru^{VI}(TMP)(O)₂ with HCl (gaseous or aqueous) has been suggested to produce the complex Ru^{IV}(TMP)(Cl)₂,^{30,31,‡} and the active catalytic species in the above system was proposed to be Ru^{VI}(TMP)(O)(Cl)⁺.³⁰ Of note, Ru^{II}(TMP)(CO) was an active catalyst precursor, and even Ru^{II}(TPP)(CO) was shown to be effective in hydroxylations. In fact Ru^{II}(TPP)(CO) was the most effective catalyst precursor, oxidizing adamantane to 1-adamantanol and adamantane-1,3-diol, with a trace of 2-adamantanone (68 : 25 : 1), the total turnover being 120000 after heating for 6 h at 80 °C in benzene.

[†] Present work to be discussed in later chapters.

[‡] The reaction of HX acids with Ru^{VI}(TMP)(O)₂ will be discussed in Chapter 6.

The first chiral picket-fence *trans*-Ru^{VI}(por*)(O)₂ complex was synthesized recently (por* = chiral porphyrin ligand, see Figure 1.6),³² and some chiral recognition was observed in the stoichiometric oxidation of *R*- and *S*-phosphine mixtures. For the $\alpha,\beta,\alpha,\beta$ isomer of the dioxoruthenium porphyrin, the oxidation of *R*- and *S*-P(CH₂Ph)(Ph)(Me) showed that the *R*-enantiomer was oxidized more selectively to the phosphine oxide (*R*:*S* = 2.4); however, the phosphorus binding-preference in the final Ru(II)-product,³³ Ru^{II}(por*)(phosphine)₂, was the *S*-configuration about phosphorus (*S*:*R* = 2.3 preference of binding to Ru).

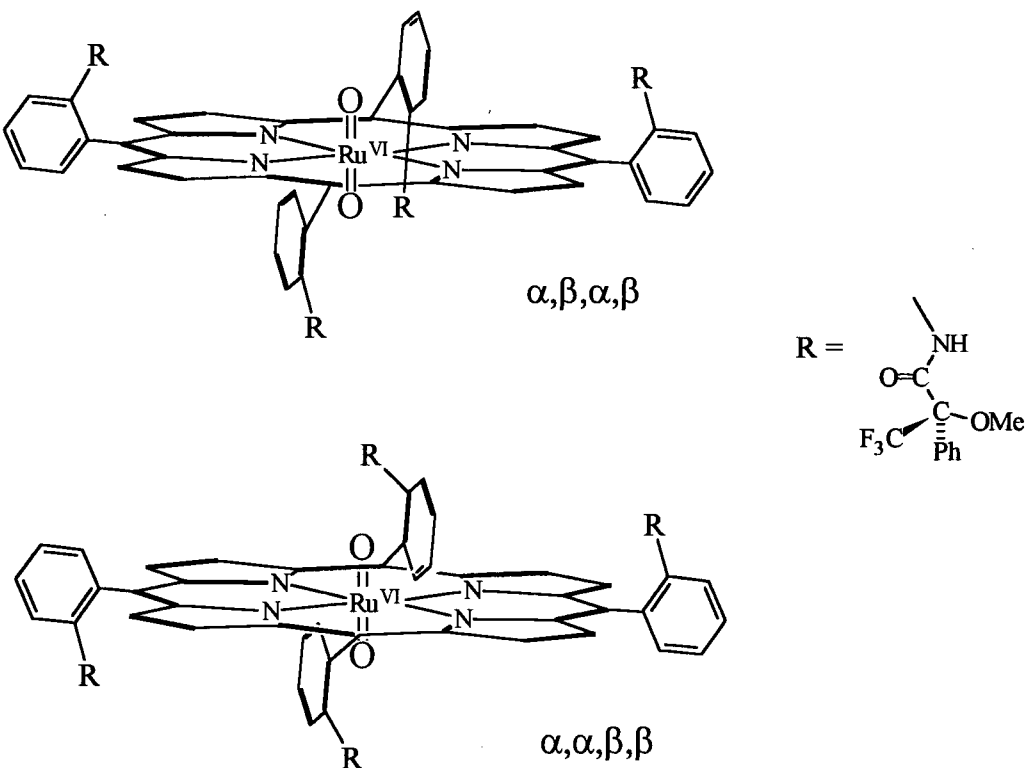


Figure 1.6. The first chiral picket-fence dioxoporphyrinato-ruthenium(VI) species. The $\alpha,\beta,\alpha,\beta$ and $\alpha,\alpha,\beta,\beta$ isomers are shown above.

Some Ru^{VI}(porp)(O)₂ species (where porp = TPP-x[†] and OEP,³⁴ the non-sterically hindered porphyrins) have been prepared without the expected formation of the inactive μ-oxo-dinuclear ruthenium(IV) species.^{2b,13} The Ru^{II}(porp)(CO)(MeOH) precursors were oxidized by *m*-CPBA in EtOH/CH₂Cl₂, which resulted in the formation of the corresponding dioxo species. A coordinating solvent such as EtOH appears to be crucial in preventing the formation of the μ-oxo-diruthenium species. Of note, the dioxo species were reported to be capable of oxidizing stoichiometrically the tertiary alkanes adamantane and methylcyclohexane to the corresponding tertiary alcohols with yields of approximately 20% based on the metal complex. Ethylbenzene was also oxidized to 1-phenylethanol and acetophenone. Epoxidations of alkenes were also reported in the studies.³⁴ In all these cases, it appears that the dioxo species eventually do form μ-oxo-dinuclear ruthenium(IV) species, thought to be due to contamination by water. The fact that these dioxo species also oxidized alcohols leads one to question the true identity of the Ru-product in the alkene oxidation reactions; Ru^{IV}(TPP)(O)•EtOH or Ru^{IV}(TPP)(OH)₂•EtOH was proposed as the Ru-product based solely on ¹H-NMR spectroscopy in a CD₃CD₂OD/CDCl₃ solvent system. Studies carried out in this thesis work show that a bis(alkoxo)ruthenium(IV) species is the inorganic product of alcohol oxidation with the Ru^{VI}(TMP)(O)₂ species,^{5a,6a} and that excess alcohol can exchange rapidly with the alkoxo ligands. It seems likely that Ru^{IV}(porp)(OR)₂ [R = CD₃ or CD₂CD₃] species are formed in the conditions noted above.

[†] TPP-x = dianion of *meso*-tetra(*para*-substituted-phenyl)porphyrin (see Figure 1.4).

A most exciting breakthrough in ruthenium porphyrin oxidation chemistry came about with the use of halogenated porphyrins, commencing with *trans*-Ru^{VI}(TDCPP)(O)₂, which was shown to be a much more robust catalyst than the TMP analogue;²⁹ an iron-TDCPP system had been demonstrated earlier to epoxidize alkenes efficiently using O-atom donors.³⁵ The Ru^{VI}(TDCPP)(O)₂ species exhibits very much the same chemistry described in Figure 1.5,^{29,†} generally with higher reactivity than the TMP analogue due to the increased electronegativity on the *meso*-phenyl rings. Recently, iron, chromium and manganese complexes of TPFPP[§] were reported to catalyze the aerobic oxidation of light alkanes, such as isobutane and propane under O₂ pressures ≤ 1000 psi at temperatures reaching 150 °C.³⁶ Further halogenation of the eight β-pyrrole positions lying on the porphyrin plane led to some remarkably reactive species. The use of Fe^{III}(TPFPP-Br₈)(Cl)[§] as a catalyst precursor afforded a system that oxidized isobutane to *tert*-butanol with turnovers of about 13000, again under 1000 psi O₂ but now the reaction proceeds at room temperature. Of note, there has been some debate as to whether a genuine oxoiron species is involved,³⁶ or whether free-radical hydroperoxide decomposition is responsible for the actual oxidation.^{16a,37} On the ruthenium front, very little work has been done on such perhalogenated Ru-porphyrins, except for the recent synthetic/structural studies with TPFPP-Cl₈ systems,¹⁴ and the work to be described in Chapter 5 on the aerobic oxidation of alcohols, alkenes and tertiary alkanes catalyzed by some Ru(TDCPP-Cl₈) species.

† Present work to be discussed in later chapters.

§ TPFPP = dianion of *meso*-tetra(2,3,4,5,6-pentafluorophenyl)porphyrin (see Figure 1.4).

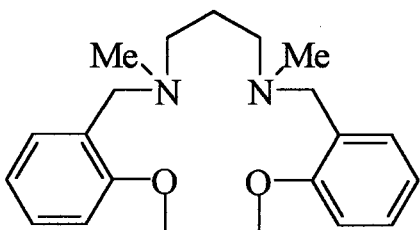
§ Refer to figure 1.4 for the abbreviations for these 3rd generation porphyrins.

The 6+ formal oxidation state is the highest observed to date for ruthenium in any ruthenium porphyrin complex, although a Ru(VI) porphyrin-radical-cation has been formed in the oxidation of $\text{Ru}^{\text{VI}}(\text{porp})(\text{O})_2$, porp = TMP or OEP, by phenoxathin hexachloroantimonate(V).³⁸ A g-value of 2.002 observed in the ESR spectrum taken at 77 K, a blue-shifted Soret band and a broad Q-band are suggestive of the formation of a porphyrin radical-cation. The oxidation of diphenylsulfide and several alkenes by these radical-cation species implied that they are stronger oxidants than the non-radical Ru(VI) counterparts. The removal of one electron from the porphyrin ligand likely increased the electrophilicity of the Ru-oxo moieties, and hence, their reactivities as well.³⁸

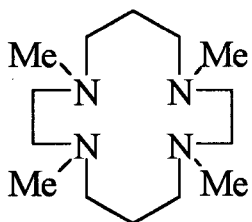
1.4.2 Ruthenium(VI) Non-porphyrin Complexes

A group of *trans*-dioxoruthenium(VI) complexes based on tetridentate tetraaza N-donor macrocycles and tetridentate dioxadiazia N- and O-donor ligands has been extensively studied in recent years.³⁹ These tetridentate ligands (some are shown in Figure 1.7) behave similarly to porphyrin ligands in their binding mode and the ligand binding geometry forces the two oxo ligands to a trans configuration. These high-valent dioxoruthenium(VI) complexes can oxidize stoichiometrically alcohols to the corresponding ketones or aldehydes in CH_2Cl_2 ,^{39b,d,e} and under air, some of these systems become marginally catalytic (2 to 3 turns) at ambient conditions.^{39d,e} Alkenes are also oxidized exclusively to epoxides.^{39a} Of note, large kinetic isotope effects ($k_{\text{H}}/k_{\text{D}}$ about 20) were observed in the stoichiometric oxidation of alcohols by these Ru(VI) complexes, in contrast with the findings on the alcohol oxidations by $\text{Ru}^{\text{VI}}(\text{TMP})(\text{O})_2$ in the present

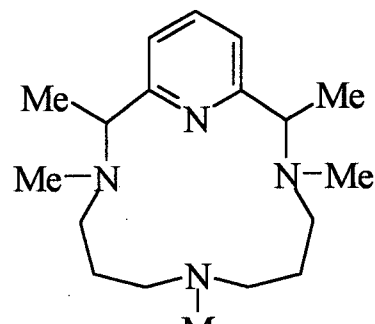
thesis (Chapter 4). The dioxoruthenium non-porphyrin species are also capable of oxidizing C-H bonds in alkanes.^{39c} The oxidation of some aromatic hydrocarbons showed the following reactivity trend: toluene < ethylbenzene < cumene, the oxidized products being benzaldehyde, acetophenone and 2-phenyl-isopropanol, respectively. A two-electron hydride or one-electron H-atom abstraction pathway was proposed as a possible mechanistic step. Kinetic isotope effects of $k_H/k_D > 10$ were observed in these alkane oxidations, indicating that C-H bond-breaking is the rate-determining step.



N,N'-dimethyl-6,7,8,9,10,11,17,18-octahydro-5*H*-dibenzo[*en*]-[1,4,8,12]dioxadiazacyclopentadecine



1,4,8,11-tetramethyl-
1,4,8,11-tetraazacyclotetradecane



meso-2,3,7,11,12-pentamethyl-
3,7,11,17-tetraazabicyclo[11.3.1]-
heptadeca-1(17),13,15-triene

Figure 1.7. Several examples of tetradentate macrocyclic tetraaza and dioxadiaz-a-N- and N/O-donor macrocyclic ligands, analogous to porphyrins, that have been used in the synthesis of dioxoruthenium(VI) complexes

Perhaps the most notable non-porphyrin oxoruthenium(VI) complex is the ruthenate ion, $\text{Ru}(\text{O})_3(\text{OH})_2^{2-}$. Once thought to be the tetrahedral RuO_4^{2-} anion, the ruthenate ion is now known to be trigonal pyramidal from crystallographic studies.⁴⁰ The ruthenate ion finds use in the oxidation of alcohols to carboxylic acids or ketones, and the system becomes catalytic in the presence of oxidizing agents such as persulfate.^{4a} Mechanistic studies by Lee and Congson¹⁹ suggest that a two-electron hydride transfer mechanism is operating in the oxidation of alcohols, which is different from the one-electron H-atom abstraction mediated by perruthenate noted in Section 1.3.

Recently, barium ruthenate has been successfully applied to the stoichiometric oxidation of alkanes at room temperature with remarkable reactivity.⁴¹ Acetic acid enhanced the reactivity of the reagent toward the hydroxylation of alkanes,^{41a} and the tertiary alkanes adamantane and methylcyclohexane were oxidized in CH_2Cl_2 in the presence of acetic acid to the corresponding tertiary alcohols within 2 h, with yields reaching 95 and 42%, respectively. For *n*-hexane, the oxidation occurred mainly at the secondary C-H bonds, forming 2- and 3-hexanone, with yields reaching 20% and 16%, respectively. The oxidation of cyclohexane yielded 60% cyclohexanone exclusively; no cyclohexanol was observed. The addition of Lewis acids such as ZnCl_2 and FeCl_3 reduced the reaction time dramatically to a few minutes, in contrast to a few hours. Cyclohexane was now oxidized to cyclohexanone with the same yield in about 5 min, with some trace cyclohexanol being detected. In another study,^{41b} trifluoroacetic acid was used instead of acetic acid, and such a change resulted in a very reactive system capable of oxidizing the light alkanes ethane and propane to acetic acid (40% yield) and acetone (65%),

respectively. Benzene was also hydroxylated to *para*-benzoquinone with a 20% yield. Dioxoruthenium(VI) acetato species were proposed to be the active oxidizing species, the reactivities of which were possibly further enhanced by the presence of Lewis acids. Of interest, the effect of the acids seems to be similar to that of HCl and HBr in the Ru(porp)/pyridine-*N*-oxide systems³⁰ mentioned earlier in Section 1.4.1, although the role of the acids in either systems is unknown.

1.5 Ruthenium(V) Complexes

Oxoruthenium(V) complexes are rare. Griffith and co-workers characterized crystallographically the product from the reaction of $[\text{RuO}_4][\text{N}''\text{Pr}_4]$ and 2-hydroxy-2-ethylbutyric acid as $[\text{Ru}^{\text{V}}(\text{O})(\text{O}_2\text{COCEt}_2)_2][\text{N}''\text{Pr}_4]$.⁴² This oxoruthenium(V) complex is a mild stoichiometric oxidant that can oxidize primary alcohols to aldehydes and secondary alcohols to ketones. Excess *N*-methylmorpholine-*N*-oxide can be used as the primary O-atom source, and the system can produce up to 25 turnovers at room temperature.

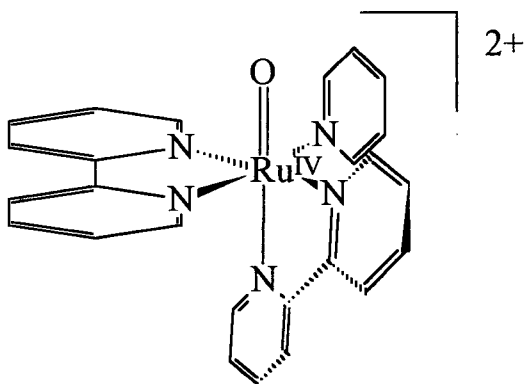
Che and co-workers have demonstrated recently that $[\text{Ru}^{\text{V}}(\text{L})(\text{O})][\text{ClO}_4]_2$ ($\text{L} =$ anion of [2-hydroxy-2-(2-pyridyl)ethyl]bis[2-(2-pyridyl)ethyl]amine) was an oxidant strong enough to oxidize cyclohexane to cyclohexanone (60% yield) in acetonitrile.⁴³ Other tertiary alkanes, such as adamantine and methylcyclohexane were oxidized exclusively to the corresponding tertiary alcohols with yields of 60% and 43%, respectively. A kinetic isotope effect $k_{\text{H}}/k_{\text{D}}$ of 5.3 was observed for the oxidation of cyclohexane, suggesting C-H bond cleavage as the rate-determining step.

1.6 Ruthenium(IV) Complexes

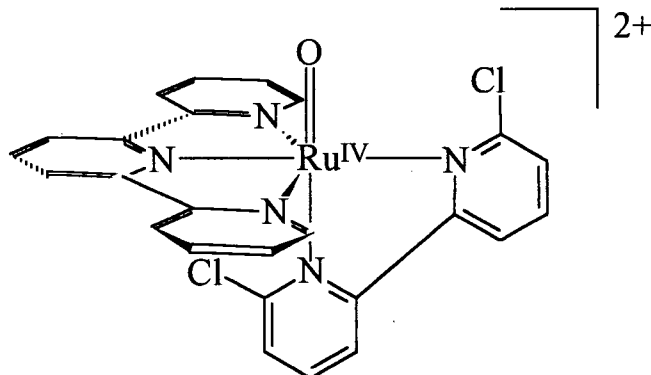
Meyer's group, and a few others, have worked extensively with *cis*-Ru(bpy)₂(py)(O)²⁺ (bpy = 2,2'-bipyridine, py = pyridine) and similar polypyridine complexes, and have studied alkene epoxidation,⁴⁴ alcohol,⁴⁵ phenol⁴⁶ and *para*-hydroquinone⁴⁷ oxidations, as well as O-atom transfer reactions to thioethers⁴⁸ and phosphines.⁴⁹ This type of Ru-complexes is shown in Figure 1.8. These stoichiometric oxidations usually were carried out in acetonitrile or acetonitrile/water solvent systems. As kinetic and mechanistic studies on Ru-oxo oxidations are rather sparse, the results for the oxidation of alcohols by Ru^{IV}(bpy)₂(py)(O)²⁺ are particularly relevant with respect to the oxidation of alcohols by Ru^{VI}(TMP)(O)₂ described in this thesis. Although the Ru-atoms are in different formal oxidation states, 4+ and 6+, respectively, both oxidations are proposed to occur via a two-electron, hydride transfer pathway. Roecker and Meyer^{45a} observed an unusually large kinetic isotope effect ($k_H/k_D = 50$) for the oxidation of benzyl alcohol, and a k_H/k_D value of 18 for ¹PrOH. The stoichiometric oxidation of ¹PrOH in benzene by Ru^{VI}(TMP)(O)₂ has a much lower value of $k_H/k_D = 1.9$ for the α -C-H bond cleavage. The discussion of this subject will be presented later in Chapter 4.

Che and co-workers have varied the Ru(bpy)₂(py)(O)²⁺ theme and replaced the polypyridine ligands with substituted polypyridines. Generally the chemistry that can be accomplished (alkene epoxidation, alcohol oxidation, etc.) by these complexes is not much different from that of their unsubstituted analogues.⁵⁰ One interesting find was that Ru^{IV}(terpy)(dcbpy)(O)²⁺ (terpy = 2,2':6',2''-terpyridine, dcbpy = 6,6':2,2'-bipyridine) (see Figure 1.8) also was capable of oxidizing stoichiometrically alkanes in

acetonitrile at room temperature. Adamantane was oxidized to 1-adamantanol with a 28% yield after 4 h, while ethylbenzene was oxidized to 70% acetophenone and 31% 1-phenylethanol in the same amount of time. The presence of the electron-withdrawing 6 and 6' Cl groups likely enhances the reactivity of the Ru=O moiety.



cis-Ru^{IV}(bipy)₂(py)(O)²⁺

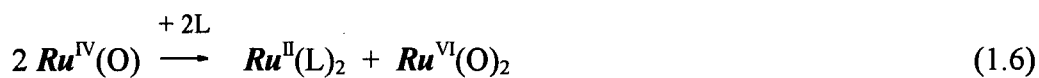
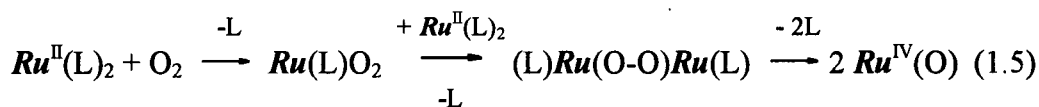


Ru^{IV}(terpy)(dcbpy)(O)²⁺

Figure 1.8. Two examples of monooxoruthenium(IV) polypyridyl complexes. These complexes have been used to oxidize stoichiometrically a variety of organic substrates (phosphines, thioethers, alcohols, alkenes).

Earlier work in this laboratory led to the discovery of Ru^{IV}(OEP⁺)(O)(Br) (OEP⁺ = OEP porphyrin radical-cation) formed from the reaction of Ru(OEP)(Br)(PPh₃) and PhIO.⁵¹ The Ru(OEP⁺)(O)(Br) was proposed as such based on ESR evidence for a porphyrin radical-cation, as well as the stoichiometry of O-atom transfer to PPh₃. Of particular importance is that this oxoruthenium(IV) moiety is isoelectronic with the proposed active Fe^{IV}=O intermediate in the P-450 system, and thus for the first time a ruthenium model of the oxoiron(IV) protoporphyrin-IX radical-cation species was available. The oxidation of cyclohexane with this oxoruthenium(IV) species was marginally catalytic on using PhIO as an oxidant, producing cyclohexanol, cyclohexanone and cyclohexylbromide in a 1:8:9 ratio, the total turnover being 1.7 based on the metalloporphyrin.

The other often quoted oxoruthenium(IV) porphyrin species is Ru^{IV}(TMP)(O), a proposed intermediate in various catalytic oxidations: epoxidation of alkenes,^{25,28} oxidative dehydrogenation of alcohols^{5a,6a} and oxidations of tertiaryarylphosphines,^{5b,6a,24} AsPh₃^{5b,6a} and SbPh₃.^{5b,6a} Equally important, Ru^{IV}(TMP)(O) is the proposed intermediate in the formation of Ru^{VI}(TMP)(O)₂ from the aerobic oxidation of Ru^{II}(TMP)(L)₂ (L = MeCN,²⁴ THF,²⁵ N₂ or vacant²⁶), which is believed to proceed via Eqs. 1.5 and 1.6 [Ru = Ru(TMP)].



The monooxo Ru(IV)-species has yet to be isolated, but ^1H -resonances assignable to $\text{Ru}^{\text{IV}}(\text{TMP})(\text{O})$ can be observed *in situ* by ^1H -NMR spectroscopy in benzene- d_6 during the oxidations of tertiaryarylphosphines,^{5b,6a,24} AsPh_3 ^{5b,6a} and SbPh_3 .^{5b,6a} The $\text{Ru}^{\text{IV}}(\text{TMP})(\text{O})$ species is paramagnetic and exhibits shifted ^1H -resonances (relative to those, for example, of diamagnetic Ru(II) species) for the TMP ligand characteristic of such Ru(IV)-porphyrin species.^{24,27,31}

In non-porphyrin work, monooxoruthenium(IV) species have been shown to undergo proton-coupled equilibria with H_2O in solution to form the *trans*-bis(hydroxo)ruthenium(IV) species.⁵² This type of equilibrium is likely to occur for $\text{Ru}^{\text{IV}}(\text{TMP})(\text{O})$ species (Eq. 1.7), and such a reaction has been invoked to account for the catalytic aerobic oxidation of alcohols.^{5a,6a} The bis(hydroxo) species depicted in Eq. 1.7



has been reported by two groups.^{29a,b,53} Preliminary work in this laboratory, reported in 1990 on the oxidation of $^i\text{PrOH}$, led to the isolation of a complex, which was proposed to be $\text{Ru}^{\text{IV}}(\text{TMP})(\text{OH})_2$ ^{29a,b} based mainly on the non-detection of any axial ligand protons by ^1H -NMR spectroscopy. In 1993, the same $\text{Ru}^{\text{IV}}(\text{TMP})(\text{OH})_2$ was reported to be isolated from the *m*-CPBA oxidation of $\text{Ru}^{\text{II}}(\text{TMP})(\text{CO})$ in $\text{EtOH}/\text{CH}_2\text{Cl}_2$, with the mention of unpublished crystallographic data on the complex.⁵³ The isolation of $\text{Ru}^{\text{IV}}(\text{TMP})(\text{O}^i\text{Pr})_2$ in the oxidation of $^i\text{PrOH}$ by $\text{Ru}^{\text{VI}}(\text{TMP})(\text{O})_2$ in benzene,^{5a,6a} and the subsequent detailed study and understanding of such alcohol oxidations (Chapter 4) strongly refute the proposal of the isolation of $\text{Ru}^{\text{IV}}(\text{TMP})(\text{OH})_2$. Indeed, the work described in Chapter 4 shows that the axial alkoxo ligands of $\text{Ru}^{\text{IV}}(\text{TMP})(\text{OR})_2$ species exchange rapidly with

excess alcohol in solution; therefore, the bis(hydroxo) species, though possibly existing as part of the equilibria of Eq. 1.7, would not be the favoured species when excess alcohol is present. Of interest, the supposed “Ru^{IV}(TMP)(OH)₂” reported by Che and co-workers⁵³ was reported to be slightly more effective than Ru^{VI}(TMP)(O)₂ for the epoxidation of norborene. Although this author believes that Ru^{IV}(TMP)(OH)₂ has not been successfully isolated under the above-mentioned conditions, recently the Ru^{IV}(TDCPP)(OH)₂ analogue was characterized crystallographically, and a Ru-O bond distance of 1.78 Å was observed,⁵⁴ which is extremely short for a Ru-O bond length for this class of Ru(IV) complexes (1.892 or 1.905 Å for Ru^{IV}(TMP)(OR)₂, where R = *i*Pr^{5a,55} or 1,3-dichloro-2-propyl,⁵⁵ respectively) and 1.944 Å in [Ru^{IV}(TPP)(*p*-OC₆H₄Me)₂]O.^{13a} A high degree of π-backbonding seems to be shortening the Ru-O bond to almost a Ru-oxo double bond,⁵⁴ which is typically *ca.* 1.73 (Ru^{VI}) to 1.78 (Ru^{IV}) Å in various dioxo- and oxoruthenium complexes.^{4c,56}

1.7 Ruthenium(III) Complexes

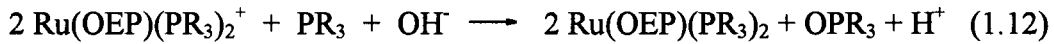
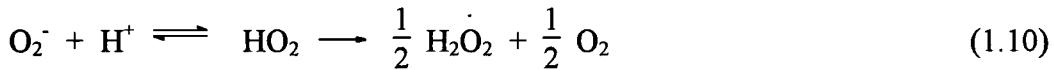
A RuCl₃•nH₂O or Ru^{II}(Cl)₂(PPh)₃ / aldehyde system was recently employed to effect the catalytic O₂-hydroxylation of alkanes under relatively mild conditions.⁵⁷ Aldehydes are known to form peracids in the presence of O₂,⁵⁸ and once formed the peracid can oxidize low-valent ruthenium(II or III) to higher-valent oxoruthenium species. In these systems, elemental iron was more effective as a catalyst precursor than the ruthenium complexes, and under 1 atm O₂, some saturated hydrocarbons (cyclohexane, methylcyclohexane, adamantane, cyclooctane, *n*-decane and ethylbenzene) were oxidized

at the secondary and tertiary positions to the corresponding ketones and tertiary alcohols.

For the $\text{RuCl}_3 \cdot n\text{H}_2\text{O}$ /heptanal/acetic acid/ CH_2Cl_2 system, cyclooctane was oxidized to cyclooctanone and cyclooctanol (3 : 1) over a period of 15 h, the total turnover being 8.4 based on the starting ruthenium.

1.8 Ruthenium(II) Complexes

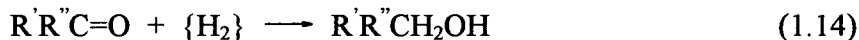
Work conducted in this laboratory throughout the 1980s led to the discovery of the production of hydrogen peroxide from H^+ and O_2 mediated by a ruthenium(II) porphyrin species (Eqs. 1.8 and 1.10).⁵⁹ In the presence of a reductant, the Ru(II) species is regenerated (Eq. 1.12), making the production of H_2O_2 catalytic. The *in situ* generated H_2O_2 then can oxidize organic substrates that are present in solution. Phosphines were studied first with this system, but the chemistry can be applied to the oxidation of thioethers. The overall reaction is catalytic in $\text{Ru}^{\text{II}}(\text{OEP})(\text{PR}_3)_2$, H^+ and OH^- . The following mechanism was proposed (Eqs. 1.8 to 1.12):



For any substrate that can be oxidized by H_2O_2 , the system can, in principle utilize O_2 as oxidant within the above scheme. As mentioned, a reductant is necessary to regenerate

the Ru(II)-catalyst (Eq. 1.12), and for an “optimum” system this reductant is preferably the substrate itself. The same basic mechanism applies to the oxidation of thioethers, namely, superoxide is first generated by an outer sphere electron transfer (Eq. 1.8), followed by the generation of H₂O₂ (Eq. 1.10), which then subsequently oxidizes the thioether to sulfoxide. Visible light from a tungsten source was necessary to assist in driving equilibria 1.8 and 1.10 to the product side.^{59a} Initial turnovers were close to 360 h⁻¹, with total turnovers of about 10000. Slowly, the catalytically less active Ru^{II}(OEP)(SR₂)(OSR₂) species containing S-bound sulfoxide was formed.

The oxidation of primary or secondary alcohols to the corresponding aldehydes or ketones is in essence a dehydrogenation reaction (Eq 1.13).



The hydrogen, {H₂}, that is liberated in Eq. 1.13 may or may not be transferred to a hydrogen acceptor R'R''C=O (Eq. 1.14). The liberation of free H₂ in a dehydrogenation reaction is an endothermic process, e.g. for ⁱPrOH, ΔH = + 66.5 kJ•mol⁻¹ at 327 °C.⁶⁰ In the aerobic oxidative-dehydrogenation of alcohols to aldehydes/ketones and H₂O, the end hydrogen acceptor is O₂ and the overall reaction becomes exothermic. It is not necessary to use O₂ as the hydrogen acceptor; for example, an imine or a ketone can accept the hydrogen from the substrate. The use of O₂ as acceptor is generally referred to as oxidation, while the use of other acceptors is usually referred to as transfer hydrogenation. Transfer hydrogenation is more generally concerned with the use of a hydrogen source other than H₂ to effect hydrogenation, and the focus is on reducing the unsaturated

substrate, not the oxidized hydrogen source. In the last few years, Bäckvall and co-workers have developed ruthenium(II)-based systems for dehydrogenating alcohols by transfer hydrogenation.⁶¹ Imines, ketones and O₂ have been used as hydrogen acceptors. With O₂, an elaborate catalytic system involving three components was employed (see Figure 1.9).^{61a} Secondary alcohols, which are more difficult to oxidize than benzyl alcohol, were oxidized to the corresponding ketones with high yields. Overall, most alcohols gave turnovers around 30 to 40 h⁻¹ at 100 °C. Of note, the reactions were more efficient under a low O₂ partial pressure, *ca.* 0.6 - 1.5% in 1 atm N₂, than those under higher O₂ partial pressures, and this was thought to be due to the sensitivity of the Ru(II)-catalytic precursor to O₂. When both the hydrogenated product and oxidized hydrogen source are valuable chemicals, this kind of transfer hydrogenation can be an extremely useful process.

1.9 Aims and Scope of this Thesis

A general overview has been presented and the diverse chemistry of Ru oxidation reagents and catalysts is very much apparent. The aims of this thesis work were two-fold. The foremost interest in the current research focussed on the use of dioxoruthenium(VI) porphyrin complexes as O₂-oxidation catalysts for the oxidation of organic substrates. Secondly, the continual need for detailed kinetic and mechanistic studies was recognized, as they may further the understanding of such oxidation reactions. As the discussion of each individual subject is at hand, the particular aims and scope (as well as success and failure!) will be explored more clearly. Chapter 2 summarizes the general experimental

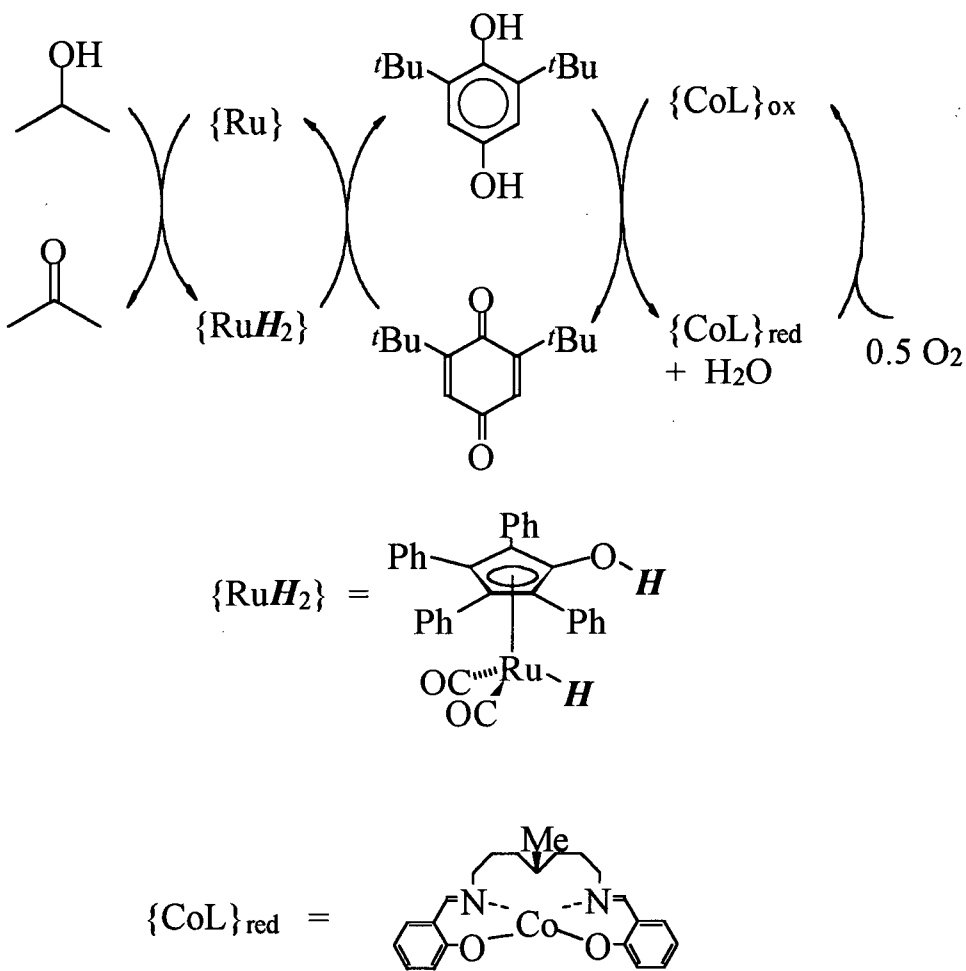


Figure 1.9. Ruthenium-based, aerobic, triple catalytic system for the O_2 -oxidation of alcohols to aldehydes and ketones. The ruthenium complex $\{Ru\}$ dehydrogenates the alcohol. Regeneration of the ruthenium catalyst is accomplished by the bulky benzoquinone. A cobalt Schiff base complex is responsible for regenerating the benzoquinone from the reduced *para*-hydroquinone. O_2 , is the sole terminal oxidant that oxidizes the reduced cobalt complex, $\{CoL\}_{red}$ (Ref. 61a).

procedures, and preparation and characterization of starting materials. Chapters 3 and 4 present kinetic and mechanistic studies on the stoichiometric and catalytic oxidations of phosphines and alcohols, respectively. Chapter 5 introduces work concerning the O₂-oxidation of alcohols and neat hydrocarbons catalyzed by ruthenium perhalogenated porphyrins. Chapter 6 includes some preliminary work on the reactions of Ru^{VII}(TMP)(O)₂ with HX acids, mono-substituted aromatics and *p*-hydroquinone. Finally, Chapter 7 presents the overall conclusions of the entire thesis work, and suggests research topics that need further study.

References

- 1 a) A. H. Haines, *Methods for Oxidation of Organic Compounds*, Academic Press, Toronto, 1988.
 b) M. Hudlický, *Oxidations in Organic Chemistry*, American Chemical Society, Washington, DC, 1990.
- 2 a) B. R. James, *Fundamental Research in Homogeneous Catalysis*, ed. A. E. Shilov, Plenum Press, Vol 1, 1986, p. 309.
 b) T. Mlodnicka and B. R. James, in *Metalloporphyrins Catalyzed Oxidations*, eds. F. Montanari and L. Casella, Kluwer Academic Publishers, Dordrecht, 1994, p. 121.
- 3 R. R. Engle and C. Djerassi, *J. Am. Chem. Soc.*, **75**, 3838 (1953).
- 4 a) W. P. Griffith, *Chem. Soc. Rev.*, **21**, 179 (1992)
 b) W. P. Griffith, *Trans. Met. Chem.*, **15**, 251 (1990)
 c) C.-M. Che and V. W.-W. Yam, *Adv. Inorg. Chem.*, **39**, 233 (1992)
- 5 a) S. Y. S. Cheng, N. Rajapakse, S. J. Rettig and B. R. James, *J. Chem. Soc., Chem. Commun.*, 2669 (1994).
 b) S. Y. S. Cheng and B. R. James, *J. Mol. Cat.*, in press.
- 6 a) S. Y. S. Cheng and B. R. James, *Proc. of the 78th Can. Chem. Conf.*, Guelph, Canada, 1995, Abstract IN-447.
 b) S. Y. S. Cheng and B. R. James, Poster Presentation at the 15th Annual BC Inorganic Research Colloquim, Victoria, Canada, June 18-20, 1993.
- 7 a) *Metalloporphyrin Catalyzed Oxidations*, eds. F. Montanari and L. Casella, Kluwer Academic Publishers, Dordrecht, 1994.
 b) *Metalloporphyrins in Catalytic Oxidations*, ed. R. A. Sheldon, Marcel Dekker, New York, 1994.
 c) B. Meunier, *Chem. Rev.*, **92**, 1411 (1992).
 d) T. Mukaiyama and T. Yamada, *Bull. Chem. Soc. Jpn.*, **68**, 17 (1995).
- 8 R. Stewart, *Oxidation Mechanisms*, W. A. Benjamin, Inc., New York, 1965.
- 9 a) *Cytochrome P-450*, eds. T. Omura, Y. Ishimura and Y. Fujii-Kuriyama, Tokyo, 2nd Ed, 1993, Chapter 2.
 b) N. Rajapakse, M. Sc. Dissertation, University of British Columbia, Vancouver, Canada, 1985.
- 10 J. T. Groves, *J. Chem. Ed.*, **62**, 928 (1985).

- 11 T. L. Poulos, B. C. Finzel, I. C. Gunzalus, Wagner and J. Kraut, *J. Biol. Chem.*, **260**, 16122 (1985).
- 12 Reference 7b, p. 113.
- 13 a) J. P. Collman, C. E. Barnes, P. J. Collins, T. Owaza, J. C. Galluci and J. A. Ibers, *J. Am. Chem. Soc.*, **106**, 5151 (1984).
b) H. Masuda, T. Tagu, K. Osaki, H. Suzimoto, M. Mori and H. Ogoshi, *J. Am. Chem. Soc.*, **103**, 2199 (1981).
- 14 a) E. R. Birnbaum, W. P. Schaefer, J. A. Labinger, J. E. Bercaw and H. B. Gray, *Inorg. Chem.*, **34**, 1751 (1995).
b) D. Mandon, P. Ochsenbein, J. Fischer, R. Weiss, K. Jayaraj, R. N. Austin, A. Gold, P. S. White, O. Brigaud, P. Battioni and D. Mansuy, *Inorg. Chem.*, **31**, 2044 (1992).
- 15 a) T. Takeuchi, H. B. Gray and W. A. Goddard III, *J. Am. Chem. Soc.*, **116**, 9730 (1994).
b) P. Ochsenbein, K. Ayougou, D. Mandon, J. Fischer, R. Weiss, R. N. Austin, K. Jayaraj, A. Gold, J. Terner and J. Fajer, *Angew. Chem. Int. Ed. Engl.*, **33**, 348 (1994).
- 16 a) M. W. Grinstaff, M. G. Hill, J. A. Labinger and H. B. Gray, *Science*, **264**, 1311 (1994).
b) J. E. Lyons and P. E. Ellis, *Catal. Lett.*, **8**, 45 (1991).
c) P. E. Ellis and J. E. Lyons, *Coord. Chem. Rev.*, **105**, 181 (1990).
d) J. E. Lyons and P. E. Ellis, *Catal. Lett.*, **3**, 389 (1989).
e) J. F. Bartoli, O. Grigaud, P. Battioni and D. Mansuy, *J. Chem. Soc., Chem. Commun.*, 440 (1991).
f) A. M. d'A. R. Gonsalves, R. A. W. Johnstone, M. M. Pereira, J. Shaw and A. J. F. do N. Sobral, *Tetrahedron Lett.*, **23**, 1355 (1991).
- 17 D. G. Lee and M. Van den Engh, *Can. J. Chem.*, **50**, 2000 (1972).
- 18 J. -L. Coudret and B. Waegell, *Inorg. Chim. Acta*, **222**, 115 (1994).
- 19 D. G. Lee and L. N. Congson, *Can. J. Chem.*, **68**, 1774 (1990).
- 20 D. G. Lee and H. Gai, *Can. J. Chem.*, **73**, 49 (1995).
- 21 R. H. Holm, *Chem. Rev.*, **87**, 1401 (1987).
- 22 T. J. Groves and R. Quinn, *Inorg. Chem.*, **23**, 3844 (1984).

- 23 M. J. Camenzind, B. R. James and D. Dolphin, *unpublished work*, Oct. 1984.
- 24 J. T. Groves and K.-H. Ahn, *Inorg. Chem.*, **26**, 3833 (1987).
- 25 J. T. Groves and R. Quinn, *J. Am. Chem. Soc.*, **107**, 5790 (1985).
- 26 M. J. Camenzind, B. R. James and D. Dolphin, *J. Chem. Soc., Chem. Commun.*, 1137 (1986).
- 27 J. T. Groves and J. S. Roman, *J. Am. Chem. Soc.*, **117**, 5594 (1995).
- 28 a) M. Tavarés, R. Ramasseul, J.-C. Marchon, B. Bachet, C. Brassy and J.-P. Mornon, *J. Chem. Soc. Perkin Trans. 2*, 1321 (1992).
b) J.-C. Marchon and R. Ramasseul, *J. Chem. Soc., Chem. Commun.*, 298 (1988).
c) B. Scharbert, E. Zeisberger and E. Paulus, *J. Organometallic Chem.*, **493**, 143 (1995).
- 29 a) N. Rajapakse, B. R. James and D. Dolphin, *Stud. Surf. Sci. Catal.*, **55**, 109 (1990).
b) N. Rajapakse, Ph.D Dissertation, University of British Columbia, 1990.
c) N. Rajapakse, B. R. James and D. Dolphin, *Catal. Lett.*, **2**, 219 (1989).
- 30 a) H. Otake, T. Higuchi and M. Hirobe, *Heterocycles*, **40**, 867 (1995).
b) H. Otake, T. Higuchi and M. Hirobe, *J. Am. Chem. Soc.*, **114**, 10660 (1992).
- 31 a) C. S. Alexander, Ph. D. Dissertation, University of British Columbia, 1995.
b) C. Sishta, Ph. D. Dissertation, University of British Columbia, 1990.
- 32 P. Le Maux, H. Bahri and G. Simonneaux, *J. Chem. Soc., Chem. Commun.*, 1287 (1994).
- 33 C. Sishta, M. J. Camenzind and B. R. James, *Inorg. Chem.*, **26**, 1181 (1987).
- 34 a) C.-M. Che and W. H. Leung, *J. Chem. Soc. Dalton Trans.*, 2932 (1991).
b) W. H. Leung and C.-M. Che, *J. Am. Chem. Soc.*, **111**, 8812 (1989).
- 35 P. S. Traylor, D. Dolphin and T. G. Traylor, *J. Chem. Soc., Chem. Commun.*, 279 (1984).
- 36 P. E. Ellis and J. E. Lyons, *J. Chem. Soc., Chem. Commun.*, 1189 (1989); 1315 (1989).
- 37 J. A. Labinger, *Catal. Lett.*, **26**, 95 (1994).

- 38 Y. Tokita, K. Yamaguchi, Y. Watanabe and I. Morishima, *Inorg. Chem.*, **32**, 329 (1993).
- 39 a) C.-M. Che, C.-K. Li, W.-T. Tang and W.-Y. Yu, *J. Chem. Soc. Dalton Trans.*, 3153 (1992).
b) C.-M. Che, W.-T. Tang, W.-O. Lee, K.-Y. Wong and T.-C. Yu, *J. Chem. Soc. Dalton Trans.*, 1551 (1992).
c) C.-M. Che, W.-T. Tang, K.-Y. Wong and C.-K. Li, *J. Chem. Soc. Dalton Trans.*, 3277 (1991).
d) C.-M. Che, T.-F. Lai and K.-Y. Wong, *Inorg. Chem.*, **26**, 2289 (1987).
e) K.-W. Wong, C.-M. Che and F. C. Anson, *Inorg. Chem.*, **26**, 737 (1986).
- 40 M. O. Elout, W. G. Haije and W. J. A. Maaskant, *Inorg. Chem.*, **27**, 10 (1988).
- 41 a) T.-C. Lau and C.-K. Mak, *J. Chem. Soc. Chem. Commun.*, 766 (1993); b) 943 (1995).
- 42 A. C. Dengel, W. P. Griffith, C. A. O'Mahoney and D. J. Williams, *J. Chem. Soc., Chem. Commun.*, 1720 (1989).
- 43 C.-M. Che, C. Ho and T.-C. Lau, *J. Chem. Soc. Dalton Trans.*, 1259 (1991).
- 44 L. K. Stultz, R. A. Binstead, M. S. Reynolds and T. J. Meyer, *J. Am. Chem. Soc.*, **117**, 2520 (1995).
- 45 a) L. Roecker and T. J. Meyer, *J. Am. Chem. Soc.*, **109**, 746 (1987).
b) J. G. Muller, J. H. Acquaye and K. J. Takeuchi, *Inorg. Chem.*, **31**, 4552 (1992).
- 46 W. K. Soek and T. J. Meyer, *J. Am. Chem. Soc.*, **110**, 7358 (1988).
- 47 R. A. Binstead, M. E. McGuire, A. Dovletoglou, W. K. Soek, L. Roecker and T. J. Meyer, *J. Am. Chem. Soc.*, **114**, 173 (1992).
- 48 a) L. Roecker, L. J. C. Dobson, W. J. Vining and T. J. Meyer, *Inorg. Chem.*, **26**, 779 (1987).
b) J. H. Acquaye, J. G. Muller and K. J. Takeuchi, *Inorg. Chem.*, **32**, 160 (1993).
- 49 a) A. Dovletoglou and T. J. Meyer, *J. Am. Chem. Soc.*, **116**, 215 (1994).
b) B. A. Moyer, B. K. Sipe and T. J. Meyer, *Inorg. Chem.*, **20**, 1475 (1981).
- 50 C.-M. Che, C. Ho and T.-C. Lau, *J. Chem. Soc. Dalton Trans.*, 1901 (1991)
- 51 T. Leung, B. R. James and D. Dolphin, *Inorg. Chim. Acta*, **79**, 180 (1983).

- 52 C.-M. Che, W.-T. Tang, W.-T. Wong and T.-F. Lai, *J. Am. Chem. Soc.*, **111**, 9048 (1989).
- 53 W.-H. Leung, C.-M. Che, C.-H. Yeung and C.-K. Poon, *Polyhedron*, **12**, 2331 (1993).
- 54 P. Dubourdeaux, M. Taverès, A. Grand, R. Ramasseul and J.-C. Marchon, *Inorg. Chim. Acta*, **240**, 657 (1995).
- 55 This thesis, Chapter 4.
- 56 J. M. Mayer, *Inorg. Chem.*, **27**, 3899 (1988).
- 57 S.-I. Murahashi, Y. Oda and T. Naota, *J. Am. Chem. Soc.*, **114**, 7913 (1992).
- 58 R. A. Sheldon and J. Kochi, *Metal-Catalyzed Oxidations of Organic Compounds*, Academic Press, Toronto, p. 25, 1981.
- 59 a) A. Pacheco, Ph. D. Dissertation, University of British Columbia, 1993.
b) A. Pacheco, B. R. James and S. J. Rettig, *Inorg. Chem.*, **34**, 3477 (1995).
c) B. R. James, A. Pacheco, S. J. Rettig and J. A. Ibers, *Inorg. Chem.*, **27**, 2414 (1988).
d) B. R. James, S. R. Mikkelsen, T. W. Leung, G. M. Williams and R. Wong, *Inorg. Chim. Acta*, **85**, 209 (1984).
e) B. R. James, T. W. Leung, F. W. B. Einstein and A. W. Willis, *Can. J. Chem.*, **62**, 1238 (1984).
- 60 *Kirk-Othmer Concise Encyclopedia of Chemical Technology*, ed. M. Grayson, D. Eckroth, E. Graber, A. Klingsberg and P. M. Siegel, John Wiley and Sons, Toronto, 1985, p. 13.
- 61 a) G.-Z. Wang, U. Andreasson and J.-E. Bäckvall, *J. Chem. Soc., Chem. Commun.*, 1037 (1994).
b) G.-Z. Wang and J.-E. Bäckvall, *J. Chem. Soc., Chem. Commun.*, 980 (1992).
c) G.-Z. Wang and J.-E. Bäckvall, *J. Chem. Soc., Chem. Commun.*, 337 (1992).
d) J.-E. Bäckvall, R. L. Chowdhury and U. Karlsson, *J. Chem. Soc., Chem. Commun.*, 473 (1991).
e) R. L. Chowdhury and U. Karlsson, *J. Chem. Soc., Chem. Commun.*, 1063 (1991).

CHAPTER 2

Experimental Methods

2.1 Materials

2.1.1 Gases

CO, Ar, N₂ and O₂ (99.99+ % pure) were supplied by Linde Gas (Union Carbide Inc.) and used without further purification. The Ar gas used for photolysis was passed through a Ridox column (Fisher Scientific) to remove any trace O₂. Trace moisture present in the gases was removed by passing the gases over activated 5 Å molecular sieves (BDH).

2.1.2 Solvents and Reagents

Common organic solvents, such as benzene, toluene, CH₂Cl₂ and CHCl₃, were supplied by Fischer Scientific as reagent or spectroscopic grade. Benzene or toluene, if required to be moisture-free, was dried over sodium/benzophenone and stored under N₂. Other solvents were dried over CaH₂ (BDH) and stored under N₂. Mesitylene (Aldrich) was used without further purification.

Deuterated solvents used for NMR studies (D₂O, benzene-*d*₆, toluene-*d*₈, CD₂Cl₂ and CDCl₃, all 99.6+% deuterated) were purchased from MSD ISOTOPES or ISOTEC Inc. When needed to be used under anaerobic conditions, these deuterated solvents were dried over ground molecular sieves (5 Å, BDH). Subsequently, three to five freeze-pump-thaw cycles were applied to remove the air. ¹PrOD-*d*₈ was purchased from Aldrich. ¹PrOD-*d*₁ was obtained by mixing 1 mL of ¹PrOH in 100 mL of D₂O, with subsequent distillation of the isopropanol-*d*₁. Any co-distilled D₂O was removed by the addition of

molecular sieves (5 Å, BDH). The absence of the -OH functional group in the $^3\text{PrOD-}d_1$ was confirmed by $^1\text{H-NMR}$ spectroscopy.

Ruthenium was obtained as $\text{RuCl}_3 \cdot 3\text{H}_2\text{O}$ on loan from Johnson Matthey Ltd. and Colonial Metals Inc. $\text{Ru}_3(\text{CO})_{12}$ was prepared from $\text{RuCl}_3 \cdot 3\text{H}_2\text{O}$ by a literature method.¹ Pyrrole (Aldrich) was distilled prior to use. BF_3 (50 % weight) in MeOH was supplied by Aldrich and was stored in a vacuum desiccator. Mesitaldehyde and 2,6-dichlorobenzaldehyde were obtained from Aldrich.

$\text{P}(p\text{-X-C}_6\text{H}_4)_3$ compounds (X = H, Me, OMe, F, Cl and CF_3) (Strem Chemicals) were recrystallized from EtOH prior to use. Triphenylphosphine oxide (Aldrich, 99% pure) was purified by column chromatography (Activity I neutral alumina), with the impurities first eluted with benzene, and the phosphine oxide subsequently eluted with acetone. The purities of the phosphines and phosphine oxide were determined by TLC analysis and ^1H and $^{31}\text{P}\{^1\text{H}\}$ -NMR spectroscopies. AsPh_3 and SbPh_3 (Eastman) were purified by recrystallization from EtOH .

MeOH , EtOH , 1- PrOH , $^3\text{PrOH}$ and benzyl alcohol were spectroscopic grade reagents obtained from Fischer Scientific, while *R,S*-1-phenylethanol and 1,3-dichloropropan-2-ol were purchased from Eastman. All the alcohols were dried over molecular sieves (5 Å, BDH) and were used without further purification. Ph_3CH and adamantane were from BDH and Aldrich, respectively. The purities of these two alkanes were verified on a gas chromatograph. Ph_3COH was from Eastman, while 1-adamantanol, 2-adamantanol and 2-adamantanone were from Aldrich. These alcohols and ketone were employed as standards for GC experiments. Methylcyclohexane (Eastman) was found by

GC analysis to contain no other impurities. 1-Methylcyclohexanol, 2-methylcyclohexanol, 2-methylcyclohexanone, 3-methylcyclohexanone and 4-methylcyclohexanone were purchased from Eastman, and were used as GC standards.

Cyclohexene, *cis*-cyclooctene (herein referred to simply as cyclooctene), cyclohexene-oxide and cyclooctene-oxide were obtained from Eastman. The alkenes were pre-purified by first passing down neutral alumina (Activity I) before being distilled. Cyclohexene was pure by GC analysis. GC analysis of the distilled cyclooctene showed another compound (~ 4%), presumably an isomer of cyclooctene, to be present; the distilled substrate was used without further purification. Cyclohexene-oxide and cyclooctene-oxide were used as standards without further purification.

N,N-Dimethylaniline (Eastman) was passed down a silica column before being atmospherically distilled. Phenol (BDH) was recrystallized twice from petroleum ether before use. *p*-Hydroquinone and *p*-benzoquinone (Aldrich) were used as received.

2.2. Instrumentation and General Experimental Procedures

2.2.1 UV-Visible Spectroscopy

UV-visible spectroscopic data were obtained with a Perkin Elmer 552A UV-Visible Spectrometer or a Hewlett-Packard HP 8452A Diode-Array Spectrophotometer, both equipped with thermoelectric temperature controllers. It should be noted that wavelength readings from the HP 8452A instrument are approximately 2 nm higher than those from the Perkin Elmer 552A instrument; all reported readings within this thesis

correlate to those from the HP 8452A instrument.[†] Extinction coefficients, ϵ , are given in units of $M^{-1}cm^{-1}$ in parentheses immediately following the reported wavelength maxima, λ_{max} .

2.2.2 Stopped-flow Kinetic Studies

A stopped-flow apparatus capable of achieving mixing within 1 to 2 ms was manufactured by Applied Photophysics Inc., and was used, for example, to study reactions of *trans*-Ru^{VII}(TMP)(O)₂ with EAr₃-type substrates (E = P, As, Sb). The apparatus was equipped with a monochromator, and both the in-slit and out-slit widths were set to 0.25 mm. The light source was a 150 W Xe arc lamp. Anaerobic conditions for the instrument, when required, were achieved by bubbling N₂ or Ar into the cooling water. In addition, TRIZMA® hydrochloride (Sigma) and sodium thiosulfite were added to the water to remove dissolved O₂ on the surface of the Teflon coils. Data acquisition was computer controlled by an Archimedes 410/I computer; the software was supplied by Applied Photophysics and was custom-made for the stopped-flow apparatus.

Figure 2.1 shows a diagram of the sample handling section of stopped-flow apparatus. The syringes that contain the sample solutions are called the “drive syringes”. An electronic trigger releases the 5 atm N₂ pressure to force the drive platform upwards, pushing the drive syringes in the same direction. The samples were mixed rapidly and at the same time the computer acquired 400 data points within a preset time interval (5 ms to 1000 s intervals are possible).

[†] The UV-visible spectrum of aqueous KMnO₄ (Mallinckrodt) obtained on the HP 8452A instrument shows absorption maxima at 508, 526 and 546 nm.

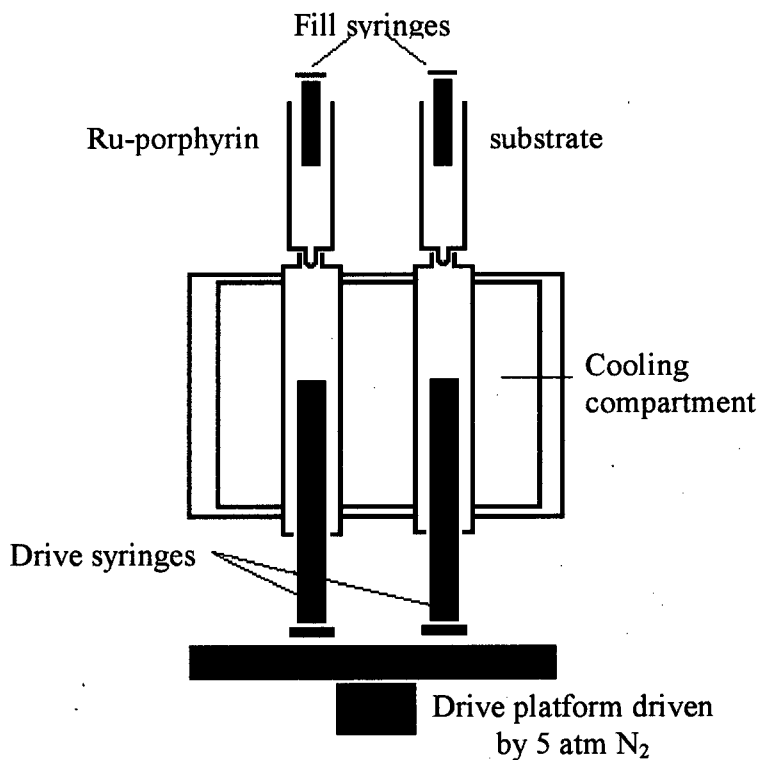


Figure 2.1. The diagram showing the various parts of the sample-handling section on the stopped-flow apparatus. Benzene solutions of Ru^{VI}(TMP)(O)₂ were loaded into the left fill-syringe via a disposal syringe from the top, while benzene solutions of P(*p*-X-C₆H₄)₃, AsPh₃ and SbPh₃ were filled on the right. The drive platform is controlled electronically via a trigger, which starts and stops a flow of pressurized N₂ gas (~ 5 atm). The mixing chamber and observation window lie in perpendicular to the sample handling unit are not shown in the diagram.

Isothermal conditions were maintained within the sample-handling compartment with the use of a thermoelectric temperature controller. The operating range of the stopped-flow apparatus itself was between 5 and 50 °C. Temperatures outside this range tend to make the drive syringe pistons either too loose or too stiff, respectively. In the course of these studies, the temperatures of the cooling source were set typically at 10, 20, 30 or 40 °C, and the exact temperatures were obtained from the digital readout at the sample compartment of the stopped-flow apparatus.

2.2.3 Infrared Spectrophotometer

Infrared spectra were taken on an ATI Mattson Genesis Series FTIR instrument.[†] The samples were prepared by one of three methods: 1) a Nujol mull sandwiched between KBr plates (referred herein as “Nujol, KBr”), 2) solid compound dispersed within a compressed KBr pellet or 3) dissolved in a solvent and then coated and dried on the surface of a KBr plate (both 2 and 3 will be referred from now as “KBr”).

2.2.4 FT-NMR Instruments

Solution NMR spectra were obtained on a Bruker AC-200E (200 MHz) or a Varian XL-300 (300 MHz) instrument in FT modes. Proton chemical shifts are given as δ in parts per million (ppm) with reference to the solvent residual [C_6H_6 at 7.15, $CHCl_3$ at 7.24 or $CH_3-C_6H_5$ at 2.09] as the internal standard, relative to TMS. $^{31}P\{^1H\}$ -NMR chemical shifts are given as δ referenced to aq. H_3PO_4 in a particular solvent. ^{19}F -NMR

[†] The IR spectrum of a polystyrene film shows absorption at $v_{C=C} = 1600 \text{ cm}^{-1}$.

chemical shifts are given as δ referenced to CF_3COOH in a particular solvent. The reported $^1\text{H-NMR}$ chemical shifts are singlets unless indicated otherwise (d = doublet; t = triplet; m = multiplet).

The Varian XL-300 instrument was equipped with a variable-temperature unit, making VT-NMR experiments possible. Toluene- d_8 was used as the solvent in all the VT-NMR studies. Typically the temperature at the NMR probe was lowered at $20\text{ }^\circ\text{C}$ intervals, and thermal equilibration was allowed to proceed for 10 min before data acquisition began.

2.2.5 Gas Chromatography Experiments

Gas chromatograms were obtained on an HP 5891A instrument, equipped with an HP17 column (cross-linked 50%-Ph-50%-Me Silicone capillary column, 25 m length, 0.32 mm diameter, 0.26 μm thick column coating) and a hydrogen-flame ionization detector (FID). The carrier gas was He, and all gases used were purified by a Supelco gas purifier system (HC 2-2445).

The column conditions and temperature programs are listed in Table 2.1 for the elution of various known standards. Sample injection volumes were typically 1 to 2 μL of solution, with typical solute concentrations between 10^{-2} to 10^{-1} M, although concentrations in the order of 10^{-3} M presented no difficulties. A split-gas flow rate of ~ 70 mL/min was employed, so that the injected sample would not overload the column.

Table 2.1. Conditions for the separation of compound mixtures by gas chromatography.

Substrate/products ^a	Temperature	Column Head Pressure (kPa)	Retention times (min)
benzyl alcohol/benzaldehyde	150 °C	45	3.6; 3.2
<i>R,S</i> -1-phenylethanol / ^b acetophenone	110 °C	40	7.2 8.1
Ph ₃ CH / Ph ₃ COH	220 °C	45	13.9 24.5
adamantane/1-adamantanol	120 °C for 6 min, then 20 °C min ⁻¹ until 200 °C	45	4.9 9.4
<i>cis</i> -cyclooctene/ cyclooctene oxide	90 °C for 4 min, then 10 °C min ⁻¹ until 140 °C	45	4.0 9.4
methylcyclohexane/ 1-methylcyclohexanol, 2-methylcyclohexanone, 3-methylcyclohexanone, 4-methylcyclohexanone ^c	50 °C for 5 min, then 10 °C min ⁻¹ until 200 °C	45	3.8 9.3 11.4 11.6 11.8
<i>N,N</i> -dimethylaniline	100 °C for 2 min., then 10°C min ⁻¹ until 200°C	45	6.82

^a These compounds were standards, obtained commercially, and were not further purified. Typically, 10⁻² to 10⁻¹ M solute was dissolved in benzene, and 1 to 2 µL were injected into the injection port, which was always set to 220 °C. The split injection flow rate was approximately 70 mL/min.

^b A racemic mixture was used.

^c CH₂Cl₂ was used as a solvent.

2.2.6 Elemental Analyses, X-ray Crystallography and Mass Spectral Analyses

Elemental analyses were obtained by Mr. P. Borda of this department. X-ray crystallographic structures were determined in this department by Dr. S. Rettig with a Ragaku X-ray Diffractometer, the X-ray source being Cu-K α or Mo-K α radiation. Mass spectral analyses were obtained in this department in a facility headed by Dr. G. Eigendorf. Both electron impact and fast atom bombardment (on thioglycerol and 3-nitrobenzylalcohol matrices) methods of ionization were used.

2.3 Techniques

A N₂-filled glove-box was used to handle air-sensitive compounds. Standard Schlenk techniques were used to carry out air-sensitive reactions and solvent transfers. Flame-sealed tubes attached to vacuum lines were used to prepared anaerobic NMR samples. These standard vacuum techniques² and the photolysis procedure to prepare Ru^{II}(TMP)(MeCN)₂ have been described elsewhere.^{2,3,7}

2.4 Synthesis and Characterization of Starting Compounds

The Ru-porphyrin complexes prepared during the course of this thesis are described below. Where known, the spectroscopic data are in excellent agreement with those from prior studies in this laboratory. Many new porphyrin species were observed *in situ*; their description will be presented later in the appropriate sections, where their reactivities will also be described in detail.

H₂TMP

H₂TMP, the free-base porphyrin *meso*-tetramesitylporphyrin, was made by a procedure reported by Groves and Nemo,⁴ which was a modification of the Rothemund synthesis.⁵ The purity of the product was determined by UV-visible and ¹H-NMR spectroscopies and TLC analysis. The data are in good agreement with those previously reported.¹¹

Molecular formula (M.W.) C₅₆H₅₄N₄ (783.07)

NMR (¹H, C₆D₆, 25 °C) 8.56 (β -pyrrole-H, 8H), 7.22 (*m*-H, 8H), 2.58 (*p*-Me, 12H), 1.80 (*o*-Me, 24H), -2.54 (N-H, 2H)

UV-Visible (CH₂Cl₂) 422, 516, 550 nm

Ru^{II}(TMP)(CO)

Carbonyl(tetramesitylporphyrinato)ruthenium(II), Ru^{II}(TMP)(CO), was prepared by a modification of a procedure that has been used to synthesize Ru^{II}(TPP)(CO).⁶ H₂TMP (500 mg, 0.063 mmol) was added to 200 mL mesitylene, and the solution was refluxed under a bubbling stream of CO gas. Ru₃(CO)₁₂ (300 mg, 0.047 mmol) was added in 18 aliquots during the next 6 h. The solution was heated for a total of 24 h, and during this time the reaction was monitored by TLC. At the end of 24 h, the mixture was rotary evaporated to remove the mesitylene, and the product was chromatographed on alumina (neutral Activity I). Unreacted TMPH₂ and Ru₃(CO)₁₂ were eluted first with benzene as purple and yellow bands, respectively. Ru^{II}(TMP)(CO) was subsequently eluted with 1:1 benzene/CH₂Cl₂ as a red-orange band. Purity was assessed by TLC analysis and UV-

visible and ^1H -NMR spectroscopies. Yield 0.30 g, 60 %. The data are in good agreement with those previously reported.¹¹

Molecular formula (M.W.) $\text{RuC}_{57}\text{H}_{52}\text{N}_4\text{O}$ (910.13)

NMR(^1H , C_6D_6 , 25 °C) 8.79 (β -pyrrole-H, 8H), 7.25 (*m*-H, 4H), 7.10 (*m*-H, 4H),
2.48 (*p*-Me, 12H), 2.20 (*o*-Me, 12H), 1.83 (*o*-Me, 12H)

UV-Visible(CH_2Cl_2) 414, 532 nm

IR (KBr) $\nu_{\text{CO}} = 1943 \text{ cm}^{-1}$

$\text{Ru}^{\text{II}}(\text{TMP})(\text{MeCN})_2$

Trans-bis(acetonitrile)(tetramesitylporphyrinato)ruthenium(II), $\text{Ru}^{\text{II}}(\text{TMP})(\text{MeCN})_2$, was prepared from $\text{Ru}^{\text{II}}(\text{TMP})(\text{CO})$ by a standard photolysis procedure described elsewhere.^{2,3,7} $\text{Ru}^{\text{II}}(\text{TMP})(\text{CO})$ (0.10 g, 0.11 mmol) was dissolved in a 5:3 benzene/acetonitrile mixture (80 mL) and the solution was transferred to a glass tube (3 cm wide, 20 cm long) with a narrow neck (1 cm wide, 20 cm long). A water-cooled condenser was fitted over this narrow neck, and the opening was covered with a rubber septum.^{2,11} A stainless steel needle was inserted into the solution through the rubber septum and the solution was purged with Ar for 30 min before it was irradiated with a 450 W Hanovia Hg-vapour lamp for 24 h. After this time a solution sample withdrawn from the mixture showed no remaining $\text{Ru}^{\text{II}}(\text{TMP})(\text{CO})$ in the IR spectrum ($\nu_{\text{CO}} = 1943 \text{ cm}^{-1}$). The remaining solvent was removed by continuing the Ar-purging without water-cooling. After about 1 h, all the solvent was removed, and the solid was isolated and dried under

vacuum for 24 h. Yield 0.08 g, 80%. The data are in good agreement with those previously reported.¹¹

Molecular formula (M.W.)	RuC ₆₀ H ₅₈ N ₆ (964.23)
NMR (¹ H, C ₆ D ₆ , 25 °C)	8.65 (β -pyrrole-H, 8H), 7.27 (<i>m</i> -H, 8H), 2.54 (<i>p</i> -Me, 12H), 2.21 (<i>o</i> -Me, 24H), -1.32 (MeCN, 6H)
Analysis, Calculated Found	C, 74.74; H, 6.06; N, 8.72 C, 74.80; H, 6.16; N, 8.56
UV-Visible (C ₆ H ₆)	410, 506 nm
IR (Nujol, KBr)	$\nu_{\text{CN}} = 2270 \text{ cm}^{-1}$

Ru^{VI}(TMP)(O)₂

Ru^{VI}(TMP)(O)₂, *trans*-dioxo(tetramesitylporphyrinato)ruthenium(VI), can be synthesized by the oxidation of Ru^{II}(TMP)(CO) with *meta*-chloroperbenzoic acid (*m*-CPBA),⁸ or by the aerobic oxidation of Ru^{II}(TMP)(N₂)₂,⁹ Ru^{II}(TMP),⁹ or Ru^{II}(TMP)(MeCN)₂.¹¹ In this thesis, Ru^{VI}(TMP)(O)₂ was produced *in situ* either by the *m*-CPBA oxidation of Ru^{II}(TMP)(CO), or by the aerobic oxidation of Ru^{II}(TMP)(MeCN)₂ in benzene or benzene-*d*₆. Two mole equivalents of MeCN were observed by ¹H-NMR spectroscopy upon the formation of Ru^{VI}(TMP)(O)₂ when the bis(acetonitrile) complex was used as the dioxo-precursor. Evacuation of the resulting solution gave a quantitative yield of the dioxo complex with no trace of the acetonitrile. The data are in good agreement with those previously reported.¹¹

Molecular formula (M.W.) RuC₅₆H₅₂N₄O₂ (914.12)

NMR (^1H , C_6D_6 , 25 °C)	9.01 (β -pyrrole-H, 8H), 7.10 (<i>m</i> -H, 8H), 2.45 (<i>p</i> -Me, 12H), 1.86 (<i>o</i> -Me, 24H)
UV-Visible (C_6H_6)	422 (280,000 $\text{M}^{-1}\text{cm}^{-1}$), 516 (22,000)nm
IR (Nujol, KBr)	$\nu_{\text{Ru=O}} = 821 \text{ cm}^{-1}$

H₂TDCPP

The free-base porphyrin H₂TDCPP, *meso*-tetra(2,6-dichlorophenyl)porphyrin, was synthesized by a literature procedure¹⁰ reported for the synthesis of H₂TMP. The modifications to the original literature preparation are described below. 2,6-Dichlorobenzaldehyde (10.0 g, 0.058 mol), pyrrole (4.0 mL, 0.058 mol) and chloranil (4.0 g, 0.0016 mol) were added in the above order to 1 L CH_2Cl_2 , which had been dried, distilled and N₂-purged. When all the aldehyde had dissolved, $\text{BF}_3\text{-MeOH}$ (50 % weight BF_3 in MeOH) (1.3 mL, 0.014 mol) was added via a syringe to the solution, which was then stirred magnetically at about 25 °C for 10 min. Then NEt_3 (2.0 mL, 0.014 mol) was added to quench the BF_3 catalyst. The resulting solution was rotary evaporated and the black tarry solid was chromatographed on a silica column (BDH 70-230 mesh). The porphyrin was eluted first with benzene as a red-purple band, although substantial amounts of dark green and violet compounds contaminated the porphyrin. MeOH (100 mL) was added to the crude porphyrin, and the solution was left sitting overnight. The purple precipitate of H₂TDCPP was collected and chromatographed again on a silica column (BDH 70-230 mesh). This time, the dark green and violet impurities that remained in the

precipitate were retained on the silica column. Yield 0.20 g, 1.6 %. The data are in good agreement with those previously reported.¹¹

Molecular formula (M.W.) C₄₄H₂₂N₄Cl₈ (890.30)

NMR (¹H, CDCl₃, 25 °C) 8.68 (β -pyrrole-H, 8H), 7.80 (*m*-H, d, 8H),
7.75 (*p*-H, t, 4H), -2.45 (N-H, 2H)

UV-Visible (C₆H₆) 420, 514, 592 nm

Ru^{II}(TDCPP)(CO)

Ru^{II}(TDCPP)(CO), carbonyl(tetra(2,6-dichlorophenyl)porphyrinato)ruthenium(II), was prepared by the same method as that used for the preparation of Ru^{II}(TMP)(CO) described above. H₂TDCPP (160 mg, 0.18 mmol) was added to a 500 mL 3-necked flask containing mesitylene (200 mL), and the solution was refluxed under a bubbling stream of CO for 48 h. Ru₃(CO)₁₂ (200 mg, 0.31 mmol) was added in 5 mg aliquots over this 48 h period, and the reaction was monitored by TLC. The mixture was then rotary evaporated to remove the mesitylene and the product was chromatographed on a neutral Activity I alumina column. Unreacted H₂TDCPP and Ru₃(CO)₁₂ were eluted first with benzene as purple and yellow bands, respectively, and Ru^{II}(TDCPP)(CO) was subsequently eluted as a red-orange band with 1:1 benzene/CH₂Cl₂. The purity of the compound was assessed by TLC analysis and UV-visible and ¹H-NMR spectroscopies. Yield 80 mg, 50%. The data are in good agreement with those previously reported.¹¹

Molecular formula (M.W.) RuC₄₅H₂₀N₄Cl₈O (1017.37)

NMR (^1H , C_6D_6 , 25 °C)	8.70 (β -pyrrole-H, 8H), 7.36 (<i>m</i> -H, d, 4H), 7.25 (<i>m'</i> -H, d, 4H), 6.90 (<i>p</i> -H, t, 4H)
UV-Visible (C_6H_6)	412, 532 nm
IR (Nujol, KBr)	$\nu_{\text{CO}} = 1951 \text{ cm}^{-1}$

Ru^{VI}(TDCPP)(O)₂

This species can be prepared either by the aerobic oxidation of Ru^{II}(TDCPP)(MeCN)₂ or by the *m*-CPBA oxidation of Ru^{II}(TDCPP)(CO), in benzene.¹¹ Ru^{VI}(TDCPP)(O)₂ was prepared via the latter route by mixing Ru^{II}(TDCPP)(CO) (40 mg, 0.04 mmol) and *m*-CPBA (120 mg, 0.12 mmol) in benzene (10 mL). After 15 min, the complete conversion to Ru^{VI}(TDCPP)(O)₂ was verified by UV-visible spectroscopy and the product was purified with on a silica column (BDH 70-230 mesh), with the dioxo species eluted first with benzene. A dark brown band remained unmoved on the column. The complex was pure by TLC analysis and UV-visible and ^1H -NMR spectroscopies, and the solid was stored in a vacuum desiccator. Yield 20 mg, 50 %. The data are in good agreement with those previously reported.¹¹

Molecular formula (M.W.)	RuC ₄₄ H ₂₀ N ₄ O ₂ Cl ₈ (1021.36)
NMR (^1H , C_6D_6 , 25 °C)	8.90 (pyrrole-H, 8H), 7.85 (<i>m</i> -H, d, 8H), 7.75 (<i>p</i> -H, t, 4H)
UV-Visible (C_6H_6)	420 (255,000 M ⁻¹ cm ⁻¹), 514 (14,000) nm
IR (Nujol, KBr)	$\nu_{\text{Ru=O}} = 822 \text{ cm}^{-1}$

Ru^{II}(TDCPP-Cl₈)(CO)

Ru^{II}(TDCPP-Cl₈)(CO), carbonyl(β -octachloro(*meso*-tetra[2,6-dichlorophenyl])-porphyrinato)ruthenium(II) was prepared by Dr. L. Xie from Dr. D. Dolphin's group in a collaborative venture with this laboratory. Ru^{II}(TDCPP)(CO) (100 mg, 0.1 mmol) that has been prepared by the previously mentioned method (H₂TDCPP was provided by Dolphin's group) was suspended in MeOH (50 mL). *N*-Chlorosuccinimide (300 mg) was then added to the MeOH suspension, and the resulting mixture was refluxed in air for 18 h. After this time, the solid Ru^{II}(TDCPP-Cl₈)(CO) that had precipitated was filtered-off and washed with a small amount of MeOH. The filtrate was green and the solid that remained was dark purple. Yield 82 mg, 64%.

Molecular formula (M.W.)	RuC ₄₅ H ₁₂ N ₄ OCl ₁₆ (1292.93)
NMR (¹ H, DMSO- <i>d</i> ₆ , 25 °C)	7.50 (<i>p</i> -H, d, 4H), 7.64 (<i>m</i> -H, t, 8H)
UV-Visible (CH ₂ Cl ₂ /C ₆ H ₆ 1:20)	418 (205,000 M ⁻¹ cm ⁻¹), 540 (17,000) nm
IR (KBr)	$\nu_{CO} = 1965\text{ cm}^{-1}$
Analysis, Calculated Found	C, 41.80; H, 0.94; N, 4.33 C, 41.79; H, 1.05; N, 4.15
Mass Spec. (EI)	[Ru(TDCPP-Cl ₈)] ⁺ , 1266 amu; loss of CO ligand

Ru^{VI}(TDCPP-Cl₈)(O)₂

The *m*-CPBA oxidation of Ru^{II}(TDCPP-Cl₈)(CO) in benzene or CH₂Cl₂ yielded Ru^{VI}(TDCPP-Cl₈)(O)₂. Only sufficient dioxo complex (< 5 mg) was made immediately prior to use as needed. Approximately 10 equivalents of *m*-CPBA were added to a suspension of Ru^{II}(TDCPP-Cl₈)(CO) in CH₂Cl₂ or benzene, as the carbonyl compound is

not very soluble either of the two solvents, and the mixture was stirred rigorously. At the end of 5 min, the completion of the reaction was confirmed by UV-visible spectroscopy. The resulting solution was chromatographed on a silica column (BDH 70- 230 mesh), using either benzene or CH_2Cl_2 as the eluent; with CH_2Cl_2 some *m*-CPBA could be eluted as well, as the colourless peracid followed very closely the yellow-brown dioxo complex as they were eluted down the column. With benzene as the eluent, the *m*-CPBA was retained by the silica; however, the dioxo complex (λ_{\max} 430 nm) in the eluent was converted to a new Ru(porp) species characterized by a Soret maximum at 422 and a Q-band at 518 nm. This porphyrin species with λ_{\max} 422 nm can be readily converted back to the dioxo species, almost quantitatively, by the addition of *m*-CPBA. The transformation of the dioxo complex to this unknown porphyrin species was slower in CH_2Cl_2 (~ 2 h). Thus, the choice of the eluent was important for the preparation of a pure sample of the dioxo species. Even in the solid state, the dioxo species degraded substantially overnight in air, evidenced by the loss of $\nu_{\text{Ru}=\text{O}}$ intensity in the IR spectrum. Presumably, $\text{Ru}^{\text{VI}}(\text{TDCPP-Cl}_8)(\text{O})_2$ reacts with impurities in the solvent, or even with the solvent itself, to give the species with λ_{\max} 422 nm.

Molecular formula (M.W.) $\text{RuC}_{44}\text{H}_{12}\text{N}_4\text{O}_2\text{Cl}_{16}$ (1296.92)

UV-Visible (C_6H_6) 430 ($200,000 \text{ M}^{-1} \text{ cm}^{-1}$), 516 (16,000) nm

IR (KBr) $\nu_{\text{Ru}=\text{O}} = 827 \text{ cm}^{-1}$

Analysis, Calculated	C, 40.75; H, 0.93; N, 4.32
Found	C, 41.95; H, 1.0 ; N, 4.04

Mass Spec. (EI and FAB) $[\text{Ru}(\text{TDCPP-Cl}_8)]^+$, 1266 amu; loss of 2 O-ligands

References

- 1 a) J. L. Dawes and J. D. Holmes, *Inorg. Nucl. Chem. Lett.*, **7**, 847 (1971).
 b) A. Mantovani and S. Cenini, *Inorg. Syn.*, **16**, 47 (1976).
- 2 C. Alexander, Ph.D. Dissertation, University of British Columbia, 1995.
- 3 M. Ke, Ph. D. Dissertation, University of British Columbia, 1988.
- 4 J. T. Groves and T. E. Nemo, *J. Am. Chem. Soc.*, **105**, 6243 (1983).
- 5 G. M. Badger, R. A. Jones and R. L. Laslett, *Aust. J. Chem.*, **17**, 1028 (1964).
- 6 D. P. Rillema, J. K. Nagle, L. F. Barringer and T. J. Meyer, *J. Am. Chem. Soc.*, **103**, 56 (1981).
- 7 A. Antipas, J. W. Buchler, M. Gouterman and P. D. Smith, *J. Am. Chem. Soc.*, **100**, 3015 (1978).
- 8 J. T. Groves and R. Quinn, *Inorg. Chem.*, **23**, 3844 (1984).
- 9 M. J. Camenzind, B. R. James and D. Dolphin, *J. Chem. Soc., Chem. Commun.*, 1137 (1986).
- 10 J. S. Lindsey, K. A. MacCrum, J. S. Tyhonas and Y.-Y. Chuang, *J. Org. Chem.*, **59**, 579 (1994).
- 11 N. Rajapakse, B. R. James and D. Dolphin, *Stud. Surf. Sci. Catal.*, **55**, 109, (1990).

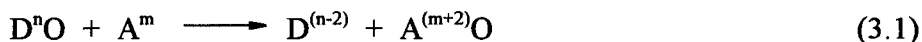
Chapter 3

Mechanism of Aerobic Oxidation of EAr₃

(E = P, As, Sb)

3.1 Introduction

Phosphines are readily oxidized to phosphine oxides. In fact, phosphines are O₂-sensitive, the tertiaryarylphosphines being air-stable only in the solid state¹ and somewhat air-oxidizable in solution.[†] Phosphines are easily oxidized and they can serve as useful test substrates for oxidation studies; a transition-metal complex to be used as an O₂-oxidation catalyst can be tested initially for the oxidation of phosphines. Moreover, the oxidation by oxometal species is a relatively simple process, an oxygen-atom transfer to the phosphorus atom, compared to other organic oxidations which might involve breakage or formation of more than one bond.² An oxygen-atom transfer generally is defined as a reaction of the type represented in Eq. 3.1. This is the simplest



representation where DⁿO is the O-atom donor and A^m is the acceptor. The O-atom does not change in its oxidation state, while the donor's and acceptor's oxidation states change by -2 and +2, respectively. For example, the O-atom transfer reaction of interest between oxoruthenium species and PPh₃ involves only cleavage of the Ru=O bond and formation of the O=P bond, unlike alcohol or alkane oxidations where O-H and C-H bonds are also involved. As a result, mechanistic studies can be carried out more easily when phosphines are used as test-substrates. In addition, the oxidation of phosphines by an oxometal species is likely to proceed via an intermediate in which the phosphine oxide product is bound to the metal before dissociating into solution.^{3a,b} Rate constants for such

[†] PPh₃ and P(*p*-X-C₆H₄)₃ are slightly air-sensitive in solution. These phosphines (in benzene solutions at ~10⁻² M) under 1 atm air at room temperature are oxidized to approximately 5% of the corresponding phosphine oxide in 24 h. AsPh₃ and SbPh₃ are not oxidized to their respective oxides under the same conditions.

dissociation reactions of phosphine oxide may be of value in the design of homogeneous catalysts that make use of hemi-labile chelating ligands, similar to the phosphine-ether bidentate type ligands used in some homogeneous catalysis systems.⁴ The oxidizable nature of phosphines allows one to determine the stoichiometry of an O-atom transfer reaction with an oxometal species, and the number of active oxo-moieties can be readily determined, thus providing a useful diagnostic tool.

3.1.1 Aims of Phosphine Oxidation in Current Work

Previous studies in this laboratory on the O₂-oxidation of thioethers catalyzed by *trans*-Ru^{VI}(TMP)(O)₂ (**1**) [from now on simply referred to as Ru^{VI}(TMP)(O)₂] led to interesting observations.⁵ Thioethers with longer alkyl chain lengths were more rapidly oxidized, the faster rates being due to more favourable ΔS[‡] values for the longer chain thioethers. One mechanistic suggestion was that the O-atom transfer from oxoruthenium species to the sulfur was induced via strong Ru=O vibrational coupling,^{3c} and for the case of the Ru=O moiety on the porphyrin a bulkier substrate was considered to be entropically more favourable.⁵

Tertiaryarylphosphines can be easily handled in the solid state as well as in solution. In addition, a whole range of P(*p*-X-C₆H₄)₃ compounds are available commercially, allowing for kinetic studies of the O-atom transfer from Ru^{VI}(TMP)(O)₂ to give a direct comparison with the earlier thioether oxidations. Also an earlier study on the same Ru^{VI}(TMP)(O)₂/PPh₃ system implied that the phosphine oxide was non-coordinating;⁶ however, the kinetic studies in the present work showed the presence of

OPPh_3 to be important in the overall reaction. The compounds PPh_3 , AsPh_3 and SbPh_3 were oxidized stoichiometrically by (1), and the rate constants and activation parameters were obtained. The para substituent on the phenyl group within a series of $\text{P}(p\text{-X-C}_6\text{H}_4)_3$ [$\text{X} = \text{OMe}$, Me , H , F , Cl and CF_3] was systematically varied so that electronic effects were also studied.

3.2 Sample Preparation and Data Analysis

3.2.1 Sample Preparation

Freshly distilled benzene was used to prepare the phosphine, arsine and stibine substrate solutions. The stopped-flow spectrophotometer was prepared for anaerobic conditions as described in Section 2.2.2. The sample solutions were purged with Ar and dried over molecular sieves (5 \AA), but samples treated in this manner gave the same kinetic data as samples that were simply prepared with freshly distilled benzene without subsequent Ar purging. The procedure required for anaerobic sample handling is time-consuming, and thus all the stopped-flow kinetic runs were performed aerobically.

Solutions of $\text{Ru}^{\text{VI}}(\text{TMP})(\text{O})_2$ were prepared by aerobically oxidizing $\text{Ru}^{\text{II}}(\text{TMP})(\text{MeCN})_2$ in freshly distilled benzene or by adding solid $\text{Ru}^{\text{VI}}(\text{TMP})(\text{O})_2$ directly (Chapter 2). Complete conversion to the dioxo species from the bis(MeCN) precursor was ensured by monitoring the UV-visible spectrum from 350 to 650 nm, and the resulting concentrations in the dioxo species, determined spectrophotometrically (Chapter 2), were of the order of 10^{-6} M . Solutions of $\text{P}(p\text{-X-C}_6\text{H}_4)_3$, AsPh_3 and SbPh_3 were prepared by dissolving appropriate weights of the compound in freshly distilled benzene, with

concentrations typically $\sim 10^{-3}$ M ($[\text{SbPh}_3] \sim 10^{-4}$ M). Solutions of $\text{P}(p\text{-X-C}_6\text{H}_4)_3$ containing OPPh_3 were prepared in the same way, with the appropriate weights of OPPh_3 added as well ($[\text{OPPh}_3] \sim 10^{-3}$ M).

The above solutions [(1) and substrate] were filled into the stopped-flow apparatus via disposal 2.5 mL syringes (Aldrich). Isothermal conditions were maintained by a water-cooled temperature controller, with the temperature at the sample compartment maintained at ± 0.1 °C for the temperature range between 5 °C and 45 °C. A computer was triggered electronically to acquire the data immediately after the porphyrin and substrate solutions were mixed. The absorbances were monitored at wavelengths of 422, 430 and 412 nm, which correspond to the loss of the dioxo species, loss of an intermediate and appearance of the product, respectively (see Figure 3.2, p. 67).

For the catalyzed O_2 -oxidations, benzene- d_6 solutions containing $\sim 10^{-4}$ M (1) were prepared, and their concentrations were determined by UV-visible spectroscopy from the known extinction coefficient of (1) (Chapter 2). $\text{P}(p\text{-X-C}_6\text{H}_4)_3$ [X = OMe, H, F, Cl] stock solutions were prepared by dissolving appropriate weights of the phosphines in 1.00 mL benzene- d_6 . All catalysis experiments were carried out in NMR tubes by adding 0.40 mL solution of (1) first. Then the NMR tubes were capped with rubber septa and secured with Parafilm. Appropriate volumes of the phosphine stock solutions subsequently were added with a 250 μL syringe (Unimetrics), so that the final concentrations of the phosphines were 0.014 and 0.027 M for the experiments under 1 atm O_2 . An O_2 atmosphere (1 atm) in these NMR tubes was created by bubbling a stream of O_2 with a stainless steel needle into the benzene- d_6 solutions for 10 min. The catalytic oxidations of

PPh_3 and $\text{P}(p\text{-F-C}_6\text{H}_4)_3$ were also studied under 1 atm air. Blank solutions with the same phosphine concentrations but containing no species (**1**) were prepared and purged with O_2 (or left under 1 atm air), so that the contributions from the autoxidation could be taken into account in the calculation of the total turnover numbers. All of the NMR samples were kept at room temperature, $24 \pm 2^\circ\text{C}$, for the duration of the experiment.

3.2.2 Data Analysis

Absorbance-time data for each phosphine oxidation run were transferred to an IBM-compatible computer as an ASCII text file. Sigma Plot for Windows on an IBM PC was used to function fit the data as a first-order exponential decay of the form represented by Eq. 3.2, of which the derivation can be found in Appendix B.

$$A = (A_0 - A_\infty)\exp(-k_{\text{obs}}t) + A_\infty, \text{ where } t = \text{time (seconds)} \text{ and } A = \text{absorbance} \quad (3.2)$$

The parameters A_0 , k_{obs} and A_∞ (A_0 = initial absorbance, k_{obs} = observed pseudo-1st-order rate constant and A_∞ = absorbance at completion of reaction) were determined by the function-fitting program in Sigma Plot. Values twice the standard errors of regression were taken to be the error estimates for the individual rate constants. Pseudo-first-order rate constants, k_{obs} , obtained from function fitting were compared to k_{obs} values obtained by the Guggenheim method⁷ and semi-log analysis (where A_0 and A_∞ were known), and the results from all three cases were in perfect agreement (see Appendix A). The raw data from the stopped-flow experiments, if in numerical form (400 data points for each absorbance-time trace), would be too voluminous to list in the present thesis. Hence, the kinetic data for the oxidations of all the substrates are tabulated in Appendix A as pseudo-

first-order rate constants for the corresponding absorbance-time traces. Samples of the actual PPh_3 oxidation absorbance-time traces are shown in Appendix A.

At the outset of the kinetic studies on the stoichiometric oxidation of PPh_3 by (1), a fast (10^{-2} to 10^{-1} s) phase, followed by a slow phase (10^1 to 10^2 s), in the overall reaction was observed. In the presence of excess PPh_3 , the slow kinetic phase exhibited non-first-order behaviour in (1): k_{obs} varied as $[(1)]$ was adjusted and exponential-decay, absorbance-time traces were not observed. The addition of excess OPPh_3 alleviated the above two problems. For the fast kinetic phase, the kinetic data exhibited first-order behaviour in (1), with and without added excess OPPh_3 . Evidently, OPPh_3 plays an important role in the slow phase of the reaction between PPh_3 and (1). For the stoichiometric oxidation of the phosphine series, $\text{P}(p\text{-X-C}_6\text{H}_4)_3$, excess OPPh_3 was added when the slow kinetic phase was monitored (see Table 3.4).

For the catalytic aerobic oxidation experiments, the ratios of oxide product to phosphine substrate in every NMR sample (including the blank solution systems) were determined from integration areas on the NMR spectra. The autoxidation contributions to the overall conversion of phosphine to the phosphine oxide within the sample solutions were taken to be equal to that of the appropriate blank solutions, and the percentages due to the blanks were subtracted from the percentages in the samples to ensure an accurate determination of the turnover numbers. For PPh_3 , $\text{P}(p\text{-OMe-C}_6\text{H}_4)_3$ and $\text{P}(p\text{-Cl-C}_6\text{H}_4)_3$, integrations in the $^{31}\text{P}\{^1\text{H}\}$ -NMR spectra were used. A pulse delay of 1.0 s was implemented initially. These relative integrations then were compared to the spectrum obtained immediately afterwards with a pulse delay of 4.0 s when the ratio of the

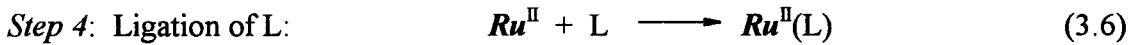
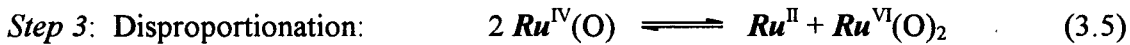
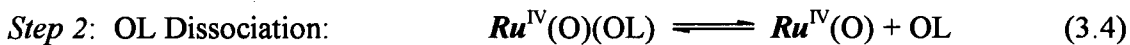
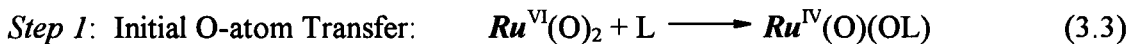
integration areas varied by approximately 7%. The process was repeated with the implementation of a 8.0 s pulse delay. No further change in the integration intensities was observed, indicating that a pulse delay of 8.0 s was sufficient to allow the ^{31}P nuclei to relax and allow for consistent integrations. For $\text{P}(p\text{-F-C}_6\text{H}_4)_3$ the integration areas on the ^{19}F -NMR spectra were used to determine the product/reactant ratios. Pulse delay experiments were performed similarly to the $^{31}\text{P}\{^1\text{H}\}$ -NMR experiments, and it was found that the product/reactant ratios were independent of pulse delay times. Of note, ^{19}F -NMR spectroscopy has the convenience of a more rapid data acquisition over that of $^{31}\text{P}\{^1\text{H}\}$ -NMR spectroscopy.

3.3 Overview of the Mechanism of Tertiaryarylphosphine Oxidation

The first mention in the literature of the oxidation of PPh_3 by $\text{Ru}^{\text{VI}}(\text{TMP})(\text{O})_2$ (**1**) was in 1987 by Groves and Ahn.⁶ The experiment involved a stoichiometric ^1H -NMR titration which monitored the conversion of (**1**) first to $\text{Ru}^{\text{IV}}(\text{TMP})(\text{O})$ and OPPh_3 , and then to $\text{Ru}^{\text{II}}(\text{TMP})(\text{PPh}_3)$ and 2 OPPh_3 , as one and three equivalents of PPh_3 were added, respectively. A successive O-atom transfer mechanism was implied in the report. Of note, the experiment was described to have taken place in benzene- d_6 , although examination of the ^1H -NMR spectrum indicated that the experiment most likely took place in CD_2Cl_2 , as indicated by the solvent residual peak at $\delta \sim 5.3$ ppm,⁸ whereas the solvent residual for benzene- d_6 is at $\delta \sim 7.15$. The results from the stoichiometric titrations implied a non-coordinating OPPh_3 , with no possible role of the phosphine oxide in the oxidation mechanism. The simple stepwise O-atom transfers suggested by the ^1H -NMR titrations

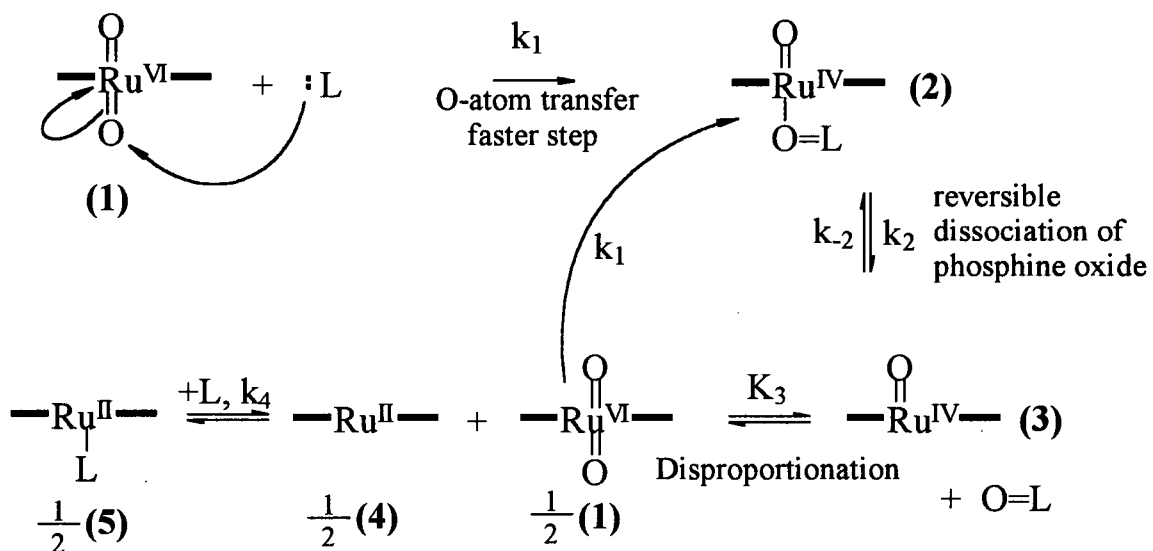
were found to be an inadequate description once kinetic studies were undertaken in this laboratory.

The mechanism of phosphine oxidation is presented first (see Figure 3.1), and the supporting data will be presented in the upcoming sections. This choice of presentation is for the benefit of the reader, as the mechanism involves several interrelated steps. The mechanism is summarized in Eqs. 3.3 to 3.6 [$\text{Ru} = \text{Ru}(\text{TMP})$, $\text{L} = \text{PPh}_3$].



The oxidation mechanism in Figure 3.1 equally applies to the other phosphines within the series $\text{P}(p\text{-X-C}_6\text{H}_4)_3$ [X = OMe, Me, F, Cl and CF_3]. When AsPh_3 and SbPh_3 were used as substrates, only their initial O-atom transfer reactions with (1) (Step 1) were monitored. Step 1 involves the O-atom transfer from $\text{Ru}^{\text{VI}}(\text{TMP})(\text{O})_2$ to PPh_3 . This fast step, the fast kinetic phase referred to in Section 3.2.2, is first-order in (1) and PPh_3 , and zero-order in OPPh_3 . Step 2 is the reversible dissociation of the OPPh_3 product from the intermediate species, $\text{Ru}^{\text{IV}}(\text{TMP})(\text{O})(\text{OPPh}_3)$ (2), to form $\text{Ru}^{\text{IV}}(\text{TMP})(\text{O})$ (3). Step 3 is the disproportionation of (3) to (1) and $\text{Ru}^{\text{II}}(\text{TMP})$ (4). In Step 4, PPh_3 readily coordinates to (4) to form $\text{Ru}^{\text{II}}(\text{TMP})(\text{PPh}_3)$ (5). Species (1) formed from the disproportionation in Step 3 can oxidize PPh_3 , and the cycle repeats to oxidize 2 equivalents of phosphine with complete formation of (5).

Oxygen-atom Transfer followed by Disproportionation



Regeneration of Catalyst (see Section 3.4)

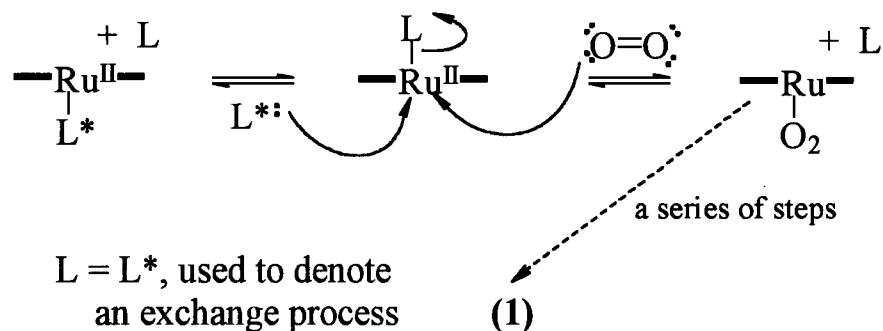


Figure 3.1. Mechanism of oxidation of $P(p\text{-X-C}_6\text{H}_4)_3$, AsPh_3 and SbPh_3 by $\text{Ru}^{\text{VI}}(\text{TMP})(\text{O})_2$ (1). The overall reaction involves the transfer of the O-atom from (1) followed by the disproportionation of $\text{Ru}^{\text{IV}}(\text{TMP})(\text{O})$. Under air or O_2 the process becomes catalytic, but the catalysis occurs at a much slower time-scale (see Section 3.4).

Steps 2, 3 and 4 were observed as an isosbestic set of UV-visible spectra, referred to in Section 3.2.2 as the slow kinetic phase, with the Soret maximum shifting from 430 to 412 nm. Figure 3.2 shows UV-visible/time traces of a benzene solution, initially containing (1) (5×10^{-6} M). In the presence of 0.1 M OPPh₃, addition of 10 equivalents of PPh₃ rapidly shifted the 422 nm Soret band [characteristic of (1)] to 430 nm (Step 1). Within the next few minutes, the spectrum's 430 nm Soret maximum shifted to 412 nm (Steps 2, 3 and 4), corresponding to that of (5) (see Section 3.4). Addition of only 1 equivalent of PPh₃, again in the presence of 0.1 M OPPh₃, shifted the Soret band to 430 nm, and then there was no further change in the position of the Soret maximum. As Groves and Ahn's ¹H-NMR studies⁶ suggested that (3) was formed on the addition of 1 equivalent of PPh₃ to (1), it is reasonable to assign the 430 nm Soret band to Ru^{IV}(TMP)(O)(OL) (2) with the OPPh₃ still coordinated to Ru. Isosbestic points at 382, 420, 484 and 538 nm for the second spectral change [(2) to (5)] are consistent with no other intermediates being formed in any significant quantity during the conversion to the product. The experiment involving the addition of 1 equivalent of PPh₃ to (1) ($\sim 10^{-3}$ M) in benzene-*d*₆ under vacuum, similar to that performed by Groves and Ahn,⁶ gave a ¹H-NMR spectrum that showed ¹H-resonances corresponding to those of free OPPh₃ and Ru^{IV}(TMP)(O) (3). The UV-visible spectrum of the same sample had absorption maxima at 424 and 518 nm. These results further support the assignment of the species with λ_{max} 430 nm as Ru^{IV}(TMP)(O)(OPPh₃) (2) (with coordinated OPPh₃). Of note, species (3) in the benzene-*d*₆ solution had decomposed when the sample was analyzed again by ¹H-NMR and UV-visible spectroscopies after 24 h.

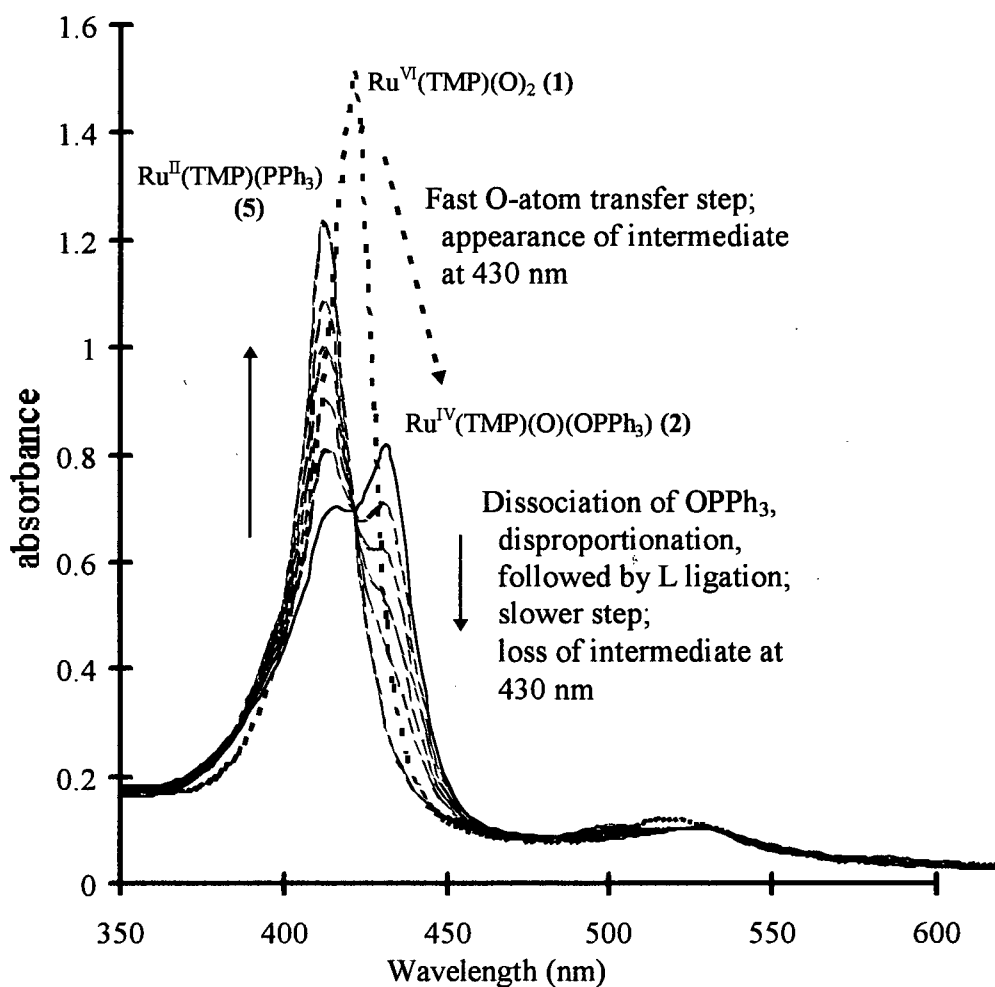


Figure 3.2. UV-visible/time traces monitoring the conversion from $\text{Ru}^{\text{VI}}(\text{TMP})(\text{O})_2$ (1) (422 nm) to $\text{Ru}^{\text{II}}(\text{TMP})(\text{PPh}_3)$ (5) (412 nm). In the presence of ~ 0.1 M OPPh_3 , addition of 10 equivalents of PPh_3 forms an intermediate at 430 nm before proceeding to form the product (5) at 412 nm. Total time < 5 min. Isosbestic points can be seen clearly at 382, 420, 484 and 538 nm. $[(1)] = 5 \times 10^{-6}$ M in benzene at room temperature under 1 atm air. $\lambda_{\text{max}} (\varepsilon, \text{M}^{-1}\text{cm}^{-1})$ values for (5) in benzene: 412(230,000) and 504(20,000) nm.

The rate expressions derived from the proposed mechanism in Figure 3.1 are represented in Eqs. 3.7 and 3.8 (see Appendix B for their derivation).

$$\text{O-atom transfer:} \quad \text{rate} = -\frac{d[(1)]}{dt} = \frac{d[(2)]}{dt} = k_1[(1)][L] \quad (3.7)$$

OL dissociation followed by disproportionation:

$$\text{rate} = -\frac{d[(2)]}{dt} = \frac{d[(5)]}{dt} = \frac{k_2 k_4 K_3^{1/2} [L][(2)]}{k_2[OL] + (k_1+k_4)K_3^{1/2}[L]} \quad (3.8)^{\dagger}$$

Under O₂ or air, the oxidation becomes catalytic. The rate-determining step is the regeneration of the catalyst, and the catalysis occurs on a much slower time-scale. The catalysis will be discussed in Section 3.4 after the mechanism of phosphine oxidation by Ru^{VI}(TMP)(O)₂ has been discussed in detail.

3.3.1 Oxygen-atom Transfer

In the present study, the fast UV-visible spectral change from 422 to 430 nm (Figure 3.2) corresponds to the initial O-atom transfer step that forms (2) as the phosphine adds to the oxo ligand. The slower, second spectral change from 430 to 412 nm, resulting in the formation of the final product (5), was inhibited by added excess OPPh₃ (Section 3.3.2). This suggests that the phosphine oxide product initially formed in fact remains coordinated to the metal centre, and that the OPPh₃ can reversibly coordinate and dissociate. Thus, the O-atom transfer reaction between (1) and PPh₃ is thought to result initially in the formation of Ru^{IV}(TMP)(O)(OPPh₃) (2). Of note, no evidence from ¹H or ³¹P{¹H}-NMR experiments was found to support the existence of a bound phosphine

[†] The k_{obs} values were the same for monitoring the loss of (2) or production of (5) at 430 and 412 nm, respectively (see Appendix A).

oxide species in the absence of added excess OPPh_3 (Section 3.4 and Ref. 6), and unfortunately similar NMR experiments in the presence of $\sim 0.1 \text{ M}$ OPPh_3 are not feasible; however, that phosphine oxides bind at axial positions of Ru(II) and Ru(IV) centres within an equatorial N_4 -ligand set as observed in other systems,^{3a,b} and that OPPh_3 slows the rate of reaction in the present system, suggest strongly the formulation of the intermediate species (**2**) as $\text{Ru}^{\text{IV}}(\text{TMP})(\text{O})(\text{OPPh}_3)$. Furthermore, that $\text{Ru}^{\text{IV}}(\text{TMP})(\text{O})$ (**3**) absorbs differently in the UV-visible spectrum (see Section 3.3) supports the formulation of (**2**) as $\text{Ru}^{\text{IV}}(\text{TMP})(\text{O})(\text{OPPh}_3)$.

Plots of k_{obs} (observed pseudo-first-order rate constant for the initial O-atom transfer) versus $[\text{L}]$ are linear throughout the concentration range studied (5×10^{-5} to $4 \times 10^{-3} \text{ M}$ for the case of PPh_3). Figure 3.3 shows the kinetic data for PPh_3 . The values for the second-order rate constants, k_1 , are given in Table 3.1 for the oxidation of all the substrates. The activation parameters for the O-atom transfer reaction to PPh_3 are $\Delta H_1^\ddagger = 18 \pm 1.4 \text{ kJ mol}^{-1}$ and $\Delta S_1^\ddagger = -94 \pm 5 \text{ J mol}^{-1}\text{K}^{-1}$ (Table 3.2), calculated from the slopes of the Eyring plots[†] (Figure 3.4). The ΔH_1^\ddagger value is lower than that for the thioether oxidations ($\Delta H^\ddagger \sim 50 \text{ kJ mol}^{-1}$),⁵ suggesting that PPh_3 is perhaps a better nucleophile than thioethers. The ΔS_1^\ddagger values are comparable, showing that both coupling reactions are unfavourable in terms of activation entropy.

No trend was found for ΔH_1^\ddagger on going from PPh_3 to AsPh_3 to SbPh_3 (Table 3.2). ΔH_1^\ddagger increases by 50% on going from PPh_3 to AsPh_3 . On the other hand, the ΔH_1^\ddagger value for SbPh_3 is about half that for the PPh_3 system. ΔH_1^\ddagger is the key factor governing the k_1

[†] Eyring Equation: $\ln \frac{k_{\text{rate}}}{T} = (-\frac{\Delta H^\ddagger}{R}) \frac{1}{T} + (\frac{\Delta S^\ddagger}{R} + \ln \frac{k_B}{h})$. See Ref. 20.

Table 3.1. Second-order rate constants, k_1 , for the initial O-atom transfer from Ru^{VI}(TMP)(O)₂ (**1**) to various phosphines, AsPh₃ and SbPh₃ substrates in benzene.

Substrate	$k_1 \times 10^{-4}, M^{-1} s^{-1}$ at 10, 20 30, and 40°C, respectively
$P(p\text{-}X\text{-}C_6H_4)_3$ $X = \text{OMe}$	8.14 ± 0.08
	10.9 ± 0.02
	14.8 ± 0.02
	19.2 ± 0.02
$X = \text{Me}$	4.29 ± 0.07
	5.88 ± 0.07
	7.69 ± 0.18
	10.0 ± 0.3
$X = \text{H}$	3.95 ± 0.14
	5.7 ± 0.3
	7.18 ± 0.14
	9.38 ± 0.15
$X = \text{F}$	7.62 ± 0.13
	10.6 ± 0.02
	14.2 ± 0.2
	18.1 ± 0.4
$X = \text{Cl}$	9.17 ± 0.11
	12.8 ± 0.2
	16.9 ± 0.2
	22.3 ± 0.03
$X = \text{CF}_3$	6.38 ± 0.17
	9.10 ± 0.3
	12.7 ± 0.3
	16.6 ± 0.4
(dichloro)(triphenylphosphine)(tris(2-pyridyl)phosphine- <i>N</i>)ruthenium(II)	0.945 ± 0.02
	1.38 ± 0.04
	2.00 ± 0.08
	2.87 ± 0.08
AsPh_3	0.0623 ± 0.0007
	0.0940 ± 0.0006
	0.147 ± 0.001
	0.212 ± 0.001
SbPh_3 (10, 15, 20, and 25°C)	285 ± 30
	303 ± 35
	325 ± 30
	362 ± 35

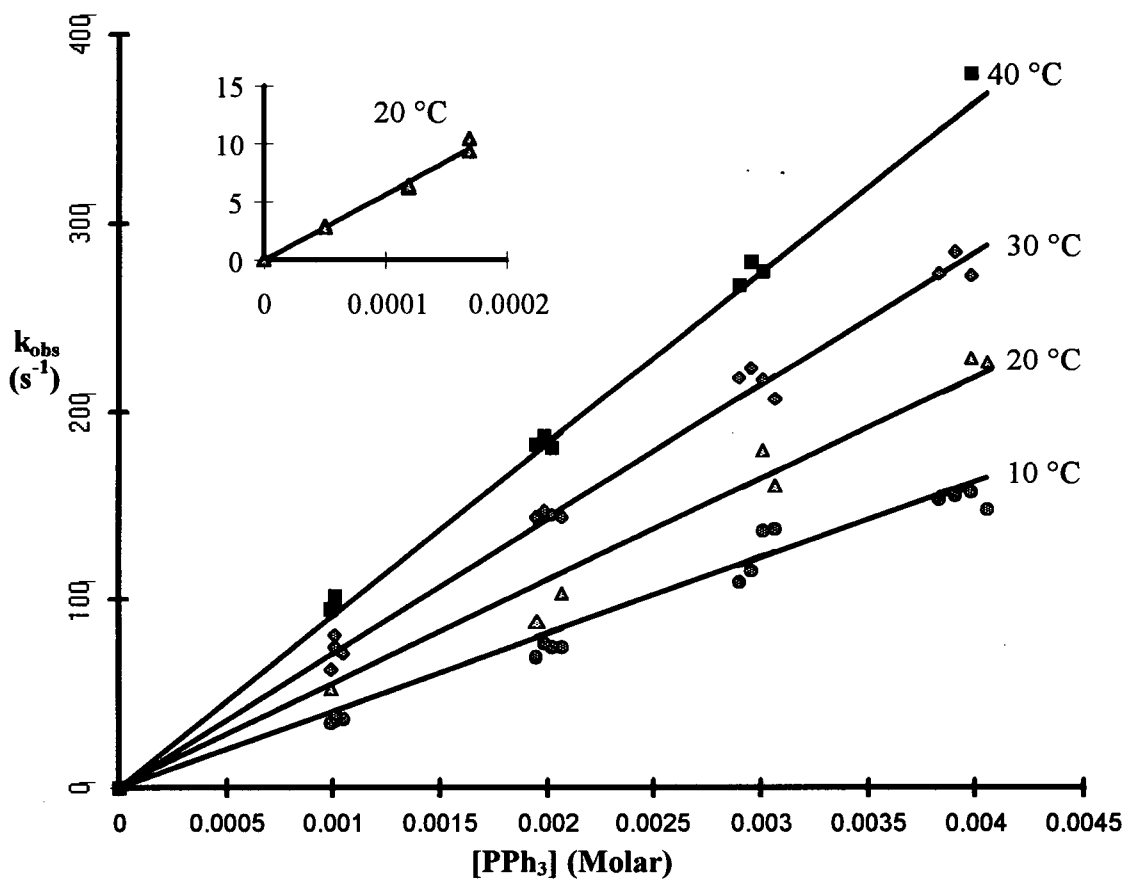


Figure 3.3. Plot of k_{obs} , pseudo-first-order rate constant, as a function of $[\text{PPh}_3]$ in benzene. k_{obs} corresponds to the rate constant for the initial O-atom transfer from $\text{Ru}^{\text{VI}}(\text{TMP})(\text{O})_2$ (**1**) to PPh_3 . Inset shows the data at 20 °C at a lower value of $[\text{PPh}_3]$. $[(\mathbf{1})] = 4.2 \times 10^{-6} \text{ M}$ ($1.6 \times 10^{-6} \text{ M}$ for the data in the inset). A tabulation of k_{obs} values can be found in Appendix A for all the different substrates listed in Table 3.1.

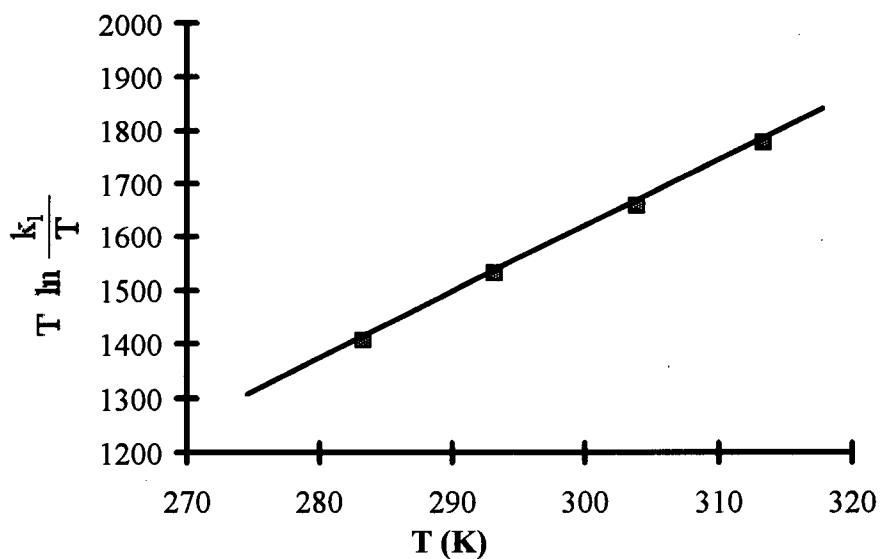
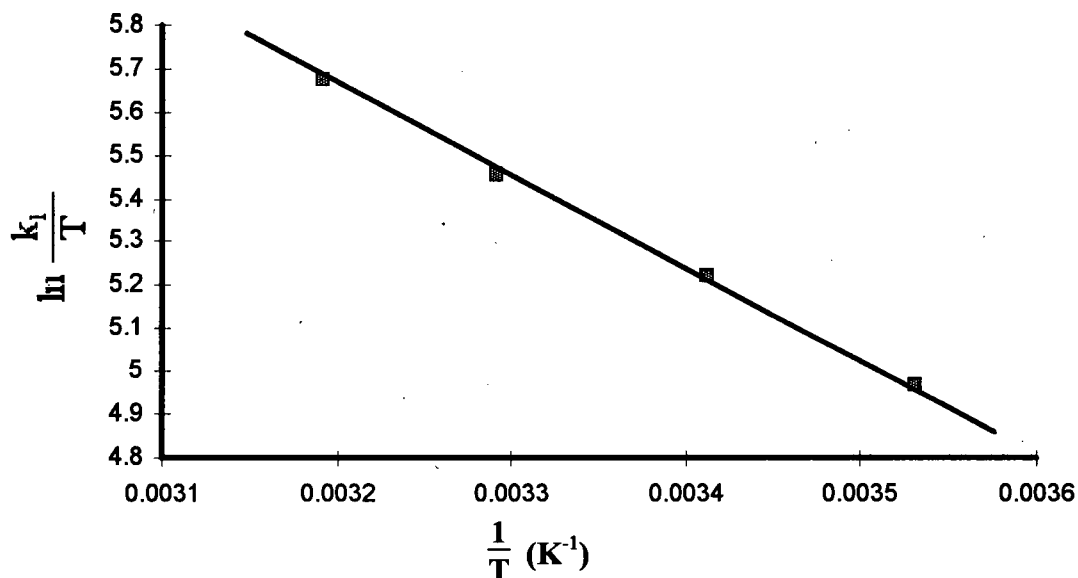


Figure 3.4. Eyring plots, $\ln(\frac{k_1}{T})$ versus $\frac{1}{T}$, and $T\ln(\frac{k_1}{T})$ versus T . From the slopes of these lines the activation parameters, ΔH_1^\ddagger and ΔS_1^\ddagger , are derived, respectively.

Table 3.2. Activation parameters, ΔH_1^\ddagger and ΔS_1^\ddagger , for the initial O-atom transfer from $\text{Ru}^{\text{VI}}(\text{TMP})(\text{O})_2$ (**1**) to phosphine, arsine and stibine substrates.

Substrates	ΔH_1^\ddagger (kJ mol ⁻¹) and ΔS_1^\ddagger (J mol ⁻¹ K ⁻¹), respectively
$\text{P}(p\text{-X-C}_6\text{H}_4)_3$ X=OMe	18 ± 1 -87 ± 5
X = Me	18 ± 1 -92 ± 5
X = H	18 ± 1.4 -94 ± 5
X = F	18.9 ± 1 -84 ± 4
X = Cl	19.4 ± 1.6 -81 ± 5
X = CF ₃	21 ± 1.4 -78 ± 5
(dichloro)(triphenylphosphine)(tris(2-pyridyl)phosphine- <i>N</i>)ruthenium(II)	25.7 ± 1 -78 ± 5
AsPh ₃	28.7 ± 1 -90 ± 3
SbPh ₃	10.2 ± 2 -85 ± 10

values for the oxidations of PPh_3 , AsPh_3 and SbPh_3 by (1), as the ΔS_1^\ddagger values are similar in all three cases. The following are some periodic trends within the series EPH_3 ($E = \text{P}, \text{As}, \text{Sb}$):⁹ 1) σ donor strength decreases in the order $\text{P} > \text{As} > \text{Sb}$; 2) steric effects due to E increases in the order $\text{P} < \text{As} < \text{Sb}$; 3) steric effects due to the Ph groups decreases in the order $\text{P} > \text{As} > \text{Sb}$. That such effects should contribute to the activation enthalpy seems feasible, but no firm conclusions can be drawn based on the current data.

An attempted Hammett correlation plot for the k_1 values for the $\text{P}(p\text{-X-C}_6\text{H}_4)_3$ substrates versus σ values¹⁰ is shown in Figure 3.5. The non-linearity observed is usually considered to indicate a change in the reaction mechanism,¹¹ but this would seem unlikely for this series of phosphine substrates. Hammett analysis is a type of linear free energy relationship, where the activation free energy, ΔG^\ddagger , is being correlated with the para substituent. More precisely (and especially in this case) the correlation is between the purely electronic effect brought about by a change in the para substituent on the P-atom, and the numerical value, σ . A conventional Hammett plot of $\log \frac{k_X}{k_H}$ versus σ can be linear only if the change in the para substituent results in one of the following three scenarios: 1) $\Delta H_1^\ddagger = \text{constant}$, implying that $\Delta(\Delta S_1^\ddagger) \propto \sigma$; 2) $\Delta S_1^\ddagger = \text{constant}$, implying that $\Delta(\Delta H_1^\ddagger) \propto \sigma$; 3) $\Delta(\Delta H_1^\ddagger) \propto \Delta(\Delta S_1^\ddagger) \propto \sigma$. As a non-linear Hammett plot is observed for the present systems, the logical alternative is to look at how the activation parameters, ΔH_1^\ddagger and ΔS_1^\ddagger , are affected by the para substituents.

Consideration of the different contributions of ΔH_1^\ddagger and ΔS_1^\ddagger (Table 3.2) suggests that the change in the values might indeed be independent of one another, and hence the phosphine systems fit none of the above three situations. The ΔH_1^\ddagger values do increase

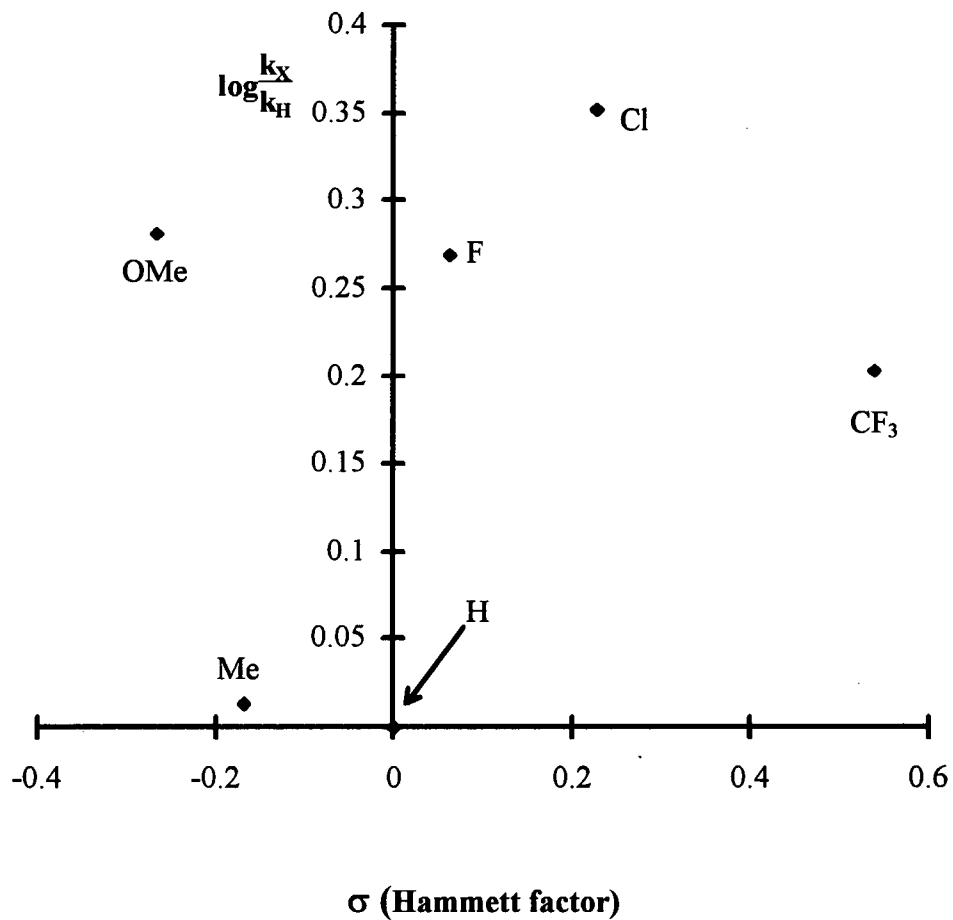
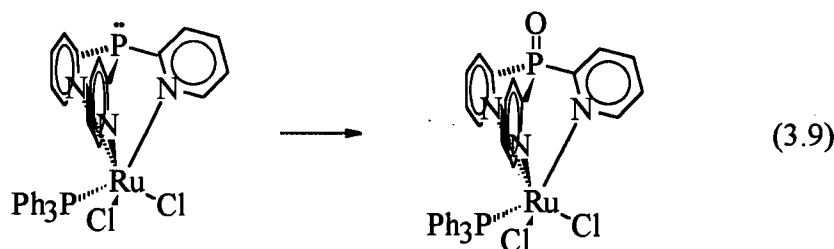


Figure 3.5. Hammett plot for $\log \frac{k_X}{k_H}$ values for the k_1 step at 20 °C (σ values taken from Ref. 10).[‡]

[‡] A supervisory member of my Ph.D. committee, M. Tanner, has suggested that the *p*-substituent effects are small, and that the Hammett plot may be horizontal.

with increasing electron-withdrawing groups (see Figure 3.6 for the modified Hammett plot). If one considers an electrophilic attack of a Ru=O moiety of (**1**) on the lone-pair of electrons on $\text{P}(p\text{-X-C}_6\text{H}_4)_3$, then withdrawal of electron density from phosphorus by X should tend to increase ΔH_1^\ddagger .

In terms of ΔS_1^\ddagger , no correlation can be seen with σ , although ΔS_1^\ddagger generally becomes more favourable, i.e. less negative, as the mass of the phosphine, arsine or stibine substrates increases (see Figure 3.7). An earlier suggestion has been made that if the O-atom transfers are induced via strong Ru=O vibrational coupling,³ the effect is perhaps reflected in a more favourable activation entropy with bulkier substrates.⁵ To test the effect of the mass of the phosphine on ΔS_1^\ddagger , the complex (dichloro)(triphenylphosphine)(tris[2-pyridyl]phosphine-*N*)ruthenium(II) (Eq. 3.9) was used as an oxidizable phosphine substrate, as the phosphorus on the coordinated tris(2-pyridyl)phosphine ligand can be oxidized to the phosphine oxide. The identities of the two species in Eq. 3.9 are known from prior work carried out in this laboratory.¹²



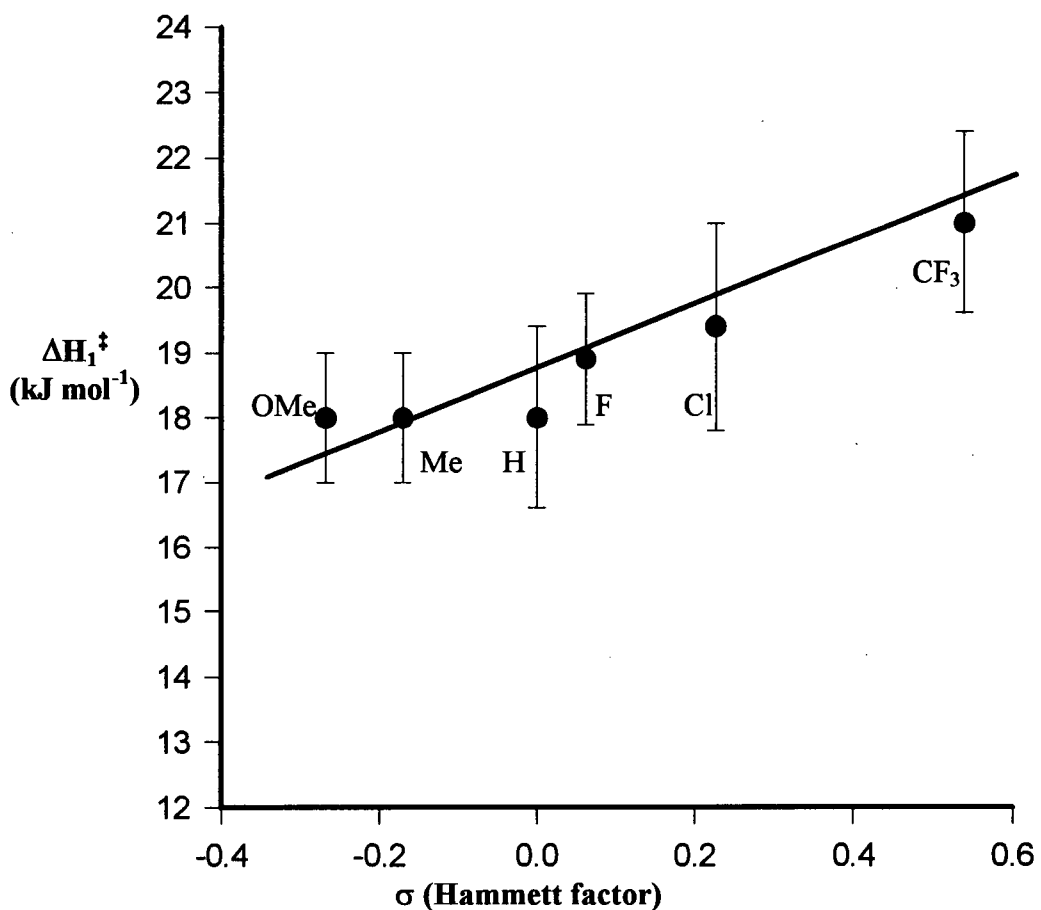


Figure 3.6. Modified Hammett plot, ΔH_1^\ddagger versus σ .

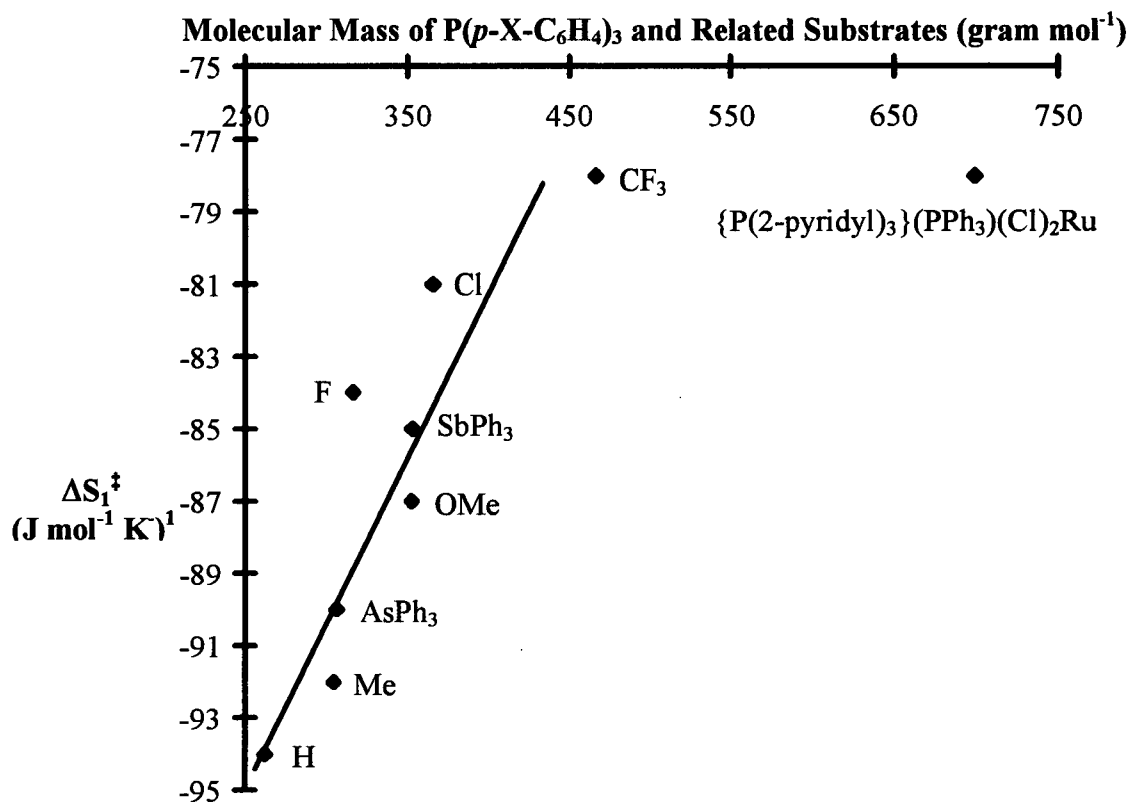


Figure 3.7. Plot of molecular mass of $P(p\text{-}X\text{-}C_6H_4)_3$ and related substrates versus ΔS_1^\ddagger .

The value of ΔS_1^\ddagger perhaps reaches some limiting value as the mass is increased; this is not surprising as the coupling reaction between (1) and L is expected to be entropically unfavourable. The tris(2-pyridyl)phosphine complex is very different structurally from the EPh₃-type substrates, and within this set an almost linear trend is established. Intuitively, one may envision this quantum mechanically in terms of the vibrational energy levels of the transition state becoming closer together as the mass becomes larger.[†]

A non-linear Hammett plot has been observed for the oxidation of *p*- and *m*-substituted styrenes by Ru^{VI}(porp)(O)₂ (porp = OEP and TPP).¹³ The non-linearity was ascribed to a shift in the electron density on the alkene C=C double bond, as the substituent on the phenyl ring varied from electron-withdrawing (NO₂) to electron-releasing (OMe) groups, and this was suggested to lead to a change in the electronic structure of the transition state. Of note, the Hammett plot was concaving upwards, with the unsubstituted styrene at the minimum of the plot. If there was some change in the electronic structure in the C=C bond, this would not necessarily occur when the substituent was H, although this was invoked in order to explain the observed experimental results. A look at the activation parameters would be more insightful in this case.

[†] Vibrational Entropy $\propto \ln q_{\text{vib}}$, where the vibrational partition function, $q_{\text{vib}} = [1 - \exp(-\frac{\hbar\nu}{kT})]^{-1}$ for a simple harmonic oscillator (Ref. 21). The vibrational frequency, $\nu \propto \mu^{-1/2}$, where μ = reduced mass. As the mass of phosphine substrate increases, the reduced mass also increases, leading to an decrease in the vibrational energy gaps, and hence a greater number of vibrational levels. A greater number of vibrational levels leads to an increase in vibrational entropy in the transition state; the macromolecules in the present system are, of course, much more complicated than the species considered in the Transition State Theory.

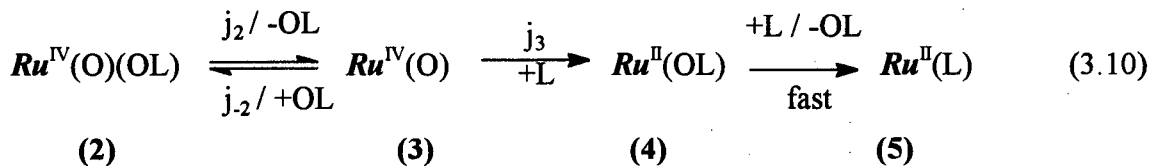
$\text{P}(p\text{-X-C}_6\text{H}_4)_3$ compounds, compared to other substrates such as alkenes or thioethers, yield the largest span of molecular mass differences, and thus this effect is perhaps the most pronounced for this series. The rates of O-atom transfer from $\text{Ru}^{\text{VI}}(\text{TMP})(\text{O})_2$ to phosphines are clearly governed by both ΔH_1^\ddagger and ΔS_1^\ddagger : ΔH_1^\ddagger becomes more favourable as the electron density around phosphorus increases, while ΔS_1^\ddagger is more favourable with more massive substituents. The increased bulk at the para position should not increase any steric hindrance,¹⁴ and should have minimum effects on the activation parameters in terms of steric considerations. The O-atom transfer is probably similar to the process in thioether oxidations, and occurs via strong Ru=O vibrational coupling, with a more massive phosphine giving rise to a more favourable ΔS_1^\ddagger via a larger vibrational entropy.

In terms of the actual mode of O-atom transfer, the phosphine could initially coordinate to Ru, followed by O-atom transfer to the phosphorus; however, the steric constraint presented by the TMP ligand makes this unlikely. The redox process could conceivably involve two successive one-electron transfers; this would be difficult to distinguish mechanistically from a single two-electron O-atom transfer pathway, although rates arising from single-electron transfers would perhaps be more likely to adhere to a Hammett correlation. The non-Hammett behaviour of this system, as well as the strong ΔS^\ddagger dependence on the substrate mass, are consistent with a single two-electron O-atom transfer pathway.

3.3.2 Disproportionation of Ru^{IV}(TMP)(O)

Figure 3.2 shows that two separate processes occur on different time-scales. The shift in the Soret maximum from 422 to 430 nm has been discussed, and corresponds to the O-atom transfer to form Ru^{IV}(TMP)(O)(OPPh₃) (**2**). The shift of the Soret maximum from 430 to 412 nm occurs on a slower time-scale and is thought to correspond to the dissociation of OPPh₃ from (**2**), followed by a disproportionation equilibrium driven to the product side by the formation of the stable Ru^{II}(TMP)(PPh₃) (**5**) (see Figure 3.1). The disproportionation reaction mechanism was summarized previously in Eqs. 3.3 to 3.6, with the resulting rate equation given in Eq. 3.8. In agreement with this mechanism for the slower second step, the rate is first-order in [(**2**)], first- to zero-order in [PPh₃], and shows an inverse dependence on [OPPh₃] (see Figure 3.8). The analysis of the kinetic data will be considered later.

An alternative simpler, but less favoured, mechanism can be proposed for the second step by assuming that the second UV-visible spectral change corresponds to a second O-atom transfer starting with dissociation of OL from (**2**), followed by oxidation of L by (**3**), and ending with the formation of (**5**) via rapid PPh₃ ligation, Eq. 3.10 (j_n = rate constants). A steady state approximation applied to the series of reactions in



Eq. 3.10 yields the rate law shown in Eq. 3.11 which is of the same form as Eq. 3.8.

$$k_{obs} = \frac{j_2 j_3 [L]}{j_{-2} [OL] + j_3 [L]} \quad (3.11)$$

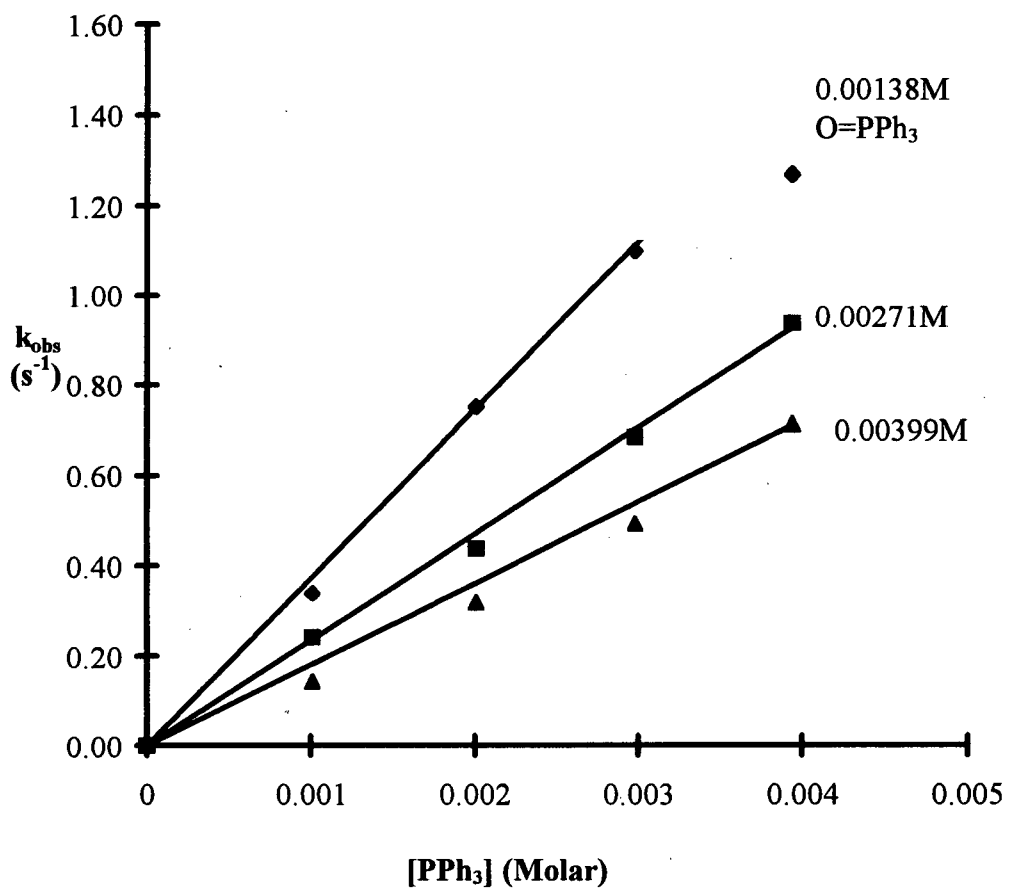


Figure 3.8. Plots of k_{obs} (2nd slower UV-visible spectral change from 430 to 412 nm) versus $[\text{PPh}_3]$ at various $[\text{OPPh}_3]$ values in benzene at 20 °C.
 $[(1)]_{\text{initial}} = 4.2 \times 10^{-6} \text{ M}$.

Rearrangement of Eq. 3.11 to the form represented by Eq. 3.12 facilitates the analysis of the kinetic data to yield values for j_2 and $\frac{j_{-2}}{j_3}$. Figure 3.9a shows the plot of

$$\frac{1}{k_{\text{obs}}} = \frac{1}{j_2} + \frac{j_{-2}[\text{OL}]}{j_2 j_3 [\text{L}]} \quad (3.12)$$

$\frac{1}{k_{\text{obs}}}$ versus $\frac{[\text{OL}]}{[\text{L}]}$ for $\text{L} = \text{PPh}_3$ at 20°C , with the slope giving $\frac{j_{-2}}{j_2 j_3}$ and the y-intercept $\frac{1}{j_2}$. (Figures 3.9b to f show similar plots for the other $\text{P}(p\text{-X-C}_6\text{H}_4)_3$ substrates). The y-intercept is near 0, hence the value obtained for j_2 is unreliable. It is possible to obtain j_2 by a different method. As $[\text{L}]$ is increased, $j_3[\text{L}] > j_{-2}[\text{OL}]$, and eventually $j_{-2}[\text{OL}]$ becomes negligible. In essence, the rate-determining step is now the dissociation of the OL ligand. 1.3×10^{-5} M OL was present (instead of $\sim 10^{-3}$ M in typical experiments as described in Section 3.2.1) in order to minimize the competition by the $j_{-2}[\text{OL}]$ term. The expected saturation kinetics are observed with the values of k_{obs} leveling-off as $[\text{L}]$ increases to nearly 0.05 M (Figure 3.10). Rearrangement of Eq. 3.12 to the form

represented in Eq. 3.13 allows the value of $\frac{1}{j_2}$ to be determined from the slope of the plot of $\frac{[\text{L}]}{k_{\text{obs}}}$ versus $[\text{L}]$ (Figure 3.11). The values of j_2 are obtained under various

$$\frac{[\text{L}]}{k_{\text{obs}}} = \frac{1}{j_2} [\text{L}] + \frac{j_{-2}}{j_2 j_3} \text{constant, for fixed [OL]} \quad (3.13)$$

temperatures (Table 3.3), and the following activation parameters may be obtained (Figure 3.12): $\Delta H_{j_2}^\ddagger = 39 \pm 13 \text{ kJ mol}^{-1}$ and $\Delta S_{j_2}^\ddagger = -85 \pm 40 \text{ J mol}^{-1}\text{K}^{-1}$; however, the Eyring plots are unsatisfactory (see below).

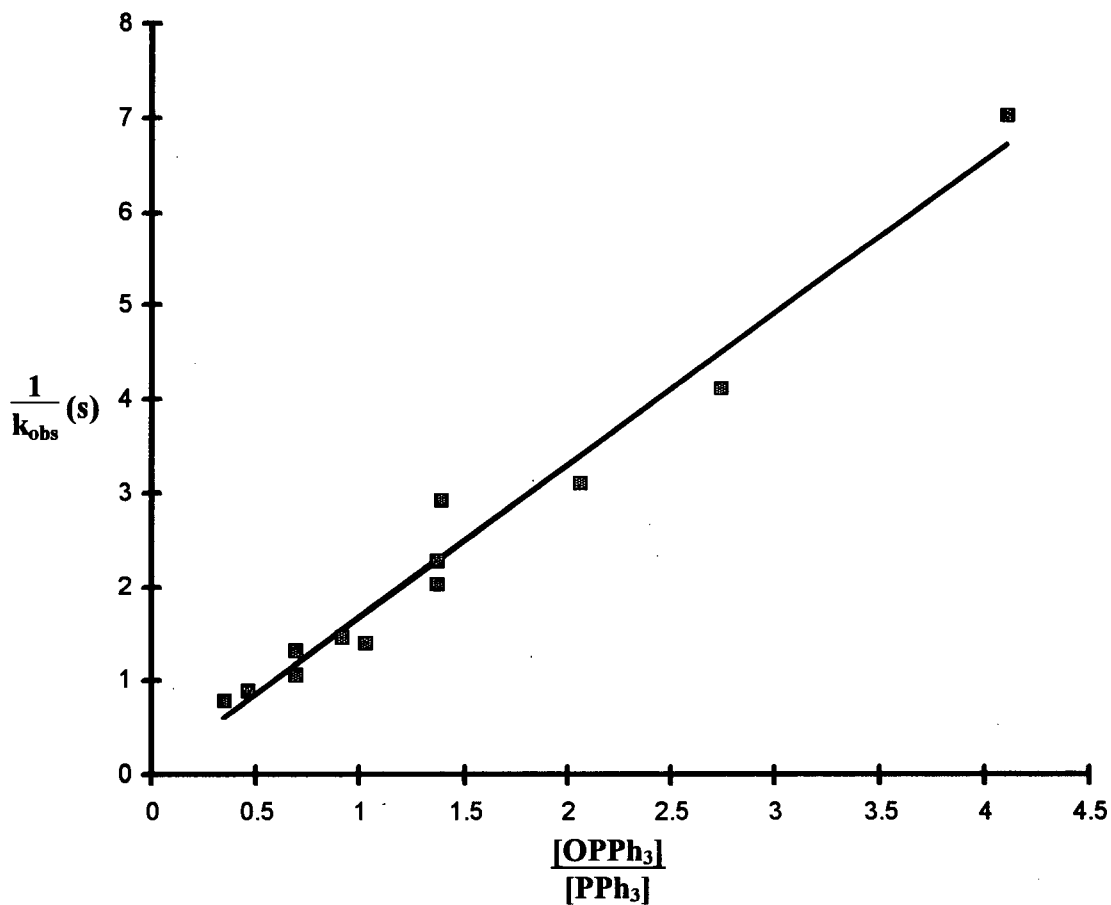


Figure 3.9a. Plot of $\frac{1}{k_{obs}}$ versus $\frac{[OPPh_3]}{[PPh_3]}$ for the kinetic data of the Soret shift from 430 to 412 nm at 20 °C, corresponding to the slower 2nd step in the overall reaction between Ru^{VI}(TMP)(O)₂ (**1**) and PPh₃. The k_{obs} values are pseudo-first-order rate constants under the conditions of added excess PPh₃ and OPPh₃. $[1]_{\text{initial}} = 4.2 \times 10^{-6}$ M. k_{obs} values for all P(*p*-X-C₆H₄)₃ substrates are tabulated in Appendix A.

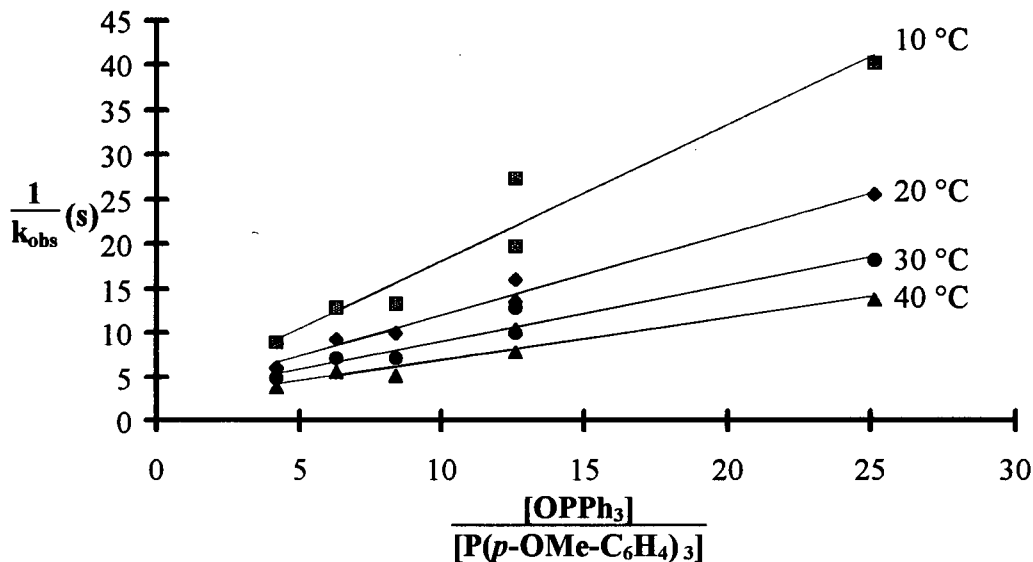


Figure 3.9b. Plot of $\frac{1}{k_{\text{obs}}} (\text{s})$ versus $\frac{[\text{OPPh}_3]}{[\text{P}(p\text{-OMe-C}_6\text{H}_4)_3]}$ for the kinetic data of the Soret shift from 430 to 412 nm (see also Appendix A).

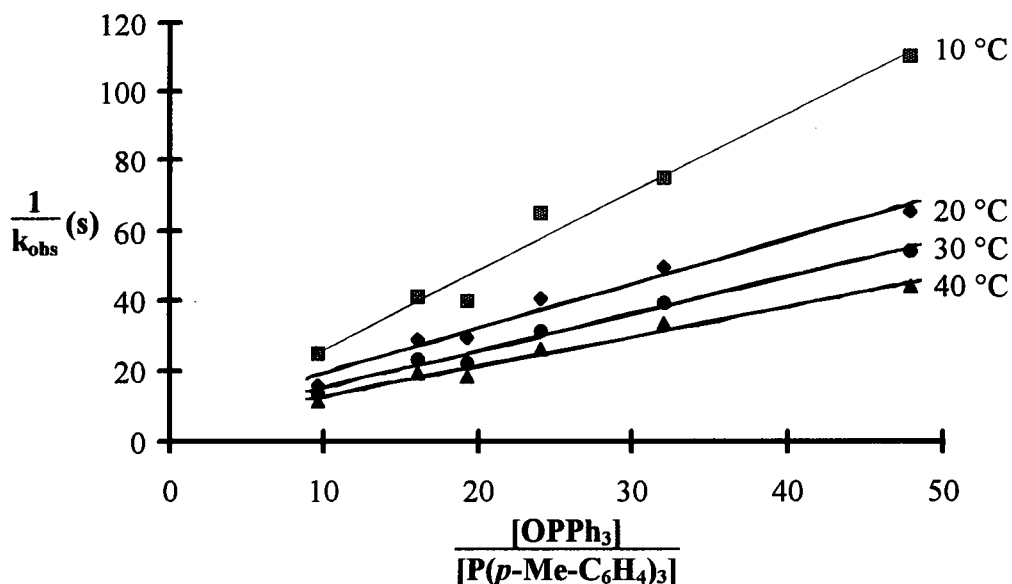


Figure 3.9c. Plot of $\frac{1}{k_{\text{obs}}} (\text{s})$ versus $\frac{[\text{OPPh}_3]}{[\text{P}(p\text{-Me-C}_6\text{H}_4)_3]}$ for the kinetic data of the Soret shift from 430 to 412 nm (see also Appendix A).

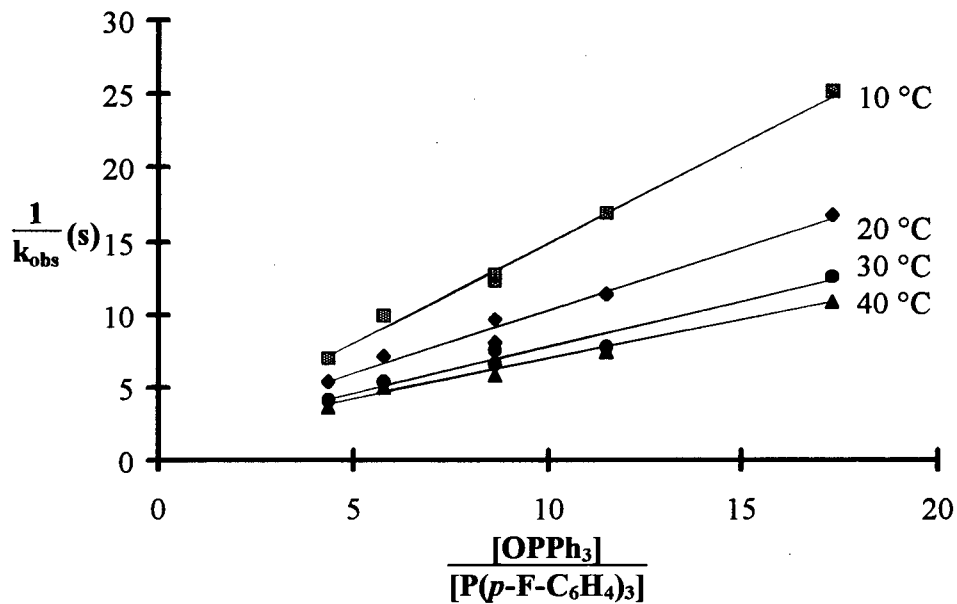


Figure 3.9d. Plot of $\frac{1}{k_{obs}}$ versus $\frac{[OPPh_3]}{[P(p-F-C_6H_4)_3]}$ for the kinetic data of the Soret shift from 430 to 412 nm (see also Appendix A).

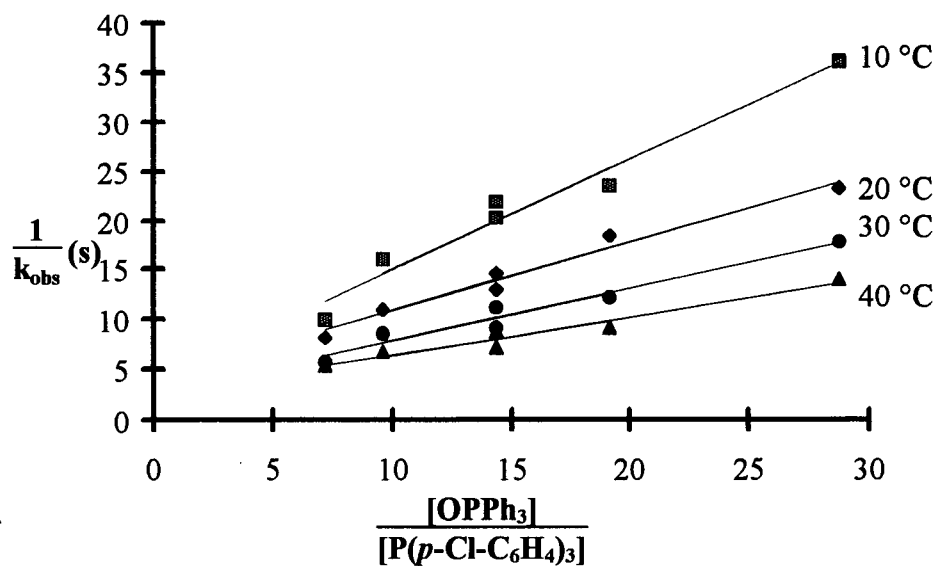


Figure 3.9e. Plot of $\frac{1}{k_{obs}}$ versus $\frac{[OPPh_3]}{[P(p-Cl-C_6H_4)_3]}$ for the kinetic data of the Soret shift from 430 to 412 nm (see also Appendix A).

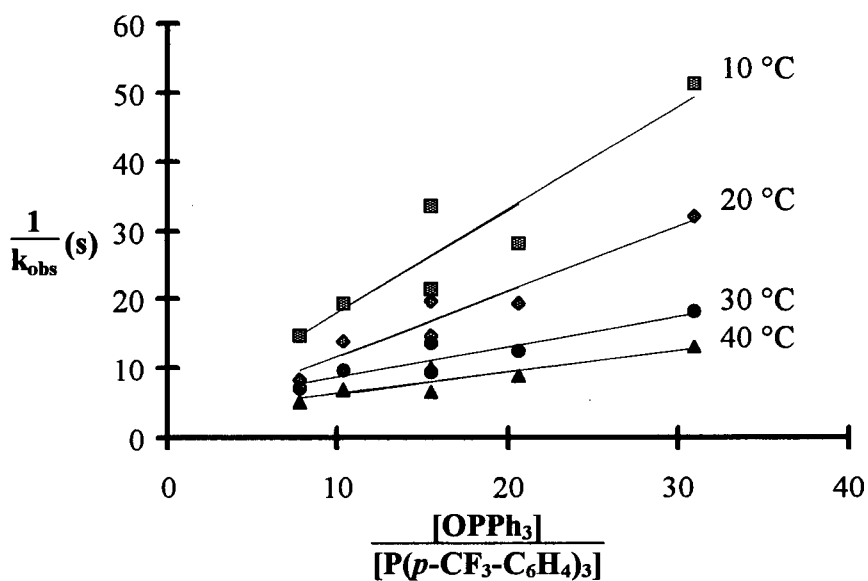


Figure 3.9f. Plot of $\frac{1}{k_{\text{obs}}}$ versus $\frac{[\text{OPPh}_3]}{[\text{P}(p\text{-CF}_3\text{-C}_6\text{H}_4)_3]}$ for the kinetic data of the Soret shift from 430 to 412 nm (see also Appendix A).

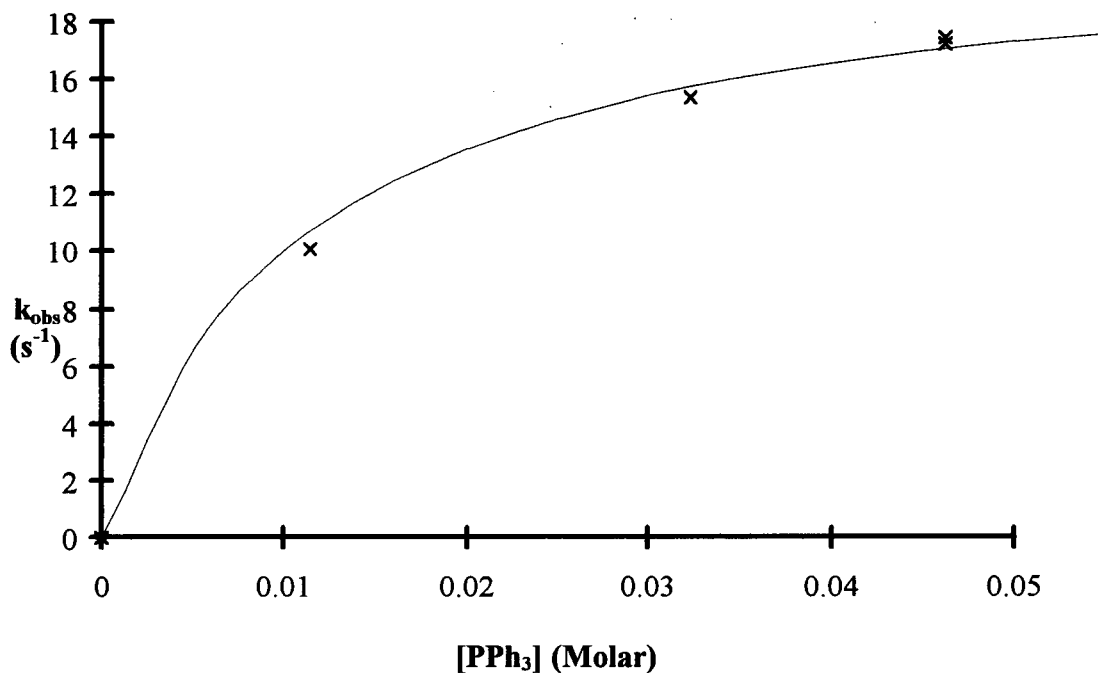


Figure 3.10. Plot of k_{obs} versus $[\text{PPh}_3]$ for the kinetic data of the Soret shift from 430 to 412 nm at 20.5 °C, corresponding to the slower 2nd step in the overall reaction between Ru^{VI}(TMP)(O)₂ (**1**) and PPh₃. The k_{obs} values are pseudo-first-order rate constants under the conditions of added excess PPh₃ and OPPh₃. The k_{obs} values at other temperatures are tabulated in Appendix A.
[OPPh₃] = 1.3 × 10⁻⁵ M, [(**1**)]_{initial} = 2 × 10⁻⁶ M

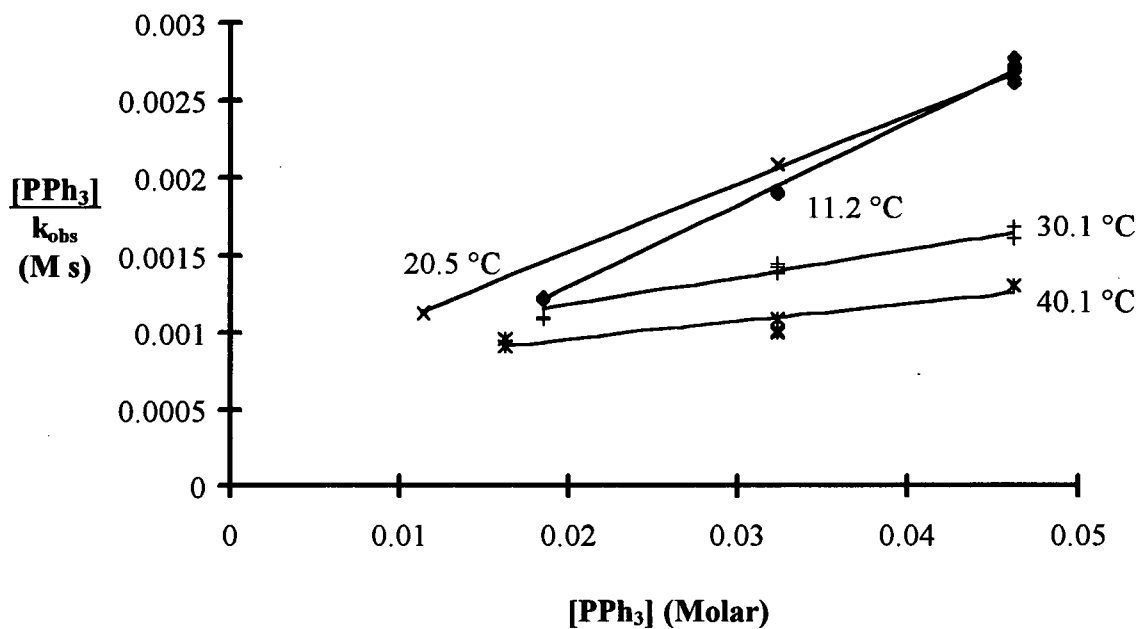


Figure 3.11. Plots of $\frac{[PPh_3]}{k_{obs}}$ versus $[PPh_3]$. Slope gives $\frac{1}{j_2}$. The k_{obs} values for the data are listed in Appendix A.

Table 3.3. Values of j_2 , dissociation of $OPPh_3$ from $Ru^{IV}(TMP)(O)(OPPh_3)$.

Temperature ($^\circ\text{C}$)	$j_2 \text{ (s}^{-1}\text{)}$
11.2	18.7 ± 1
20.5	22.7 ± 1
30.1	55.7 ± 9
40.1	82 ± 25

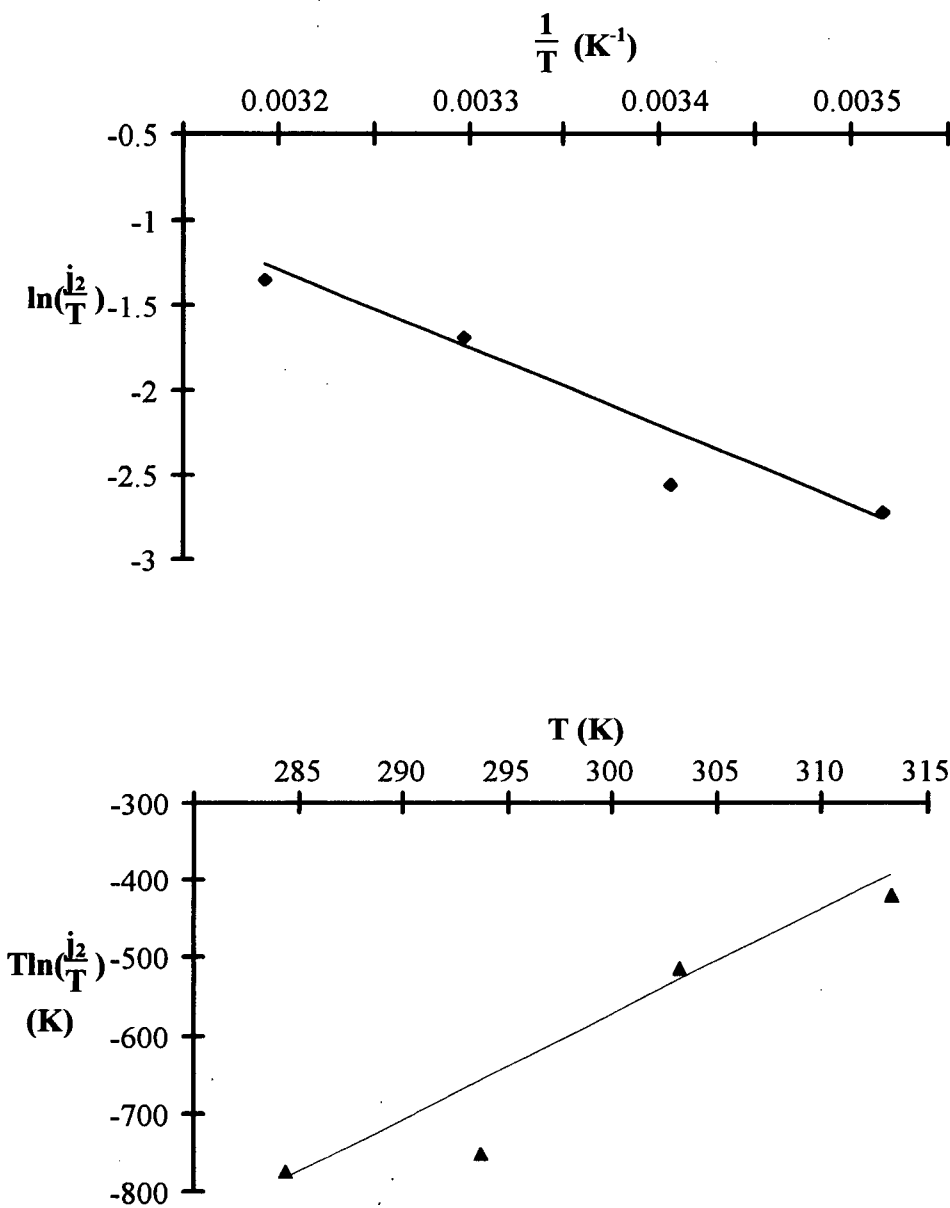
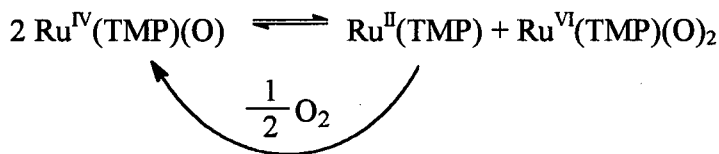
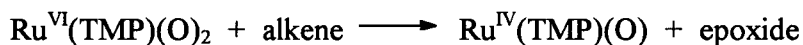


Figure 3.12. Eyring plots, $\ln(\frac{j_2}{T})$ versus $\frac{1}{T}$, and $T \ln(\frac{j_2}{T})$ versus T . From the slopes of these lines the activation parameters, ΔH_{j2}^\ddagger and ΔS_{j2}^\ddagger , are derived.

The large negative ΔS_{j2}^\ddagger value would thus correspond to the loss of OPPh_3 , a dissociation reaction. This is unusual, but could be ascribed in part to solvent effects, perhaps due to some solvation of the transition state, if its geometry approximates that of $\text{Ru}^{\text{IV}}(\text{TMP})(\text{O})$. As written, this second O-atom transfer follows the dissociation of OL from (2), while the coordination of OL inhibits the O-atom transfer. This is contrary to the mechanism suggested for thioether oxidations by (1),⁵ where $\text{Ru}^{\text{IV}}(\text{TMP})(\text{O})(\text{OSR}_2)$ is considered more active than (1) as an O-atom transfer agent (see later).

The disproportionation mechanism (Eqs. 3.3 to 3.6) is favoured for the phosphine oxidation reaction as explained below. First, the disproportionation of $\text{Ru}^{\text{IV}}(\text{TMP})(\text{O})$ to $\text{Ru}^{\text{II}}(\text{TMP})$ and $\text{Ru}^{\text{VI}}(\text{TMP})(\text{O})_2$, although not directly established, presents a “consistent” explanation for the $\text{Ru}^{\text{VI}}(\text{TMP})(\text{O})_2$ oxidation chemistry demonstrated for a range of different systems studied. The O_2 -oxidation of alkenes catalyzed by (1) has been proposed to involve a disproportionation process^{15,16} as depicted below.



The generation of $\text{Ru}^{\text{VI}}(\text{TMP})(\text{O})_2$ from $\text{Ru}^{\text{II}}(\text{TMP})(\text{MeCN})_2$ upon exposure to air^{5,6} also has been suggested to occur via the disproportionation of $\text{Ru}^{\text{IV}}(\text{TMP})(\text{O})$. In addition, the catalytic O_2 -dehydrogenation of primary and secondary alcohols to aldehydes and ketones, respectively (Chapter 4), is proposed to involve this disproportionation reaction.

According to the disproportionation mechanism, the pseudo-first-order rate constant, k_{obs} , assumes the form represented in Eq. 3.8, and the observed saturation

kinetics yield not j_2 (the OL dissociation rate constant), but rather the combination of rate constants, $k' = \frac{k_2 k_4}{k_1 + k_4}$, where k_2 alone represents the OL dissociation rate constant (see Appendix B). The Eyring plots in Figure 3.12 are performed on k' , and the observed ΔS^\ddagger value of $-85 \text{ J mol}^{-1}\text{K}^{-1}$ is probably not meaningful. The Eyring equation applied to k' is not expected to yield a linear plot, and the scatter of the data in Figure 3.12 suggests that the Eyring plots are probably non-linear. The dissociation of OL from $\text{Ru}^{\text{IV}}(\text{TMP})(\text{O})(\text{OL})$ is a necessity within the disproportionation mechanism, as a vacant site is required for the disproportionation of $\text{Ru}^{\text{IV}}(\text{TMP})(\text{O})$ to take place.¹⁶

The slope from the plot in Figure 3.9a gives the value of $k'' = \frac{k_2}{k_2 k_4 K_3^{1/2}}$ at 20°C for the PPh_3 system [the values at other temperatures, as well as those for other $\text{P}(p\text{-X-C}_6\text{H}_4)_3$ systems, are listed in Table 3.4]. Excess OPPh_3 was used throughout each study, as the dominant oxide present would then be OPPh_3 regardless of the phosphine substrate. The inhibition of the rates of reaction by OPPh_3 in all the $\text{P}(p\text{-X-C}_6\text{H}_4)_3$ systems (see data in Appendix A and the linear $\frac{1}{k_{\text{obs}}}$ versus $\frac{[\text{OPPh}_3]}{[\text{P}(p\text{-X-C}_6\text{H}_4)_3]}$ plots, Figures 3.9b to 3.9f) implies that the k_2 and k_{-2} steps involve a rapid replacement of $\text{OP}(p\text{-X-C}_6\text{H}_4)_3$ by excess OPPh_3 , and hence the reversible dissociation and coordination reactions involve mainly OPPh_3 . K_3 is independent of the phosphine substrate as well. Thus, the smaller the value of $\frac{k_2}{k_2 k_4 K_3^{1/2}}$, the larger the relative value of k_4 . From Table 3.4, the relative rate of binding of L to Ru(II) follows the order: $\text{Cl} > \text{F} > \text{CF}_3 \sim \text{OMe} > \text{H} \sim \text{CH}_3$ at 10°C .

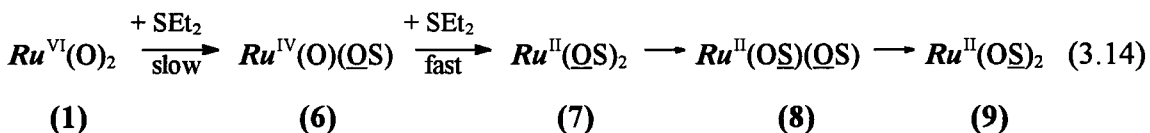
Table 3.4. Values of $\frac{k_2}{k_2 k_4 K_3^{1/2}}$ obtained from the kinetic data for the spectral change of the Soret maximum from 430 to 412 nm.

P(<i>p</i> -X-C ₆ H ₄) ₃ , X=	$\frac{k_2}{k_2 k_4 K_3^{1/2}}^a$ at 10, 20 30 and 40°C
OMe	1.52 ± 0.2
	0.92 ± 0.07
	0.63 ± 0.08
	0.48 ± 0.08
Me	2.25 ± 0.17
	1.27 ± 0.1
	1.05 ± 0.06
	0.846 ± 0.07
H	2.16 ± 0.2
	1.62 ± 0.09
	1.26 ± 0.1
	1.06 ± 0.1
F	1.38 ± 0.06
	0.864 ± 0.06
	0.628 ± 0.06
	0.536 ± 0.05
Cl	1.12 ± 0.1
	0.69 ± 0.06
	0.52 ± 0.054
	0.38 ± 0.045
CF ₃	1.48 ± 0.3
	0.94 ± 0.14
	0.444 ± 0.09
	0.31 ± 0.07

^a k_2 , k_2 and $K_3^{1/2}$ are considered to be the same for every reaction (see text). Excess OPPh₃ was used in every study to allow for a comparison of k_4 between different phosphine systems.

The orders are slightly different at other temperatures: Cl > F > OMe > CF₃ > CH₃ > H at 20 °C, CF₃ > Cl > F > OMe > CH₃ > H at 30 °C, and CF₃ > Cl > OMe > F > CH₃ > H at 40 °C. The data suggest that the electron-rich groups tend to give the smaller relative k₄ values. Perhaps the electron-rich Ru(II)-centre favours π-acceptor ligands; for example S-bound sulfoxides are generally favoured over O-bound sulfoxides in Ru(II)-complexes.^{5,17} A more electron-deficient phosphine may act as a better π-acceptor. The coordination of L to Ru(II) may well be the driving force for the effective disproportionation of Ru^{IV}(TMP)(O).

In hindsight, the two-stage oxidation of thioethers may follow the same mechanism as the phosphines, via disproportionation, rather than via two successive O-atom transfers.⁵ The time-scale of the O-atom transfer from (1) to aliphatic thioethers is of the order of hours, and any Ru^{IV}(TMP)(O) that may have formed should have rapidly disproportionated. The scheme represented in Eq. 3.14 [Ru = Ru(TMP), S = SEt₂; O and S imply oxygen- and sulfur-bonding sulfoxides, respectively] is the mechanism of thioether



oxidation proposed in Reference 5. More careful examination of the data in Reference 5 shows that the formulation of species (7) as the bis(O-bonded sulfoxide) complex may be incorrect. In Reference 5a, the ¹H-NMR spectrum of Ru^{II}(TMP)(SEt₂)₂, produced *in situ* from the reaction of Ru^{II}(TMP)(MeCN)₂ and excess SEt₂, is found to be identical to that assigned to (7). This also possibly suggests that the formulation for species (8) as written in Eq. 3.14 is also incorrect, and it might be the Ru^{II}(TMP)(SEt₂)(OSEt₂) species. This

chemistry would be consistent with the labile nature of an O-bound Et₂SO ligand in the Ru(TMP) system.⁵ A plausible route to these Ru(II) thioether and S-bound sulfoxide species is from the disproportionation of Ru^{IV}(TMP)(O) to Ru^{II}(TMP) and (1), followed by rapid ligation of thioether and sulfoxide to the Ru(II)-centre.

3.4 Ru^{II}(TMP)(L) Species and Catalytic Aerobic Oxidation of Phosphines

3.4.1 Ru^{II}(TMP)(L) Species

Stoichiometric ¹H-NMR titrations (see Section 3.3) performed by Groves and Ahn⁶ showed Ru^{II}(TMP)(PPh₃) (**5**) along with 2 equivalents of OPPh₃, to be the products of the reaction between Ru^{VI}(TMP)(O)₂ (**1**) and 3 equivalents of PPh₃. It was assumed initially that perhaps the bis(phosphine) complex, Ru^{II}(TMP)(PPh₃)₂, would form if more than 3 equivalents of PPh₃ were added to (**1**), as Ru^{II}(TMP)(PⁿBu₃)₂ and Ru^{II}(OEP)(PPh₃)₂ have been synthesized previously in this laboratory;¹⁸ however, ¹H and ³¹P{¹H}-NMR experiments showed that only (**5**) was formed even when more than 3 equivalents of PPh₃ reacted with (**1**).

Figure 3.13 shows the ¹H-NMR spectrum of (**5**), the product from the reaction of (**1**) with 3 equivalents of PPh₃ in benzene-*d*₆. That two distinct *ortho*-Me ¹H-resonances are observed is indicative of (**5**) possessing C_{4v} symmetry.⁵ Of note, addition of 1 equivalent of PPh₃ to Ru^{II}(TMP)(MeCN)₂ yields a product giving a ¹H-NMR spectrum identical to that of (**5**), with production of free MeCN. This rules out the possibility that OPPh₃ coordinates to the Ru-centre [as Ru^{II}(TMP)(L)(OL) also exhibits C_{4v} symmetry] when (**5**) is produced via PPh₃ oxidation by (**1**), where 2 equivalents of OPPh₃ is produced.

Thus, the formulation of (**5**) as the mono-phosphine complex $\text{Ru}^{\text{II}}(\text{TMP})(\text{PPh}_3)$ is correct.

Also shown in Figure 3.13 is the ^1H -NMR spectrum of the same benzene- d_6 solution at room temperature containing (**5**), formed via the reaction between (**1**) and 30 of equivalents PPh_3 . The two ^1H -NMR spectra for the systems containing no excess PPh_3 and excess PPh_3 are generally the same, except that the *ortho*-Me protons of TMP were exchanged broadened and the signals of the coordinated PPh_3 protons had disappeared for the system containing the excess PPh_3 . Most likely, rapid PPh_3 exchange via nucleophilic attack at the Ru centre is causing the broadening of the *ortho*-Me protons signals.

The ligand exchange process of (**5**) with excess PPh_3 was verified in variable temperature ^1H and $^{31}\text{P}\{^1\text{H}\}$ -NMR studies. Figure 3.14 shows the ^1H and $^{31}\text{P}\{^1\text{H}\}$ -NMR spectra in benzene- d_6 of (**5**) formed from the reaction of (**1**) with 60 equivalents PPh_3 . At 10°C , the *ortho*-Me signals were exchange broadened, and the signals of the PPh_3 protons disappeared. At -78°C , ^1H -resonances due to the two inequivalent *ortho*-Me groups, as well as ^1H -resonances for the protons on the coordinated PPh_3 , were detected, as the ligand exchange rate at the lower temperature was decreased. Also at -78°C , the $^{31}\text{P}\{^1\text{H}\}$ -resonance for the coordinated PPh_3 was observed (Figure 3.14). These results clearly suggest that a five-coordinate mono-phosphine complex is favoured. That no other $\text{Ru}^{\text{II}}(\text{TMP})$ species can be detected in these NMR studies indicates that the bis(phosphine) species is present only in a trace amount needed to effect phosphine ligand exchange,

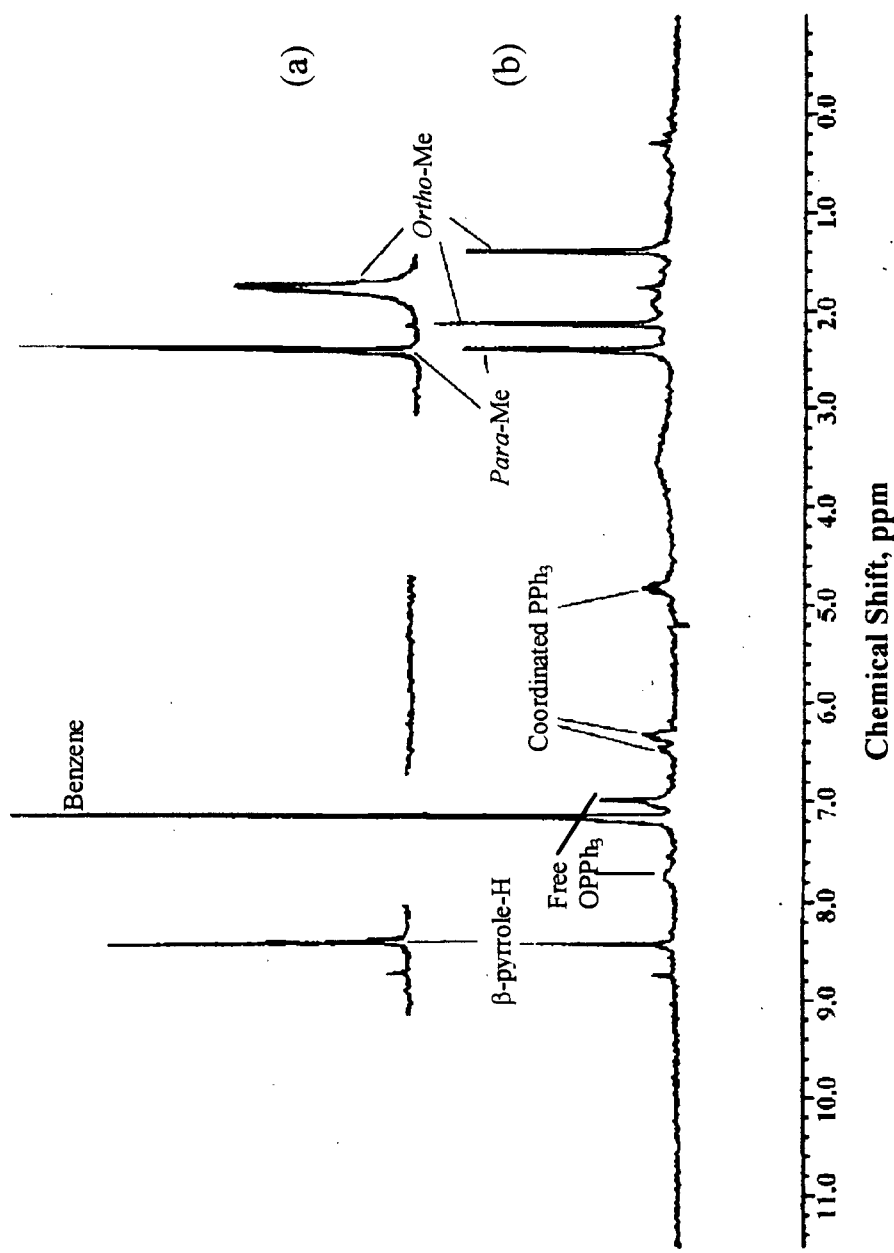


Figure 3.13. ^1H -NMR (200 MHz) spectra of $\text{Ru}^{\text{II}}(\text{TMP})(\text{PPh}_3)$ (**5**) ($\sim 1 \times 10^{-3}$ M) with (a) and without (b) excess PPh_3 in benzene- d_6 at 25 °C. The coordinated Ph-proton resonances disappeared for the system containing excess PPh_3 . For the case without excess phosphine, (**5**) was formed from the reaction of (1) and 3 equivalents of PPh_3 , 30 equivalents of PPh_3 were added to (1) in the system containing excess phosphine.

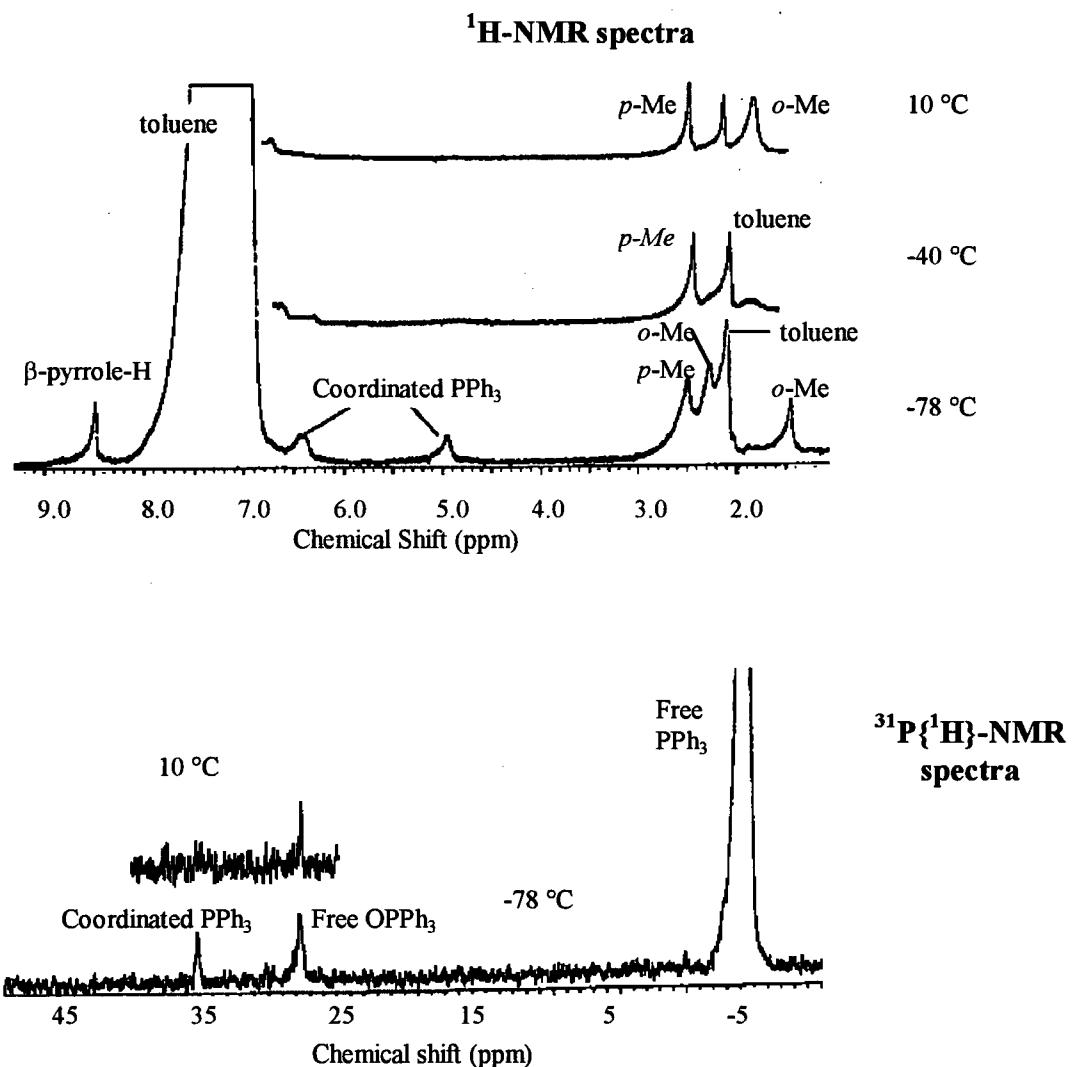
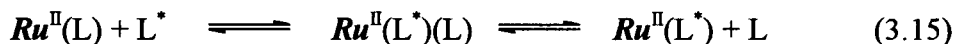


Figure 3.14. Variable-temperature ^1H and $^{31}\text{P}\{^1\text{H}\}$ -NMR (300 MHz) spectra of $\text{Ru}^{\text{II}}(\text{TMP})(\text{PPh}_3)$ (**5**) (5×10^{-4} M) containing excess PPh_3 (3×10^{-2} M) in toluene- d_8 . Species (**5**) was formed by reacting (**1**) with 60 equivalents of PPh_3 , and free OPPh_3 is observed in the $^{31}\text{P}\{^1\text{H}\}$ -NMR spectra. The partial $^{31}\text{P}\{^1\text{H}\}$ -NMR spectrum at 10 °C shows only OPPh_3 ; the signal due to the coordinated PPh_3 is not observed.

which would make the *ortho*-Me protons become equivalent (Eq. 3.15 [$\text{Ru} = \text{Ru}(\text{TMP})$]).

The UV-visible spectrum of (**5**) (Figure 3.2) did not change when more



phosphine was added (up to ~ 0.1 M), a strong indication that there is no significant amount of $\text{Ru}^{\text{II}}(\text{TMP})(\text{PPh}_3)_2$ in solution, if any.

$\text{Ru}^{\text{II}}(\text{TMP})(\text{L})$ [$\text{L} = \text{P}(p\text{-X-C}_6\text{H}_4)_3$, X = OMe, Me, F, Cl and CF_3] species can also be formed from the reaction of (**1**) with 3 equivalents of L, and the NMR data obtained for these species produced *in situ* are tabulated in Table 3.5. The reaction of (**1**) with 3 equivalents of EPh_3 ($\text{E} = \text{As}$ and Sb) also afforded the $\text{Ru}^{\text{II}}(\text{TMP})(\text{EPh}_3)$ species. The ^1H -NMR spectra of the solutions containing excess phosphine L show the same exchange broadening of the *ortho*-Me protons and non-detection of the coordinated ligand phenyl protons, as observed for the PPh_3 system, showing that the phosphines within the $\text{P}(p\text{-X-C}_6\text{H}_4)_3$ series do not form complexes of the type $\text{Ru}^{\text{II}}(\text{TMP})(\text{L})_2$. It seems that only stronger σ -donor phosphines such as $\text{P}''\text{Bu}_3$ can form the $\text{Ru}^{\text{II}}(\text{TMP})(\text{P}''\text{Bu}_3)_2$ complex in solution; however, the second $\text{P}''\text{Bu}_3$ ligand within the complex can be removed at 270 °C under a vacuum of $\sim 10^{-5}$ torr.¹⁸

3.4.2 Catalytic Aerobic Oxidation of Phosphines

$\text{Ru}^{\text{IV}}(\text{TMP})(\text{O})$, $\text{Ru}^{\text{VI}}(\text{TMP})(\text{O})_2$ and $\text{Ru}^{\text{II}}(\text{TMP})(\text{L})$ were observed in benzene- d_6 solutions of $\text{Ru}^{\text{II}}(\text{TMP})(\text{L})$ (initially made from (**1**) + 3 L) [$\text{L} = \text{P}(p\text{-X-C}_6\text{H}_4)_3$, AsPh_3 and SbPh_3] when these solutions were exposed to air for approximately 2 min. Free L was not observed during the reaction, and within 10 min OL and (**1**) were the only species in

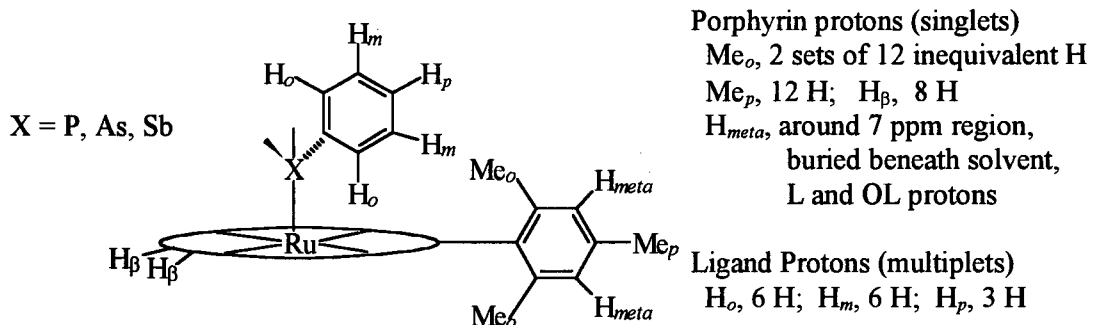
Table 3.5. ^1H and $^{31}\text{P}\{^1\text{H}\}$ -NMR data for various $\text{Ru}^{\text{II}}(\text{TMP})(\text{L})$ species
(L = substituted phosphine, AsPh_3 or SbPh_3).

$\text{Ru}^{\text{II}}(\text{TMP})(\text{L})^a$	Chemical shifts, ^{b,c} δ						
	H_β	Me_p	Me_o	H_m	H_o	H_p	$^{31}\text{P}\{^1\text{H}\}$
$\text{L} = \text{PPh}_3$	8.42	2.41	2.18, 1.40	6.32	4.80	6.44	35.3 ^d
$\text{L} = \text{P}(p\text{-OMe-C}_6\text{H}_4)_3$	8.45	2.41	2.32, 1.41	6.07	4.88	-	-
$\text{L} = \text{P}(p\text{-Me-C}_6\text{H}_4)_3$	8.45	2.43	2.23, 1.70	6.25	4.86	-	29.6 ^d
$\text{L} = \text{P}(p\text{-F-C}_6\text{H}_4)_3$	8.38	2.43	2.23, 1.29	6.10	4.64	N/A	31.7
$\text{L} = \text{P}(p\text{-Cl-C}_6\text{H}_4)_3$	8.37	2.43	2.23, 1.28	6.39	4.57	N/A	35.1 ^d
$\text{L} = \text{P}(p\text{-CF}_3\text{-C}_6\text{H}_4)_3$	8.37	2.43	2.19, 1.20	6.65	4.69	N/A	29.5
$\text{L} = \text{AsPh}_3$	8.28	2.38	1.92, 1.78	6.54	5.35	6.67	N/A
$\text{L} = \text{SbPh}_3$	8.55	2.38	2.25, 1.55	6.38	5.18	6.52	N/A
$\text{Ru}^{\text{II}}(\text{TMP})(\text{P}^n\text{Bu}_3)^e$	8.45	2.63	2.47, 1.72		N/A		53.09
$\text{Ru}^{\text{II}}(\text{TMP})(\text{P}^n\text{Bu}_3)_2^e$	8.43	2.48	2.43 ^f		N/A		-0.38

^a $\text{Ru}^{\text{II}}(\text{TMP})(\text{L})$ species produced *in situ* from the reaction between $\text{Ru}^{\text{VI}}(\text{TMP})(\text{O})_2$ and 3 equivalents of L .

^b ^1H relative to TMS; $^{31}\text{P}\{^1\text{H}\}$ relative to $\text{H}_3\text{PO}_{4\text{(aq)}}$; 200 MHz machine at 25 °C in benzene- d_6 unless indicated otherwise.

^c Legend:



^d Temperature at -68 °C in toluene- d_8 on a 300 MHz instrument.

^e Reference 18.

^f Singlet for the *ortho*-Me ^1H -resonance is indicative of the complex possessing D_{4h} symmetry.

solution. Figure 3.15 shows the ^1H -NMR spectrum of a benzene- d_6 solution of $\text{Ru}^{\text{II}}(\text{TMP})(\text{AsPh}_3)$ [formed from (1) reacting with 3 AsPh_3], which has been exposed to air for approximately 2 min. Other substrate systems generally give the same type of ^1H -NMR spectrum under the corresponding conditions: namely, $\text{Ru}^{\text{IV}}(\text{TMP})(\text{O})$, $\text{Ru}^{\text{VI}}(\text{TMP})(\text{O})_2$ and $\text{Ru}^{\text{II}}(\text{TMP})(\text{L})$ are observed. For the spectrum of the AsPh_3 system shown in Figure 3.15, an unassigned upfield ^1H -resonance at $\delta \sim -8$ ppm that is not present in the spectra of the other systems is observed. This broad signal disappeared in the spectrum that was acquired after a total time of ~ 4 min of exposure to air. This unassigned δ value could result from a species formed from the binding of OAsPh_3 to $\text{Ru}^{\text{IV}}(\text{TMP})(\text{O})$. If $\text{Ru}^{\text{IV}}(\text{TMP})(\text{O})(\text{OAsPh}_3)$ is indeed present, the ligand binding is expected to be weak, and the ^1H -chemical shifts of $\text{Ru}^{\text{IV}}(\text{TMP})(\text{O})$ moiety generally might not be perturbed to a great extent; nonetheless, the perturbation on the β -pyrrole-H signal might be large enough to be detected. The β -pyrrole-H signals of the paramagnetic $\text{Ru}^{\text{IV}}(\text{porp})^{5,19,\dagger}$ species are very sensitive to the environment about the ruthenium and might possibly discriminate between $\text{Ru}^{\text{IV}}(\text{TMP})(\text{O})$ and $\text{Ru}^{\text{IV}}(\text{TMP})(\text{O})(\text{OAsPh}_3)$.

As the exposure of $\text{Ru}^{\text{II}}(\text{TMP})(\text{L})$ species to air in solution regenerates $\text{Ru}^{\text{VI}}(\text{TMP})(\text{O})_2$ (1), oxidizing L catalytically with O_2 is clearly viable. Initial qualitative

[†] The β -pyrrole protons within $\text{Ru}^{\text{IV}}(\text{TMP})(\text{OR})_2$ ($\text{R} = \text{Me}, \text{C}_6\text{H}_5, {}^1\text{Pr}, \text{Et}$) species exhibit very different chemical shifts (-21.8, -30.45, -11.95, -17.6 ppm, respectively), while the Me_{para} and Me_{ortho} ^1H -chemical shifts differ by ~ 0.3 ppm. See Chapter 4.

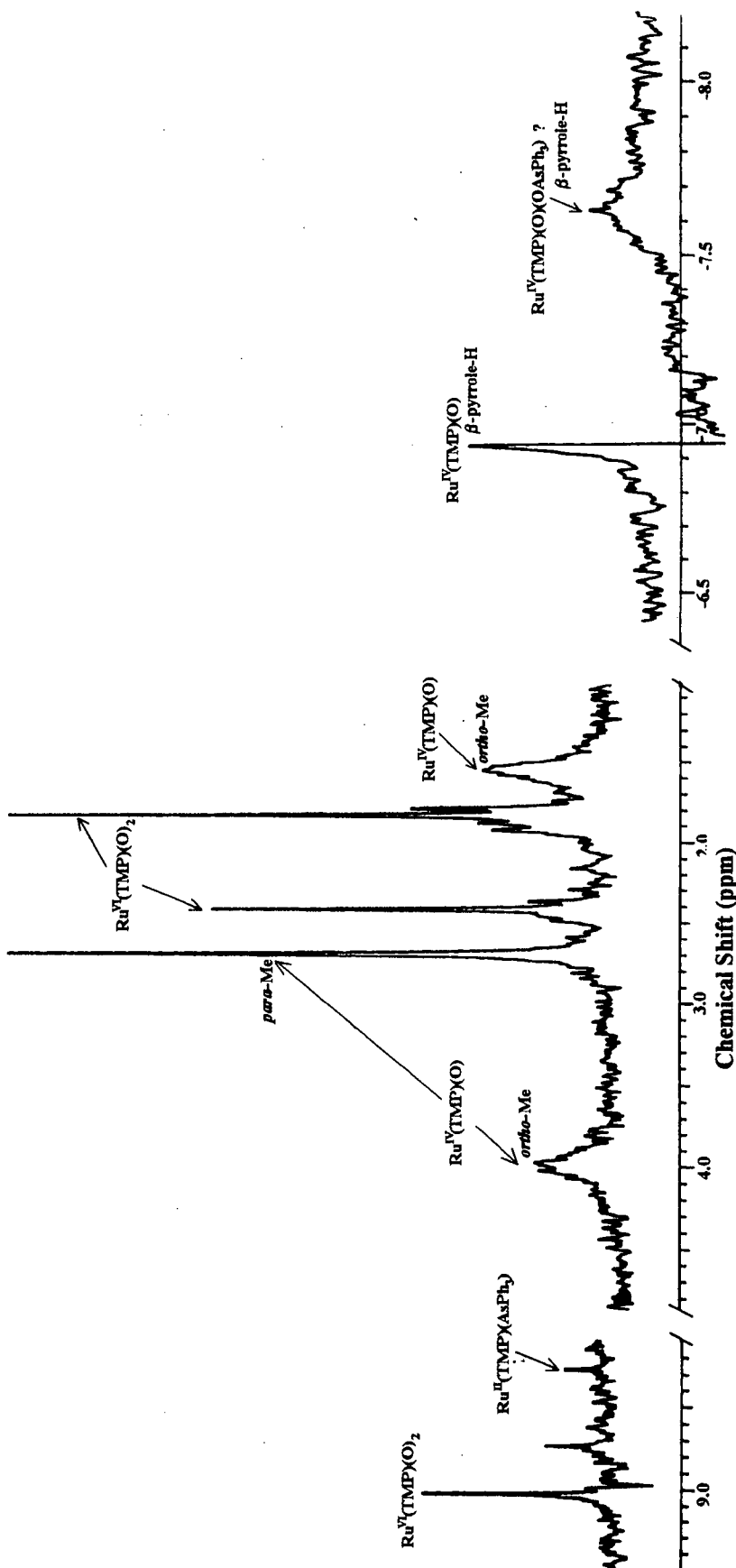


Figure 3.15. ${}^1\text{H}$ -NMR (300 MHz) spectrum of $\text{Ru}^{\text{V}}(\text{TMP})(\text{AsPh}_3)$ in benzene- d_6 exposed to air for ~ 2 min at 25 °C.
 $\text{Ru}^{\text{V}}(\text{TMP})(\text{AsPh}_3)$ was generated *in situ* from the reaction of $\text{Ru}^{\text{VI}}(\text{TMP})(\text{O})_2$ and 3 AsPh_3 .

experiments showed that PPh_3 can be O_2 -oxidized using (1) as the catalyst, with total turnovers of approximately 20 at the end of 24 h at room temperature under 1 atm air. The turnover frequency of about 1 h^{-1} (exclusive of the initial 2 equivalents of phosphine oxide formed from the stoichiometric reaction) is low considering that the O-atom transfer and disproportionation steps to form $\text{Ru}^{\text{II}}(\text{TMP})(\text{PPh}_3)$ (5) are complete within a few minutes. The relatively slow regeneration of (1) from (5) most likely is initiated via O_2 attack at the vacant axial site in (5) (Figure 3.1), and the excess PPh_3 competes against this O_2 -binding.

Catalysis studies were done on various phosphine systems under 1.0 atm O_2 and/or air (Table 3.6 and Figs. 3.16a to d). The catalytic activity of (1) generally is higher under 1 atm O_2 , but the turnovers obtained are not too much greater than those obtained under 1 atm air, especially during the initial 24 h of the catalytic runs. The diffusion of O_2 from the gas phase into the benzene- d_6 solutions within the NMR tubes to replenish the consumed O_2 is expected to be slow and dependent upon various factors, and thus no firm conclusions regarding the effect of O_2 on the rate of catalysis can be drawn from the current data; indeed diffusion may be rate-limiting. There is generally little effect of the concentration of phosphine on the catalytic activity, especially when the experimental errors are taken into consideration. A possible exception might be the $\text{P}(p\text{-Cl-C}_6\text{H}_4)_3$ system, which gave higher turnovers at a higher value of [phosphine]. Again, the O_2 -diffusion problem precludes any discussion regarding the effect of [phosphine], as the key step in the catalytic process, that of the regeneration of (1), must depend on both phosphine and O_2 binding to (5).

Table 3.6. Total turnovers of various phosphines catalytically oxidized at 24 °C in benzene-*d*₆ under 1 atm O₂ in the presence of Ru^{VI}(TMP)(O)₂ (1).

Substrate (Molar) ([Ru ^{VI} (TMP)(O) ₂] in parentheses)	Time (hours)	Blank contributions (% of initial L)	Turnovers based on Ru ^{VI} (TMP)(O) ₂ ^a
PPh₃ 64 excess; 0.0147 M (2.3 x 10 ⁻⁴ M)	22	3.5	31 ± 3
	22	3.0	21 ± 3
	22	5.0	36 ± 5
	22	5.5	14 ± 3
P(p-F-C₆H₄)₃ 175 excess; 0.0148 M (8.5 x 10 ⁻⁵ M)	19	0.8	9 ± 2
	48	1.4	82 ± 4
	62	2.3	96 ± 5
	19	1.3	14 ± 2
	48	2.7	80 ± 3
	62	4.2	112 ± 6
	22	1.5	11 ± 2
	49	3.4	27 ± 3
	70	7.6	40 ± 4
	22	3.0	13 ± 2
	49	7.0	32 ± 3
	70	15.0	40 ± 4
P(p-OMe-C₆H₄)₃ 166 excess; 0.0144 M (8.7 x 10 ⁻⁵ M)	19.75	1.7	24 ± 3
	48.75	4.2	131 ± 10
	60	5.6	166 ± 12
	19.75	3.4	19 ± 2
	48.75	8.5	180 ± 15
	60	11.5	190 ± 20
	20	1.4	7 ± 1
	48	3.0	64 ± 5
	62.5	4.0	71 ± 6
	20	2.4	15 ± 2
	48	5.9	110 ± 10
	62.5	6.2	115 ± 10

^a Autoxidation by O₂ has been taken into account in these reported turnover numbers.

Refer to Section 3.2.2 on the quantification of OL and L.

^b Experiment done under 1 atm air (~ 0.20 atm O₂)

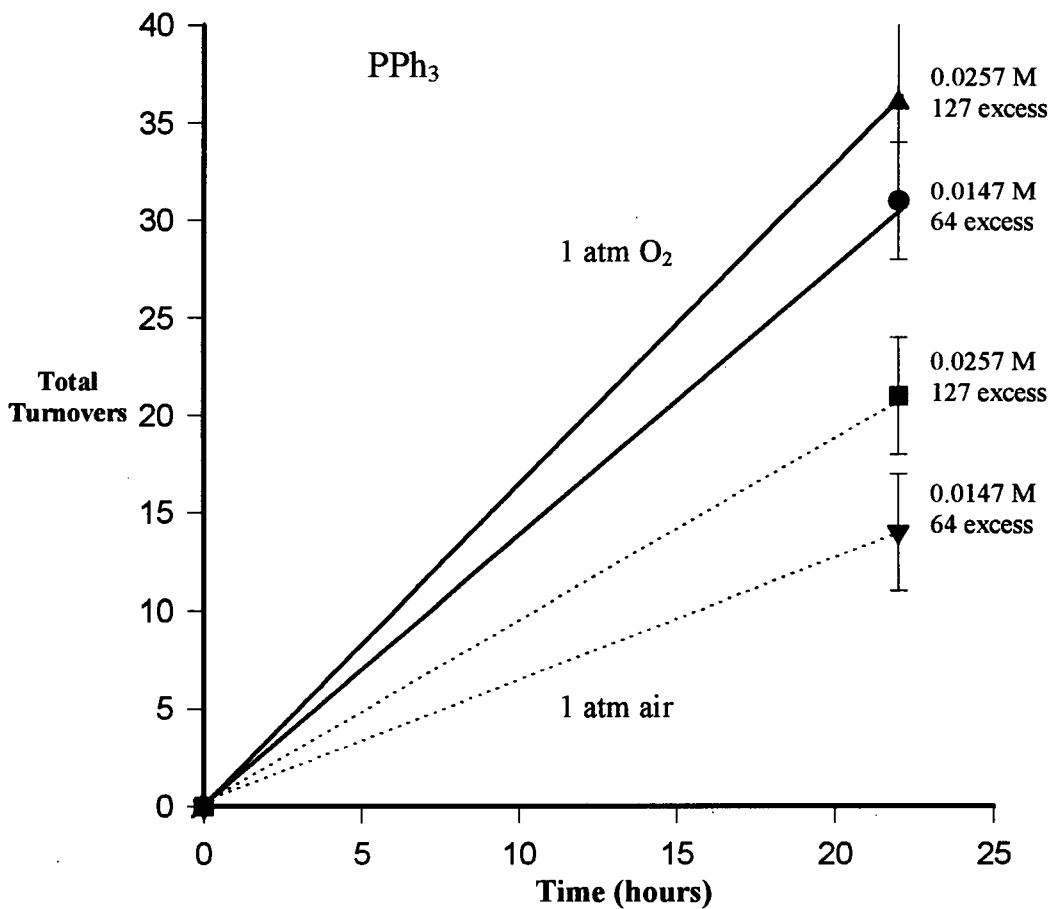


Figure 3.16a. Catalytic oxidation of PPh_3 in the presence of $\text{Ru}^{\text{VI}}(\text{TMP})(\text{O})_2$ ($\sim 2 \times 10^{-4}$ M) under 1 atm air or O_2 in benzene- d_6 at 24 °C. Linear dependences are assumed, based on related systems—see Figs. 3.16b to d.

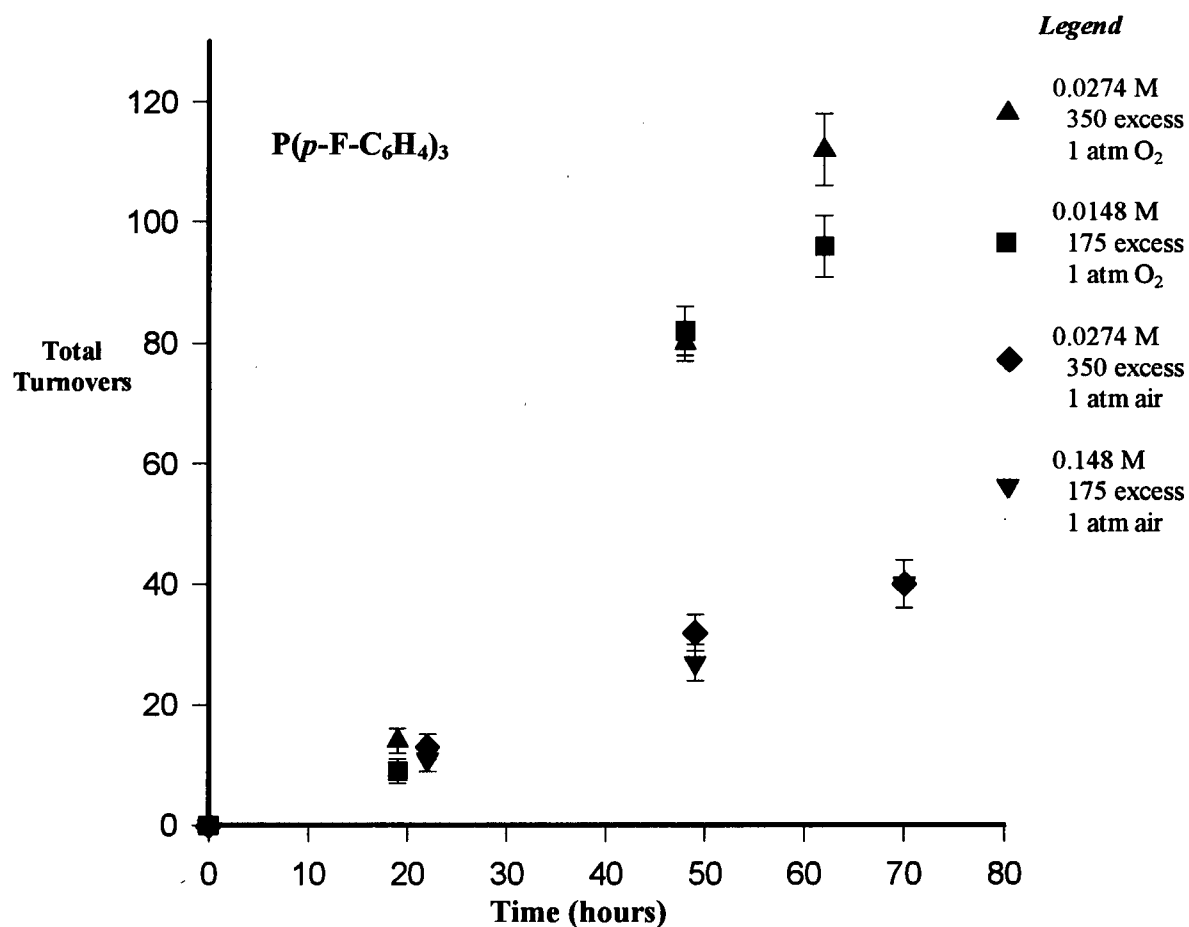


Figure 3.16b. Catalytic oxidation of $\text{P}(p\text{-F-C}_6\text{H}_4)_3$ in the presence of $\text{Ru}^{\text{VI}}(\text{TMP})(\text{O})_2$ (**1**) under 1 atm air and O_2 in benzene- d_6 at 24 °C. $[(\mathbf{1})] \sim 2 \times 10^{-4}$ M for experiments under 1 atm air and $\sim 8 \times 10^{-5}$ M under 1 atm O_2 .

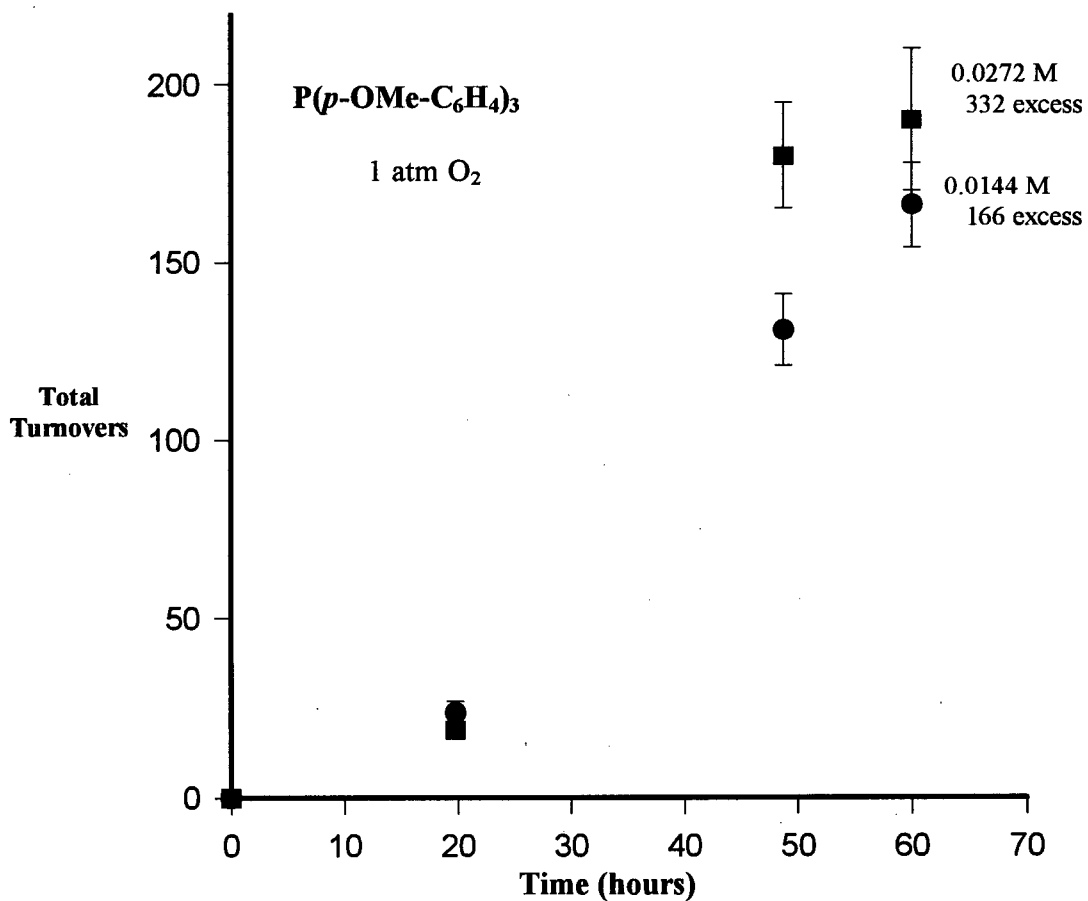


Figure 3.16c. Catalytic oxidation of $\text{P}(p\text{-OMe-C}_6\text{H}_4)_3$ in the presence of $\text{Ru}^{\text{VI}}(\text{TMP})(\text{O})_2$ ($\sim 8 \times 10^{-5}$ M) under 1 atm O_2 in benzene- d_6 at 24°C .

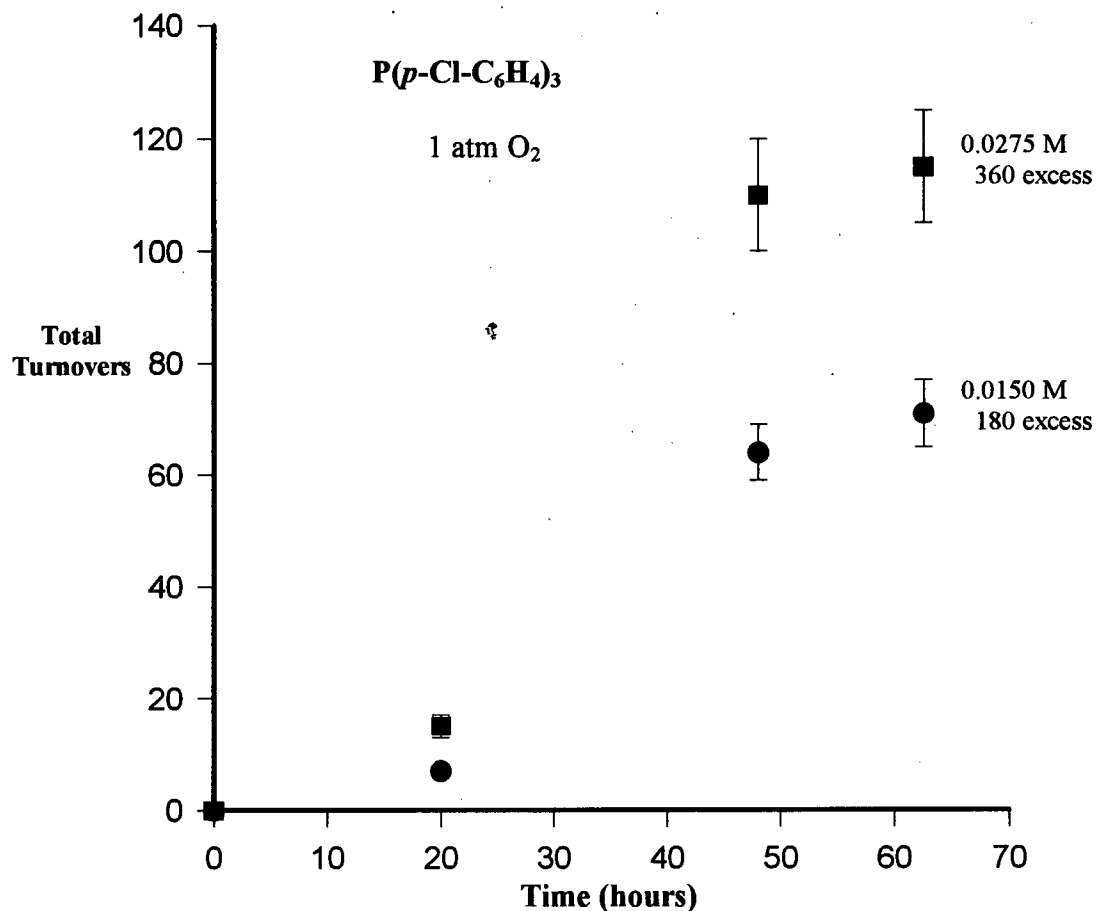


Figure 3.16d. Catalytic oxidation of P(*p*-Cl-C₆H₄)₃ in the presence of Ru^{VI}(TMP)(O)₂ ($\sim 8 \times 10^{-5}$ M) under 1 atm O₂ in benzene-*d*₆ at 24 °C.

3.5. Conclusions

This chapter presented some kinetic data for the O-atom transfer from *trans*-Ru^{VI}(TMP)(O)₂ to tertiaryarylphosphines, AsPh₃ and SbPh₃. The increasing ΔH_1^\ddagger for the O-atom transfer upon withdrawing electron density around phosphorus suggests that the Ru-oxo moieties are electrophilic in nature, and that the reaction proceeds via an electrophilic attack of the Ru=O moieties on the lone pair of phosphorus. Alternatively, a nucleophilic attack of the phosphorus lone pair on the empty Ru=O π^* -orbital, with the phosphorus atom coordinating to Ru, as suggested for O-atom transfer reactions with organic sulfides within non-porphyrin Ru=O systems,²² is also a possibility, but unlikely due to the steric constraints presented by the mesityl groups on TMP. Furthermore, the O-atom transfer appears to occur via strong Ru=O vibrational coupling, as reflected in the trend found for ΔS_1^\ddagger .

In contrast to the conclusions drawn for the thioether oxidations,⁵ a successive two O-atom transfer mechanism is not favoured for the phosphine systems. Rather, an initial O-atom transfer from Ru^{VI}(TMP)(O)₂, followed by a disproportionation reaction of the Ru(IV) formed to generate Ru(II) and Ru(VI), is favoured. This type of disproportionation is more consistent in explaining Ru(TMP) oxidation chemistry in general, for example, in alkene^{13,14} and alcohol oxidations (Chapter 4). Indeed, the thioether oxidations may also proceed via the same disproportionation mechanism as that for the phosphine oxidations; the reported kinetic data⁵ could equally well be rationalized in terms of the disproportionation mechanism, as discussed in Section 3.3.2.

References

- 1 R. A. Sheldon and J. K. Kochi, *Metal-Catalyzed Oxidations of Organic Compounds*, Academic Press, Toronto, 1981, p. 395.
- 2 R. H. Holm, *Chem. Rev.*, **87**, 1401 (1987).
- 3
 - a) B. A. Moyer, B. K. Sipe and T. J. Meyer, *Inorg. Chem.*, **20**, 1475 (1981).
 - b) A. Dovletoglou and T. J. Meyer, *J. Am. Chem. Soc.*, **116**, 215 (1994).
 - c) L. Roecker, J. C. Dobson, W. J. Vinning and T. J. Meyer, *Inorg. Chem.*, **26**, 779 (1987).
- 4 E. Lindner and M. Haustein, *Coord. Chem. Rev.*, in press.
- 5
 - a) N. Rajapakse, Ph. D. Dissertation, University of British Columbia, 1990.
 - b) N. Rajapakse, B. R. James and D. Dolphin, *Stud. Surf. Sci. Catal.*, **55**, 109 (1990).
- 6 J. T. Groves and K.-H. Ahn, *Inorg. Chem.*, **26**, 3831 (1987).
- 7 B. Borderie, D. Lavalire, G. Levy and J. C. Michaeu, *J. Chem. Ed.*, **67**, 459 (1990).
- 8 *Deuterated NMR Solvents-Handy Reference Data*, Merck and Co., Quebec, Canada, 1992.
- 9 F. A. Cotton and G. Wilkinson, *Advanced Inorganic Chemistry*, 5th edition, John Wiley and Sons, Toronto, 1988, p. 432.
- 10 C. D. Johnson, *The Hammett Equation*, Cambridge University Press, Chapter 1, 1973.
- 11 P. R. Wells, *Chem. Rev.*, **62**, 171 (1962).
- 12 R. Schutte, Ph. D. Dissertation, University of British Columbia, 1995.
- 13 C. Ho, W.-H. Leung and C.-M. Che, *J. Chem. Soc., Dalton Trans.*, 2933 (1991).
- 14
 - a) C. A. Tolman, *Chem. Rev.*, **77**, 313 (1977).
 - b) P. B. Dias, M. E. Minas de Piedale and J. A. Martinho Simões, *Coord. Chem. Rev.*, **135/136**, 737 (1994).
- 15 J. T. Groves and R. Quinn, *J. Am. Chem. Soc.*, **107**, 5790 (1985).

- 16 J. T. Groves and J. S. Roman, *J. Am. Chem. Soc.*, **117**, 5594 (1995).
- 17 a) D. T. T. Yapp, J. Jaswal, S. J. Rettig, B. R. James and K. A. Skov, *Inorg. Chim. Acta.*, **177**, 199 (1990).
b) D. T. T. Yapp, J. Jaswal, S. J. Rettig, B. R. James and K. A. Skov, *J. Chem. Soc., Chem. Commun.*, 1528 (1992).
- 18 C. Sishta, M. J. Camenzind, B. R. James and D. Dolphin, *Inorg. Chem.*, **26**, 1181 (1987).
- 19 S. Y. S. Cheng, N. Rajapakse, S. J. Rettig and B. R. James, *J. Chem. Soc., Chem. Commun.*, 2669 (1994).
- 20 H. E. Avery, *Basic Reaction Kinetics and Mechanisms*, Macmillan Education, London, 1974, p. 66.
- 21 G. M. Barrow, *Physical Chemistry*, 4th Edition, McGraw-Hill, Toronto, 1979, p. 228.
- 22 D. G. Lee and H. Gai, *Can. J. Chem.*, **73**, 49 (1995).

Chapter 4

Catalytic Aerobic Oxidation of Alcohols and Alkanes

4.1 Introduction

The recent developments in the use of ruthenium complexes in the oxidation of saturated hydrocarbons were discussed in Chapter 1. Most of the complexes discussed were represented by examples from non-porphyrin oxoruthenium species.¹ Attention is now turned to the discussion of the oxidation of alcohols and alkanes catalyzed by dioxoruthenium(VI) complexes containing porphyrin ligands that were studied in the present thesis.

Work carried out as a part of this thesis led to the development of a ruthenium porphyrin-based system exhibiting remarkable activity for the catalytic aerobic oxidation of alcohols. The complexes Ru^{VI}(porp)(O)₂ [porp = TMP (**1a**) and TDCPP (**1b**)] catalyzed the aerobic oxidation of primary and secondary alcohols to the corresponding aldehydes and ketones, respectively, under mild conditions. An intermediate in the oxidation of PrOH to acetone was identified to be a bis(alkoxo)ruthenium(IV) species, Ru^{IV}(TMP)(O'Pr)₂ (**2a**), which was characterized crystallographically.² To the best of the author's knowledge, this represents the first structurally characterized, monomeric alkoxo complex of ruthenium porphyrins; the results clarify earlier proposals by this group³ and others⁴ that the intermediate was possibly the bis(hydroxo) species, Ru^{IV}(TMP)(OH)₂.

The ability of some dioxoruthenium porphyrins⁵ similar to (**1a**) and non-porphyrin oxoruthenium species⁶ to hydroxylate tertiary alkanes stoichiometrically prompted further studies on (**1a**) and (**1b**) in their abilities to oxidize alkanes. Species (**1a**) catalyzes the aerobic oxidation of Ph₃CH to Ph₃COH, while species (**1b**) [but not (**1a**)] also catalyzes the aerobic oxidation of adamantine to 1-adamantanol, although the rates were slow and

the overall turnovers were low. The question regarding whether (**1a**) or (**1b**) can oxidize alkanes; either stoichiometrically or catalytically, has been raised,^{3b} and the catalytic aerobic oxidation of the above tertiary alkanes clearly answers that question, as well as demonstrating some significant chemistry within these ruthenium porphyrin systems.

4.1.1 Scope of Alcohol Oxidations in Current Work

As mentioned, the nature of the intermediate in the stoichiometric oxidation of ⁱPrOH by Ru^{VI}(TMP)(O)₂ (**1a**), tentatively proposed in previous studies to be Ru^{IV}(TMP)(OH)₂,^{3,4} was unresolved, and it was the initial goal to establish its identity. Also, it was hoped that a better understanding of the oxidation mechanism could be realized through kinetic studies and deuterium-isotope labeling experiments. Furthermore, in the initial thesis work the Ru^{VI}(TMP)(O)₂/ⁱPrOH system was found to be marginally catalytic under 1 atm air (Section 4.3), and thus a considerable effort was devoted to enhance the lifetime and reactivity of the catalyst.

4.2 Sample Preparation and Data Analysis

4.2.1 Sample Preparation

The kinetics for the stoichiometric oxidation of ⁱPrOH and benzyl alcohol were followed by ¹H-NMR spectroscopy. In typical experiments, solutions of (**1a**) (made from the aerobic oxidation of Ru^{II}(TMP)(MeCN)₂, Chapter 2), 1 to 5 x 10⁻⁴ M in benzene-*d*₆ (0.30 to 0.40 mL), were purged with Ar for 30 min. During this time, the NMR probe was preset at the desired temperature, between 18 and 35 °C. At the end of this time,

¹PrOH or benzyl alcohol, dried over molecular sieves (5 Å, BDH), was injected (1 to 5 µL) into the benzene-*d*₆ solution, with resulting concentrations of the alcohol between 10⁻² and 10⁻¹ M.

The catalytic aerobic oxidations of ¹PrOH and benzyl alcohol were generally carried out at 24 or 50 °C (\pm 2) under 1 atm air. Typical solutions of (1a) 10⁻⁴ to 10⁻³ M in benzene-*d*₆ (0.40 mL) were prepared, and the alcohols were added via syringe (Unimetrics), with resulting concentrations between 10⁻² and 10⁻¹ M. The conversions of the alcohols to the ketone or aldehyde were monitored periodically (usually between 24 h intervals) by ¹H-NMR spectroscopy, with the relative amounts of the reactant to product determined from the integration intensities of Me₂CHOH (¹PrOH), Me₂CO (acetone), PhCH₂OH (benzyl alcohol) and PhCHO (benzaldehyde) at 3.68, 1.58, 4.31 and 9.62 ppm, respectively.

In gas chromatography experiments, the aerobic oxidations of benzyl alcohol and 1-phenylethanol were carried out at 50 °C under 1 atm air. Benzene solutions (0.40 mL) of (1a) or (1b) [see Chapter 2 for the preparation of (1a) or (b)] in the concentration range between 10⁻⁶ and 10⁻⁴ M were prepared in screw-capped glass vials. The caps were lined with Teflon tape to ensure that the benzene did not evaporate. The vials then were immersed in an oil-bath, which was maintained at a temperature of 50 \pm 2 °C. At the end of approximately every 24 h, a sample (1 to 2 µL) of the solution was withdrawn and analyzed by a gas chromatograph to determine the total turnover number. The retention times of the various substrates and the column conditions of the GC runs are tabulated in Section 2.2.5, Table 2.1.

For the above catalysis studies, the deuterated and non-deuterated benzene solvents were not dried and were used directly from the bottle. The concentration of H₂O in benzene-d₆ directly from the bottle that has not been pre-dried was determined to be approximately 4×10^{-3} M from the ¹H-NMR spectra using MeCN as the standard. The concentration of H₂O in benzene directly from the bottle was assumed to be of the same order of magnitude as in benzene-d₆. H₂O saturated benzene-d₆ (with H₂O/benzene-d₆ as a two-phase system) was found to have a water concentration of 1.0×10^{-2} M in the organic phase. In both the NMR and GC catalysis experiments, no additional water, 50 μ L water, or 50 μ L 3.0 M aqueous KOH was added to the benzene or benzene-d₆ solutions.

The catalytic hydroxylations of Ph₃CH by (**1a**) and Ph₃CH and adamantane by (**1b**) were studied in benzene solutions at 24 ± 2 °C under 1 atm air in the same type of vials that were used for the catalytic oxidation of alcohols. Complex (**1a**) [1.2×10^{-4} M in 0.40 mL benzene generated from the bis(acetonitrile) precursor] was prepared and 50 μ L 0.026 M Ph₃CH in benzene solution was added to the solution of (**1a**). The resulting excess of alkane over (**1a**) was 29-fold. Complex (**1b**) (2.4×10^{-4} M in benzene) was prepared by the *m*-CPBA oxidation of Ru^{II}(TDCPP)(CO) (Chapter 2). 25 μ L of 0.10 M adamantane in benzene was added to 0.40 mL of benzene solution containing (**1b**), giving rise to a 26-fold excess of alkane over (**1b**). 25 μ L of 0.074 M Ph₃CH in benzene was added to 0.40 mL benzene solution containing (**1b**), giving rise to a 19.4-fold excess of alkane over (**1b**).

X-ray quality crystals of Ru^{IV}(TMP)(O*i*Pr)₂ (**2a**) and Ru^{IV}(TMP)(O*i*CH(CH₂Cl)₂)₂ (**2b**) were obtained from concentrated benzene-d₆ solutions that were used for ¹H-NMR

analyses of the stoichiometric oxidations of the $^i\text{PrOH}$ and 1,3-dichloro-2-propanol substrates. Extended evacuation of these solutions to dryness at ambient temperatures yielded crystals suitable for X-ray diffraction.

4.2.2 Data Acquisition and Analysis

The kinetics of the stoichiometric oxidations of $^i\text{PrOH}$ and benzyl alcohol under 1 atm Ar were followed by the integrations of the *para*-methyl protons of (**1a**) and the product $\text{Ru}^{\text{IV}}(\text{TMP})(\text{O}^i\text{Pr})_2$ (**2a**) or $\text{Ru}^{\text{IV}}(\text{TMP})(\text{OCH}_2\text{Ph})_2$ (**2c**), respectively. The combined integrations of (**1a**) and (**2a**) or (**2c**) were normalized to 100%, since no porphyrin intermediates[†] were observed by NMR, ESR or UV-visible spectroscopies. The natural logarithm of the mole fraction of (**1a**), $\ln(X_{1a})$, was plotted versus time. For the $^i\text{PrOH}$ oxidations, the half-lives were 3 to 4 h in typical experiments, and it was practical to follow only one of the reactions for more than three half-lives to establish first-order dependence in (**1a**) (see Figure 4.1). Subsequent reactions, where the concentrations for both (**1a**) and $^i\text{PrOH}$ or benzyl alcohol were systematically varied (Appendix C), were monitored only for 1 to 2 h. Of note, $^1\text{H-NMR}$ spectroscopy, rather than UV-visible spectroscopy, was chosen as the method to follow the kinetics for the stoichiometric oxidation of alcohols, because the concentration of (**1a**) in UV-visible experiments is $\sim 10^{-6}$ M. The alcohol oxidations become catalytic in the presence of O_2 , and removing O_2

[†] i) Species (**1a**) and (**2a**) were the only ones observed in solution during the reaction, as monitored by $^1\text{H-NMR}$ spectroscopy. ii) A frozen benzene- d_6 solution of “(**1a**) + $^i\text{PrOH}$ ” under Ar at 110 K showed no ESR signals (see later). iii) Previous work (Ref. 3) followed the conversion of (**1a**) to (**2a**) by UV-visible spectroscopy in benzene, and the set of spectra showed isosbestic points, suggesting that (**1a**) and (**2a**) are the dominant species in solution.

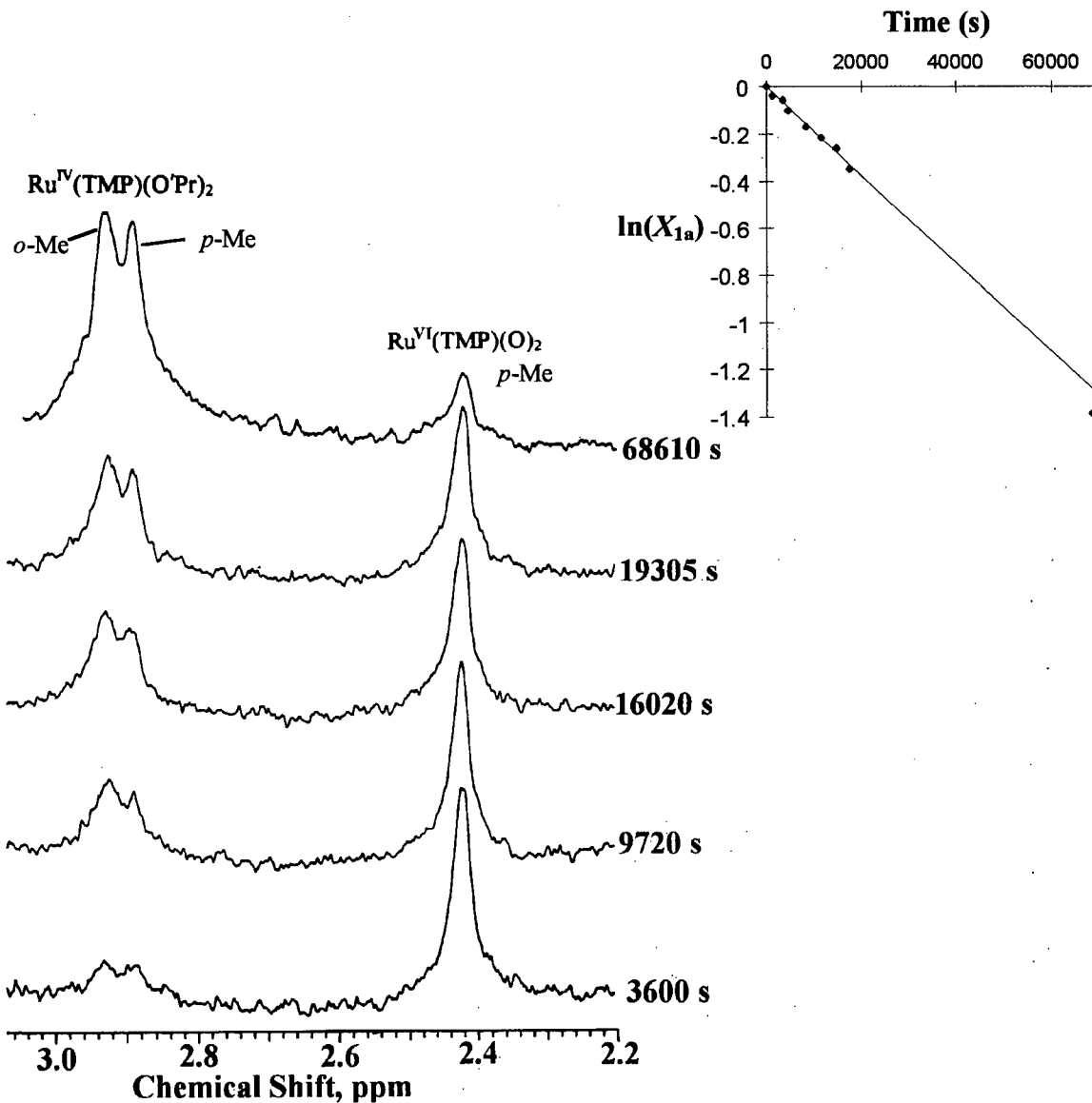


Figure 4.1. The kinetics of the stoichiometric oxidation of ¹PrOH by Ru^{VI}(TMP)(O)₂, (**1a**), in benzene-*d*₆ under 1 atm Ar at 18.2 °C followed by ¹H-NMR spectroscopy (300 MHz) in the 2 to 3 ppm region. Inset shows the plot of $\ln(X_{1a})$ versus time (X_{1a} = mole fraction of starting porphyrin (**1a**) = $\text{Int}_{p\text{-Me}(\text{Ru(VI)})}/[\text{Int}_{p\text{-Me}(\text{Ru(VI)})} + 1/3 \text{ Int}_{p+o\text{-Me}(\text{Ru(IV)})}]$), the slope of which gives the pseudo-first -order rate constant, k_{obs} . [**1a**] = 4.0×10^{-4} M; [¹PrOH] = 0.0568 M.

to the extent that it becomes less than 10^{-6} M, such that (**1a**) does not regenerate, is not feasible.

The catalytic oxidations of $^3\text{PrOH}$ and benzyl alcohol were followed by $^1\text{H-NMR}$ spectroscopy and GC analysis, with results in agreement. The products of oxidation were solely acetone and benzaldehyde, respectively; benzaldehyde was not further oxidized to benzoic acid under the conditions described in Section 4.2.1. In both $^1\text{H-NMR}$ and GC experiments, the identities of the products were determined with the use of known standards. The combined integrations of the alcohols and products were normalized to 100%, and subsequently the percentage conversions were calculated. Knowledge of the initial ratios of substrates to the catalyst (**1a**) or (**1b**) allowed the catalytic turnovers to be determined as the reactions progressed.

The catalytic hydroxylations of adamantane to 1-adamantanol and Ph_3CH to Ph_3COH by (**1a**) and (**1b**) in benzene were followed by GC analysis. The retention times of the solutes were determined from authentic samples of the starting alkanes and alcohol products (Chapter 2, Table 2.1). The response factors of adamantane and 1-adamantanol to the FID detector were proportional to the molar concentrations of the analyte. The same also applies to the $\text{Ph}_3\text{CH}/\text{Ph}_3\text{COH}$, benzyl alcohol/benzaldehyde and 1-phenylethanol/acetophenone systems. In the GC analyses, the starting alkanes and tertiary alcohol products accounted for all the organics present, and thus the conversions were calculated based on the relative intensity of the alkane and alcohol signals.

The kinetic data for the stoichiometric oxidation of $^3\text{PrOH}$ and benzyl alcohol by (**1a**) are tabulated in Appendix C. The data from the catalytic oxidation of benzyl alcohol

are also tabulated in Appendix C. The alkane hydroxylation data can also be found in Appendix C. The supplementary data for the crystal structures of (**2a**) and (**2b**) are given in Appendix D.

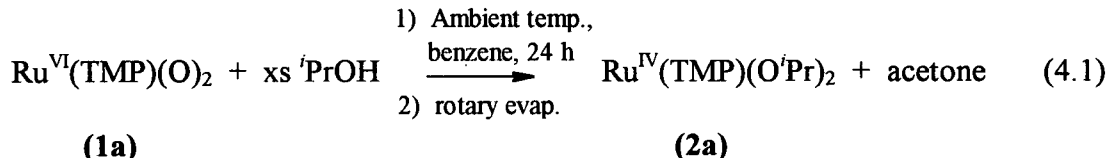
4.3 Stoichiometric Oxidation of Alcohols by Oxo Ruthenium Species

Kinetic and mechanistic studies on the stoichiometric oxidation of alcohols by monooxoruthenium(IV) and dioxoruthenium(VI) complexes have been reported, mainly by the groups of Meyer,⁷ Lee,⁸ Griffith¹ and Che^{6a,9,15}. Nonetheless, further detailed kinetic and mechanistic studies on the oxidation of alcohols by oxoruthenium complexes are invaluable in order to understand better such oxidations in general; this can aid in the design of better oxidation catalysts. Further, the Ru-porphyrin catalysts reported in this thesis are the first to utilize effectively O₂ as the oxidant in alcohol oxidations.

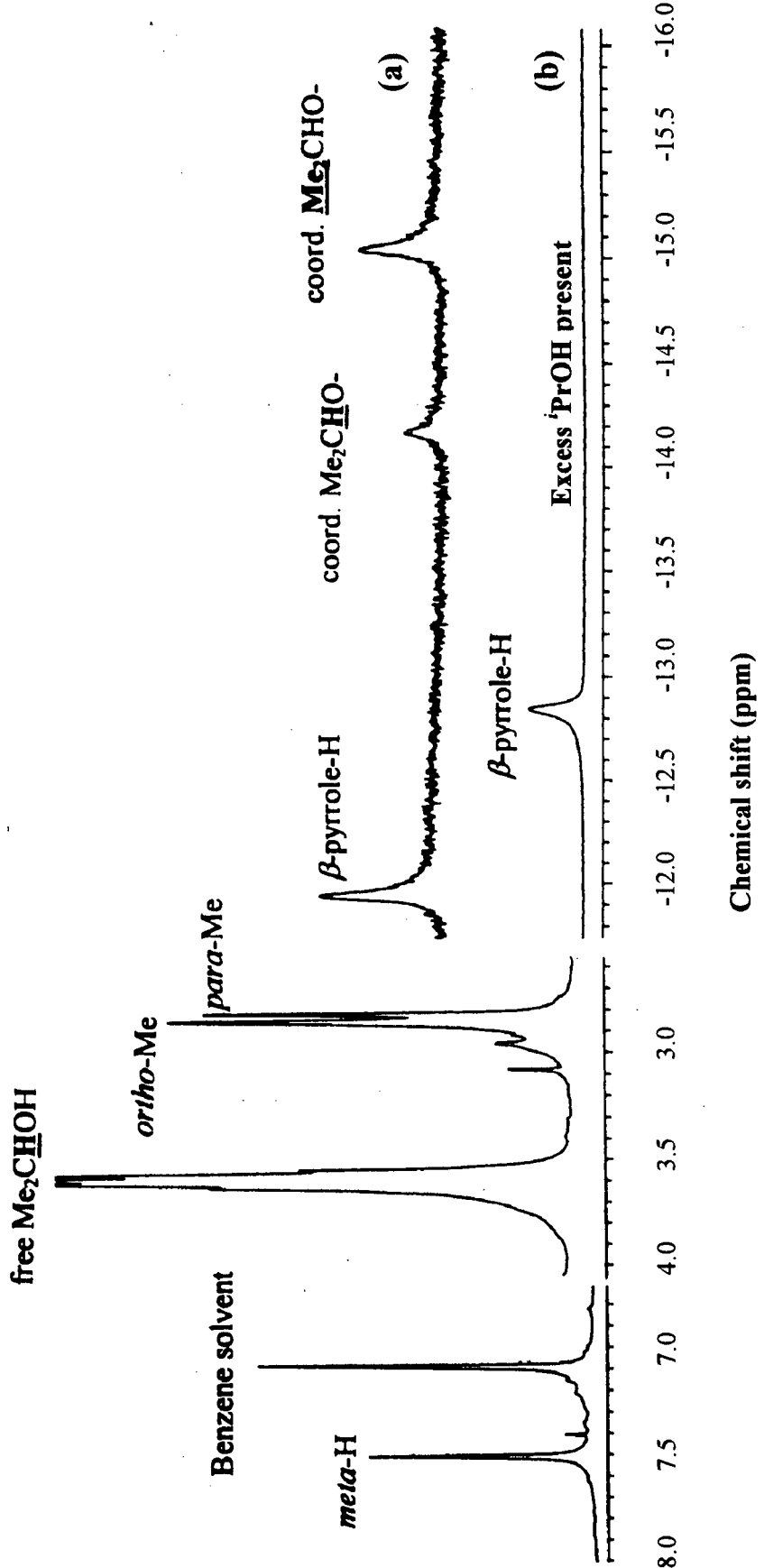
4.3.1 Bis(alkoxo)porphyrinatoruthenium(IV) Species

The kinetic studies on the stoichiometric oxidation of ⁱPrOH to acetone and benzyl alcohol to benzaldehyde by (**1a**) were studied, and the proposed mechanism will be discussed in the next section. The metalloporphyrin products in these alcohol oxidations were the corresponding bis(alkoxo) species, Ru^{IV}(TMP)(OR)₂ [R = ⁱPr (**2a**) or CH₂Ph (**2c**)]. For the stoichiometric oxidation of ⁱPrOH by (**1a**), the Ru-porphyrin product proposed from preliminary work in this laboratory was Ru^{IV}(TMP)(OH)₂, the underlying reason being mainly the non-detection of axial ⁱPrO ligand protons by ¹H-NMR.

spectroscopy.³ This proposal now seems incorrect. Previously in this laboratory,^{3a} (**2a**) was prepared following the scheme represented in Eq. 4.1 (not balanced).



In the earlier work,^{3a} the removal of solvent and excess ¹PrOH by rotary evaporation gave a compound, the elemental analysis (C 68.87; H 5.76; N 5.55%) corresponding neither to that calculated for Ru^{IV}(TMP)(OⁱPr)₂ (C 74.45; H 6.65; N 5.60%)^{3a} nor Ru^{IV}(TMP)(OH)₂ (C 73.42; H 5.94; N 6.12%); however, the non-detection of the axial ligand protons and magnetic susceptibility measurement³ ($\mu_{\text{eff}} = 2.96 \mu_B$; S = 1) favoured the formulation of **(2a)** as Ru^{IV}(TMP)(OH)₂ at the time. In the present thesis work, the preparation of **(2a)** in an NMR tube from which the solvent and excess ¹PrOH were removed completely under vacuum overnight gave a ¹H-NMR spectrum that showed the chemical shifts for the axial ¹PrO ligand protons (Figure 4.2). Heating the sample (> 100 °C) under vacuum to remove the solvent and ¹PrOH led to decomposition of the complex, while pumping under vacuum at a lower temperature was not always effective in removing all of the ¹PrOH (see also Section 4.3.3). A satisfactory elemental analysis of **(2a)** still is not obtained, presumably due to the above-mentioned difficulties; however, the fact that the axial ligands were alkoxo, and not hydroxo, was shown unambiguously through the X-ray structural analyses of **(2a)** and its bis(1,3-dichloro-2-propoxo) analogue **(2b)**. Thus, the earlier incorrect proposals from this group³ and others⁴ that Ru^{IV}(TMP)(OH)₂ existed in the presence of excess alcohol were clarified.

**Figure 4.2.**

$^1\text{H-NMR}$ (300 MHz) spectra of $\text{Ru}^{\text{IV}}(\text{TMP})(\text{O}'\text{Pr})_2$ (**2a**) with (b) and without (a) excess $^{\prime}\text{PrOH}$. The ^1H -chemical shifts for the axial $^{\prime}\text{PrO}$ ligands were observed when the excess PrOH was removed by pumping under vacuum over extended periods of time (see text). The β -pyrrole ^1H -resonances are not at exactly the same chemical shift, presumably due to the slightly different temperatures at which the spectra were obtained (at room temperature). Ref. 3a contains $^1\text{H-NMR}$ data for (**2a**) between -60 and +60 $^{\circ}\text{C}$.

Of note, the TDCPP analogue, Ru^{IV}(TDCPP)(OH)₂, recently has been characterized crystallographically (see Section 4.3.3).

X-ray analyses of (**2a**) and (**2b**) revealed structures with inversion centres, with the Ru-atom being essentially octahedral, sitting in the centre of the porphyrin plane with coordinated axial 'PrO or 1,3-dichloro-2-propoxo ligands (Figures 4.3 and 4.4). The tetramesityl groups on the porphyrin ring are perpendicular to the porphyrin plane and the Ru(TMP) moiety essentially has the same dimensions as those found in Ru^{II}(TMP)(MeCN)₂.³ There are no significant non-bonding interactions between the axial alkoxo ligand and the porphyrin in either (**2a**) or (**2b**) less than 3.6 Å (see Appendix D).

The crystal structures of (**2a**) and (**2b**), even though exhibiting disorder about the axial ligands due to high thermal motion, unambiguously show the complexes to contain axial alkoxo ligands. In terms of the Ru-O distances, 1.892(3) Å in (**2a**) and 1.905(6) Å in (**2b**), these values lie within the range found for similar Ru(IV)-porphyrin complexes [1.929(9) Å within Ru^{IV}(TMP)(OEt)₂[†] and 1.944 Å within the coordinated *para*-cresol for [Ru^{IV}(TPP)(*p*-OC₆H₄Me)]₂O,¹⁰ although the latter is a Ru(IV) diamagnetic species]. On the other hand, the average Ru(III)-O bond length for the coordinated ethanol/ethoxo in Ru^{III}(OEP)(OEt)(EtOH) is longer at 2.019 Å.¹¹ The marginally longer Ru-O bond length in (**2b**) over that in (**2a**) is presumably due to the inductive electron-withdrawing effect of the two chlorine atoms, which reduces the extent of π -backbonding from the oxygen to the ruthenium. Such backbonding is evident in the large Ru-O-C bond angles

[†] The axial ligand was unidentified due to severe disorder in the axial ligands, but the axial ligand was most likely ethoxo. See Reference 4.

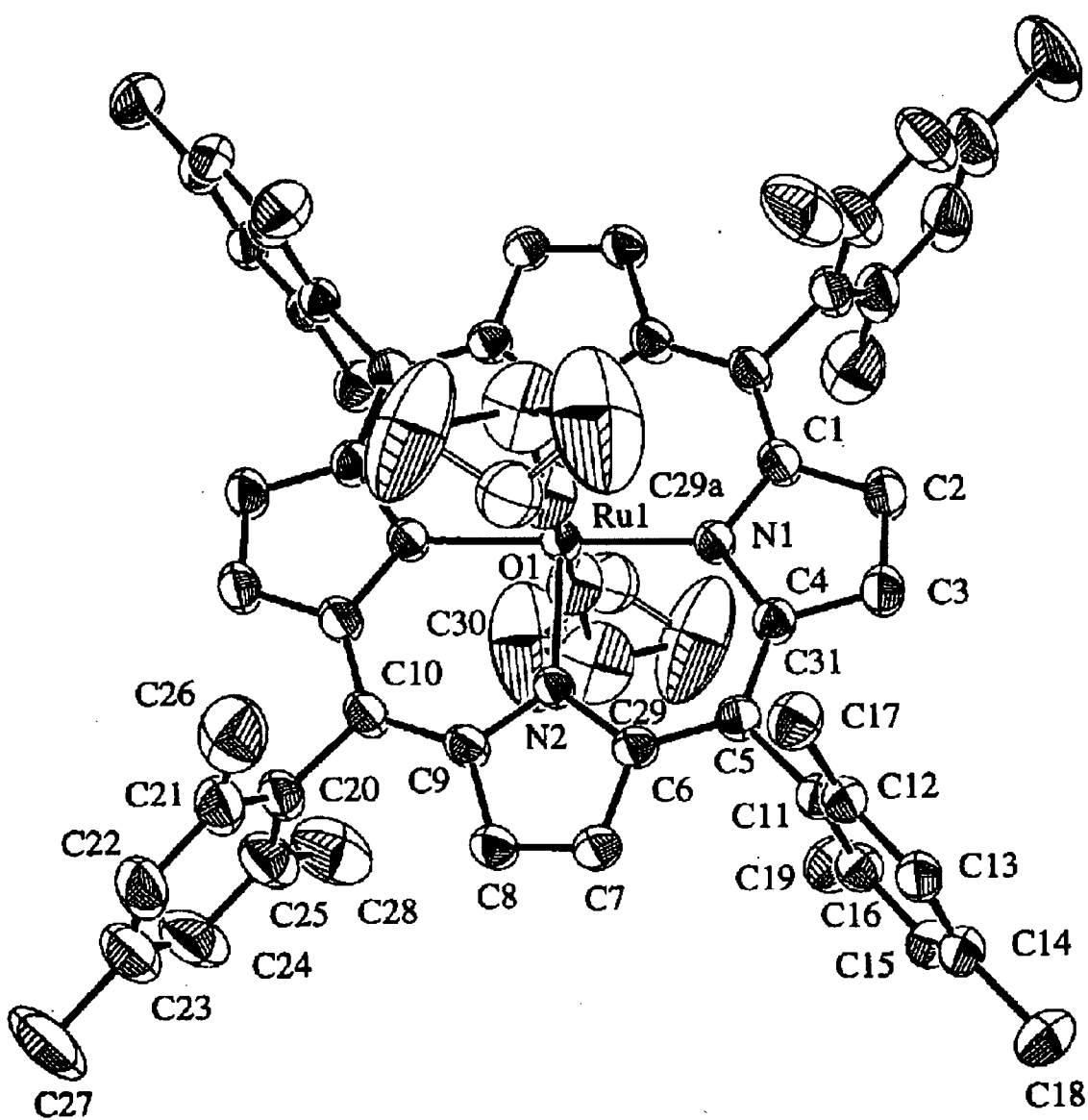


Figure 4.3. The structure of Ru^{IV}(TMP)(O'Pr)₂ (**2a**) (H-atoms omitted for clarity). Selected bond lengths (Å) and angles (°): Ru-O(1) 1.892(3), av. Ru-N 2.033, O(1)-C(29a) 1.18(3), O(1)-C(29) 1.34(1), C(29)-C(31) 1.55(2), C(29a)-C(31) 1.47(3), C(29)-C(30) 1.56(1), C(29a)-C(30) 1.66(3); Ru-O(1)-C(29) 139.7(5), Ru-O(1)-C(29a) 155(1), O(1)-C(29)-C(31) 103(1), O(1)-C(29)-C(30) 100(1), O(1)-C(29a)-C(30) 101(1), O(1)-C(29a)-C(31) 117(2). At the Ru, all *cis*-angles are $90 \pm 1.2^\circ$. Additional crystallographic data can be found in Appendix D.

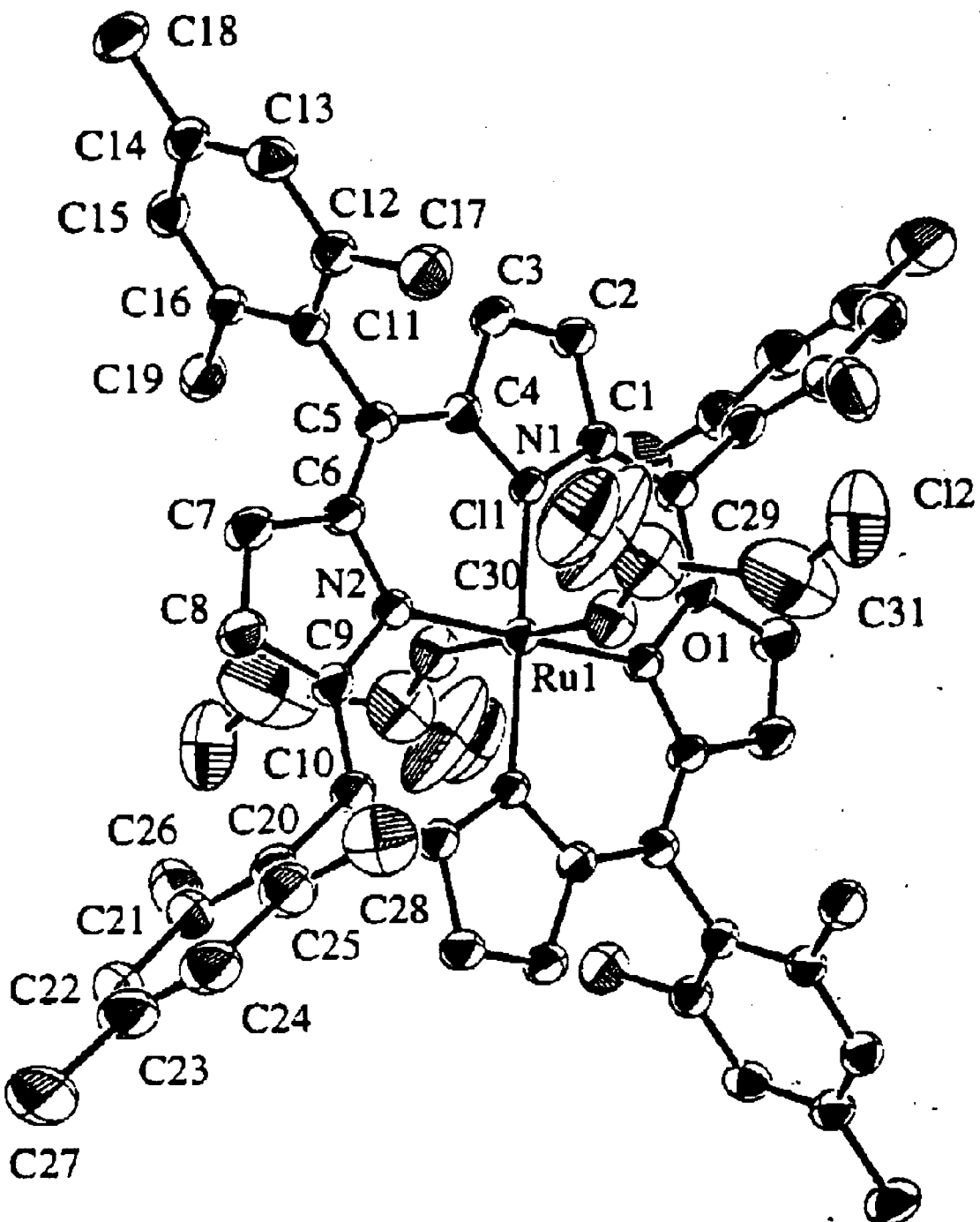


Figure 4.4. The structure of $\text{Ru}^{\text{IV}}(\text{TMP})(\text{OCH}(\text{CH}_2\text{Cl})_2)_2$ (**2b**) (H-atoms omitted for clarity). Selected bond lengths (Å) and angles (°). Ru-O(1) 1.905(6), Ru-N(av.) 2.036; Ru-O(1)-C(29) 146(1), Ru-O(1)-C(29a) 150(2). Additional crystallographic data can be found in Appendix D.

of 139.7 and 155° in (**2a**) and 146 and 151° in (**2b**), and in both complexes the bond angles deviate significantly from the ideal value of a sp_3 hybrid expected at the O-atom of the alkoxo ligand. Unfortunately, the disorder problem precludes any direct comparison between the bond angles of (**2a**) and (**2b**), and masks the information pertaining to the difference in degree of backbonding as a result of the two chlorines.

The ability of Ru^{VI}(TMP)(O)₂ (**1a**) to oxidize alcohols was tested with some primary and secondary alcohols, and the spectroscopic evidence suggests that the Ru-porphyrin intermediates are the corresponding bis(alkoxo) species, Ru^{IV}(TMP)(OR)₂ (see later, Table 4.1). The products of the stoichiometric oxidation of these alcohols are aldehydes or ketones, and the reactions are most likely general for any primary or secondary alcohol, although the methanal and ethanal products from the oxidations of MeOH and EtOH, respectively, are not identified by ¹H-NMR spectroscopy, as the characteristic aldehyde ¹H-resonances for the two aldehyde products are not observed. The non-detection of the methanal and ethanal products is likely due to polymer formation, which is known to occur with these aldehydes,¹¹ and as the stoichiometries of the ¹PrOH and benzyl alcohol oxidations have been established (see Section 4.3.2), no further attempts were made to detect the methanal and ethanal products.

The ¹H-NMR chemical shifts of various Ru^{IV}(TMP)(OR)₂ species are reported in Table 4.1. These Ru^{IV}(TMP)(OR)₂ species [R = Me, Et, ¹Pr, 1-Pr, PhCH₂, (CH₂Cl)₂CH, PhCH(Me)] were observed *in situ* in benzene-*d*₆ under 1 atm Ar in ¹H-NMR studies when the corresponding primary and secondary alcohols were oxidized by (**1a**) to the aldehyde and ketone, respectively. The data for these Ru^{IV}(TMP)(OR)₂ species are entirely consistent with Ru(IV) species possessing D_{4h} symmetry, as all known Ru^{IV}(TMP)(X)₂

Table 4.1 ^1H -NMR data^a for *trans*-Ru^{IV}(TMP)(OR)₂ species.

OR ^b =	<i>meta</i> -H ^c	<i>para</i> -Me	<i>ortho</i> -Me ^d	pyrrole-H
O <i>i</i> Pr (2a) ^e	7.52	2.85	2.90	-11.95
1,3-dichloropropoxo (2b)	7.69	not observed ^f		-28.8
OMe	7.40	2.93	2.70	-21.8
OEt ^g	7.40	2.85	2.76	-17.6
1-PrO	7.49	2.78	2.93	-16.4
benzoxo (2c)	7.48	2.74	2.92	-20.6
1-phenylethoxo ^h	7.66, 7.60	2.91, 2.83	3.00, 2.96	-19.4
phenoxy ^{i,k}	7.63	3.00	2.90	-30.5
<i>para</i> -OC ₆ H ₄ OH ^{j,k}	7.63	3.00	2.90	-30.45

^a Chemical shifts, δ ppm, in benzene-*d*₆ relative to TMS at \sim 25 °C.

^b These bis(alkoxo) species are typically generated *in situ* by the addition of corresponding excess alcohol (1.0×10^{-2} M) to (**1a**) ($\sim 5.0 \times 10^{-4}$ M) under 1 atm Ar in benzene-*d*₆. Excess alcohol is present, which generally leads to exchange broadening and non-observance of axial ligand protons. Extended heating under (~ 100 °C) vacuum can remove all the alcohol, but this leads to decomposition of the complex as well (see text). Axial ligand ^1H -chemical shifts are reported if observed.

^c Single *meta*-H peak indicates a D_{4h} symmetry about the porphyrin plane.

^d Single *meta*-Me peak indicates a D_{4h} symmetry about the porphyrin plane.

^e Axial ligand protons observed after removal of excess $^i\text{PrOH}$: -OCH₂, 2H, -14.22; CH(CH₃)₂, 12 H, -15.2.

^f The ^1H -chemical shifts for the free alcohol are in the \sim 3 ppm range and overlap with those for the bis(alkoxo) complex.

^g Ligand protons observed after removal of excess EtOH: -OCH₂, 4H, -7.48; -CH₃, 6H, -12.90.

^h Racemic 1-phenylethanol was used, leading to a mixture of 3 isomers: a 1:1 enantiomeric mixture of Ru(TMP)(OR^R)(OR^R) and Ru(TMP)(OR^S)(OR^S) accounts for 50%; Ru(TMP)(OR^S)(OR^R) accounts for the other 50%. Two sets of axial ligand ^1H -chemical shifts, unassigned, are observed (excess alcohol not removed) in the NMR spectra of the solution containing the above set of compounds: -18.9 and -18.4; 7.91 and 8.02; 15.2 and 13.9.

ⁱ Generated *in situ* in benzene-*d*₆ under 1 atm Ar from “(**2a**) + excess phenol” (see text). Axial ligand protons (excess phenol not removed): *para*-H, 2H, -71.9; *ortho*-H, 4H, -68.2; *meta*-H, 4 H, 49.7.

^j Axial ligand protons: *para*-OH, 2H, -71.85; *ortho*-H, 4H, -68.19; *meta*-H, 4 H, 49.68 (Ref. 3).

^k The bis(*p*-hydroquinoxo) complex has been incorrectly assigned as such (Ref. 3) and is in fact the bis(phenoxy) complex (see Section 6.4.1).

species belonging to the D_{4h} point group exhibit single *meta*-H and *ortho*-Me signals.^{3,4,12}

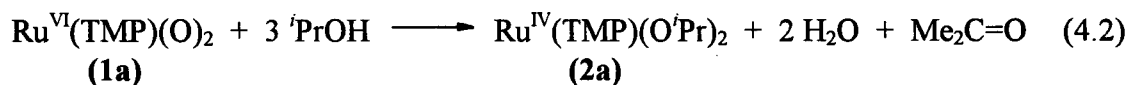
Previously in this laboratory, the ^1H -chemical shifts for the bis(isopropoxo) and bis(phenoxo) species have been measured between -60 and +60 °C.^{3a} The isotropic ^1H -chemical shifts for the TMP ligand within these paramagnetic Ru(IV) species, and also within other paramagnetic $\text{Ru}^{\text{IV}}(\text{TMP})(\text{X})_2$ species^{4,12} ($\text{X} = \text{Cl}$ and Br), vary with inverse temperature, showing the existence of a single spin state over this temperature range. The paramagnetic nature of the $\text{Ru}^{\text{IV}}(\text{TMP})(\text{OR})_2$ complexes suggests bonding similar to that found in $\text{Ru}(\text{porp})(\text{X})_2$ species ($\text{X} = \text{Cl}$, Br), which accommodate two unpaired electrons in a closely spaced t_{2g} set (with either d_{xy} or $d_{xz,yz}$ being lowest in energy).¹²

Among the complexes listed in Table 4.1, only the protons of the axial EtO, ^1PrO , 1-phenylethoxo, and phenoxo ligands within the $\text{Ru}^{\text{IV}}(\text{TMP})(\text{OR})_2$ species are observed by $^1\text{H-NMR}$ spectroscopy. In general, the alkoxo ligands exchange readily with the corresponding alcohol in solution, leading to line-broadening in the $^1\text{H-NMR}$ spectra and undetectable axial ligand chemical shifts, although the 1-phenylethoxo and phenoxo ligands could be detected even in the presence of the corresponding alcohols. The increased steric bulk of the 1-phenylethoxo ligand perhaps slows the rate of exchange, while for the phenoxo ligands, the slow exchange may be due to steric as well as possible electronic effects of the aromatic ring. The exchangeability of the ^1PrO ligands was used to prepare the bis(phenoxo) analogue *in situ*. Phenol (~ 50-fold excess) was added to an Ar-purged benzene- d_6 solution of (2a) (~ 5×10^{-4} M). Within the time required to acquire a $^1\text{H-NMR}$ spectrum (~15 min), quantitative axial ligand exchange, with the liberation of free $^1\text{PrOH}$, was observed, with no trace of (2a). Of note, the product from the above-

mentioned phenol exchange shows ^1H -resonances nearly identical to those of a complex previously proposed to be $\text{Ru}^{\text{IV}}(\text{TMP})(p\text{-OC}_6\text{H}_4\text{OH})_2$ (Table 4.1);³ the significance of this will be discussed in Chapter 6. The exchange of the ^iPrO ligands with alcohol in solution was observed readily when (**2a**) ($\sim 10^{-6}$ M) was dissolved in benzene containing $\sim 10^{-3}$ M EtOH or MeOH; almost instantaneous shifts (within seconds) of the Soret band of (**2a**) from 412 to 408 and 406 nm were observed, respectively, indicating formation of the different $\text{Ru}^{\text{IV}}(\text{TMP})(\text{OR})_2$ species in solution. The UV-visible data for these $\text{Ru}^{\text{IV}}(\text{TMP})(\text{OR})_2$ species in benzene are [$\lambda_{\text{max}}/\text{nm}$ ($\epsilon/10^{-3}\text{ M}^{-1}\text{cm}^{-1}$)]: R = ^iPr , 412 (240), 522(29.0); R = Et, 408(230), 520(25.4); R = Me, 406(200), 520(26.7).

4.3.2 Mechanism of Alcohol Oxidation by $\text{Ru}^{\text{VI}}(\text{TMP})(\text{O})_2$

Previous work in this laboratory,³ in addition to the knowledge from the crystallographic structure of the metalloporphyrin product (**2a**) from the $^i\text{PrOH}$ oxidation, allow the overall stoichiometry of the oxidation reaction to be established (Eq. 4.2). One equivalent of acetone and two equivalents of water^{3a} were observed by $^1\text{H-NMR}$ spectroscopy upon complete formation of (**2a**).



The oxidation of benzyl alcohol presumably follows the same stoichiometry as that for $^i\text{PrOH}$; again, one equivalent of benzaldehyde was observed by $^1\text{H-NMR}$ spectroscopy, although no special precautions were taken to remove all the water from the system, and the water stoichiometry was assumed to be the same as in Eq. 4.2. Thus (**1a**)

in reaction 4.2 is an overall two-electron oxidant, similar to other oxoruthenium(VI or IV) complexes.^{5-9,13,15}

The kinetics of ¹PrOH oxidation by (**1a**) under 1 atm Ar showed a first-order dependence in (**1a**) (see Figure 4.1 in Section 4.2.2). The first-order dependence was also assured, as the kinetics monitored for [¹PrOH] = 0.218 M were independent of [(**1a**)] (2.0 vs. 4.0×10^{-4} M; see Appendix C). Under pseudo-first-order conditions at about 18 °C, the ¹PrOH dependence is first-order at [¹PrOH] values below 0.3 M (Figures 4.5). In this linear range, the use of ¹PrOD-*d*₈ showed that a kinetic isotope effect of 1.9 ± 0.3 is exhibited at the α -C-H bond, while the use of ¹PrOD gave no kinetic isotope effect. The k_{obs} versus [¹PrOH] plot for the oxidation of ¹PrOH by (**1a**) tends to level-off at [¹PrOH] values beyond 0.4 M (see later); that is, the oxidation of ¹PrOH by (**1a**) exhibits saturation kinetics as the concentration of ¹PrOH increases. The oxidation of benzyl alcohol by (**1a**) is more rapid; the concentration range studied (Figure 4.6) is lower than that for ¹PrOH, and there is no obvious fall-off of k_{obs} from a first-order dependence on [benzyl alcohol].

Regarding the non-linear k_{obs} versus [¹PrOH] plot (Figure 4.5), the phenomenon is likely due to solvent effects. Addition of an inert alcohol, ¹BuOH, to simulate the high ¹PrOH content, slows the rate of oxidation of ¹PrOH by (**1a**). At 18.2 °C with [¹PrOH] = 0.130 M, the k_{obs} value for the ¹PrOH oxidation is $(4.2 \pm 0.5) \times 10^{-5} \text{ s}^{-1}$. At the same value of [¹PrOH], but with [¹BuOH] = 0.177 and 0.530 M, $k_{\text{obs}} = (9.2 \pm 0.7) \times 10^{-6} \text{ s}^{-1}$ and $(3.6 \pm 0.5) \times 10^{-6} \text{ s}^{-1}$, respectively. Hence, it seems very likely that the levelling-off of the k_{obs} values as the ¹PrOH content increases is attributed to some solvent effect.

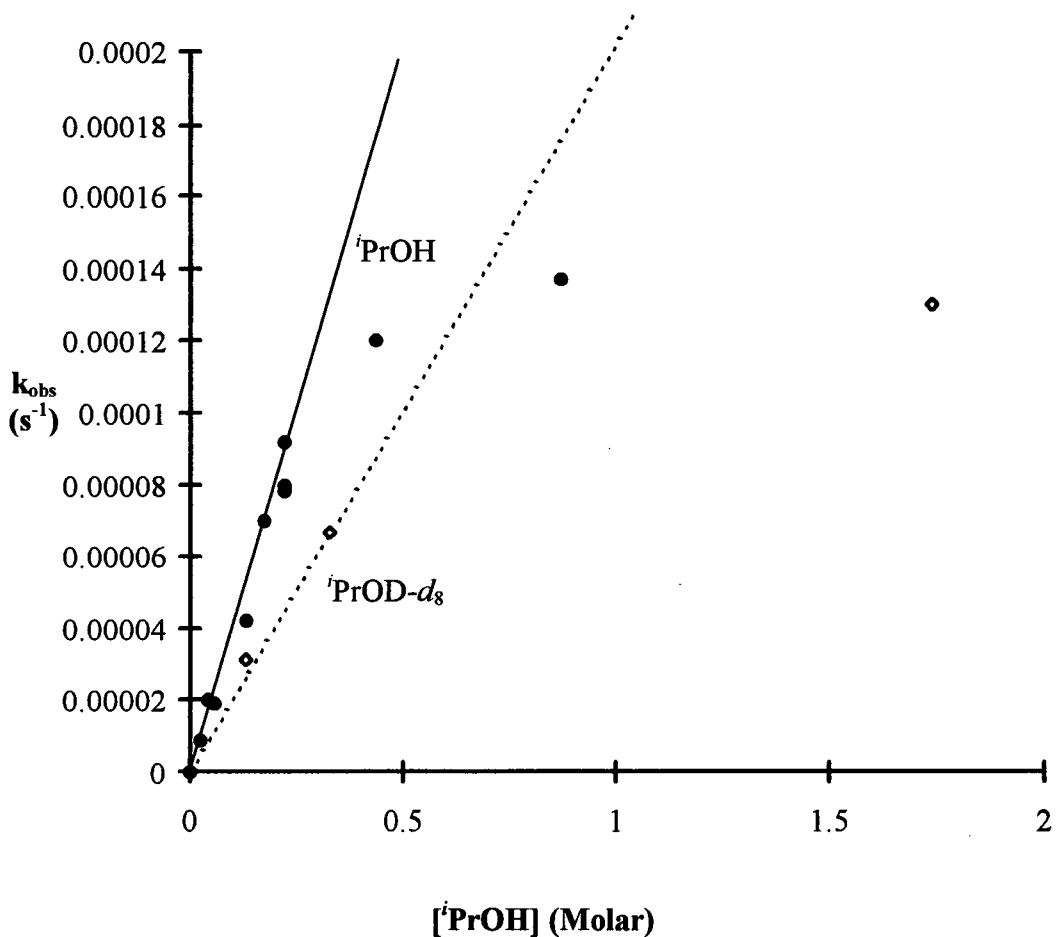


Figure 4.5. Pseudo-first-order rate constant, k_{obs} , as a function of excess $'\text{PrOH}$ concentration in benzene- d_6 under 1 atm Ar at 18.2°C . A kinetic isotope effect of $k_H/k_D = 1.9 \pm 0.3$ was observed at low concentrations of alcohol (< 0.3 M). The k_{obs} values for both $'\text{PrOH}$ and $'\text{PrOD}-d_8$ at higher [alcohol] values level-off at about $1.3 \times 10^{-4} \text{ s}^{-1}$. See Appendix C for a list of the raw data.

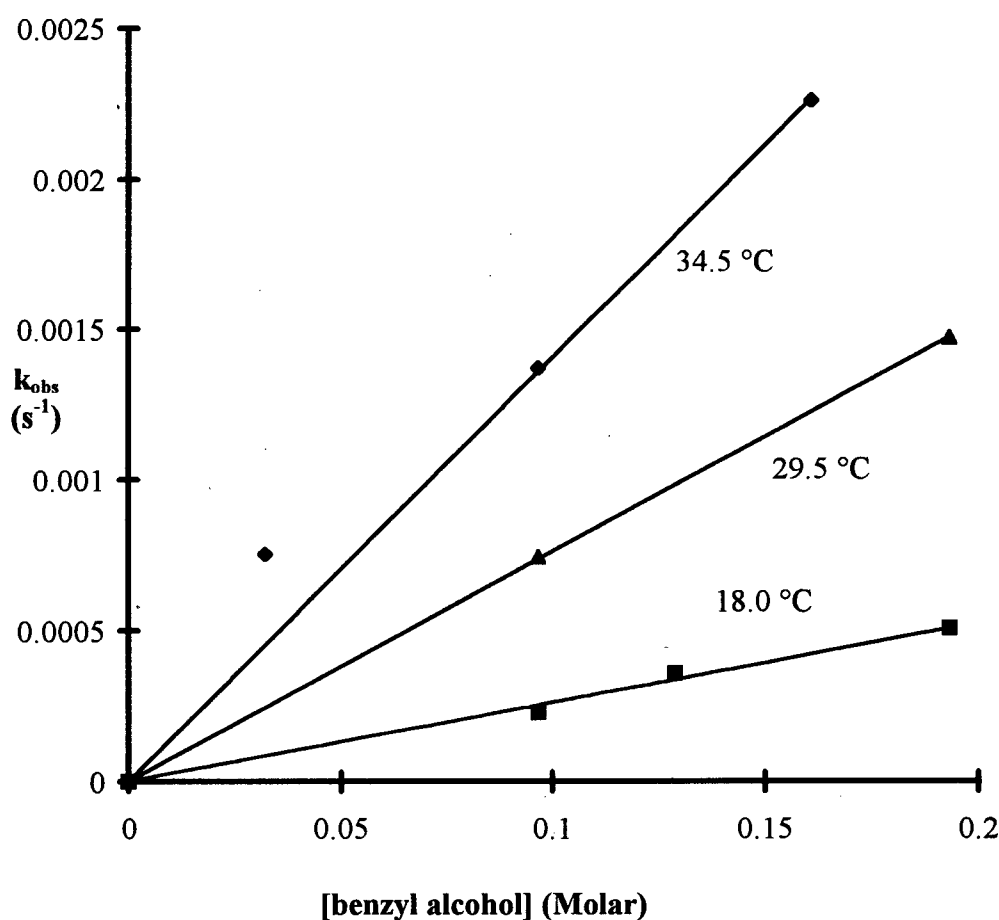
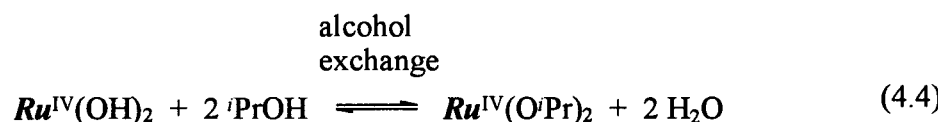
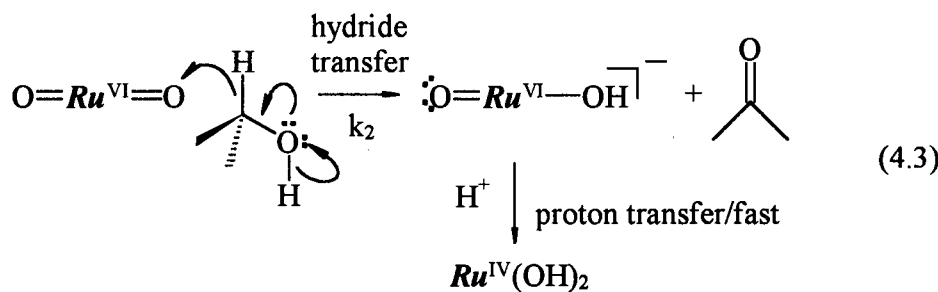


Figure 4.6. Pseudo-first-order rate constant, k_{obs} , as a function of [benzyl alcohol] at various temperatures in benzene- d_6 under 1 atm Ar.

The following mechanism [Eqs. 4.3 and 4.4; $\text{Ru} = \text{Ru}(\text{TMP})$] for the oxidation of alcohols by (1a) is favoured by the experimental evidence, which will be further presented after the introduction of the mechanism.



A hydride transfer pathway seems appropriate (Eq. 4.3) because the addition of KOH/'PrOH and KO'Bu/'PrOH increases the rate of oxidation (see Table 4.2). The electrophilic Ru=O moiety (Chapter 3) would favour attack of the α -C-H bond of the ' PrO over that of ' PrOH . In the presence of base, (**1a**) attacks the α -C-H bond of an alkoxide, followed by stepwise hydride and proton transfers to the oxo ligands to generate $\text{Ru}^{\text{IV}}(\text{TMP})(\text{OH})_2$ (Eqs 4.5, 4.6; $\text{B}^- = \text{OH}^-$ or ' BuO^-).

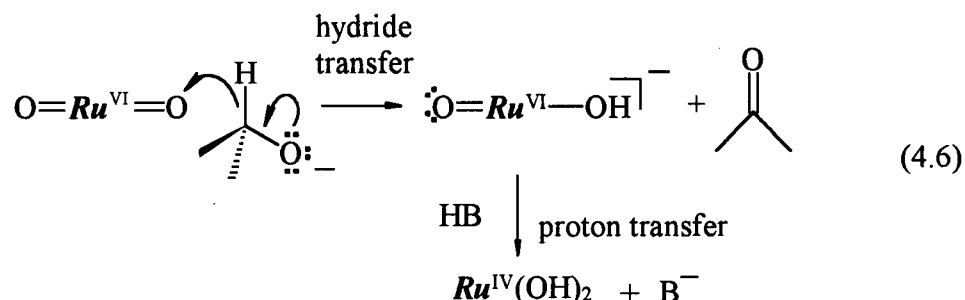


Table 4.2. Selected pseudo-first-order rate constants, k_{obs} for the stoichiometric oxidation of $^i\text{PrOH}$ to acetone by $\text{Ru}^{\text{VI}}(\text{TMP})(\text{O})_2$ (**1a**).

$[^i\text{PrOH}]^a$ (M)	KOH/ $^i\text{PrOH}$ ^b KO'Bu/ $^i\text{PrOH}$	pseudo-1st-order rate constant, k_{obs} (s ⁻¹)
0.0568 ^c	-	$(1.87 \pm 0.1) \times 10^{-5}$
0.131 ^c	-	$(4.21 \pm 0.5) \times 10^{-5}$
0.0408	4×10^{-6} M KOH	$(0.9 \pm 0.2) \times 10^{-4}$
0.0408	2×10^{-5} M KOH	$(1.2 \pm 0.2) \times 10^{-4}$
0.0816	4×10^{-6} M KOH	$(1.1 \pm 0.2) \times 10^{-4}$
0.130	1.2×10^{-4} M KO'Bu	$(5.4 \pm 0.8) \times 10^{-4}$
0.130	1.6×10^{-3} M KO'Bu	$(5.6 \pm 0.8) \times 10^{-3}$

^a $[\text{Ru}^{\text{VI}}(\text{TMP})(\text{O})_2] = 10^{-4}$ to 10^{-3} M in benzene- d_6 at 18.2 °C under 1 atm Ar.

^b Various solutions of $^i\text{PrOH}$ with dissolved KOH or KO'Bu were prepared and injected into the benzene- d_6 solutions, and the [base] values refer to those in the diluted solutions. The approximately constant rate of oxidation, apparently independent of the concentrations of KOH and $^i\text{PrOH}$, is likely due to the insolubility of KOH in benzene such that a saturation concentration has been reached. Hence, a maximum increase of rate is reached.

^c See Figure 4.5 for the k_{obs} versus $[^i\text{PrOH}]$ plot and Appendix C for the raw data.

That KOH or KO'Bu accelerated the rate of oxidation suggests bond cleavage by the Ru=O moiety at the α -C-H bond (Eq. 4.5). At lower $[^i\text{PrOH}]$ values where the k_{obs} versus $[^i\text{PrOH}]$ plots are linear, the $k_{\text{H}}/k_{\text{D}}$ ratio is approximately 1.9. The oxidation of $^i\text{PrOH}$ by (**1a**), based on the observed kinetic isotope effect, also seems reasonably consistent with the cleavage of the alcohol α -C-H bond by a Ru=O moiety as the initial oxidation step (Eq. 4.3), although the isotope effect of 1.9 is clearly very small, especially considering that a $k_{\text{H}}/k_{\text{D}}$ value is expected to be ~6.9, if $v_{\text{C}-\text{H}}$ and $v_{\text{C}-\text{D}}$ zero point energies are the only factors under consideration. In non-porphyrin systems, the oxidations of alcohols by oxoruthenium(IV)^{7a,9,13} and *trans*-dioxoruthenium(VI)^{15b} complexes have been observed to give kinetic isotope effects larger than the theoretical value of 6.9, including

k_H/k_D values as high as 50 and 18 for the oxidations of benzyl alcohol and $^1\text{PrOH}$, respectively.^{7a} The data for the $^1\text{PrOH}$ oxidation at 18.2 °C (Figure 4.5) show that the k_{obs} versus [alcohol] plots for $^1\text{PrOH}$ and $^1\text{PrOD-}d_8$ both level-off at approximately the same value of $k_{\text{obs}} \sim 1.3 \times 10^{-4} \text{ s}^{-1}$, which means that the under such conditions, the k_H/k_D ratio is approximately 1.0. The levelling-off of the k_{obs} values has been shown to be an artifact resulting from a solvent effect at the high $^1\text{PrOH}$ concentration (see earlier). It is not known why the oxidation of $^1\text{PrOH}$ by (1a) exhibits such a small kinetic isotope effect if α -C-H bond cleavage is involved, or why the k_H/k_D values becomes ~ 1.0 at higher $^1\text{PrOH}$ concentrations. One interpretation of the findings is that significant solvent effects (perhaps due to the alcohol content itself), in addition to direct α -C-H bond cleavage by the Ru=O moiety, may be involved in the oxidation reaction.

An alternative explanation for the levelling-off of the k_{obs} values (saturation kinetics) is the operation of a preassociation step, forming a {Ru-alcohol} adduct prior to the actual oxidation step, which has been invoked in alcohol oxidations by non-porphyrin oxoruthenium(IV) species.^{7a} Roecker and Meyer studied the stoichiometric oxidation of some alcohols using $\text{Ru}^{\text{IV}}(\text{bpy})_2(\text{py})(\text{O})^{2+}$ as the oxidant in MeCN solutions, and they observed non-linear k_{obs} versus [benzyl alcohol] plots which were attributed to a preassociation step;^{7a} however, a linear plot was observed once the solution ionic strength in MeCN was rendered constant by the addition of 0.10 M TEAP or when the reaction took place in H_2O . Neither the $\text{Ru}^{\text{VI}}(\text{TMP})(\text{O})_2$ nor $\text{Ru}^{\text{IV}}(\text{byp})_2(\text{py})(\text{O})^{2+}$ ^{7a} system shows any spectroscopic evidence for the formation of a preassociation complex in the respective oxidation reactions. Hence, the observed levelling-off of the k_{obs} values, at least in the

$\text{Ru}^{\text{VI}}(\text{TMP})(\text{O})_2$ system, is considered due mainly to a solvent effect caused by high ${}^{\text{i}}\text{PrOH}$ concentrations used.

As for the formation of the bis(alkoxo) product (**2a**), a likely path is via a metathesis reaction of ${}^{\text{i}}\text{PrOH}$ with $\text{Ru}^{\text{IV}}(\text{TMP})(\text{OH})_2$ (Eq. 4.4). There is no evidence for the existence of $\text{Ru}^{\text{IV}}(\text{TMP})(\text{OH})_2$, nor is there any direct proof regarding the rapid exchange of the hydroxo ligands with the alcohol in solution to form (**2a**), although rapid alcohol exchange with the axial alkoxo ligands within the $\text{Ru}^{\text{IV}}(\text{TMP})(\text{OR})_2$ species has been observed (Section 4.3.1); it is feasible that the formation of $\text{Ru}^{\text{IV}}(\text{TMP})(\text{OH})_2$ is disfavoured over that of (**2a**) in the presence of excess ${}^{\text{i}}\text{PrOH}$. There is indirect support that $\text{Ru}^{\text{IV}}(\text{TMP})(\text{OH})_2$ exists in solution, as the bis(hydroxo) analogue of TDCPP, $\text{Ru}^{\text{IV}}(\text{TDCPP})(\text{OH})_2$, has been characterized crystallographically recently,¹⁴ of interest the complex was isolated from a toluene filtrate solution (that had been left standing at -25 °C) obtained during the preparation of $\text{Ru}^{\text{VI}}(\text{TDCPP})(\text{O})_2$. The stoichiometric oxidations of alcohols by some non-porphyrin *trans*-dioxoruthenium(VI) species have been shown, based on UV-visible data, to form oxo(aquo)ruthenium(IV) species.^{15b} These Ru(IV) species also have been suggested to isomerize to the bis(hydroxo)-Ru(IV) species via proton migration.¹⁵ Of note, ${}^1\text{H}$ -resonances assignable to $\text{Ru}^{\text{IV}}(\text{TMP})(\text{O})$ were detected in the O_2 -oxidation of *p*-hydroquinone to *p*-benzoquinone catalyzed by (**1a**) (Section 6.4.1). As for the present $\text{Ru}^{\text{VI}}(\text{TMP})(\text{O})_2/{}^{\text{i}}\text{PrOH}$ system, ${}^1\text{H}$ -resonances corresponding to $\text{Ru}^{\text{IV}}(\text{TMP})(\text{O})$ or $\text{Ru}^{\text{IV}}(\text{TMP})(\text{O})(\text{OH}_2)$ were not detected; the only observable ${}^1\text{H}$ -resonances in the ${}^{\text{i}}\text{PrOH}$ system corresponding to Ru(TMP) species are those assignable to (**1a**) and (**2a**). Although $\text{Ru}^{\text{IV}}(\text{TMP})(\text{O})$ has not been detected in the ${}^{\text{i}}\text{PrOH}$ system (but

as Ru^{IV}(TMP)(O) has been detected in the *p*-hydroquinone system), it can still be envisaged that the initial hydride transfer (Eq. 4.3) yields Ru^{IV}(TMP)(O), while the Ru^{IV}(TMP)(OH)₂ could form subsequently via reaction of Ru^{IV}(TMP)(O) and H₂O similar to that proposed in the Ru(IV) non-porphyrin systems¹⁵ (see also Section 4.4.3 regarding the role of H₂O in a Ru^{VI}(TMP)(O)₂/alkene oxidation system).

The slopes of the lines in Figures 4.5 and 4.6 give the second-order rate constants, k_2 , for the stoichiometric oxidation of ¹PrOH and benzyl alcohol by (1a) (Table 4.3). The Eyring plots derived for these k_2 values, Figures 4.7 and 4.8, give the following activation parameters: $\Delta H_2^\ddagger = 45 \pm 7$ and 65 ± 11 kJ mol⁻¹, and $\Delta S_2^\ddagger = -167 \pm 10$ and -70 ± 20 J mol⁻¹ K⁻¹ for ¹PrOH and benzyl alcohol, respectively, a marked difference being noted. The rates of alcohol oxidations in the Ru^{VI}(TMP)(O)₂ system are limited by large and negative ΔS_2^\ddagger values, and that benzyl alcohol is oxidized approximately 10 times faster than ¹PrOH is due entirely to a more favourable ΔS_2^\ddagger ; indeed, the relative ΔH_2^\ddagger values favour oxidation of ¹PrOH. In comparison, the activation parameters for the oxidation of ¹PrOH and benzyl alcohol by Ru^{IV}(bpy)₂(py)(O)²⁺ in MeCN are $\Delta H^\ddagger = +33.5$ and $+24.2$ kJ mol⁻¹, and $\Delta S^\ddagger = -176$ and -160 J mol⁻¹ K⁻¹, respectively;^{7a} although the ΔS^\ddagger values are large and negative, as in the Ru^{VI}(TMP)(O)₂ systems, the ΔH^\ddagger term is the major factor affecting the differences in the rate constants.

An alternative mechanism for the stoichiometric ¹PrOH oxidation by (1a) involves oxidative addition of the alcohol α -C-H bond across the Ru=O moiety of (1a), leading to an organoruthenium intermediate (as proposed for a RuO₃²⁻/alcohol system),⁸ although the lack of cis sites at the Ru makes this unlikely. The Ru=O moiety of (1a) could perhaps

abstract a hydrogen atom from the α -C-H bond to form $\text{Ru}^{\text{V}}(\text{TMP})(\text{O})(\text{OH})$ and an in-cage organic radical $\text{Me}_2\text{C}^{\bullet}\text{-OH}$; a single-electron transfer from $\text{Me}_2\text{C}^{\bullet}\text{-OH}$ to $\text{Ru}^{\text{V}}(\text{TMP})(\text{O})(\text{OH})$, followed by loss of H^+ from $\text{Me}_2\text{C=OH}^+$, will give the same products as those shown in Eq. 4.3. This hydrogen abstraction path is disfavoured somewhat as no ESR signals due to either an organic radical and/or a Ru(V) paramagnetic species were observed at 110 K in a frozen benzene solution of (1a) and $^{\text{i}}\text{PrOH}$; however, as the organic radical and Ru(V) species might be unable to escape from each other in a solvent cage in the frozen environment, an electron transfer from the radical to the Ru(V) species may have occurred prior to the attempted detection of the radicals by ESR spectroscopy, and thus the hydrogen abstraction mechanism cannot be ruled out completely.

Table 4.3. Second-order rate constants, k_2 , for the stoichiometric oxidations of $^{\text{i}}\text{PrOH}$ and benzyl alcohol in benzene- d_6 by $\text{Ru}^{\text{VI}}(\text{TMP})(\text{O})_2$ (1a).

Temperature (Kelvin) [for benzyl alcohol]		$k_2 (\text{M}^{-1} \text{s}^{-1})^a$
	$^{\text{i}}\text{PrOH}$	benzyl alcohol
291.4 [291.2]	3.8×10^{-4}	2.6×10^{-3}
301.7 [302.7]	$7.4 \times 10^{-4}^b$	7.6×10^{-3}
308.7 [307.7]	$1.05 \times 10^{-3}^b$	1.4×10^{-2}

^a The kinetics were monitored by $^1\text{H-NMR}$ spectroscopy in benzene- d_6 under 1 atm Ar.

^b These k_2 values were derived from a single k_{obs} value determined at $[^{\text{i}}\text{PrOH}] = 0.161$ and 0.174 M at 301.7 and 308.7 K, respectively. These $[^{\text{i}}\text{PrOH}]$ values are well within the linear region of the k_{obs} versus [alcohol] plots (Figures 4.5 and 4.6), and hence are deemed reliable in the calculation of k_2 .

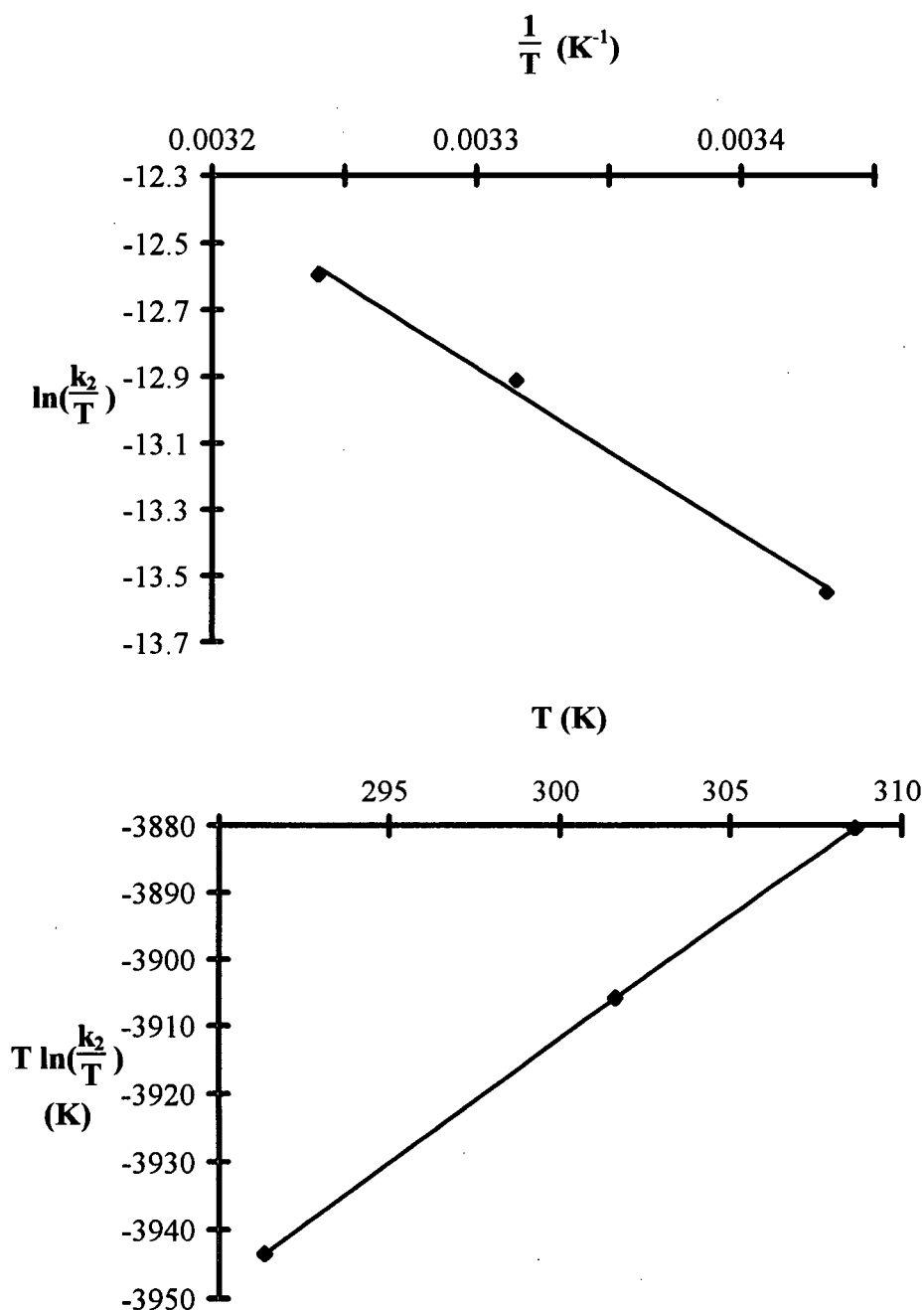


Figure 4.7. Eyring plots for the stoichiometric oxidation of $'\text{PrOH}$ by $\text{Ru}^{\text{VI}}(\text{TMP})(\text{O})_2$ under 1 atm Ar in benzene- d_6 .

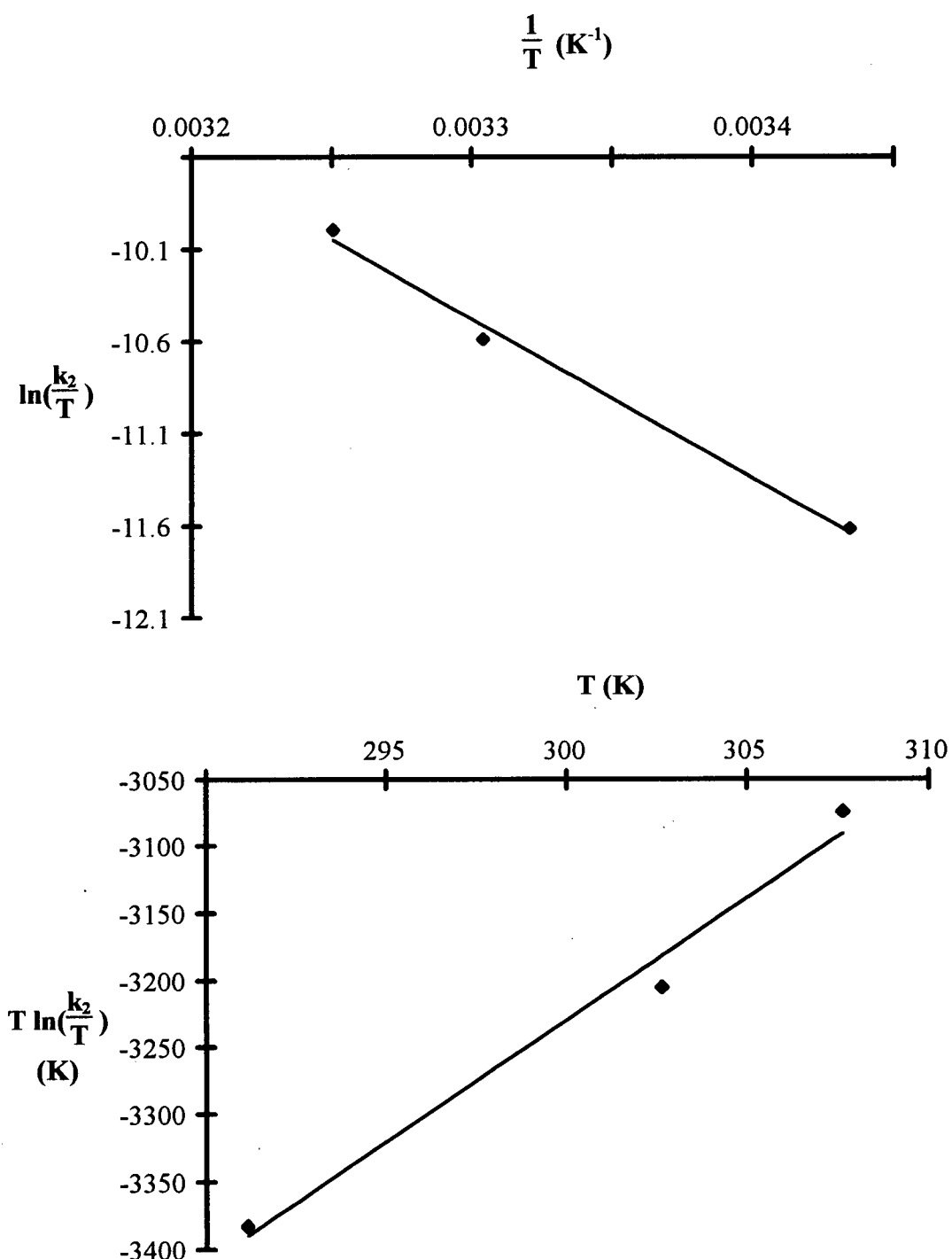
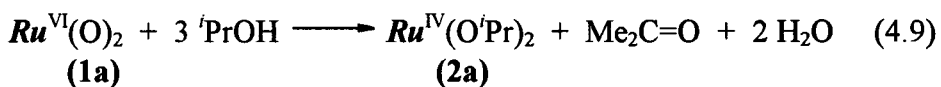
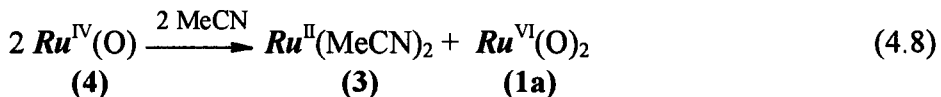
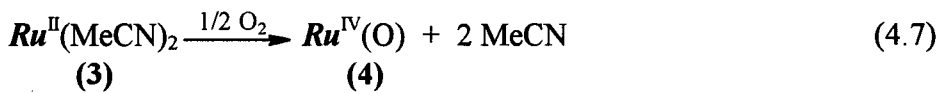


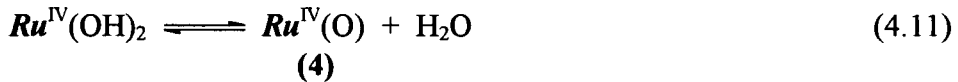
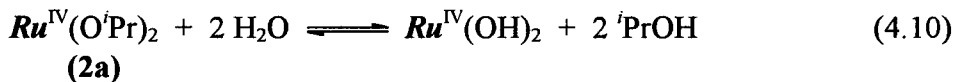
Figure 4.8. Eyring plots for the stoichiometric oxidation of benzyl alcohol by $\text{Ru}^{\text{VI}}(\text{TMP})(\text{O})_2$ under 1 atm Ar in benzene- d_6 .

4.3.3 Aerobic Oxidations of Alcohols to Aldehydes and Ketones

The implication for **(1a)** to function catalytically in the aerobic oxidation of alcohols was noticed in $^1\text{H-NMR}$ experiments where excess $^1\text{PrOH}$ was added to a vacuum-degassed sample of **(1a)** [generated *in situ* in benzene- d_6 from the aerobic oxidation $\text{Ru}^{II}(\text{TMP})(\text{MeCN})_2$ (**3**)]. Complete conversion of **(1a)** to **(2a)** and the formation of one equivalent of acetone after about 24 h under vacuum, in accordance with Eq. 4.2, were observed by $^1\text{H-NMR}$ spectroscopy. After an additional 48 h, the same sample was analyzed again by $^1\text{H-NMR}$ spectroscopy, and ^1H -resonances characteristic of species (**3**) (~10%) were detected (β -pyrrole-H, 8.65; *o*-Me, 2.21; *p*-Me, 2.54; MeCN, -1.32 ppm). At the end of 2 weeks, when no further noticeable changes were observed in the $^1\text{H-NMR}$ spectrum of the sample, greater than 90% of **(2a)** was converted to **(3)**. Also, almost two, instead of the original one, equivalents of acetone were detected. This regeneration of **(3)**, coupled with the fact that **(3)** under air or O_2 can reform **(1a)** (Chapter 2), suggests that the O_2 -oxidation of alcohols can be catalyzed by **(1a)**.

The mechanism for the aerobic oxidation of alcohols catalyzed by **(1a)** is proposed to follow the pathways represented in Eqs. 4.7 to 4.11 [$\text{Ru} = \text{Ru}(\text{TMP})$], and the evidence suggesting the operation of these pathways will be presented below.





The formation of $\text{Ru}^{\text{II}}(\text{TMP})(\text{MeCN})_2$ (**3**), as well as the production of an additional equivalent of acetone in vacuum, observed in the previously mentioned ^1H -NMR experiment, can be accommodated by the proposed catalytic mechanism (Eqs. 4.7 to 4.11). In the absence of O_2 , Eq. 4.7 is removed from the scheme for the catalytic oxidation, and the 1/2 equivalent of $\text{Ru}^{\text{II}}(\text{TMP})$ formed from the disproportionation of 1 equivalent of (**4**) can no longer regenerate (**1a**). Thus only 1/2 equivalent of (**1a**) oxidizes the excess PrOH , and in the next cycle the 1/2 equivalent of (**4**) disproportionates to reform only 1/4 equivalent of (**1a**), and so forth. All the cycles added together as an infinite sum[†] would yield exactly one additional equivalent of acetone and one equivalent of $\text{Ru}^{\text{II}}(\text{TMP})$ [which is coordinated readily by MeCN to form (**3**)]; the net, overall reaction is given in Eq. 4.12, $\text{Ru} = \text{Ru}(\text{TMP})$.



Evidence for reaction 4.10 can be inferred from the following experiment, where an isolated sample of (**2a**) dissolved in benzene- d_6 and exposed to air regenerated (**1a**), with acetone forming concurrently, as monitored by ^1H -NMR spectroscopy. Moisture was crucial in the regeneration of (**1a**), as (**2a**) dissolved in benzene- d_6 containing dry O_2 gave no reaction. During the regeneration of (**1a**), no free PrOH was observed at any

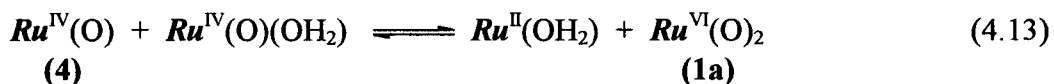
[†] $\frac{1}{2} + (\frac{1}{2})^2 + (\frac{1}{2})^3 + \dots = \frac{1}{2}(\frac{1}{1-\frac{1}{2}}) = 1$, Reference 27.

time [\sim 30 min for complete regeneration of (**1a**)]. Of note, the complete removal of $^i\text{PrOH}$ from (**2a**) was a problem (mentioned earlier in Section 4.3.1), and as high as 10 equivalents of acetone have been observed on one occasion when a sample of (**2a**) was exposed to air. Typically less $^i\text{PrOH}$ is present, although usually more (3 to 6 equivalents) than the expected two equivalents of acetone are formed. The slightly excess $^i\text{PrOH}$ was not observed in the $^1\text{H-NMR}$ spectrum, presumably due to the rapid exchange of the axial alkoxo ligands with the alcohol (Section 4.3.1).

Because water is crucial in the regeneration of the active catalyst (**1a**) from (**2a**), H_2O is proposed to exchange with the axial alkoxo ligands of (**2a**) to form $\text{Ru}^{\text{IV}}(\text{TMP})(\text{OH})_2$, followed by conversion to $\text{Ru}^{\text{IV}}(\text{TMP})(\text{O})$ (**4**) (Eqs. 4.10 and 4.11, respectively). Species (**4**) then disproportionates (cf. Eq. 4.8) to (**1a**) and $\text{Ru}^{\text{II}}(\text{TMP})$. The pathways shown in Eqs. 4.7 and 4.8, although not fully established, generally represent the accepted mechanism¹⁶ for generating (**1a**) from the aerobic oxidation of $\text{Ru}^{\text{II}}(\text{TMP})(\text{L})_2$ species ($\text{L} = \text{THF}$,¹⁷ MeCN ,¹⁸ N_2 or vacant¹⁹), with the disproportionation of (**4**) to (**1a**) and $\text{Ru}^{\text{II}}(\text{TMP})$ (cf. Eq. 4.8) occurring via attack of the $\text{Ru}=\text{O}$ moiety on the vacant site of another molecule of (**4**).²⁰ In addition, (**4**) is also the supposed intermediate in the catalytic epoxidation of alkenes by (**1a**).^{17,20,21}

Of note, a recent study showed that the addition of water promoted the catalytic O_2 -oxidation of alkenes by (**1a**).²¹ No explanation was offered by the authors; however, noting the above observations in the present $^i\text{PrOH}$ system, two possible proposals may explain the H_2O effect. The rate-determining step in the epoxidation of alkenes catalyzed by (**1a**) appears to be the dissociation of the epoxide product from

$\text{Ru}^{\text{IV}}(\text{TMP})(\text{O})(\text{epoxide})$ (Figure 4.9), as the catalysis is independent of alkene concentration and O_2 partial pressures.¹⁷ Hence, water could displace the epoxide from the Ru-centre and speed up the disproportionation of (4) to (1a) and $\text{Ru}^{\text{II}}(\text{TMP})$. The lack of a trans or cis site leaves a seven-coordinate associative mechanism as the only possibility for a water-assisted dissociation of epoxide, but considering the steric constraints presented by the TMP mesityl groups, an associative mechanism is unlikely. Another potential role of water might be its participation in the disproportionation reaction shown in Eq. 4.12 [$\text{Ru} = \text{Ru}(\text{TMP})$]. Such reactions (and their reverse reactions)



are suggested to be proton-coupled, electron transfer processes (the H^+ coming from H_2O) in the non-porphyrin oxoruthenium(III, IV, V, VI) systems,^{7b,15} based on electrochemical studies. If H_2O can speed up the disproportionation of (4), the rates of epoxidation will also be increased.

The results for the aerobic oxidation of $^{\text{t}}\text{PrOH}$ and benzyl alcohol catalyzed by (1a) and (1b) are tabulated in Table 4.4. Complex (1a) is a far more effective catalyst than (1b) for the oxidation of benzyl alcohol. This was initially surprising as (1b) is generally more reactive than (1a) due to the presence of the electron-withdrawing Cl-groups on the TDCPP ligand.³ That (1b) is less reactive than (1a) is due to the former being more susceptible to deactivation during the catalysis, to form the inactive $\text{Ru}^{\text{II}}(\text{TDCPP})(\text{CO})$ species, as evidenced by the appearance of UV-visible and IR absorption bands characteristic of the carbonyl complex (Chapter 2). Species (1a) is also deactivated, as

well as decomposed, but more slowly (see later); the formation of Ru^{II}(TMP)(CO) is a problem not only in alcohol oxidations, but also in epoxidations of alkenes.^{17,21}

Ruthenium(II) is known to have a strong affinity for CO and other π -acid ligands (e.g. S-bound is favoured over O-bound sulfoxides),^{3,22,23} where π -backbonding stabilizes the Ru(II) centre. Decarbonylation of carbonyl-containing organic compounds by Ru-porphyrins is not without precedent; for example, earlier work from this laboratory showed Ru(TPP)(phosphine)₂ species to be competent catalysts in the thermal decarbonylation of aldehydes.²³

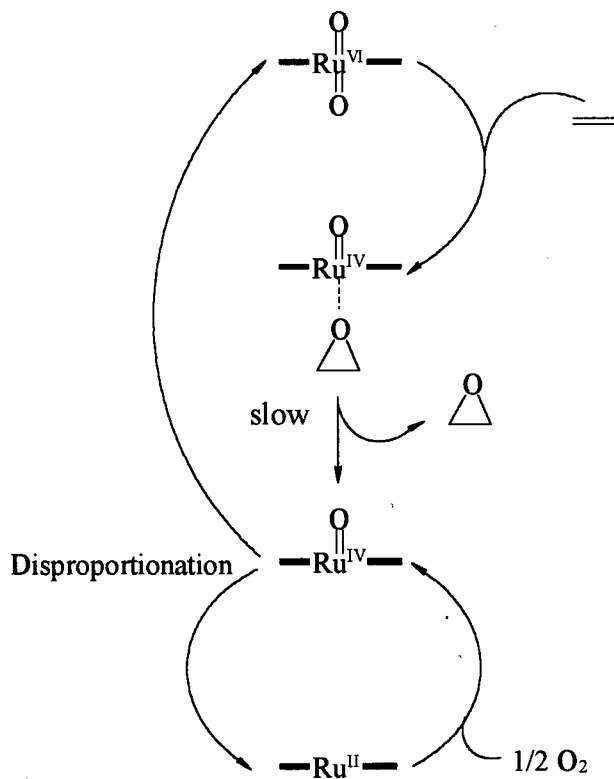


Figure 4.9. Mechanism of alkene epoxidation catalyzed by Ru^{VII}(TMP)(O)₂. The dissociation of the epoxide from the Ru(IV) centre is interpreted as being the rate-determining step, as the rate of catalysis is the insensitive to the alkene concentration and O₂ partial pressure (Ref. 17).

The data in Table 4.4 show that (**1a**) is a far more effective catalyst for oxidizing benzyl alcohol than $^1\text{PrOH}$. The aerobic oxidation of 1-phenylethanol to acetophenone catalyzed by (**1a**) and (**1b**) also was studied briefly, and as with $^1\text{PrOH}$, only a few total turnovers were achieved at room temperature ($\sim 20^\circ\text{C}$); carbonylation of the catalyst to $\text{Ru}^{II}(\text{porp})(\text{CO})$ (porp = TMP and TDCPP) within 24 h was the main deactivation pathway, as evidenced by $^1\text{H-NMR}$ and UV-visible spectroscopies. Benzyl alcohol is an order of magnitude more reactive than $^1\text{PrOH}$ and, under the optimum conditions, a total turnover of 2000 was achieved in a period of 13 d. The presence of water which created a two-phase system enhanced the rates of catalysis, and the addition of 3.0 M aqueous KOH increased, at least for benzyl alcohol, the turnovers even further (Figure 4.10). Of note, the turnover numbers were independent on the O_2 partial pressure (1 atm air versus 1 atm O_2 ; see Table 4.4).

Figure 4.10 shows the turnovers in the initial 24 h as a function of [benzyl alcohol], while Figure 4.11 shows the progress of the aerobic oxidation of benzyl alcohol catalyzed by (**1a**) as a function of time. The daily turnovers in Figure 4.10 show that an upper limit in the effectiveness of the catalyst (in terms of turnover numbers) is reached beyond certain [benzyl alcohol] values ($> 0.2 \text{ M}$); therefore, it is plausible that the rate-limiting step in the catalysis, when [benzyl alcohol] values are below 0.2 M, is the alcohol oxidation step (Eq. 4.9). As the [benzyl alcohol] values increase, the turnovers per day versus [benzyl alcohol] plots level-off, and one of the processes (Eqs. 4.7, 4.8, 4.10 or 4.11) involving the regeneration of (**1a**) may become the rate-limiting step in the catalytic cycle. The generation of (**1a**) from Ru(II)-porphyrin species,¹⁶ when exposed to air or O_2 ,

is known to occur rapidly (usually within minutes, see also Chapter 3); therefore, the rate-limiting step is likely reaction 4.10 or 4.11. Figure 4.11 shows that the activity of the system slowly degrades over time and, as mentioned earlier, the catalyst becomes carbonylated to Ru^{II}(TMP)(CO) at 24 °C; the aldehyde or ketone product is presumably decarbonylated, but this was not checked experimentally. At 50 °C, the Ru(TMP)(OR)₂ species in the ¹PrOH and benzyl alcohol systems also decompose, as evidenced by the disappearance of the ¹H-resonances in the NMR spectrum characteristic of the TMP ligand; the relative contributions from carbonylation of versus destruction of Ru(TMP) species are not known, although at 24 °C deactivation to Ru^{II}(TMP)(CO), as evidenced by ¹H-NMR spectroscopy, was the primary deactivation pathway. It is not obvious from the data or graphs, but an important point is that the presence of aqueous KOH extended the catalytic activity of (**1a**) to over 10 d and, although the addition of H₂O increased the turnover numbers, the catalyst did not survive for more than 4 d in typical experiments. A finding relevant to this is that substantial decomposition of (**1a**) occurs in a benzene solution under 1 atm air overnight,[†] with the instability thought to be due to the presence of trace acid impurities.³ In direct support of this postulation, addition of ~25 µL 3.0 M aqueous KOH to ~5 x 10⁻⁶ M benzene solution of (**1a**), again in air, led to the preservation of the 422 nm Soret band of (**1a**) overnight, while solutions of (**1a**) without added base lost this characteristic Soret band (a new band appears at 414 nm).

[†] At room temperature under 1 atm air, a substantial portion of (**1a**) (~ 10⁻⁶ M) decomposes in the benzene solution overnight. Under the same conditions (**1b**) converts to Ru^{II}(TDCPP)(CO) in solution, as well as in the solid state, via an unknown process (see Chapter 5).

Table 4.4. Catalytic activity of Ru^{VI}(porp)(O)₂ [porp = TMP (**1a**) and TDCPP (**1b**) towards O₂-oxidation of ¹PrOH and benzyl alcohol under mild conditions in benzene.

[(1a) or (1b)] ^a (M)	[alcohol] (M)	turnovers within 1st 24 h ^b	total turnovers; % conversion [time] ^c	3.0 M KOH _(aq) , H ₂ O, or <i>NONE</i> ^d
(1a) 20 °C	¹ PrOH			
4.0 x 10 ⁻⁴ ^e	0.033	1.5 ± 0.1	-	NONE
50 °C				
7.0 x 10 ⁻⁶	0.242	6.0 ± 0.5	-	NONE
2.0 x 10 ⁻⁴ ^e	0.0325	10.6 ± 1	-	H ₂ O
2.0 x 10 ⁻⁴ ^e	0.0325	6.3 ± 0.5	-	D ₂ O
20 °C	PhCH ₂ OH			
2.0 x 10 ⁻⁴ ^e	0.0242	30 ± 2.5	-	NONE
	0.0484	40 ± 3	-	NONE
	0.121	50 ± 4	-	NONE
50 °C				
1.5 x 10 ⁻⁴ ^{e,f}	0.0242	24 ± 2	-	NONE
1.5 x 10 ⁻⁴	0.0242	28 ± 2	-	NONE
1.5 x 10 ⁻⁴	0.0483	42 ± 3	-	NONE
2.35 x 10 ⁻⁴ ^e	0.121	50 ± 4	122; 77% (67.5 h)	NONE
8.33 x 10 ⁻⁵	0.00083	5.5 ± 0.4	-	H ₂ O
8.33 x 10 ⁻⁵	0.00167	14 ± 1	-	H ₂ O
8.33 x 10 ⁻⁵	0.0321	28 ± 5	-	H ₂ O
2.1 x 10 ⁻⁴	0.0321	34 ± 3	-	H ₂ O
2.0 x 10 ⁻⁴	0.121	77 ± 6	-	H ₂ O
8.33 x 10 ⁻⁵	0.138	72 ± 6	-	H ₂ O
2.0 x 10 ⁻⁴	0.362	137 ± 9	-	H ₂ O
7.5 x 10 ⁻⁵	0.362	101 ± 8	-	H ₂ O
7.5 x 10 ⁻⁵	0.725	113 ± 9	-	H ₂ O
2.63 x 10 ⁻⁵	0.121	111 ± 9	440; 9.5% (259 h)	KOH
2.63 x 10 ⁻⁵	0.241	274 ± 22	950; 10% (234 h)	KOH
2.63 x 10 ⁻⁵	0.483	297 ± 25	1860; 10% (334h)	KOH
2.63 x 10 ⁻⁵	0.876	272 ± 22	2000; 5.3% (308h)	KOH
(1b) 50 °C	PhCH ₂ OH			
9.0 x 10 ⁻⁵	0.121	10 ± 1	complete loss of	H ₂ O
9.0 x 10 ⁻⁵	0.242	18 ± 1.5	catalytic activity	H ₂ O
2.19 x 10 ⁻⁴	0.0966	15 ± 1.2	after about	KOH
2.19 x 10 ⁻⁴	0.387	20 ± 1.6	2 d	KOH

^a In benzene, under 1 atm air, followed by GC analysis, unless otherwise indicated.

^b Turnovers are typically obtained during a period between 18 to 25 h and are normalized to 24 h.

^c At 50 °C, (**1a**) decomposes gradually and the systems loses its catalytic activity.

^d Benzene directly out of the bottle contains H₂O at a concentration of the order of 10⁻³ M, and "NONE" means that no further H₂O has been added. Addition of H₂O (or KOH_(aq)) to benzene creates a 2-phase system, with the benzene phase containing H₂O at ~10⁻² M (Section 4.2.1).

^e Followed by ¹H-NMR spectroscopy in benzene-d₆. ^f Under 1 atm O₂.

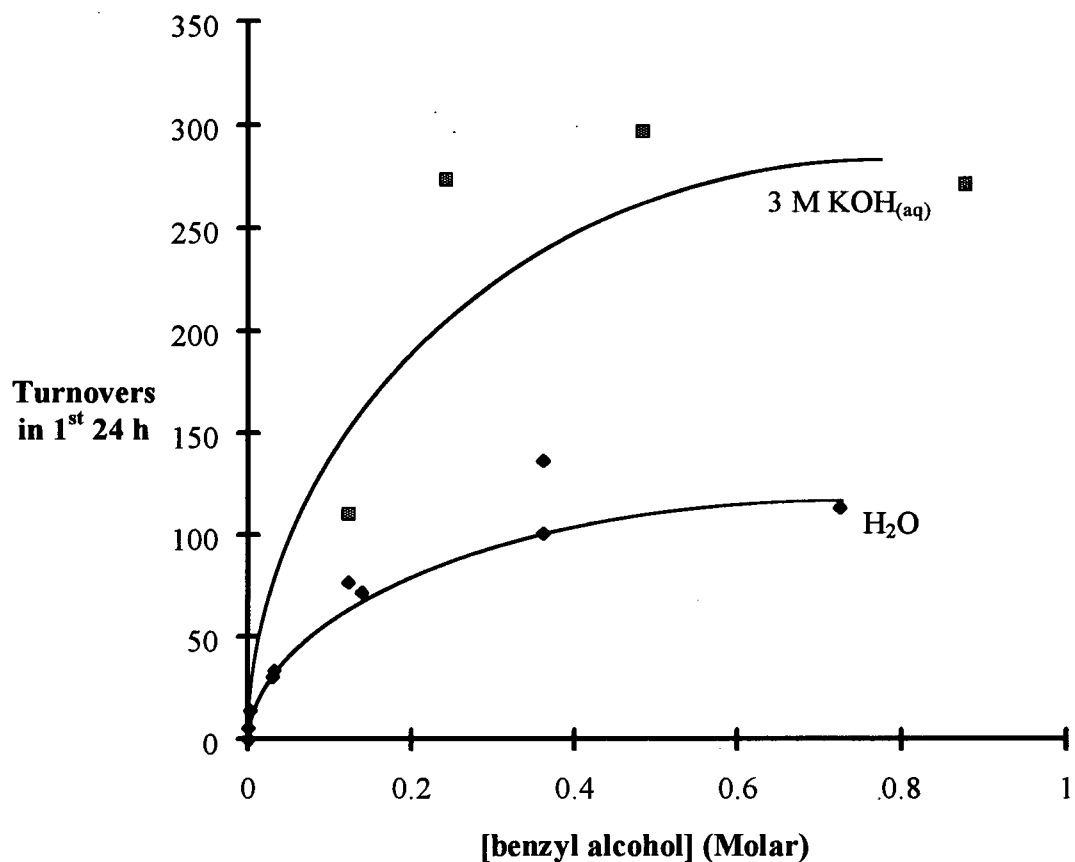


Figure 4.10. Daily turnovers versus [benzyl alcohol] for the aerobic oxidation of benzyl alcohol catalyzed by Ru^{V6}(TMP)(O)₂ (**1a**) at 50 °C.
[(**1a**)] ~ 10⁻⁴ M in benzene (see also Table 4.4).

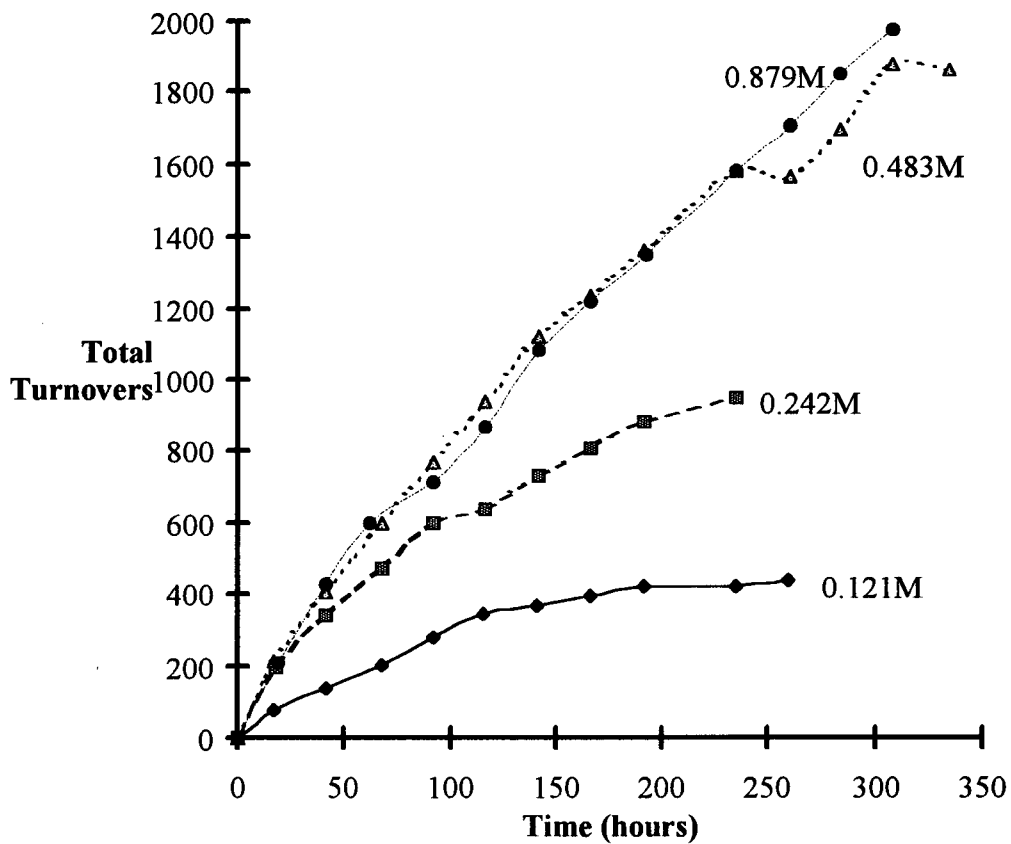


Figure 4.11. Total turnovers versus time for the aerobic oxidation of benzyl alcohol (concentrations indicated) catalyzed by $\text{Ru}^{\text{VI}}(\text{TMP})(\text{O})_2$ (**1a**) at 50°C . $[(\textbf{1a})] = 2.63 \times 10^{-5} \text{ M}$ in benzene (see also Table 4.4).

Of note, a recent report on the use of the same catalysts, namely $\text{Ru}^{\text{VI}}(\text{porp})(\text{O})_2$ species (porp = TMP and TDCPP), using pyridine-*N*-oxides as oxidants, demonstrated efficient catalytic activity for the oxidation of alcohols, with total turnovers for the conversion of benzyl alcohol to benzaldehyde being ~140 (80 % yield).²⁴ The oxidation of adamantane in the same $\text{Ru}^{\text{VI}}(\text{TMP})(\text{O})_2/\text{pyridine-}N\text{-oxide}$ system was more impressive; up to 14000 total turnovers were realized. Active species other than $\text{Ru}^{\text{VI}}(\text{porp})(\text{O})_2$ must account for such high activities, as the studies described in Section 4.4 show that the dioxo species are only barely able to oxidize the more active alkanes adamantane and Ph_3CH . Acids such as HCl and HBr were present in the pyridine-*N*-oxide system, and were essential for the enhanced reactivity, and $\text{Ru}^{\text{VI}}(\text{TMP})(\text{O})(\text{X})^+$ species ($\text{X} = \text{Cl}, \text{Br}$) have been suggested to be the active oxidant;²³ the coordination of the pyridine-*N*-oxide to the ruthenium centre may play a role in the system's high catalytic reactivity. In addition, a Ru-porphyrin catalyzed decomposition of pyridine-*N*-oxide to generate perhaps an O-atom, and thus initiate a possible radical-chain reaction, might lead to such high activities.

4.4 Aerobic Oxidation of Tertiary Alkanes Catalyzed by $\text{Ru}^{\text{VI}}(\text{porp})(\text{O})_2$ Species

At 24 °C under 1 atm air in benzene, (**1a**) catalyzes the aerobic oxidation of Ph_3CH to Ph_3COH , while (**1b**), but not (**1a**), can also catalyze the aerobic oxidation of adamantane to 1-adamantanol; however, the reactions are sluggish (< 1 turnover per day). As the dioxoruthenium(VI) species are subject to degradation, particularly (**1a**), kinetic studies were deemed to be impractical, and no kinetics studies were undertaken on

these alkane systems. In $^1\text{H-NMR}$ studies in benzene- d_6 , ^1H -resonances corresponding to **(1a)** ($\sim 10^{-3}$ M) can still be detected after 24 h (i.e. not all of **(1a)** at this higher concentration has decomposed after this time, see end of Section 4.3.3); ^1H -resonances corresponding to $\text{Ru}^{\text{IV}}(\text{TMP})(\text{O})$ (see Section 3.4.2) also can be observed [~ 5 % of the total Ru]. The progress of the catalyses is shown in Figure 4.12. The presence of electron-withdrawing Cl-groups makes **(1b)** more reactive, and almost four times the turnovers are achieved for the Ph_3CH oxidation catalyzed by **(1b)** over that by **(1a)**. The addition of 2,6-ditertbutyl-4-methylphenol (BHT, 0.01 M)[†] to the $\text{Ru}^{\text{VI}}(\text{TMP})(\text{O})_2/\text{Ph}_3\text{CH}$ system does not inhibit the oxidation, and thus the oxidation most likely is due to direct attack of the tertiary C-H bond by the Ru=O moiety.

The mechanism of oxidation is proposed to occur via Eq. 4.14 [Ru = Ru(TMP) or Ru(TDCPP)]; whether the reaction in Eq. 4.14 proceeds via an H-atom abstraction followed by electron transfer is unknown. For example, oxidation of alkanes by Fe(TMP)(Cl)(O) species has been proposed to occur via a hydride transfer pathway,²⁵ while oxidations by non-porphyrin oxoruthenium species have been proposed to undergo a homolytic H-atom abstraction pathway.^{6b} For the $\text{Ru}^{\text{VI}}(\text{TMP})(\text{O})_2$ system, a homolytic cleavage of the tertiary C-H bond by a Ru=O moiety to initiate the alkane oxidation reaction, with the $^{\bullet}\text{OH}$ being transferred to the R^{\bullet} fragment within a solvent cage, is consistent with the results in Chapter 5, where the catalytic oxidation of hydrocarbons occurs via radical-chain pathways, possibly initiated by a homolytic C-H

[†] The addition of BHT (~ 0.01 M) to $\text{Ru}^{\text{VI}}(\text{TMP})(\text{O})_2$ ($\sim 10^{-6}$ M) in benzene, under 1 atm air, gave no reaction, as evidenced by UV-visible spectroscopy.

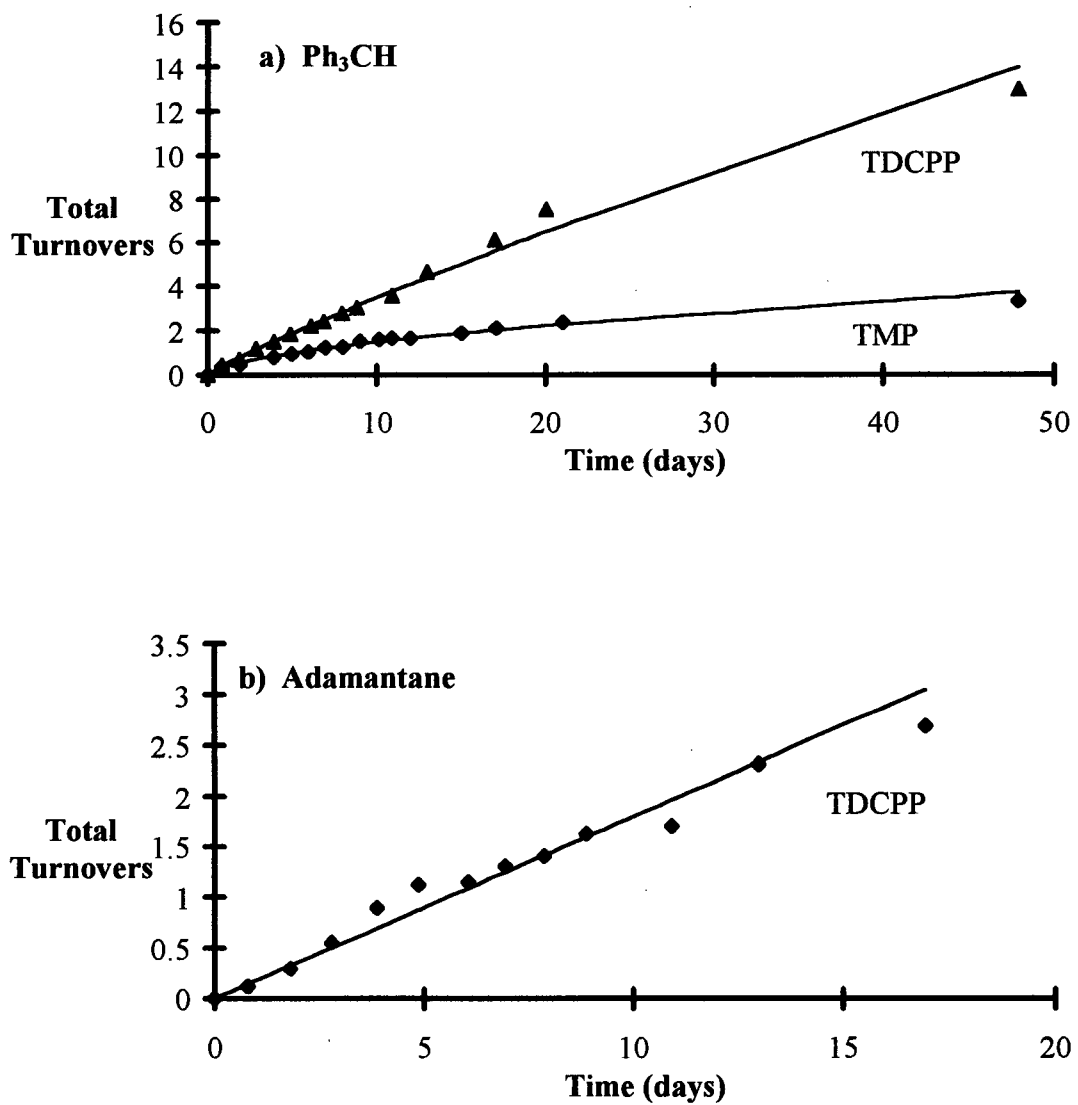


Figure 4.12. Total turnovers versus time for the aerobic oxidations of a) Ph_3CH and b) adamantane catalyzed by $\text{Ru}^{\text{VI}}(\text{porp})(\text{O})_2$ [$\text{porp} = \text{TMP}$ (**1a**) and TDCPP (**1b**)] at $24 \pm 2^\circ\text{C}$ in benzene.
 a) TMP: $[(\text{1a})] = 1.2 \times 10^{-4} \text{ M}$; $[\text{Ph}_3\text{CH}] = 2.89 \times 10^{-3} \text{ M}$
 TDCPP: $[(\text{1b})] = 2.4 \times 10^{-4} \text{ M}$; $[\text{Ph}_3\text{CH}] = 4.64 \times 10^{-3} \text{ M}$
 b) $[(\text{1b})] = 2.4 \times 10^{-4} \text{ M}$; $[\text{adamantane}] = 6.28 \times 10^{-3} \text{ M}$.

bond cleavage by Ru=O moieties. Eq. 4.14 corresponds to the oxygen-rebound mechanism²⁶ proposed for the ubiquitous cytochrome P-450 enzyme, where the •OH group is transferred to the R^{*} fragment before the substrate leaves the protein cavity.

4.5 Conclusion

The description and plausible mechanism of an efficient catalytic aerobic system based on *trans*-dioxoporphyrinato(ruthenium(VI)) species, capable of oxidizing benzyl alcohol, ¹PrOH and 1-phenylethanol to the corresponding aldehydes and ketones, have been presented. The initiation of the oxidation via a hydride transfer from the alcohol α -C-H bond was proposed. At 50 °C under 1 atm air, benzyl alcohol was oxidized selectively to benzaldehyde with daily turnovers up to 300 d⁻¹, and total turnovers reaching 2000 in 13 d. This is among the most efficient of Ru-based catalyst systems for the aerobic oxidation of alcohols.¹ The Ru^{VI}(porp)(O)₂ species (porp = TMP and TDCPP) can also catalyze the aerobic oxidations, although slowly, of Ph₃CH to Ph₃COH and adamantine to 1-adamantanol under 1 atm air at 24 °C.

References

- 1 W. P. Griffith, *Chem. Soc. Rev.*, **21**, 179 (1992).
- 2
 - a) S. Y. S. Cheng, N. Rajapakse, S. J. Rettig and B. R. James, *J. Chem. Soc., Chem. Commun.*, 2669 (1994).
 - b) S. Y. S. Cheng and B. R. James, *Proc. of the 78th Can. Chem. Conf.*, Guelph, Canada, 1995, Abstract IN-447.
- 3
 - a) N. Rajapakse, Ph. D. Dissertation, University of British Columbia, 1990.
 - b) N. Rajapakse, B. R. James and D. Dolphin, *Stud. Surf. Sci. Catal.*, **55**, 105 (1990).
- 4 W.-H. Leung, C.-M. Che, C.-H. Yeung and C.-K. Poon, *Polyhedron*, **12**, 2331 (1993).
- 5
 - a) C.-M. Che and W. H. Leung, *J. Chem. Soc. Dalton Trans.*, 2932 (1991).
 - b) W. H. Leung and C.-M. Che, *J. Am. Chem. Soc.*, **111**, 8812 (1989).
- 6
 - a) C.-M. Che, C. Ho and T.-C. Lau, *J. Chem. Soc. Dalton Trans.*, 1259 (1991).
 - b) M. S. Thompson and T. J. Meyer, *J. Am. Chem. Soc.*, **104**, 5070 (1982).
- 7
 - a) L. Roecker and T. J. Meyer, *J. Am. Chem. Soc.*, **109**, 746 (1987).
 - b) M. S. Thompson and T. J. Meyer, *J. Am. Chem. Soc.*, **104**, 4106 (1982).
- 8 D. G. Lee and L. N. Congson, *Can. J. Chem.*, **68**, 1774 (1990).
- 9 C.-M. Che, W.-T. Tang, W.-O. Lee, K.-Y. Wong and T.-C. Lau, *J. Chem. Soc. Dalton Trans.*, 1551 (1992).
- 10 J. P. Collman, C. E. Barnes, P. J. Brothers, T. J. Collins, T. Ozawa, J. C. Galluci and J. A. Ibers, *J. Am. Chem. Soc.*, **106**, 5151 (1984).
- 11 R. J. Fessenden and J. S. Fessenden, *Organic Chemistry*, 3rd Edition, Brookes/Cole, Monterey, 1986, p. 523-524.
- 12
 - a) C. Sishta, M. Ke, B. R. James and D. Dolphin, *J. Chem. Soc., Chem. Commun.*, 787 (1987).
 - b) M. Ke, C. Sishta, B. R. James and D. Dolphin, *Inorg. Chem.*, **30**, 4776 (1991).
 - c) C. S. Alexander, Ph. D. Dissertation, University of British Columbia, 1995.
- 13 J. G. Muller, J. H. Acquaye and K. J. Takeuchi, *Inorg. Chem.*, **31**, 4552 (1992).

- 14 P. Dubourdeaux, M. Taverès, A. Grand, R. Ramasseul and J.-C. Marchon, *Inorg. Chim. Acta.*, **240**, 657 (1995).
- 15 a) C.-M. Che, W.-T. Tang, W.-T. Wong and T.-F. Lai, *J. Am. Chem. Soc.*, **111**, 9048 (1989).
b) C.-K. Li, C.-M. Che, W.-F. Tong and T.-F. Lai, *J. Chem. Soc. Dalton Trans.*, 813 (1992).
- 16 T. Mlodnicka and B. R. James, in *Metalloporphyrins Catalyzed Oxidations*, eds. F. Montanari and L. Casella, Kluwer Academic Publishers, Dordrecht, 1994, p. 121.
- 17 J. T. Groves and R. Quinn, *J. Am. Chem. Soc.*, **107**, 5790 (1985).
- 18 J. T. Groves and K.-H. Ahn, *Inorg. Chem.*, **26**, 3833 (1987).
- 19 M. J. Camezind, B. R. James and D. Dolphin, *J. Chem. Soc., Chem. Commun.*, 1137 (1986).
- 20 J. T. Groves and J. S. Roman, *J. Am. Chem. Soc.*, **117**, 5594 (1995).
- 21 B. Scharbert, E. Zeisberger and E. Paulus, *J. Organometallic Chem.*, **493**, 143 (1995).
- 22 a) D. T. T. Yapp, J. Jaswal, S. J. Rettig, B. R. James and K. A. Skov, *Inorg. Chim. Acta.*, **177**, 199 (1990).
b) D. T. T. Yapp, J. Jaswal, S. J. Rettig, B. R. James and K. A. Skov, *J. Chem. Soc., Chem. Commun.*, 1528 (1992).
- 23 G. Domazetis, B. Tarpey, D. Dolphin and B. R. James, *J. Chem. Soc., Chem. Commun.*, 939 (1980).
- 24 a) H. Ohtake, T. Higuchi and M. Hirobe, *Heterocycles*, **40**, 867 (1995).
b) H. Ohtake, T. Higuchi and M. Hirobe, *J. Am. Chem. Soc.*, **114**, 10660 (1992).
- 25 J. T. Groves and T. E. Nemo, *J. Am. Chem. Soc.*, **105**, 6243 (1983).
- 26 J. T. Groves, *J. Chem. Ed.*, **62**, 928 (1985).
- 27 J. F. Hurley, *Intermediate Calculus*, Saunders College, Philadelphia, 1980, p. 682.

Chapter 5

Reactivities of Ru(TDCPP-Cl₈) Species

5.1 Introduction

The development of metalloporphyrins as catalysts in O₂-oxidations of organic compounds, a particular aim being the oxidation of light alkanes, entered a new stage with the introduction of the so-called third-generation porphyrins (See Section 1.4.1). The methodology behind the development of this class of compounds is based on the extensive halogenation of the TPP ligand at its β -pyrrole positions and on the *meso*-phenyl rings to stabilize the porphyrin against oxidative destruction in the oxidizing medium of the reaction mixture. Furthermore, the saddle shape conformation¹ for these extensively halogenated metalloporphyrins favours monomeric structures and prevents their “dimerization” to μ -oxo-dinuclear species,² a cause for catalyst deactivation. Adding to these properties a very reactive oxometal moiety due to the addition of electron-withdrawing halogen groups (if the systems indeed generate M=O moieties as the active catalytic centres), a potentially powerful reagent is thus available for oxidizing organic compounds.

Of particular significance is the work of Lyons and Ellis on the O₂-oxidation of light alkanes catalyzed by Fe(porp) species [porp = octa- β -fluoro, chloro and bromo-tetra(pentafluorophenyl)porphyrins] under mild conditions; for example, total turnovers for an isobutane system exceeded 10000 mol⁻¹.³ One of the aims of the present thesis is to extend the periodic analogy of Fe to Ru and examine the reactivity of similar Ru-porphyrins of the third generation. One difficulty is the insertion of ruthenium into the free-base porphyrins having a large number of electron-withdrawing halogens. Collaboration with Dolphin and Xie led to successful preparation of one of the first

perhalogenated Ru-porphyrin complexes, $\text{Ru}^{\text{II}}(\text{TDCPP-Cl}_8)(\text{CO})$ (TDCPP-Cl_8 = dianion of octa- β -chloro-tetra(2,6-dichlorophenyl)porphyrin], whose reactivity is the subject of this chapter.

5.1.1 Ru-Perhalogenated Porphyrins: Aims and Scope

Although a wide range of transition metals across the periodic table has been inserted into free-base porphyrins, the metallation of the highly-halogenated third-generation porphyrins, to the best of the author's knowledge, has been limited until very recently to the first row transition metals.⁴ Metalloporphyrins of such type, particularly iron porphyrins, have been shown to exhibit high activity in the hydroxylation of alkanes.³ Only recently have there been reports on the second row (Ru) congeners,^{5,†} although no catalysis studies on these Ru-porphyrins are yet reported.

The metallation of Ru into these highly-halogenated porphyrins is non-trivial. The common procedure of Ru-insertion is to reflux $\text{Ru}_3(\text{CO})_{12}$ and the free-base porphyrin (eg. TPP) in a high-boiling organic solvent, such as mesitylene⁶ under 1 atm CO for extended periods of time, or more recently, heating $\text{Ru}(\text{DMF})_6^{3+}$ and water-soluble free-base porphyrins in DMF.⁷ Initial attempts in this thesis work to metallate H_2TPFPP (which contains twenty F-groups, and does not have any β -pyrrole-halo groups) via the $\text{Ru}_3(\text{CO})_{12}$ route [see Chapter 2 regarding the preparation of $\text{Ru}^{\text{II}}(\text{porp})(\text{CO})$, where porp = TMP and TDCPP] gave low yields of $\text{Ru}^{\text{II}}(\text{TPFPP})(\text{CO})$ (<10% approximated by spectrophotometry and TLC), and the application of the $\text{Ru}_3(\text{CO})_{12}$ route to other highly-

[†] Work described in the present thesis was being carried out when the papers of Ref. 5 appeared in the literature.

halogenated porphyrins was assumed to be similarly difficult. Recently, Murahashi *et al.*⁸ reported the reaction of Ru₃(CO)₁₂ and H₂TPFPP in decalin to give Ru^{II}(TPFPP)(CO) in a 49% yield; this solvent was also used in the preparation of Ru^{II}(TDCPP)(CO) by Dubourdeaux *et al.*⁹ Also, Birnbaum *et al.*⁵ reported the insertion of ruthenium into H₂TPFPP-Cl₈, the reaction involving heating Ru₃(CO)₁₂ and the free-base porphyrin in refluxing perfluorobenzene to form Ru^{II}(TPFPP-Cl₈)(CO).⁵ Clearly, the choice of the solvent for the Ru₃(CO)₁₂ route is critical for the successful preparation of Ru-porphyrins containing a large number of electron-withdrawing groups. Again, at the time when the current research was in progress, the reports of Birnbaum *et al.*⁵ were unpublished, and an alternative route to obtain the highly-chlorinated Ru-porphyrin, Ru^{II}(TDCPP-Cl₈)(CO), (1), was discovered in a collaborative effort with Dolphin and Xie (Chapter 2). Following the successful preparation of (1), *trans*-Ru^{VI}(TDCPP-Cl₈)(O)₂, (2), was obtained from the *m*-CPBA oxidation of (1). (1) and (2) were tested as catalyst precursors in the O₂-oxidations of alcohols, alkenes and alkanes.

5.2 Sample Preparation and Data Analysis

5.2.1 Sample Preparation in Catalysis Studies

The catalytic O₂-dehydrogenations of benzyl alcohol and 1-phenylethanol (up to 0.58 M) were studied at 50 °C in benzene under 1 atm air using an experimental procedure similar to that outlined in Section 4.2.1. Concentrations of (2) were 10⁻⁵ - 10⁻⁴ M in benzene, these being determined spectrophotometrically using the extinction coefficient of the complex (Chapter 2). The aerobic oxidation of Ph₃CH (~10⁻² M) to Ph₃COH catalyzed by (2) (~10⁻⁴ M) in benzene also follows the same setup as that

described in Section 4.2.1.

The O₂-oxidations of neat *cis*-cyclooctene (referred to as cyclooctene), cyclohexene and methylcyclohexane were studied under 1 atm O₂. The 1 atm O₂ environment created by the continual purge of O₂ into the neat hydrocarbons resulted in some solvent losses in the cyclohexene and methylcyclohexane systems, and the experimental setup shown in Figure 5.1 was employed to minimize the evaporation of the hydrocarbons. The reactions were done in a 25 mL, three-neck, conical flask topped with a water-cooled (10 °C) condenser, although under such an experimental setup, ~20% losses of methylcyclohexane and cyclohexene were still observed over the time of the experiment,[†] typically < 24 h. Alkane or alkene (5 mL) was added into the flask, and subsequently ~0.5 mg (1) or (2) was added into the hydrocarbons. A 25 µL aliquot of the neat hydrocarbon containing the Ru-porphyrin was diluted in 1 mL benzene, and the diluted concentration of (1) or (2) was determined spectrophotometrically in the benzene solution; typical concentrations of the Ru-porphyrin in the original neat hydrocarbons, where significant catalysis occurred (see Sections 5.4 and 5.5), were calculated to be ~ 3 x 10⁻⁵ M. The reaction vessel was submerged into an oil-bath heated by an electric hot-plate, with the desired temperature (35 to 100 °C) maintained within ± 1 °C. O₂ was introduced into the solution through a stainless steel needle, with the gas continually purging through the solution at ~5 mL min⁻¹.

Physical changes were observed approximately 1 h after the cyclooctene system was heated to 93 °C. The darker brown colour of the alkene solutions due to the presence

[†] The 20% losses in volumes were assumed to contain mostly methylcyclohexane and cyclohexene, as they are the most volatile component in the respective systems.

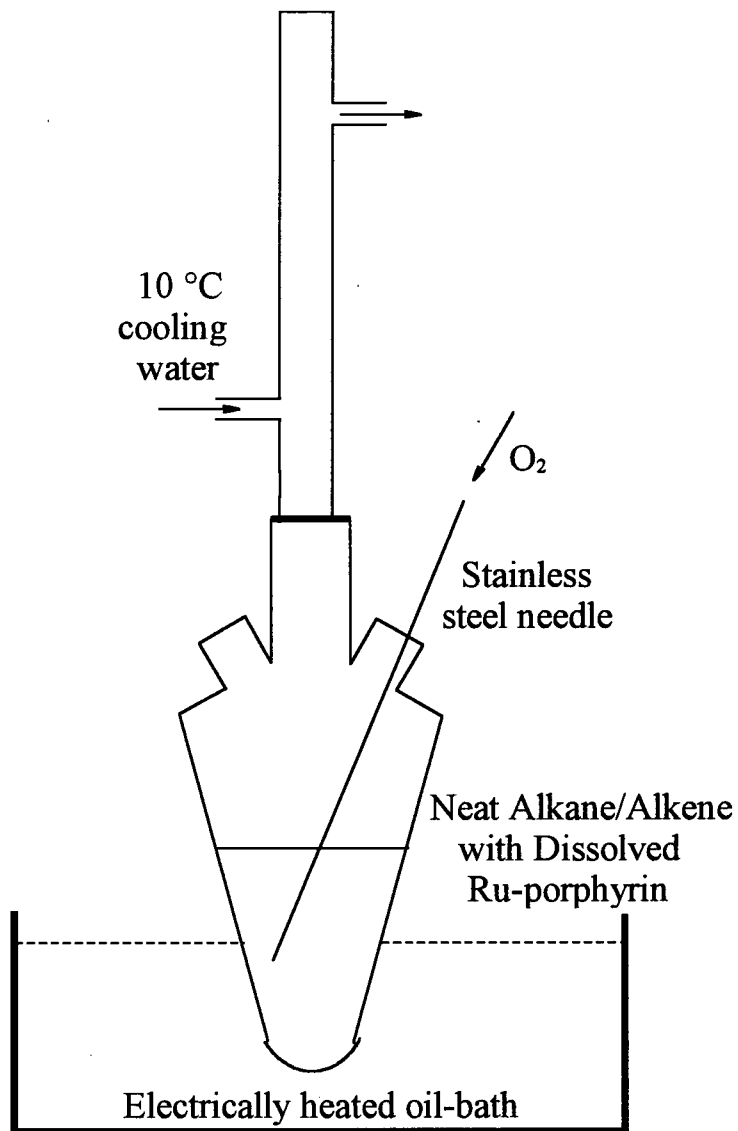


Figure 5.1. Experimental setup for the oxidations of neat cyclohexene, cyclooctene and methylcyclohexane under 1 atm O₂. The constant purge of O₂ necessitated the use of a water-cooled condenser. ~20% losses of cyclohexene or methylcyclohexane (see text) were observed over a period of ~24 h.

of (**2**) turned greenish-yellow after this time; however, a Soret absorption, although gradually disappearing as the reaction progressed, was still observed at 422 nm at this time. Of note, the Soret λ_{max} for (**2**) is at 430 nm; however, (**2**) reacts with the neat cyclooctene almost immediately at room temperature, and the resulting Ru-porphyrin species absorbs at 422 nm. At the end of 24 h, < 30% of the intensity of the Soret maximum at 422 nm remained, indicating that a substantial amount of the Ru-porphyrin had decomposed. After 55 h, a very small (< 5%) Soret absorption was still observed in the cyclooctene system, but a large UV-visible absorption, presumably due to the organic products (starting from ~ 420 nm and rising steeply below this wavelength), made an accurate determination of the amount of intact porphyrin difficult. The methylcyclohexane system showed no oxidation after 2 h of heating at 90 °C; however, the solution became bleached after 24 h, when no Soret absorbances were evident.

5.2.2 Preparation of *trans*-Ru^{VI}(TDCPP-Cl₈)(O)₂

That *trans*-Ru^{VI}(TDCPP-Cl₈)(O)₂ (**2**) contains two oxo ligands is shown by its ability to oxidize 2 equivalents of P(*p*-F-C₆H₄)₃ to the corresponding phosphine oxide in CDCl₃ under 1 atm Ar, as observed by ¹⁹F-NMR spectroscopy.[†] The IR absorption due to ν_{Ru=O} within (**2**) is observed at 827 cm⁻¹ (solid KBr), in agreement with values for other *trans*-Ru^{VI}(porp)(O)₂ species (porp = TMP,¹⁰ TDCPP,¹¹ OEP and TPP¹²), whose ν_{Ru=O} values range between 820 and 823 cm⁻¹. Hence a trans geometry for the oxo ligands in (**2**)

[†] 5 equivalents of P(*p*-F-C₆H₄)₃ (2.5 × 10⁻³M) were added to a CD₂Cl₂ solution of (**2**) (5.0 × 10⁻⁴M) under 1 atm Ar, and the amount of oxide product was determined from integrations on the ¹⁹F-NMR spectrum (acquired ~ 30 min after the addition of the phosphine): OP(*p*-F-C₆H₄)₃ and P(*p*-F-C₆H₄)₃ at δ = -30.7 and -36.4, respectively (see also Chapter 3).

seems reasonable. Purification of (**2**) by column chromatography (activity I neutral alumina) using benzene as the eluent gives a product with Soret and Q-bands at 430 and 516 nm, respectively (Chapter 2); however, when species (**2**) is left in benzene, within 1 h the Soret maximum shifts to 422 ($\epsilon \sim 150,000 \text{ M}^{-1} \text{ cm}^{-1}$) and the Q-band to 518 nm ($\epsilon \sim 14,000 \text{ M}^{-1} \text{ cm}^{-1}$). Using CH_2Cl_2 as the eluent leads to the same Soret and Q-band shifts, although the time for the transformation is typically longer (~ 2 h) than that in benzene. The loss of the dioxo ligands in these solution species is certain, as the Soret shift from 430 to 422 nm is accompanied by the loss of the 827 cm^{-1} absorption band in the IR spectrum of a recovered solid sample. Of note, the addition of ~ 10 equivalents of *m*-CPBA to the benzene solution containing the unknown Ru(porp) species with λ_{\max} 422 nm regenerates almost quantitatively (**2**).

Addition of 0.50 mL HCl-saturated benzene solution to a fresh benzene solution of (**2**) ($\sim 4 \times 10^{-6} \text{ M}$, 5.00 mL), within 1 min, yielded a new species which absorbed at 424 and 528 nm, with ϵ values of 140,000 and $14,000 \text{ M}^{-1}\text{cm}^{-1}$, respectively. The reaction of HCl with $\text{Ru}^{\text{VI}}(\text{porp})(\text{O})_2$ species, which will be discussed in Chapter 6, gives $\text{Ru}^{\text{IV}}(\text{porp})(\text{Cl})_2$ products. The benzene solution was pumped to dryness, and the solid that remained was analyzed by mass spectrometry (Figure 5.2); the mass peak at 1336 amu corresponds to the parent peak for $[\text{Ru}^{\text{IV}}(\text{TDCPP-Cl}_8)(\text{Cl})_2]^+$, which suggests that the bis(chloro) species was present in the solid. This reaction of (**2**) with HCl gives further indirect evidence that (**2**) is the dioxo species.

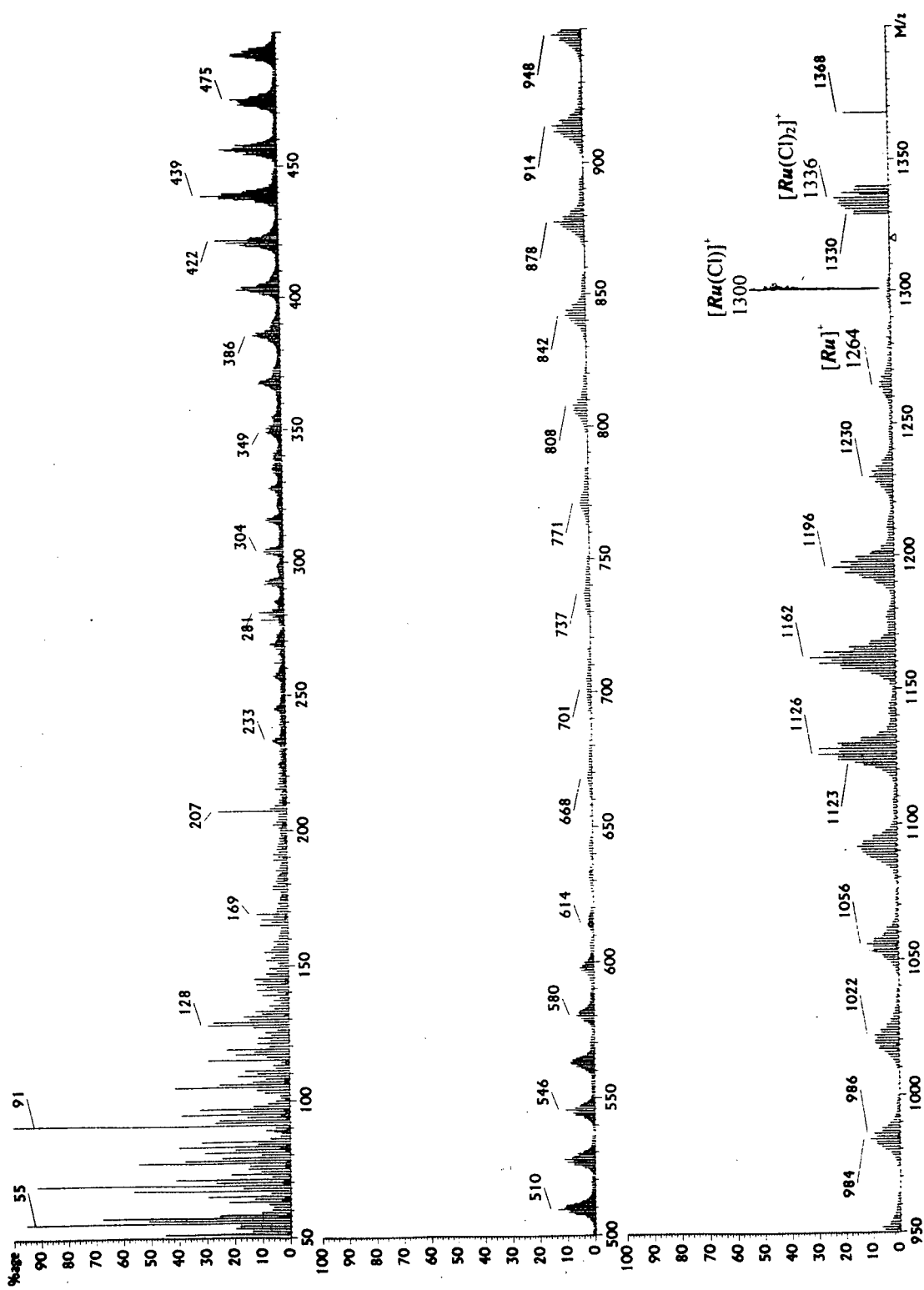


Figure 5.2. Mass spectrum (EI) of $\text{Ru}^{\text{V}}(\text{TDCPP-C18})(\text{Cl})_2$ made from the reaction of $\text{Ru}^{\text{VI}}(\text{TDCPP-C18})(\text{O})_2$ with HCl (see text).
 $\text{Ru} = \text{Ru}(\text{TDCPP-C18})$.

The identity of the Ru(TDCPP-Cl₈) species with a Soret maximum at 422 nm is unknown. Most likely the sixteen Cl-groups on the porphyrin makes the Ru=O moieties within (**2**) extremely reactive, and (**2**) perhaps react with any trace impurities in the solvents[†] presumably to form reduced, lower-valent Ru-species. When a solution (benzene or CH₂Cl₂) of (**2**) is left standing for 1 week in air, the Soret maximum shifts further to 418 nm, and at this time an IR absorption due to ν_{CO} can be observed at 1965 cm⁻¹. Even more remarkable is that a solid sample of (**2**) left exposed to air for 1 month shows the presence of an IR stretch at ν_{CO} = 1965 cm⁻¹.

5.2.3 Data Acquisition and Analysis

The progress of all the catalytic oxidations (alcohol and hydrocarbon systems) was monitored by GC analysis. The procedure and methodology have been described already in Sections 2.2.5 and 4.2.2. Known standards, when available, were used to identify the oxidation products (Chapter 2). In addition, GC-MS analyses were employed to ascertain the identities of some of the products from the neat cyclohexene, cyclooctene and methylcyclohexane systems, where known standards were unavailable for all of the oxidation products. The GC-MS data are compiled in Appendix E, as are the raw data from the GC analyses for the catalysis studies on these neat hydrocarbons systems.

[†] The benzene and CH₂Cl₂ eluents used were HPLC grade solvents from Fisher, and were used without further purification.

5.3 Catalytic Aerobic Oxidation of Alcohols

$\text{Ru}^{\text{VI}}(\text{TDCPP-Cl}_8)(\text{O})_2$ (**2**) was tested as a catalyst for the aerobic oxidation of alcohols. In Chapter 4, the aerobic oxidation of alcohols in benzene catalyzed by the $\text{Ru}^{\text{VI}}(\text{porp})(\text{O})_2$ species (porp = TMP and TDCPP) was discussed, and the TDCPP analogue was more susceptible to deactivation via decarbonylation pathways (total loss of catalytic activity within 24 h). The activity of (**2**) is of the same order of magnitude as that of $\text{Ru}^{\text{VI}}(\text{TMP})(\text{O})_2$ (Chapter 4); this is surprising as the reactivity of (**2**) had been thought to resemble that of the TDCPP analogue, also highly chlorinated, and (**2**) was expected to be similarly susceptible to deactivation. That (**2**) does not lose catalytic activity as rapidly as $\text{Ru}^{\text{VI}}(\text{TDCPP})(\text{O})_2$ under similar conditions suggests perhaps that the highly distorted and sterically crowded environment about the ruthenium prevents decarbonylation of the aldehyde or ketone products (Chapter 4); however, inspection of the 1-phenylethanol system after ~ 7 d shows the presence of $\text{Ru}^{\text{II}}(\text{TDCPP-Cl}_8)(\text{CO})$, as evidenced by the presence of ν_{CO} at 1965 cm^{-1} in the IR spectrum.

The aerobic oxidations of benzyl alcohol and 1-phenylethanol catalyzed by (**2**) are shown in Figures 5.3 and 5.4. About 1200 turnovers are obtained for benzyl alcohol after 15 d; no benzoic acid is detected under the conditions described below. The conditions used in this system are the optimum ones found for the Ru(TMP)/benzyl alcohol system: addition of 3.0 M aqueous KOH (50 μL) to benzene (0.40 mL) and moderate reaction conditons (1 atm air at 50 °C). Of interest, the unknown species with a characteristic λ_{max} 422 nm described in Section 5.2.2 gives almost the same turnover numbers as those by (**2**) (see later).

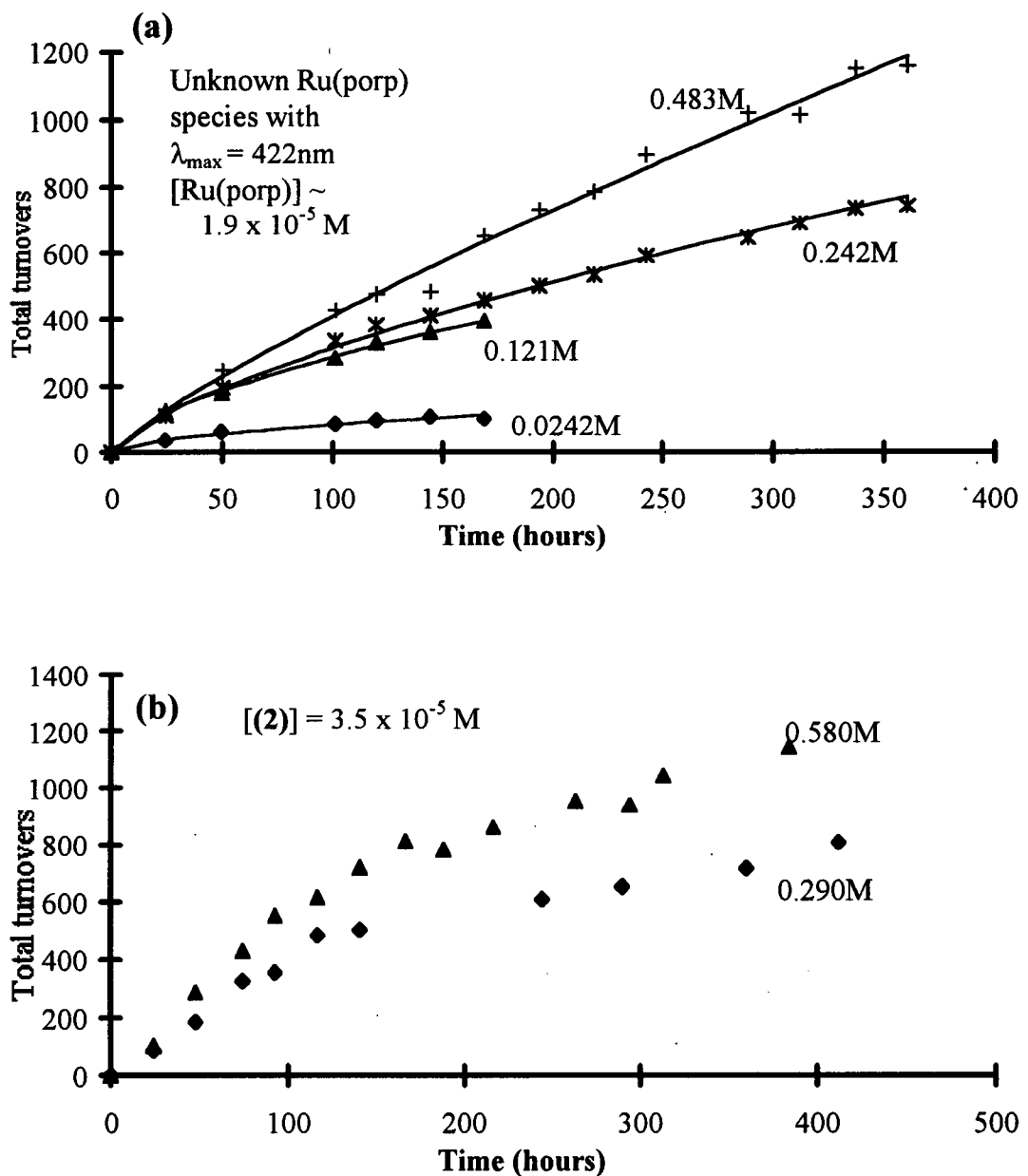


Figure 5.3. Aerobic oxidation of benzyl alcohol to benzaldehyde catalyzed by $\text{Ru}^{\text{VI}}(\text{TDCPP-Cl}_8)(\text{O})_2$ (**2**) under 1 atm air in benzene at 50 °C (2-phase system containing 0.40 mL benzene/50 μL 3.0 M aqueous KOH, see text). The unknown Ru-porphyrin species with characteristic Soret absorption at 422nm (a) exhibits almost the same activity as (**2**) (b).

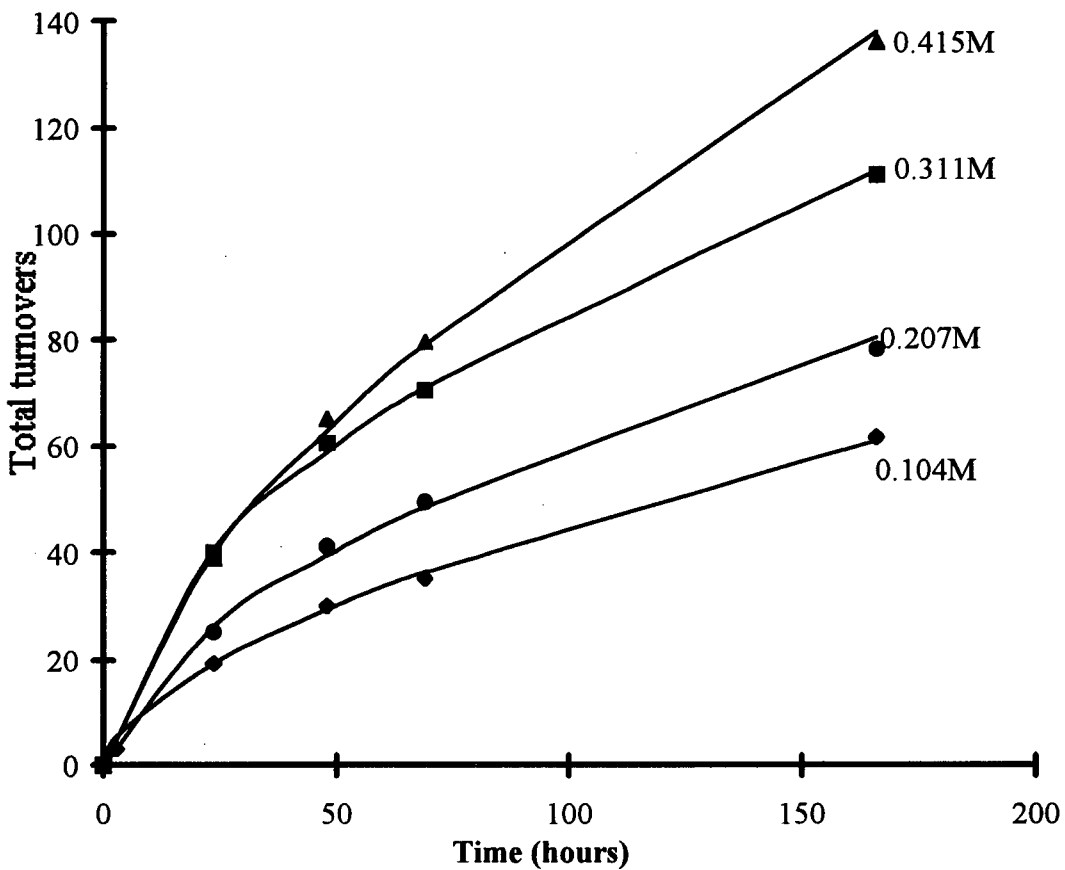
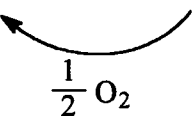
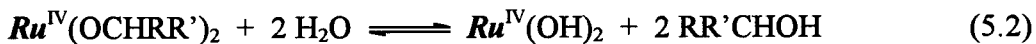
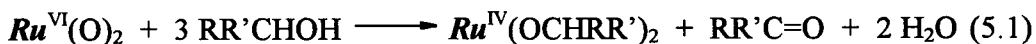


Figure 5.4. Aerobic oxidation of *R,S*-1-phenylethanol to acetophenone catalyzed by Ru^{VI}(TDCPP-Cl₈)(O)₂ (**2**) under 1 atm air in benzene at 50 °C (2-phase system containing 0.40 mL benzene/50 μL 3.0 M aqueous KOH, see text). [(**2**)] = 2.1 × 10⁻⁴ M.

Addition of the common radical inhibitor, 2,6-ditertbutyl-4-methylphenol (BHT, 0.1 M) to the benzyl alcohol system did not hinder the oxidation, thus ruling out the operation of a radical-chain mechanism. The selective oxidation of benzyl alcohol to benzaldehyde without further conversion to benzoic acid also strongly suggests a mechanism not involving free-radicals. The catalytic process most likely is analogous to that of the Ru^{VI}(TMP)(O)₂ system, which has been fully discussed in Section 4.3.3, and is summarized again in Eqs. 5.1 through 5.4 [*Ru* = Ru(TDCPP-Cl₈)].



Of note, the addition of 10 μL of benzyl alcohol (1×10^{-2} M) to (2) (3.0×10^{-6} M in benzene under air), after ~ 30 min, gives a Ru-species which absorbs at 422 and 518 nm; this spectral change is the same, and occurs on the same timescale, as that observed with (2) alone in benzene solution (see earlier). If the present system exhibits chemistry similar to that of the TMP system (Chapter 4), the Ru-product in the benzyl alcohol reaction is expected to be Ru^{IV}(TDCPP-Cl₈)(OCH₂Ph)₂. That the unknown Ru(TDCPP-Cl₈) species with λ_{max} 422 nm formed from (2) alone in benzene exhibits almost the same reactivity as that of (2) implies that it is an equally effective catalyst precursor, presumably exhibiting similar chemistry as (2) (Eqs. 5.1 to 5.4); this suggests that the λ_{max} 422 nm

species is similar in nature to $\text{Ru}^{\text{IV}}(\text{O})$, $\text{Ru}^{\text{IV}}(\text{L})_2$ or $\text{Ru}^{\text{II}}(\text{L}')_2$ species (L , L' = ligands that are labile or exchangeable with water or alcohol; see Chapter 4).

The catalytic activity of (2) is vastly superior to that of $\text{Ru}^{\text{VI}}(\text{TDCPP})(\text{O})_2$ and is comparable to that of $\text{Ru}^{\text{IV}}(\text{TMP})(\text{O})_2$ for the aerobic oxidation of benzyl alcohol. In addition, (2) gives ~ 130 turnovers for the catalytic aerobic oxidation of 1-phenylethanol to acetophenone, while $\text{Ru}^{\text{VI}}(\text{porp})(\text{O})_2$ species (porp = TMP or TDCPP) give only a few turnovers before being deactivated completely (Chapter 4). Hence, (2) might offer a greater potential as an alcohol oxidation catalyst, and possibly is more useful for a greater range of alcohol substrates.

5.4 Oxidation of Alkenes

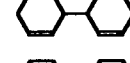
The O_2 -oxidations of cyclohexene and *cis*-cyclooctene catalyzed by (2) give total turnovers of the order of 10^5 when the neat alkenes are used without any solvent. The epoxide is the main product in the cyclooctene oxidation; however, cyclohexene-2-ol and cyclohexene-2-one, allylic C-H bond cleavage compounds, are the main products in the cyclohexene oxidation. Table 5.1 lists the results from the oxidation of cyclohexene and cyclooctene catalyzed by (1) and (2). The addition of BHT (either 0.01 or 0.1 M) completely inhibits oxidation in both alkene systems, and both active systems test positive (KI/starch) for the presence of organic peroxides. The BHT experiment and the predominant production of allylic C-H bond cleavage products within the cyclohexene system suggest a free-radical oxidation mechanism. It is clear from blank studies at higher temperatures that (1) and (2) are necessary in these alkene oxidations, and a reasonable

conclusion is that the Ru-porphyrins are involved in the decomposition of organic peroxides to propagate a radical-chain process at a lower temperature (see later, Figure 5.7).

The O₂-oxidations of alkenes using radical initiators have been well-studied,¹³ and the reactions generally follow the mechanism outlined in Figure 5.5. Two main propagating pathways, addition of RO₂[•] to alkenes (Eq. 5.7) and H-abstraction from alkenes by RO₂[•] (Eq. 5.9), are identified within this mechanism, with the former leading to epoxides as products (Eq. 5.8). Clearly, for every equivalent of epoxide formed, one equivalent of alkoxyl radical must be accounted for (Eqs. 5.8, 5.10, 5.11 and possibly 5.12); therefore, the maximum yield of epoxide should never exceed 50%, if addition is the only epoxide yielding path. Mayo mentioned the possibility of an alkoxyl radical giving directly an epoxide (Eq. 5.12);^{13c} however, how such a reaction can proceed was not indicated in the report and the actual mechanism for such an epoxide forming route is not obvious. The yields of the various products in the cyclohexene system are consistent with radical pathways in operation; however, the cyclooctene system gives as high as 87% cyclooctene-oxide among the products (see also Figure 5.6), which is far higher than the expected maximum of 50% based on an addition pathway alone.

Cyclooctene is known to be an unusual substrate in autoxidation studies in that it is not as autoxidizable compared to its cyclohexene, cyclopentene and cycloheptene homologues.^{13b} A most intriguing, and still unexplained, observation by de Roch and Balaceanu was that the autoxidation of cyclooctene at 106 °C in the presence of

Table 5.1. Oxidation of alkenes catalyzed by Ru^{II}(TDCPP-Cl₈)(CO) (**1**) and Ru^{VI}(TDCPP-Cl₈)(O)₂ (**2**) under 1 atm O₂.

Substrate	Products (% of starting alkene) [% Distribution of oxidation products]					Total Products (% of starting alkene)
cyclohexene ^a	 ^d	 ^d	 ^d	 ^{e,f}		
					+other dimers ^e	
Blank 24 h	0.012 [2.8]	0.16 [37]	0.23 [54]	0.0032 [0.74]	0.023 [5.4]	0.42 ± 0.1
[(1)] ^b = 3.15 × 10 ⁻⁵ M 23 h	1.05 [3.6]	13.4 [45]	12.8 [43]	0.031 [1.0]	2.1 [7.0]	29.6 ± 1 [92000 turnovers] ^g
cyclooctene ^a	 ^d		-C=O, -OH and -OOH ^f containing and rearrangement products ^e			
Blank 23 h ^c	8.2 [73]		3.1 [27]			11.3 ± 1
[(2)] ^b = 5.0 × 10 ⁻⁵ M 26 h	35.8 [87]		5.4 [13]			41.2 ± 4 [63000 turnovers] ^{h,i}

^a Reaction conditions: 5 mL neat alkene under 1 atm O₂; 35 ± 1 °C for cyclohexene and 93 ± 1 °C for cyclooctene, unless indicated otherwise.

^b Similar conversion were obtained in qualitative studies under the same conditions using (**2**) as the catalyst. Again, cyclohexene-2-ol and cyclohexene-2-one were the major products.

^c 110 ± 1 °C

^d Identification of product from the correlation of retention times with known standards, as well as by GC-MS (Appendix E).

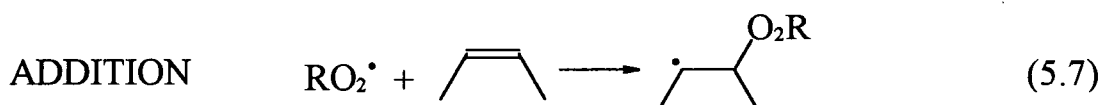
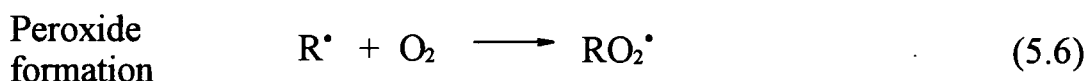
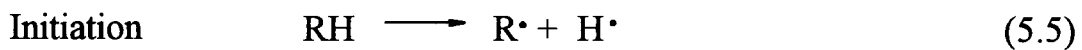
^e Formulation of product identity based on GC-MS only (Appendix E).

^f Presence of hydroperoxides suggested from a positive KI/starch test result.

^g Turnovers based on [neat cyclohexene] = 9.86 M.

^h Turnovers based on [neat cyclooctene] = 7.69 M.

ⁱ Progress of this reaction beyond 26 h is shown in Figure 5.6.



&

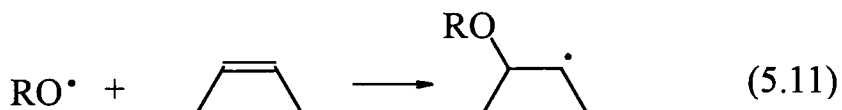
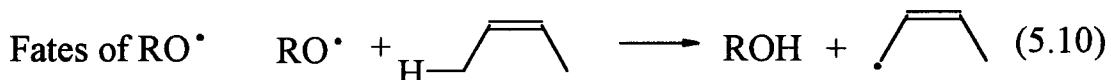
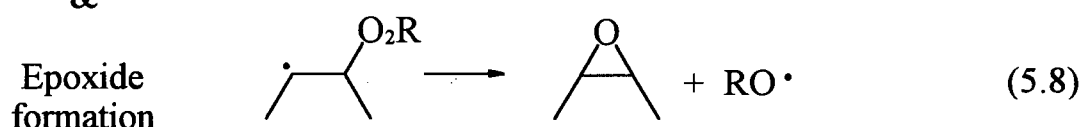


Figure 5.5. Radical-chain mechanism proposed for the oxidation of alkenes (Ref. 13). Chain propagation proceeds through either an ADDITION or ABSTRACTION pathway.

cobalt(II) stearate gave over 70% yield in the epoxide.¹⁴ At about the same time, Van Sickle *et al.* conducted similar experiments (ABN-initiated autoxidation) and found that only 40% cyclooctene-oxide was obtained at 70 °C;^{13b} the high epoxide yield observed by de Roch and Balaceanu was viewed with skepticism. The present cyclooctene system using (2) as the catalyst yields 87 % epoxide among the oxidation products after 26 h; there is no doubt that a > 50 % yield of epoxide is generated.

Approximately 60000 turnovers per day are realized at 93 °C when (2) is added to the cyclooctene, and the catalytic activity does not decrease much as the reaction proceeds (see Figure 5.6). As < 30% of the starting Ru-porphyrin remains in the cyclooctene system after 24 h (Section 5.2.1), the almost linear turnover versus time plot suggests that Ru-porphyrin species are not solely responsible for the catalytic activity (see Section 5.5 later). Worth noting is that the reaction involving cyclooctene and (2) is relatively clean and that the epoxide content among the products remains almost constant throughout the reaction (Figure 5.6). Autoxidation at 93 °C in the absence of (2) is negligible (< 0.4 % product after 24 h), but at 110 °C some 11 % cyclooctene autoxidation is evident (blank study, Table 5.1); the amount of epoxide obtained at 110 °C (blank study) is 73 ± 4 % of the total products, which is close to the distribution seen when (2) is present as a catalyst at 93 °C.

Earlier work by Mayo's group on the ABN-initiated autoxidation of cyclohexene at 60 °C (closed system initially under ~5 atm O₂) achieved a 6.15 % overall conversion in 13.5 h; among the products observed were cyclohexene-2-peroxide (80.4 %), cyclohexene-2-ol (7.0 %), cyclohexene-2-one (4.7 %), cyclohexene-oxide (0.9 %) and

dimers (7.0 %).^{13b} In comparison, the present cyclohexene system catalyzed by (1) shows a higher activity (30 vs. 6 % conversion) at a lower temperature (35 vs. 60 °C) and pressure (1 vs. 5 atm O₂). Thus, (1) and (2) are effective catalyst precursors, and are even more effective than some free-radical initiators (e.g. ABN) in promoting the free-radical propagated O₂-oxidation of cyclohexene and cyclooctene.

At lower temperatures (24 and 50 °C) under 1 atm air in benzene solvent [$\sim 10^{-2}$ M alkene, $\sim 5 \times 10^{-4}$ M (1) or (2)], (1) is completely inactive as a catalyst, while (2) shows marginal activity in the epoxidation of cyclohexene and cyclooctene. Under such

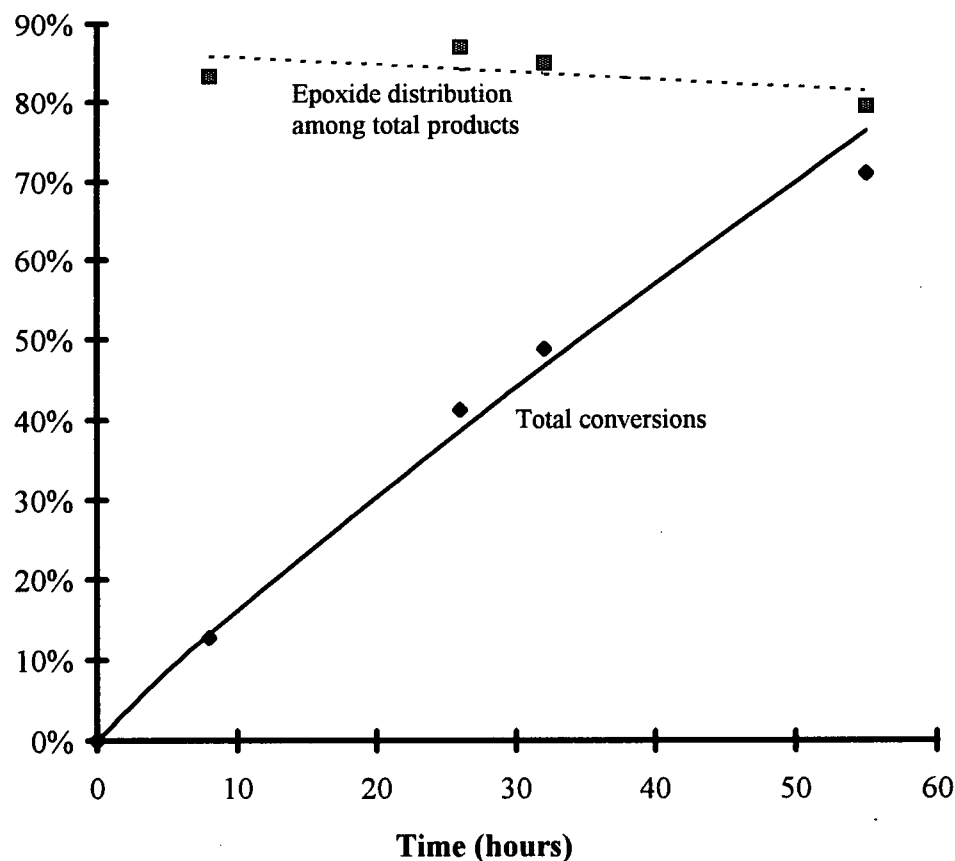


Figure 5.6. O₂-oxidation of cyclooctene under 1 atm O₂ at 93 ± 1 °C catalyzed by Ru^{VI}(TDCPP-Cl₈)(O)₂ (2). [(2)] = 5.0 × 10⁻⁵ M. Excess of alkene to (2) corresponds to 150000 : 1.

conditions, approximately 1 turnover per day is realized (total turnovers \sim 10) for either alkene when (2) is employed as the catalyst, and the turnovers obtained are invariant with temperature. Under 1 atm O₂ at 35 °C, (2) (3.5×10^{-5} M in benzene) also gives only 1 turnover after 16 h for the oxidation of cyclohexene (1.5×10^{-2} M) to cyclohexene-oxide. The Soret intensity at 422 nm has not changed when the solution is inspected after 24 h, unlike in the reactions involving the neat cyclooctene, indicating that the Ru-porphyrin remains intact in the reaction medium. The oxidation of both cyclohexene and cyclooctene, at dilute concentrations in benzene, produces exclusively the corresponding epoxides, a direct contrast with the neat alkene systems. An O-atom transfer mechanism, suggested by the specificity for epoxide formation, is most likely in operation in the case where the alkenes are dilute in the benzene solutions.

5.5 Oxidation of Alkanes

Lyons and Ellis have suggested that their isobutane and propane oxidations (\sim 13000 turnovers for isobutane) catalyzed by Fe(TPFPP-Br₈)(Cl) occur via a high-valent oxoiron intermediate, with the Fe=O moiety attacking the hydrocarbon C-H bonds.³ Recent work by Grinstaff *et al.*,¹⁵ however, demonstrated that the oxidations involve the decomposition of organic peroxides by Fe-porphyrins via a radical-chain mechanism (Figure 5.7). The inhibition of any oxidation in the presence of 0.01 M BHT, as well as the >99% selectivity for the tertiary C-H bond, led to the conclusion that the main reaction pathway was a free-radical one.¹⁵ Also, computer simulation studies based on free-radical

propagation of oxidation via Fe(porp) decomposition of hydroperoxides closely accounted for the actual experimental observations.¹⁶

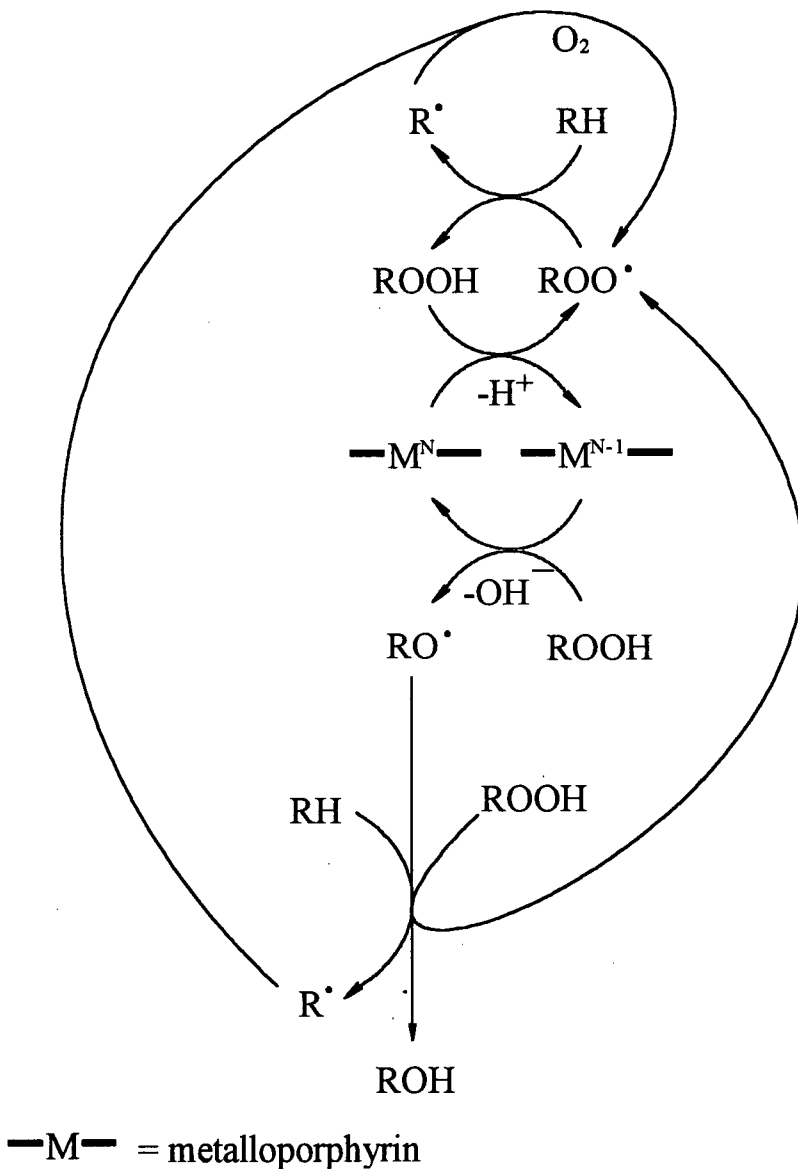


Figure 5.7. Radical-chain mechanism for the oxidation of alkanes via peroxide decomposition catalyzed by Fe-porphyrin species. Adapted from Ref. 15. Ru(TDCPP-Cl₈) species can be considered to undergo similar chemistry, catalyzing the decomposition of hydroperoxides.

In the present study, (1) and (2) are also effective in initiating the O₂-oxidation of methylcyclohexane at 90 °C via a radical-chain pathway, likely via a mechanism similar to the one proposed by Grinstaff *et al.* (Figure 5.7).¹⁵ The results for the methylcyclohexane oxidation catalyzed by (1) and (2) are listed in Table 5.2. A blank study conducted at 100 °C under 1 atm O₂ shows that the autoxidation gives only 0.67% oxidized products, which are distributed between 57 % 1-methylcyclohexanol, 26% secondary alcohols and 17% ketones. The selectivity for oxidation at the tertiary C-H bond over secondary ones normalized on a per bond basis[†] is approximately 12.4 for the autoxidation within the the blank solution. When (1) or (2) is present, a similar tertiary bond selectivity of 13 ± 3 (average of the three runs involving (1) and (2) in Table 5.2) is observed. Hence, the presence of (1) or (2) does not have any effect on the selectivity of oxidation, and the role of Ru-porphyrin species in the oxidation likely involves the catalytic decomposition of organic peroxides, similar to that of Fe-porphyrins in the scheme shown in Figure 5.7. Although the systems containing (1) or (2) give the same distribution of products as that in the blank, the Ru-porphyrin species are clearly effective in promoting oxidation of the methylcyclohexane by about 10-fold (Table 5.2). Of note, when BHT (0.01 M) was added, (1) and (2) were completely ineffective in promoting the autoxidation of methylcyclohexane, this result being consistent with a free-radical mechanism.

[†] no. 3° CH bond = 1; no. 2° CH bonds = 10; bond selectivity = $\frac{\sum 3^\circ \text{ products}}{\sum 2^\circ \text{ products}} \times 10$.

Table 5.2. Oxidation of methylcyclohexane catalyzed by Ru^{II}(TDCPP-Cl₈)(CO) (**1**) and Ru^{VII}(TDCPP-Cl₈)(O)₂ (**2**) under 1 atm O₂.

CONDITIONS	Products (% of starting alkene) ^a				e	C ₇ H ₁₄ O ₃ ^e Mixture of ring-opened acids and/or peroxides ^f	Total Yield (% of starting alkane)
	% Distribution of oxidation products						
Blank ^b 24 h	0.38, 0.17 [57, 26]	0.032, 0.058, 0.026 [4.7, 8.6, 3.9]	NONE	TRACE ^f		0.67 ± 0.07	
[1] = 3.15 × 10 ⁻⁵ 20 h ^c	2.1, 0.52 [41, 10]	0.36, 0.87, 0.35 [7.0, 17.0, 6.8]	0.29 [5.6]	0.64 [12.6]		5.2 ± 0.6 [13000 turnovers] ^g	
[2] = 1.14 × 10 ⁻⁵ 17.5 h ^c	0.98, 0.32 [35.4, 11.5]	0.19, 0.41, 0.17 [6.9, 14.9, 6.2]	0.20 [7.1]	0.50 [17.9]		2.8 ± 0.3 [19300 turnovers] ^g	
[2] = 3.15 × 10 ⁻⁵ 22.5 h ^b	3.65, 0.59 [37, 5.9]	0.57, 1.53, 0.59 [5.8, 15.4, 5.9]	1.06 [10.6]	1.95 [19.7]		9.9 ± 1 [25000 turnovers] ^g	

^a Losses due to evaporation of 20% of methylcyclohexane (b.p. 101 °C) have been taken into account in the tabulated results (see text).

^b 100 ± 1 °C

^c 93 ± 1 °C

^d Identification of product from the correlation of retention times with known standards, as well as by GC-MS (Appendix E).

^e Formulation of product identity based on GC-MS only (Appendix E).

^f Presence of hydroperoxides suggested from a positive KI/starch test result.

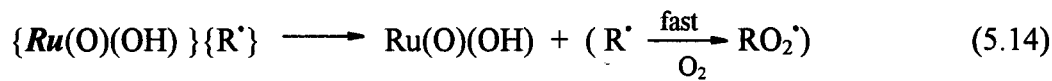
^g Turnovers based on [neat methylcyclohexane] = 7.8 M.

As a further test for catalytic activity, Ru^{VI}(TMP)(O)₂ (1.5×10^{-4} M) was added to neat methylcyclohexane, and the solution heated at 93 °C under 1 atm O₂. At the end of 16 h, approximately 3.6 % of oxidation products were present, with product distribution (52 % 1-methylcyclohexanol, 9 % secondary alcohols, 34 % ketones and 5 % other products) similar to that shown for systems containing (1) or (2) (see Table 5.2). An important observation is that after 16 h the brown colour due to Ru^{VI}(TMP)(O)₂ was completely bleached, and a small amount of black residue was present in the solution. In an attempt to increase the amount of the black residue formed, 5 mg Ru^{VI}(TMP)(O)₂ (10^{-3} M) was added to 5 mL methylcyclohexane and the procedure was repeated; however, almost no oxidation occurred after 16 h, and the oxidation products accounted for approximately 0.1% of the total organics (~ 8 turnovers), an amount even less than that for the blank study (Table 5.2). Also in this case, by visual inspection the colour of Ru^{VI}(TMP)(O)₂ was still present and no black residue was formed. A similar experiment, performed by adding 5 mg (1) (10^{-3} M) to 5 mL methylcyclohexane under corresponding conditions, also showed negligible oxidation after 16 h.

These “ineffective oxidation” experiments involving Ru^{VI}(TMP)(O)₂ and (1) correspond to porphyrin concentrations of approximately 10^{-3} M, while experiments that generated oxidation products have porphyrin concentrations that are 1 to 2 orders of magnitude more dilute. The reduced forms of the Ru-porphyrins, when present at higher concentrations, may react with the hydroperoxides to form Ru(porp)(O)₂ species,⁶ rather than decomposing them according to the scheme in Figure 5.7, and thus the radical-chain does not propagate (see below).

Ru(TMP) species are known to decompose hydroperoxides. Hansen studied the decomposition of cyclohexyl hydroperoxide catalyzed by Ru(porp) species (porp = TMP, TDCPP and TPP),¹⁷ and the following results are particularly relevant to the present TDCPP-Cl₈ system: i) the Ru^{II}(porp)(CO) precursors are initially oxidized to the corresponding Ru^{VI}(porp)(O)₂ species by the cyclohexyl hydroperoxide; ii) the decomposition rate of the cyclohexyl hydroperoxide is almost linear for about 120 min, although ~ 90 % of the Ru(TDCPP) species are destroyed in about 30 min; iii) the use of the radical scavenger, galvinoxyl, slows the rate of decomposition of hydroperoxides to 54% that of the reaction without any added radical scavenger; and iv) ESR studies show that the system contains ESR-active species which give rise to g-values of 2.0023 and 2.35, with the latter suggested to belong to a Ru non-porphyrin species.

In the present TDCPP-Cl₈ system, an almost linear rate in the cyclooctene oxidation was observed (Figure 5.6), although > 70% of the Ru(TDCPP-Cl₈) species had been destroyed in the first 24 h. This result suggests that Ru-porphyrin species are not solely responsible for the catalytic oxidation within the neat hydrocarbon systems; complementing this proposal are Hansen's studies,¹⁷ which suggest that Ru non-porphyrin species are responsible, at least partly, for the decomposition of cyclohexyl hydroperoxide. Dioxoruthenium(VI) porphyrin species may act as initiators for oxidation via a radical-chain pathway (Eqs. 5.13 and 5.14, [Ru = Ru(porp)]) by initially producing R[·] (and thus RO₂[·]) radicals; in Chapter 4, the oxidation of tertiary alkanes by Ru^{VI}(TMP)(O)₂ was



discussed, and a homolytic C-H cleavage was proposed as a possible mechanism (Eq. 5.13). When the Ru(porp) (porp = TDCPP-Cl₈ and TMP) concentrations are $\sim 10^{-3}$ M, which are ineffective in initiating any oxidation, the hydroperoxides formed (Eq. 5.14) may not be decomposed according to the scheme in Figure 5.7, but rather, the reduced Ru(porp) species react with the hydroperoxides preferentially to give the corresponding dioxo complexes.^{6,17} When the Ru(porp) concentrations are lower (10^{-4} to 10^{-5}), the systems become effective, operating via radical-chain pathways, for the oxidation of methylcyclohexane and cyclooctene; in these active systems, the destruction of the Ru(porp) species is noted. Hence, it is feasible that Ru non-porphyrin,¹⁷ decomposition products, not Ru(TDCPP-Cl₈) species, are responsible for mediating the radical-chain pathways depicted in Figure 5.7. As the Ru(porp) species are clearly destroyed during the oxidations, the usefulness of the porphyrin ligands is questionable (see below).

The black residue mentioned above is most likely RuO₂, but this as yet is unsubstantiated; demetallation of Ru-porphyrin species to give RuO₂ under oxidizing conditions has been demonstrated in this laboratory.¹⁸ It is difficult to increase the amount of Ru-porphyrin to give more decomposition product as the metallocporphyrin itself, when present at a higher concentration, inhibits the oxidation (and the demetallation seems to occur as the oxidation progresses). Of note, the essentially insoluble RuCl₃•3H₂O (5 mg, ~20 μmol, in 5 mL methylcyclohexane at 90 °C under 1 atm O₂ for 20 h) gives approximately 2% oxidation products for the methylcyclohexane system [35 % 1-methylcyclohexanol, 5.4 % secondary alcohols, 29.3 % ketones and 30.3% other products; cf. Table 5.2]. It is plausible that some RuCl₃ is oxidized to RuO₂ under the

above conditions, and the dioxide in turn can catalyze the generation and decomposition of hydroperoxides similar to a recently used RuCl₃/aldehyde/saturated hydrocarbon O₂-oxidation system, where the formation of high-valent Ru-oxo species was invoked.¹⁹ In this thesis work, RuCl₃•3H₂O and RuO₂•2H₂O, although essentially insoluble in neat cyclooctene, were also found to be effective in catalyzing the oxidition of the alkene: after 16 h at 92 °C, the RuCl₃•3H₂O system gave an 8% conversion (with 72% epoxide formation), while the RuO₂•2H₂O system gave a 16% conversion; after 56 h, the latter system showed almost 80% conversion (with 86% epoxide formation).

At room temperature (24 °C) under 1 atm air, the aerobic oxidation of Ph₃CH to Ph₃COH in benzene catalyzed by (2) is similar to that catalyzed by Ru^{VII}(porp)(O)₂ species (porp = TMP and TDCPP) (Section 4.4). Figure 5.8 shows the progress of the aerobic oxidation of Ph₃CH catalyzed by (2). The catalytic activity is marginal, and at the end of 20 d three turnovers are realized. As BHT (0.01 M) does not inhibit the oxidation, the mechanism most likely does not involve hydroperoxide decomposition, and is presumably similar to that described for the TMP and TDCPP systems (Chapter 4).

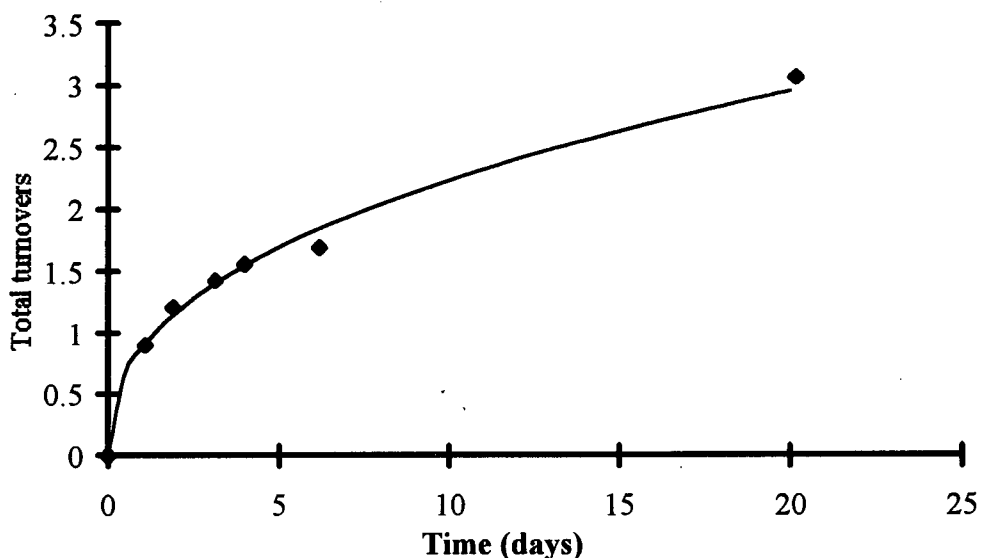


Figure 5.8. Aerobic oxidation of Ph_3CH to Ph_3COH catalyzed by $\text{Ru}^{\text{VI}}(\text{TDCPP-Cl}_8)(\text{O})_2$ (**2**) in benzene under 1 atm air at $24 \pm 1^\circ\text{C}$. $[\text{2}] = 3.1 \times 10^{-4}$ M; $[\text{Ph}_3\text{CH}] = 0.0223$ M

5.6 Conclusions

That $\text{Ru}(\text{TDCPP-Cl}_8)$ species can catalyze O_2 -oxidations of hydrocarbons via a radical-chain propagation pathway is clearly demonstrated in this chapter; however, the Ru-porphyrin species are completely destroyed in the methylcyclohexane system, as the colour of the Ru-porphyrin is completely bleached. For the neat cyclooctene system ~ 70% of the initial porphyrin most certainly disappears after 24 h.

Among the oxidations discussed in this chapter, the oxidation of alcohols to aldehydes or ketones in benzene catalyzed by (**2**) appears to be the only efficient oxidation

that proceeds via a high-valent oxoruthenium species. The Ru(TMP and TDCPP) systems were well-studied (Chapter 4) and the activity of Ru^{VI}(TDCPP-Cl₈)(O)₂ resembled that of the TMP analogue. The exclusive production of benzaldehyde from benzyl alcohol without further oxidation to benzoic acid, as well as the fact that BHT has no effect on the catalysis, suggest a process not involving a radical-chain pathway. The higher activity of (2), over that of the TMP and TDCPP analogues (Chapter 4), in catalyzing the aerobic oxidation of 1-phenylethanol suggests that (2) may be potentially more useful in the oxidation of other alcohols.

References

- 1 P. Ochsenbein, K Ayougou, D. Mandon, J. Fischer, R. Weiss, R. N. Austin, K. Jayaraj, A. Gold, J. Terner and J. Fajer, *Angew. Chem. Int. Ed. Engl.* **33**, 348 (1994).
- 2
 - a) J. P. Collman, C. E. Barnes, P. J. Collins, T. Owaza, J. C. Galluci and J. A. Ibers, *J. Am. Chem. Soc.*, **106**, 5151 (1984).
 - b) H. Masuda, T. Tagu, K. Osaki, H. Suzimoto, M. Mori and H. Ogoshi, *J. Am. Chem. Soc.*, **103**, 2199 (1981).
- 3
 - a) J. E. Lyons and P. E. Ellis, *Catal. Lett.*, **8**, 45 (1991).
 - b) P. E. Ellis and J. E. Lyons, *Coord. Chem. Rev.*, **105**, 181 (1990).
 - c) J. E. Lyons and P. E. Ellis, *Catal. Lett.*, **3**, 389 (1989).
- 4 T. P. Wijesekera and D. Dolphin, in *Metalloporphyrins in Catalytic Oxidations*, ed. R. A. Sheldon, Marcel Dekker, Inc., New York, p. 218, 1994.
- 5
 - a) E. R. Birnbaum, W. P. Schaefer, J. A. Labinger, J. E. Bercaw and H. B. Gray, *Inorg. Chem.*, **34**, 1751 (1995).
 - b) E. R. Birnbaum, J. A. Hodge, M. W. Grinstaff, W. S. Schaefer, L. Henling, J. A. Labinger, J. E. Bercaw and H. B. Gray, *Inorg. Chem.*, **34**, 3625 (1995).
- 6 N. Rajapakse, B. R. James and D. Dolphin, *Stud. Surf. Sci. Catal.*, **55**, 109 (1990).
- 7 C. J. Ware, M. Sc. Thesis, University of British Columbia, 1994.
- 8 S.-I. Murahashi, T. Naota and N. Komiya, *Tetrahedron Lett.*, **36**, 8059 (1995).
- 9 P. Dubourdeaux, M. Taverès, A. Grand, R. Ramasseul and J.-C. Marchon, *Inorg. Chim. Acta.*, **240**, 657 (1995).
- 10 J. T. Groves and R. Quinn, *Inorg. Chem.*, **23**, 3844 (1984).
- 11 N. Rajapakse, Ph.D. Dissertation, University of British Columbia, 1990.
- 12
 - a) C.-M. Che and W. H. Leung, *J. Chem. Soc. Dalton Trans.*, 2932 (1991).
 - b) W. H. Leung and C.-M. Che, *J. Am. Chem. Soc.*, **111**, 8812 (1989).
- 13
 - a) F. R. Mayo, *Acc. Chem. Research*, **1**, 193 (1968).
 - b) D. E. Van Sickle, F. R. Mayo and R. M. Arluck, *J. Am. Chem. Soc.*, **87**, 4824 (1965).
 - c) F. R. Mayo, *J. Am. Chem. Soc.*, **80**, 2497 (1958).
- 14 I. S. de Roch and J. C. Balaceanu, *Bull. Soc. Chim. Fr.*, 1393 (1964).

- 15 M. W. Grinstaff, M. G. Hill, J. A. Labinger and H. B. Gray, *Science*, **264**, 1311 (1994).
- 16 J. A. Labinger, *Catal. Lett.*, **26**, 95 (1994).
- 17 a) C. B. Hansen, Ph.D. Dissertation, Utrecht University, Netherlands, 1991.
b) C. B. Hansen, F. P. W. Agterberg, A. M. C. van Eijndhoven and W. Drenth, *J. Mol. Cat.*, **102**, 117 (1995).
- 18 B. R. James, S. R. Mikkelsen, T. W. Leung, G. W. Williams and R. Wong, *Inorg. Chim. Acta*, **85**, 209 (1984).
- 19 S.-I. Murahashi, Y. Oda and T. Naota, *J. Am. Chem. Soc.*, **114**, 7913 (1992).

Chapter 6

Preliminary Work:

**Reactions of Ru^{VI}(TMP)(O)₂ with HX Acids
and
Oxidation of Phenol and *N,N*-Dimethylaniline**

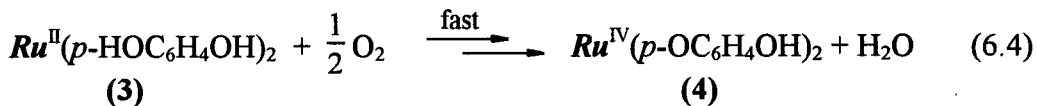
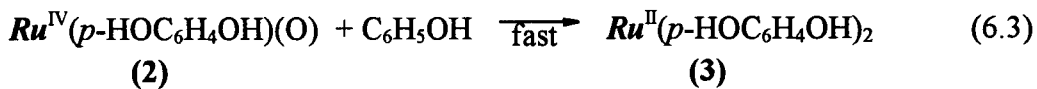
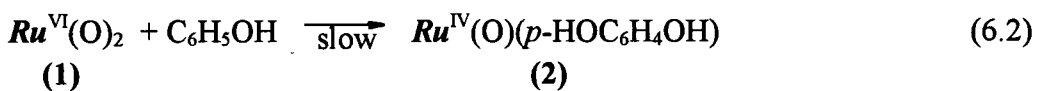
6.1 Introduction

The formation of $\text{Ru}^{\text{IV}}(\text{TMP})(\text{X})_2$ species ($\text{X} = \text{Cl}$, CF_3COO and CHCl_2COO) from the reaction represented in Eq. 6.1 (reaction not balanced) [$\text{Ru} = \text{Ru}(\text{TMP})$] was



discovered in the course of this thesis work. The effects of acids and bases on the rates of oxidation of alcohols (Chapter 4) were examined, and the above-mentioned acids were found to react with $\text{Ru}^{\text{VI}}(\text{TMP})(\text{O})_2$ (1) instead of giving a possible rate enhancement effect, as observed for the $\text{BaRuO}_3/\text{HOAc}$ ¹ and $\text{Ru}(\text{porp})/\text{pyridine-N-oxide}$ ² systems used for the hydroxylation of hydrocarbons. Some preliminary data on the characterization of these $\text{Ru}^{\text{IV}}(\text{TMP})(\text{X})_2$ species are discussed in this chapter; they are unexpected products and are characterized mainly *in situ*.

Preliminary studies have been carried out earlier in this laboratory on the stoichiometric oxidation of phenol by (1), and the Ru-porphyrin product was thought to be a bis(hydroquinoxo)ruthenium(IV) species.³ The mechanism represented in Eqs. 6.2 to 6.4 was proposed based on the evidence available at the time [$\text{Ru} = \text{Ru}(\text{TMP})$].



While the intermediate (**2**) [or the analogous Ru^{IV}(TMP)(O)] was not observed, ¹H-resonances characteristic of Ru^{II}(TMP) and Ru^{IV}(TMP) species, tentatively formulated as (**3**) and (**4**) in Eq. 6.4, respectively, were observed under anaerobic conditions in an approximately 2:3 ratio.^{3a} Under 1 atm O₂ or air, only ¹H-resonances due to the paramagnetic Ru^{IV}(TMP) species (**4**) were detected. This phenol system is re-examined, and compared to the chemistry of Ru(TMP) species within the phosphine and alcohol systems (Chapters 3 and 4).

The use of *N,N*-dimethylaniline as a mono-substituted aromatic substrate seemed a logical step in testing the reactivity of (**1**), and preliminary work showed that (**1**) oxidizes *N,N*-dimethylaniline to *p*-hydroxy-*N,N*-dimethylaniline both stoichiometrically, and in the presence of air, catalytically.

6.2 Experimental: Sample Preparation and Data Analysis

The reactions of (**1**) with HX acids (X = Cl, CF₃COO and CHCl₂COO) were studied *in situ* by ¹H-NMR, ESR and UV-visible spectroscopies. Ru^{IV}(TMP)(CF₃COO)₂ (**5**) was isolated and subjected to mass (by FAB ionization) and elemental analyses. Ru^{II}(TMP)(MeCN)₂ (10 mg, 0.01 mmol) was dissolved in air in 5 mL benzene until the aerobic oxidation to (**1**) was complete (< 30 min). Subsequently CF₃COOH (10 µL, 0.13 mmol) was added, when an instantaneous darkening (from brown to dark green) of the solution was observed. After 10 min the solvent and excess acid were removed by pumping under vacuum, and the solid (**5**) that remained was dried at 100 °C under vacuum for a further 24 h. Ru^{IV}(TMP)(CHCl₂COO)₂ (**6**) was prepared *in situ* in benzene

(1 mL) in an NMR tube by adding CHCl₂COOH (1 μ L, 0.012 mmol) to (1) (formed from the aerobic oxidation of Ru^{II}(TMP)(MeCN)₂, 0.001 mmol), when an instantaneous darkening of the solution was observed. After 10 min, the solvent and excess acid were removed under vacuum at room temperature for 12 h. Toluene-*d*₈ (1 mL) was then vacuum transferred to the NMR tube containing (6), which was used in ¹H-NMR experiments (see later, Figures 6.6, 6.8 and Table 6.2). A sample of (5) for NMR studies was prepared in the same way as that for (6); however, the solvent and excess CF₃COOH were removed with heat (100 °C) under vacuum, instead of at room temperature. This sample did not exhibit any characteristic TMP ¹H-resonances, implying that compound (5) had decomposed. Subsequently, (5) was prepared *in situ* by adding CF₃COOH (1 μ L, 0.013 mmol) to (1) (from bis(MeCN) precursor, 0.001 mmol) in toluene-*d*₈ (1 mL) under 1 atm air, and the excess acid was not removed. Attempts to purify compound (5) by column chromatography were unsuccessful, as the compound moved down the column in streaks using either benzene or CH₂Cl₂ as the eluent. Elemental analysis of (5), compared with the theoretical formulation as Ru^{IV}(TMP)(CF₃COO)₂, gave the following data:

Analysis, calculated for C ₆₀ H ₅₂ N ₄ O ₄ F ₆ Ru	C, 65.03; H, 4.73; N, 5.06
Found	C, 57.21; H, 4.92; N, 5.13.

Mass spectral analysis of (5) (FAB ionization in a 3-nitrobenzylalcohol matrix) showed the following ion mass peaks: [Ru(TMP)(CF₃COO)₂]⁺ at 1108, [Ru(TMP)(CF₃COO)]⁺ at 995 and [Ru(TMP)]⁺ at 822 amu (see Figure 6.1). A frozen benzene solution of (5) at 110 K did not show any ESR signals, suggesting that Ru(III) or Ru(V) species are absent.

The kinetics of the stoichiometric oxidation of phenol by (1) in benzene were monitored by UV-visible spectroscopy, using an HP 8452A Diode-Array instrument for

experiments involving $[\text{phenol}] < 0.1 \text{ M}$ and a stopped-flow spectrophotometer for $[\text{phenol}]$ values between 0.1 and 1.0 M. The experimental setup, sample preparations and data analysis for the phosphine oxidations have been described in Sections 2.2.2 and 3.2, and these procedures are equally applicable to the phenol oxidation kinetics monitored on the stopped-flow instrument. For the kinetic experiments using the HP 8452A instrument, phenol solutions (1.00 mL) of the appropriate concentrations (0.001 to 0.1 M) were prepared in benzene and added to a UV-visible quartz cell (1 cm path-length), which were then equilibrated thermally at $20 \pm 1^\circ\text{C}$. After 10 min, appropriate volumes of a benzene solution containing (1) ($\sim 10^{-3} \text{ M}$) were added to the cell to arrive at diluted concentrations of $\sim 10^{-6} \text{ M}$, and the kinetics were monitored over the 340 - 650 nm range. Figure 6.2 shows a typical isosbestic set of spectra acquired during a kinetic run (0.0943 M phenol; (1) $5 \times 10^{-6} \text{ M}$; 1 atm O₂ at 20°C). The values of the pseudo-first-order rate constants, k_{obs} , were derived from the absorbance changes at the Soret maximum for (1) at 422 nm for all the kinetic experiments. The kinetic data and k_{obs} values are tabulated in Appendix F.

The reaction of (1) with *N,N*-dimethylaniline under 1 atm air or 1 atm Ar was studied *in situ* by ¹H-NMR spectroscopy. The Ru-porphyrin product from the reaction of (1) with *N,N*-dimethylaniline in benzene-*d*₆ under air was isolated by pumping off the solvent (see also Section 6.5), and the solid that remained was analyzed by mass spectrometry (Figure 6.3). The data from the mass spectrum suggest a mixture of compounds to be present (see later, Section 6.5). The catalytic oxidation of *N,N*-dimethylaniline in benzene employed the same procedure as that used for the alcohol oxidations, which has been described previously in Sections 4.2 and 5.2.

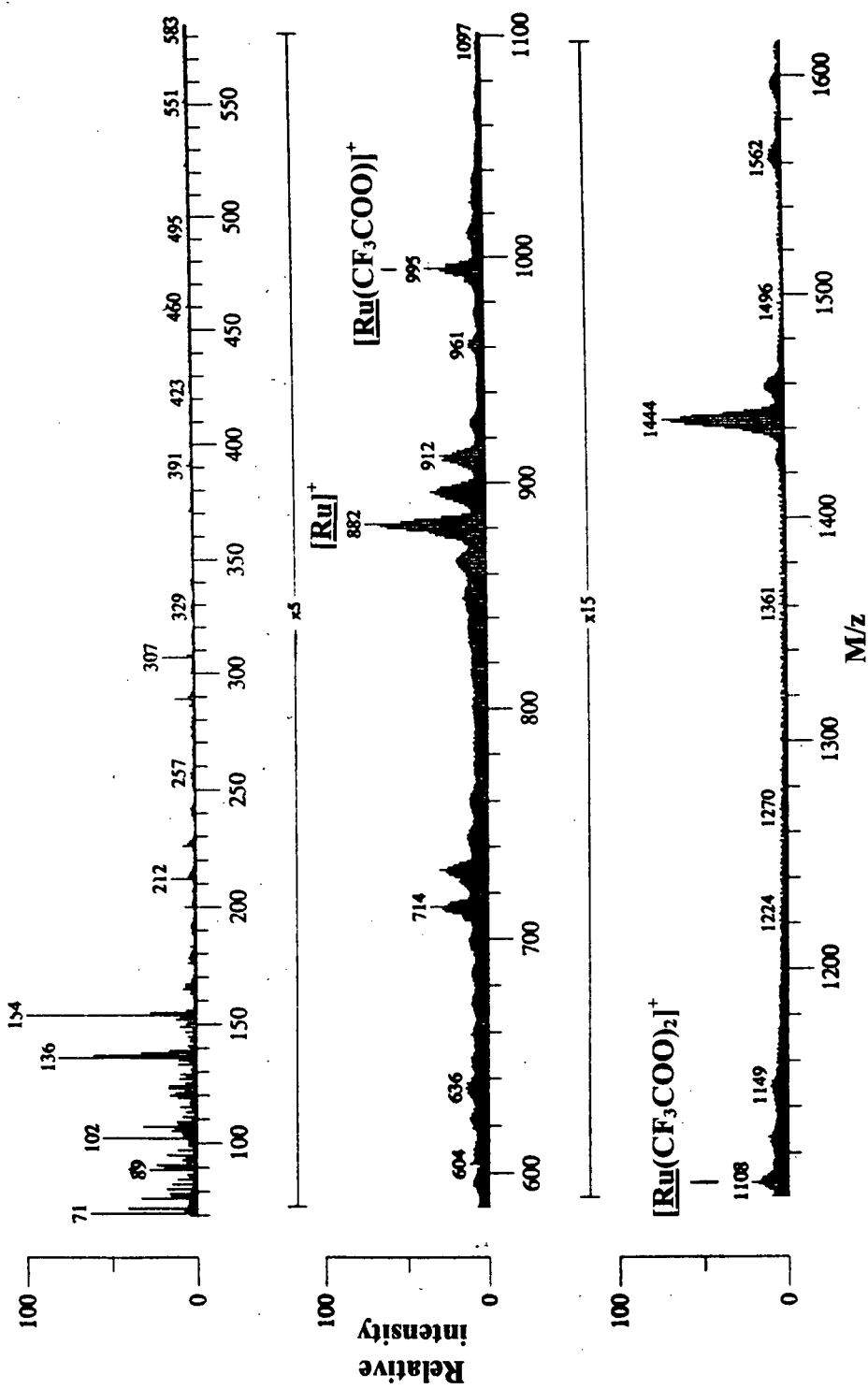


Figure 6.1. Mass spectrum of $\text{Ru}^{IV}(\text{TMP})(\text{CF}_3\text{COO})_2$, (5). FAB ionization of (5) supported in a 3-nitrobenzyl alcohol matrix.

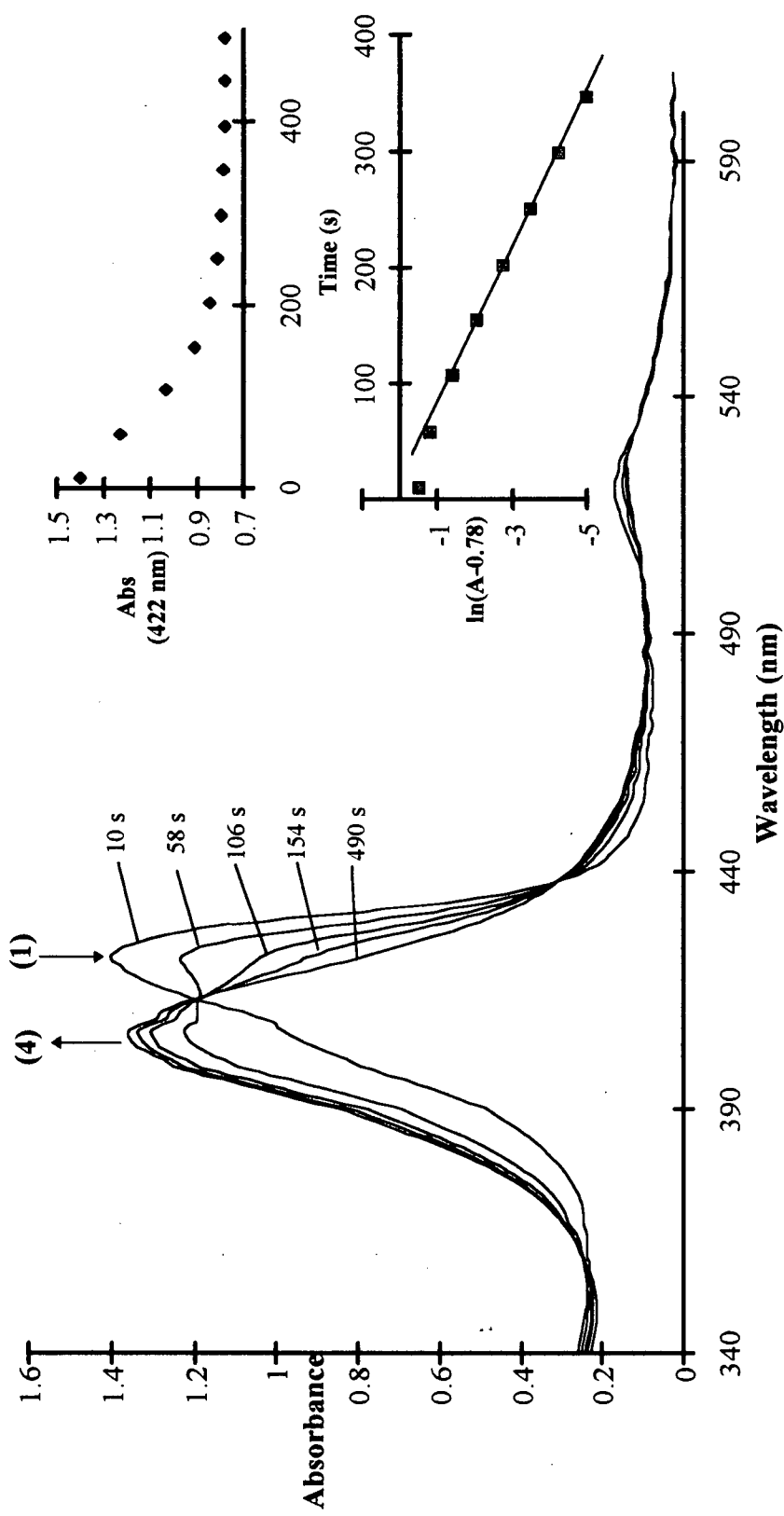


Figure 6.2. UV-visible spectra for the reaction between Ru^{IV}(TMP)(O)₂ (1) (5×10^{-6} M) and phenol (9.43×10^{-2} M) in benzene, under 1 atm O₂ to form Ru^{IV}(TMP)(OC₆H₅)₂ (4). The insets show the absorbance-time trace monitored for the loss of (1) at 422 nm, and the corresponding semilog plot, ln(A-A_∞) versus time (A_∞ = 0.78), from which the value of $k_{\text{obs}} = 1.40 \times 10^{-2} \text{ s}^{-1}$ is derived.

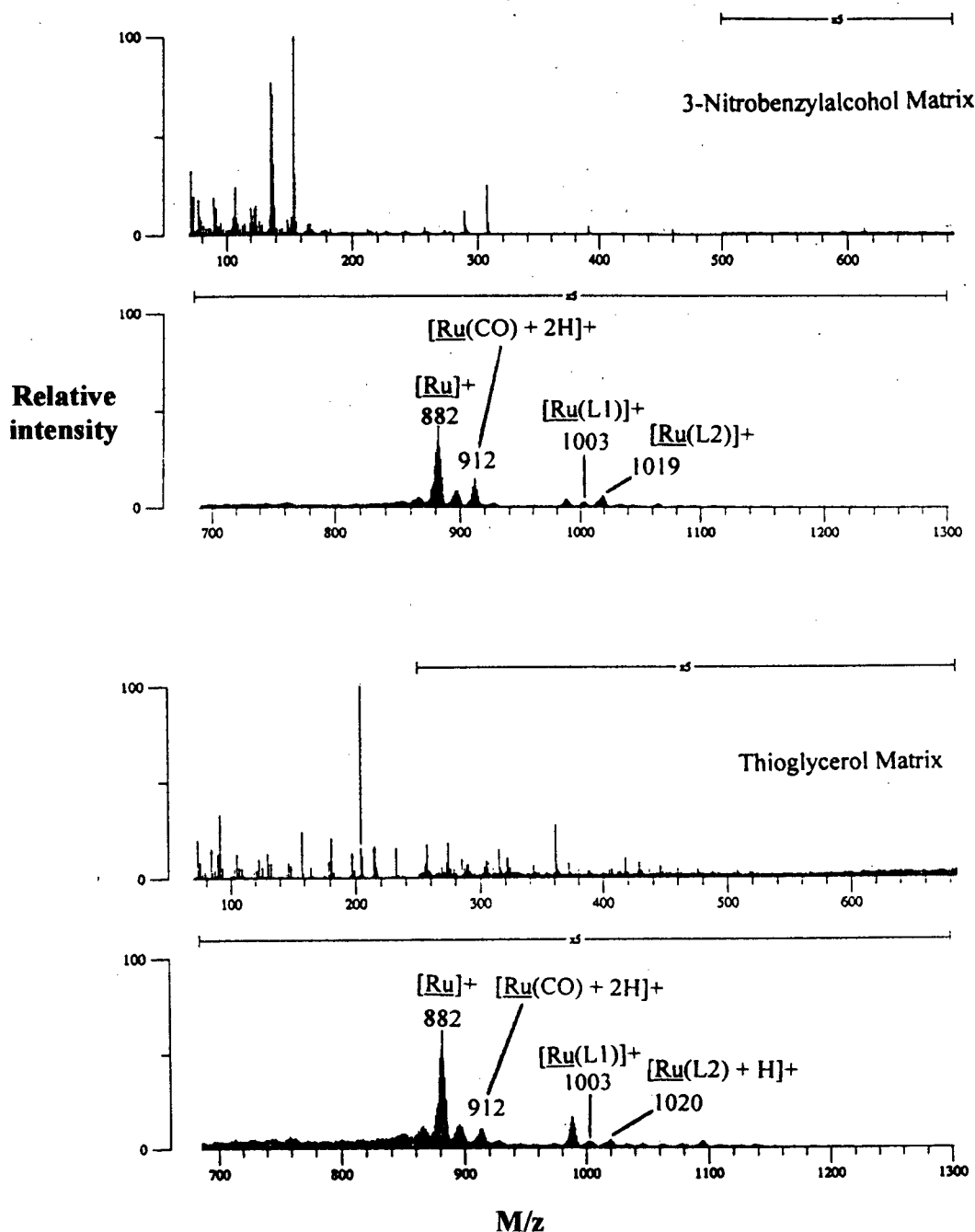


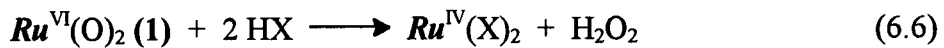
Figure 6.3 Mass spectra of solid sample isolated from the reaction between $\text{Ru}^{\text{VI}}(\text{TMP})(\text{O})_2$ and N,N -dimethylaniline in benzene- d_6 under 1 atm air. The results suggest a mixture of $\text{Ru}^{\text{II}}(\text{TMP})(p\text{-NMe}_2\text{-C}_6\text{H}_4\text{-X})$ species, where $\text{X} = \text{H}$ (L1) and OH (L2), to be present. (FAB ionization of the compound supported in (a) 3-nitrobenzylalcohol and (b) thioglycerol matrices). See also Section 6.5.

6.3 Ru^{IV}(TMP)(X)₂ Species

Ru^{IV}(TMP)(X)₂ species (X = Cl and Br) have been synthesized and characterized previously in this laboratory.⁴ The preparation of these compounds follows the scheme represented in Eq. 6.5 [*Ru* = Ru(TMP) and X = Cl or Br]. The presence of air or O₂ has



been noted to accelerate the rate of the reaction as depicted in Eq. 6.5, if the air or O₂ is introduced into the system after the HX has been added.^{4b} Recently the formation of Ru^{IV}(TMP)(Cl)₂, via the reaction of Ru^{VI}(TMP)(O)₂ (**1**) with anhydrous HCl in benzene, was reported,² and it was found independently during the course of this thesis work that exposure of a benzene solution of (**1**) to gaseous HCl or 12 M aqueous HCl gives Ru^{IV}(TMP)(Cl)₂ quantitatively, the reaction being complete within a few minutes at room temperature, as evidenced by ¹H-NMR and UV-visible spectroscopies. Furthermore, the addition of the strong organic acids, CF₃COOH and CHCl₂COOH, to benzene solutions of (**1**) produces rapid changes in the UV-visible spectra (Figure 6.4); the expected products are bis(substituted-acetato)-Ru(IV) complexes (see below). Of note, the oxidation products in the reactions between (**1**) and HX, presumably derived from the acids themselves, are presently unknown; one way to balance reaction 6.1 is to consider H₂O₂ as the oxidation product [Eq. 6.6; *Ru*=Ru(TMP)], but this is unlikely chemically.



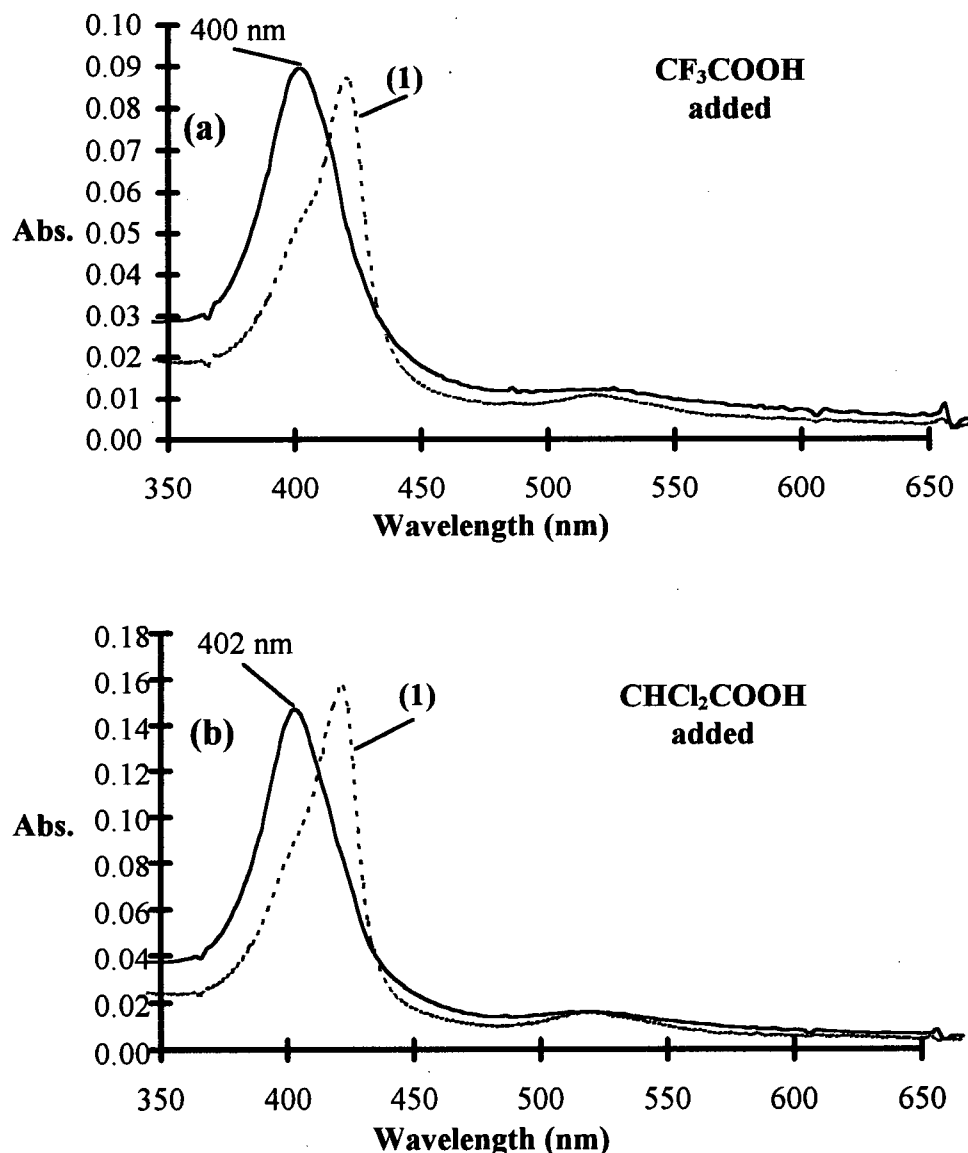


Figure 6.4. UV-visible spectra of Ru^{VI}(TMP)(O)₂, (1), in 1 mL benzene at 25 °C followed by the addition of 5 μL (a) CF₃COOH and (b) CHCl₂COOH. [(1)] = 6.4 × 10⁻⁷ M in (a) and 1.1 × 10⁻⁶ M in (b).

The 1000 cm^{-1} region in the IR spectra of Ru(TMP) complexes contains what is known as the “oxidation state marker”, the name arising from the strong IR signal which varies depending upon the oxidation state of the ruthenium centre. This property has been used by other workers^{5,6} to demonstrate a change in the oxidation state of the Ru within Ru-porphyrin complexes; however, the IR database has been somewhat limited to a few complexes. Earlier work carried out in this laboratory led to the preparation of a variety of alkoxo (Chapter 4), alkyl and haloruthenium(IV and III)⁴ TMP complexes, and thus a larger number of complexes has become available and firmer comparisons may be drawn (Table 6.1, see also Figures 6.9 and 6.10 later).

The IR data from Table 6.1 are consistent with assigning an oxidation state of 4+ for the Ru-centre in the proposed bis(acetato)ruthenium(IV) species. A sample of (**5**), generated *in situ* from the reaction of (**1**) and excess CF_3COOH in benzene- d_6 for ^1H -NMR experiments, exhibits a solution magnetic susceptibility value of $\mu_{\text{eff}} = 2.5\ \mu_{\text{B}}$ measured by the Evan's method.⁷ The μ_{eff} value suggests a Ru(IV) S = 1 spin state.

The ^1H -NMR spectrum of (**5**) in toluene- d_8 is shown in Figure 6.5 and that of the CHCl_2COO analogue, $\text{Ru}^{\text{IV}}(\text{TMP})(\text{CHCl}_2\text{COO})_2$ (**6**), in Figure 6.6. Single *m*-H and *o*-Me ^1H -resonances of the TMP ligand in (**5**) and (**6**) are indicative of these species possessing D_{4h} symmetry,^{3,4} and coordination of two acetate ligands would give the observed single *m*-H and *o*-Me ^1H -resonances. The ^{19}F -NMR spectrum of (**5**) (Figure 6.5 inset) clearly indicates the presence of coordinated CF_3COO at δ 25.4. The upfield-shifted β -pyrrole ^1H -resonances at -61.10 for (**5**) and -63.33 ppm for (**6**) at ~290 K are reminiscent of those of the paramagnetic $\text{Ru}^{\text{IV}}(\text{TMP})(\text{X})_2$ ($\text{X} = \text{Br}^{4a}$ and Cl^{4b}) complexes.

Table 6.1. IR absorption frequencies for some Ru(TMP) complexes in the 1000 cm⁻¹ region.

Ru(TMP) species	IR Absorption Frequency ^a (cm ⁻¹)	Reported Source
Ru ^{II} (TMP)(PPh ₃)	1000 ^b	Groves <i>et al.</i> ⁵
Ru ^{II} (TMP)(MeCN) ₂	1001 (1003) ^b	this thesis (Groves <i>et al.</i> ⁵)
Ru ^{II} (TPP)(NH ₂ 'Bu) ₂	1000	Huang <i>et al.</i> ^{6c}
Ru ^{II} [(MeO) ₁₂ TPP](NH ₂ 'Bu) ₂ ^c	1004	Huang <i>et al.</i> ^{6c}
Ru ^{III} (TMP)(NH ₃)(Cl) ^d	1005	this thesis
Ru ^{III} (TMP)(NH ₃)(Br) ^d	1004	this thesis
Ru ^{IV} (TMP)(O)	1011 ^b	Groves <i>et al.</i> ⁵
Ru ^{IV} (TMP)(O'Pr) ₂	1010	this thesis
Ru ^{IV} (TMP)(OEt) ₂	1010 (1011)	this thesis (Leung <i>et al.</i> ^{6b})
Ru ^{IV} (TMP)(Cl) ₂ ^{d,e}	1007	this thesis
Ru ^{IV} (TMP)(Me) ₂ ^d	1007	this thesis
Ru ^{IV} (TMP)(Ph) ₂ ^d	1007	this thesis
Ru ^{IV} (TMP)(CF ₃ COO) ₂	1011	this thesis
Ru ^{IV} (TMP)(CHCl ₂ COO) ₂ ^f	1011	this thesis
Ru ^{IV} [(MeO) ₁₂ TPP](O)(NH ₂ 'Bu) ^c	1016	Huang <i>et al.</i> ^{6c}
Ru ^{IV} (TPP)(O)(NH ₂ 'Bu)	1016	Huang <i>et al.</i> ^{6c}
Ru ^{VI} (TMP)(O) ₂	1019 ^b	Groves <i>et al.</i> ⁵
Ru ^{VI} (TPP)(O) ₂	1017	Leung <i>et al.</i> ^{6a}
Ru ^{VI} [(MeO) ₁₂ TPP](O) ₂ ^c	1019	Huang <i>et al.</i> ^{6c}

^a IR spectra in this thesis are obtained in Nujol mulls in KBr plates, unless indicated otherwise. IR spectra reported by other workers are in Nujol mulls, unless indicated otherwise.

^b Solution IR in benzene.

^c (MeO)₁₂TPP = dianion of *meso*-tetra(3,4,5-MeO-phenyl)porphyrin.

^d These compounds were prepared by Dr. C. S. Alexander (Ref. 4b) of this laboratory.

^e Prepared by the reaction of (1) with HCl_(g).

^f IR spectrum obtained from a benzene solution, which was dried on a KBr plate, initially containing (1) and added CHCl₂COOH (see Section 2.2.3).

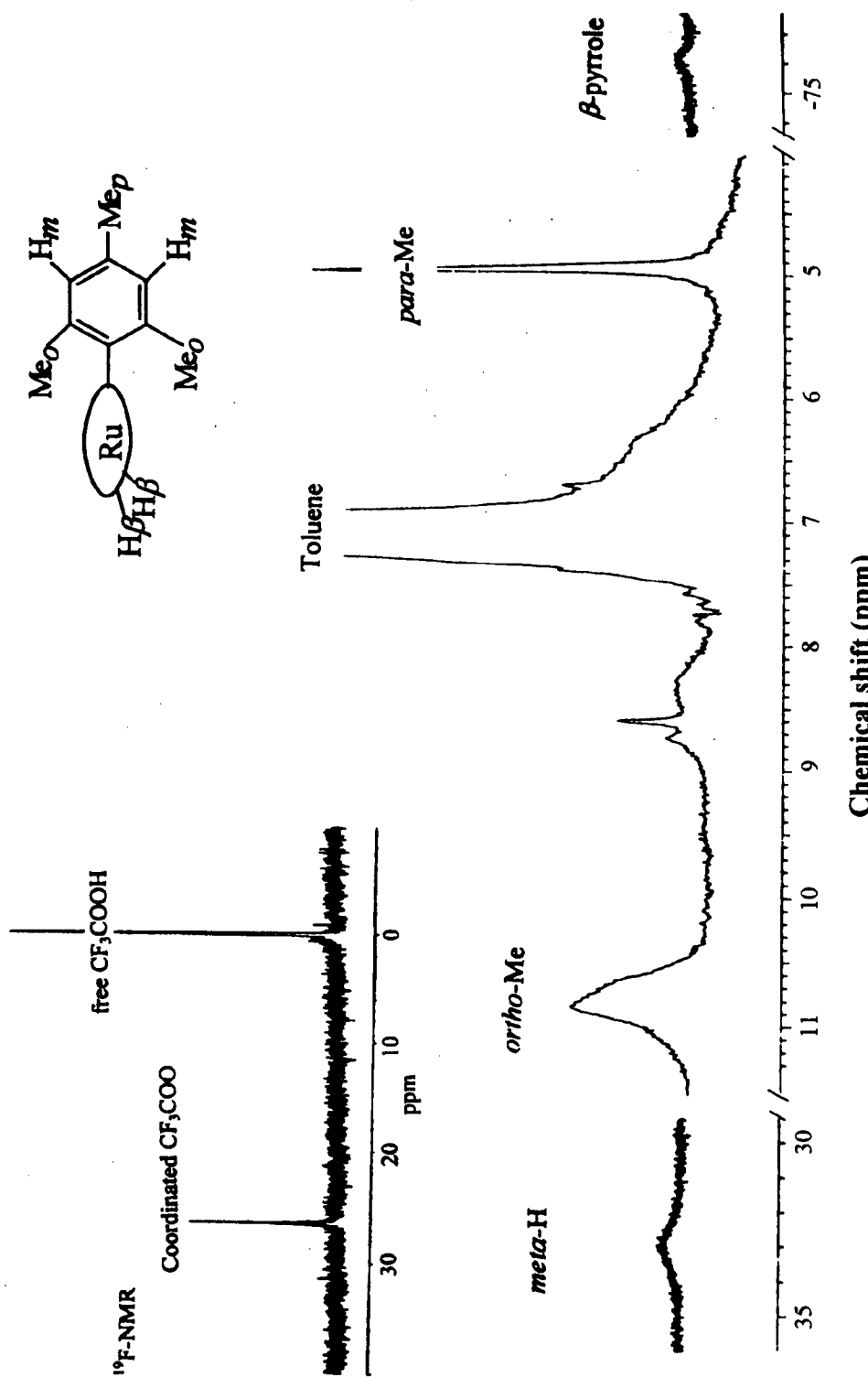


Figure 6.5. $^1\text{H-NMR}$ (300 MHz) spectrum of $\text{Ru}^{\text{V}}(\text{TMP})(\text{CF}_3\text{COO})_2$ (**5**) in toluene- d_8 at -57.1 °C. Inset shows the $^{19}\text{F-NMR}$ (188 MHz) spectrum of the same sample at 25 °C. (**5**) was prepared *in situ* by adding excess CF_3COOH to $\text{Ru}^{\text{VI}}(\text{TMP})(\text{O})_2$ (1.0×10^{-3} M) in toluene- d_8 under 1 atm air (see Section 6.2). The $^1\text{H-NMR}$ spectrum at -57.1 °C, rather than that at other temperatures (Table 6.2), is shown here so that the *ortho*-Me ^1H -resonances can be displayed clearly.

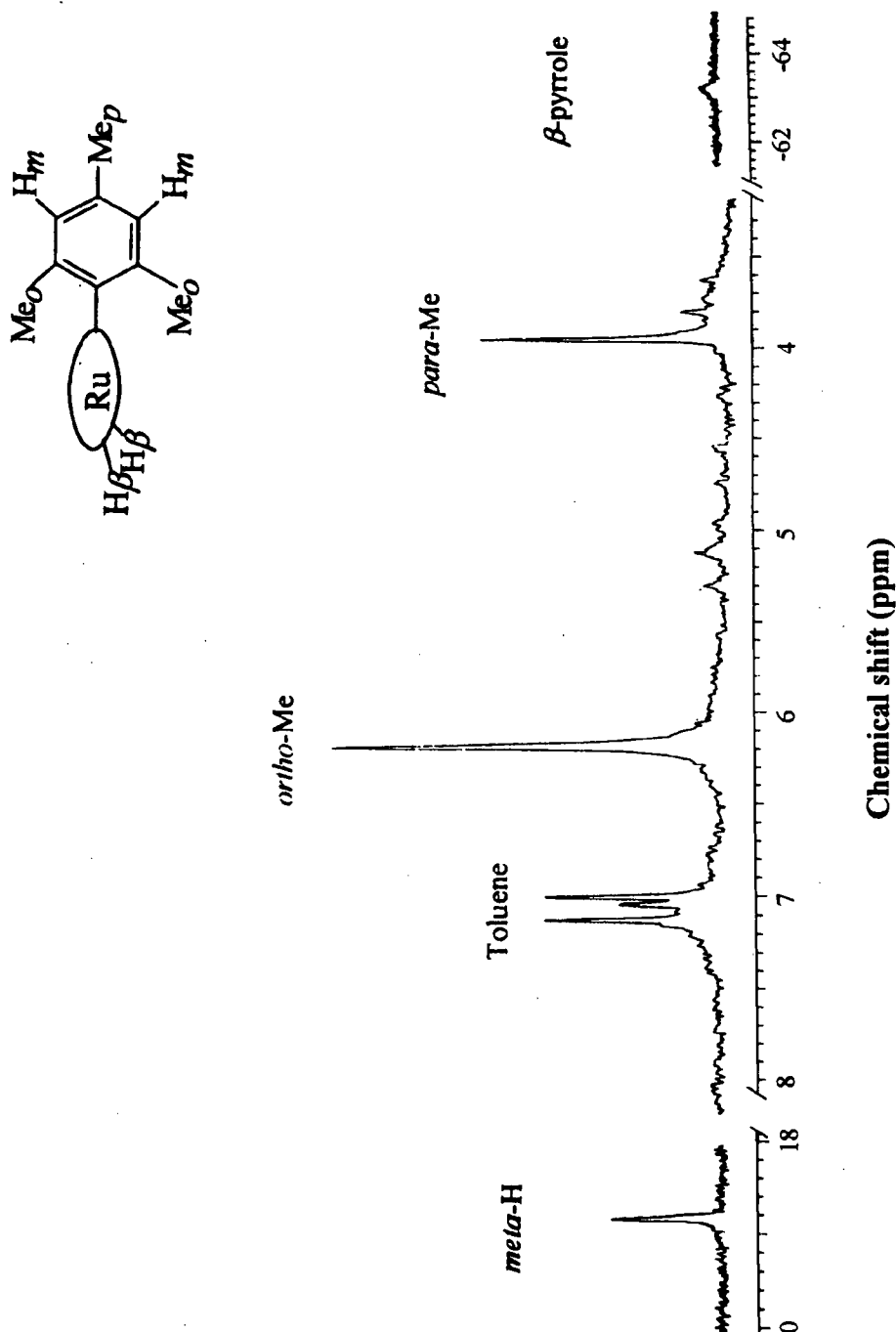


Figure 6.6. ¹H-NMR (300 MHz) spectrum of Ru^V(*TMP*)(CHCl₂COO)₂ (**6**) (1.0×10^{-3} M) in toluene-*d*₈ at 17.3 °C *in vacuo*. (**6**) was prepared by adding excess CHCl₂COOH to Ru^V(*TMP*)(O)₂ in benzene, followed by removal of solvent and excess acid under vacuum (see Section 6.2).

$\text{Ru}^{\text{IV}}(\text{TMP})$ paramagnetic species⁴ delocalize the spin density to the empty $4e(\pi^*)$ orbitals on the porphyrin through $\text{Ru}(d_{xz,yz}) \rightarrow \text{porp}(\pi^*)$ charge transfer.⁸ This interaction is reflected in the inverse temperature dependence of the ^1H -chemical shifts within the TMP ligand, with the β -pyrrole ^1H -resonances within $\text{Ru}^{\text{IV}}(\text{TMP})$ species varying most noticeably with temperature.^{3,4}

The ^1H -chemical shifts of the TMP ligand in (5) and (6) vary with inverse temperature (see Figures 6.7 and 6.8), suggestive of a single spin state for (5) and (6) over the observed temperature range. Of interest, the *m*-H and *o*-Me ^1H -resonances are more strongly temperature-dependent, as well as being much more downfield-shifted than those of the analogous $\text{Ru}^{\text{IV}}(\text{TMP})(\text{X})_2$ complexes ($\text{X} = \text{Cl}, \text{Br}$; Table 6.2). In contrast, the ^1H -resonances of the TMP ligand in $\text{Ru}^{\text{IV}}(\text{TMP})(\text{OR})_2$ species ($\text{R} = \text{C}_6\text{H}_5$ and ^iPr)³ are relatively temperature-insensitive except those for the β -pyrrole hydrogens.

The CO stretching frequencies for the acetate groups within (5) and (6) show that the coordinated acetates have ν_{CO} values shifted to lower wavenumbers than those of the corresponding free acids. In (5), $\nu_{\text{CO}} = 1670 \text{ cm}^{-1}$ with a weaker shoulder at 1709 cm^{-1} , while for the free acid $\nu_{\text{CO}} = 1783 \text{ cm}^{-1}$ (Figure 6.9). In (6), $\nu_{\text{CO}} = 1648 \text{ cm}^{-1}$ with a weaker shoulder at 1667 cm^{-1} , while for the free acid $\nu_{\text{CO}} = 1732 \text{ cm}^{-1}$ (Figure 6.10).

An acetate ligand is expected to give two ν_{CO} absorptions ($\nu_{\text{C=O}}$ and $\nu_{\text{C-O}}$), and the difference between the two reflects its bonding mode within the complex. For example, the difference between the two ν_{CO} absorptions for the free CH_3COO^- ion is 144 cm^{-1} , and a coordinated CH_3COO^- is considered to be η^1 -monodentate if the difference between the

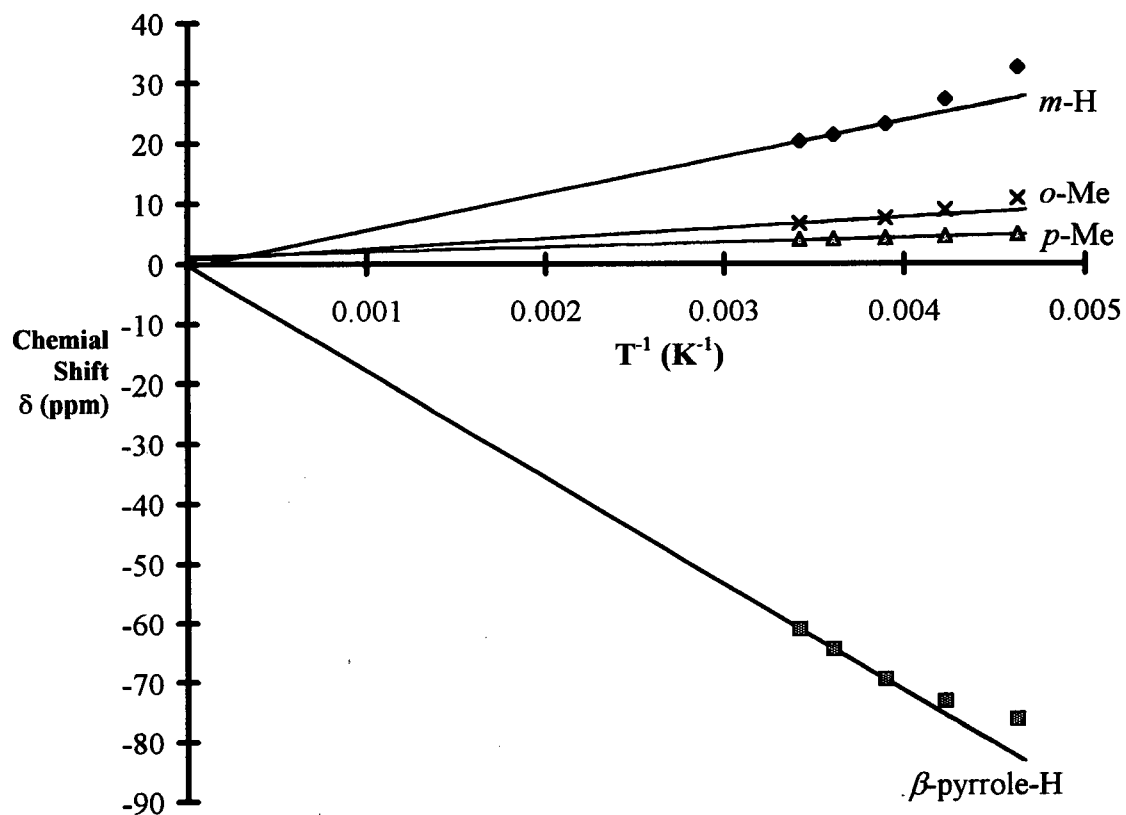


Figure 6.7. Inverse temperature plot, ^1H -chemical shifts (300 MHz) versus T^{-1} for $\text{Ru}^{\text{IV}}(\text{TMP})(\text{CF}_3\text{COO})_2$ (**5**) in toluene- d_8 (same sample as for Figure 6.5).

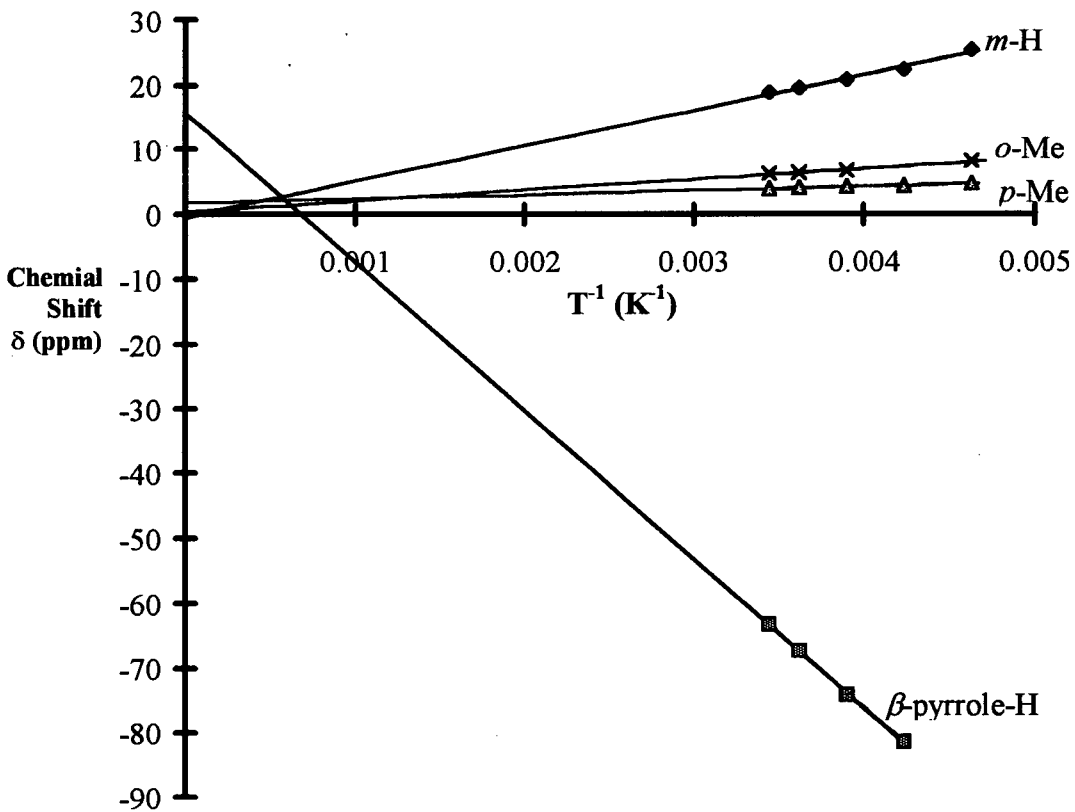


Figure 6.8. Inverse temperature plot, ^1H -chemical shifts (300 MHz) versus T^{-1} for $\text{Ru}^{\text{IV}}(\text{TMP})(\text{CHCl}_2\text{COO})_2$ (**6**) in toluene- d_8 (same sample as for Figure 6.6)

Table 6.2. Observed variable temperature ^1H -NMR chemical shifts^a for selected $\text{Ru}^{\text{IV}}(\text{TMP})(\text{X})_2$ species.

$\text{Ru}^{\text{IV}}(\text{TMP})(\text{X})_2$	Temp. (K) ^g	β -pyrrole H	meta-H ^h	ortho-Me ^h	para-Me
Cl^b	223.55	-79.75	14.44	4.41	4.71
	274.65	-59.35	12.82	3.93	4.19
	291.15	-55.42	12.50	3.83	4.07
Br^b	204	-63.29	16.20	5.37	4.93
	243	-54.22	14.69	4.84	4.40
	303	-43.24	13.15	4.27	3.88
$\text{O}'\text{Pr}^c$	213.15	-13.22	7.79	3.12	3.35
	253.15	-12.70	7.69	3.10	3.10
	293.15	-11.92	7.59	2.90	2.91
$p\text{-OC}_6\text{H}_5^{c,d}$	213.15	-45.44	8.13	3.69	3.49
	253.15	-36.88	7.87	3.15	3.19
	298.15	-29.89	7.60	2.79	2.98
CF_3COO^e (5)	216.05	-76.44	32.62	10.82	4.93
	236.25	-73.30	27.27	8.92	4.58
	256.65	-69.61	23.13	7.55	4.29
	277.15	-64.53	21.33	-	4.12
	292.45	-61.10	20.25	6.72	4.00
$\text{CHCl}_2\text{COO}^f$ (6)	215.95	-	25.46	8.09	4.67
	236.15	-81.41	22.40	-	4.37
	256.15	-74.20	20.77	6.66	4.16
	276.25	-67.38	19.55	6.36	4.02
	290.45	-63.33	18.79	6.16	3.92

^a In toluene- d_8 ; data acquired on a 300 MHz instrument.

^b Selected data for X = Br and Cl from Ref. 4a and 4b, respectively.

^c Selected data from Ref. 3a.

^d This species is shown in the present thesis work to contain OC_6H_5 axial ligands, rather than $p\text{-OC}_6\text{H}_4\text{OH}$ ligands (see Section 6.4.1).

^e [(5)] = 1.0×10^{-3} M *in situ*, [CF₃COOH] = 1.5×10^{-2} M, in toluene- d_8 under 1 atm air (see Section 6.2).

^f [(6)] = 1.0×10^{-3} M *in situ*, under vacuum without any excess acid (see Section 6.2).

^g Uncertainty in T = ± 0.5 K.

^h Single ^1H -resonance indicates D_{4h} symmetry for these Ru(TMP) species.

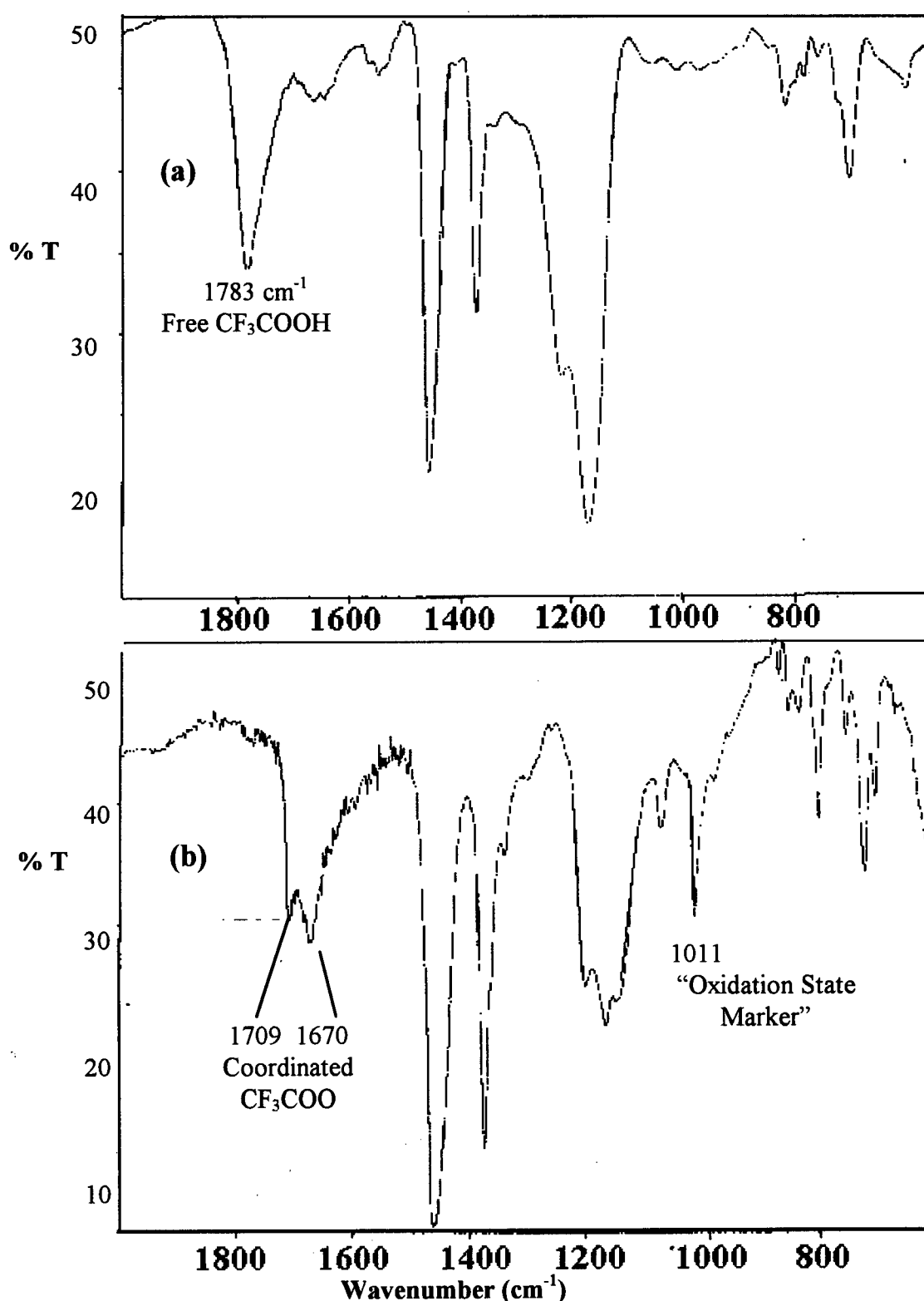


Figure 6.9. Infrared spectra of (a) free CF_3COOH and (b) $\text{Ru}^{\text{IV}}(\text{TMP})(\text{CF}_3\text{COO})_2$ (5), obtained as Nujol mulls in KBr plates.

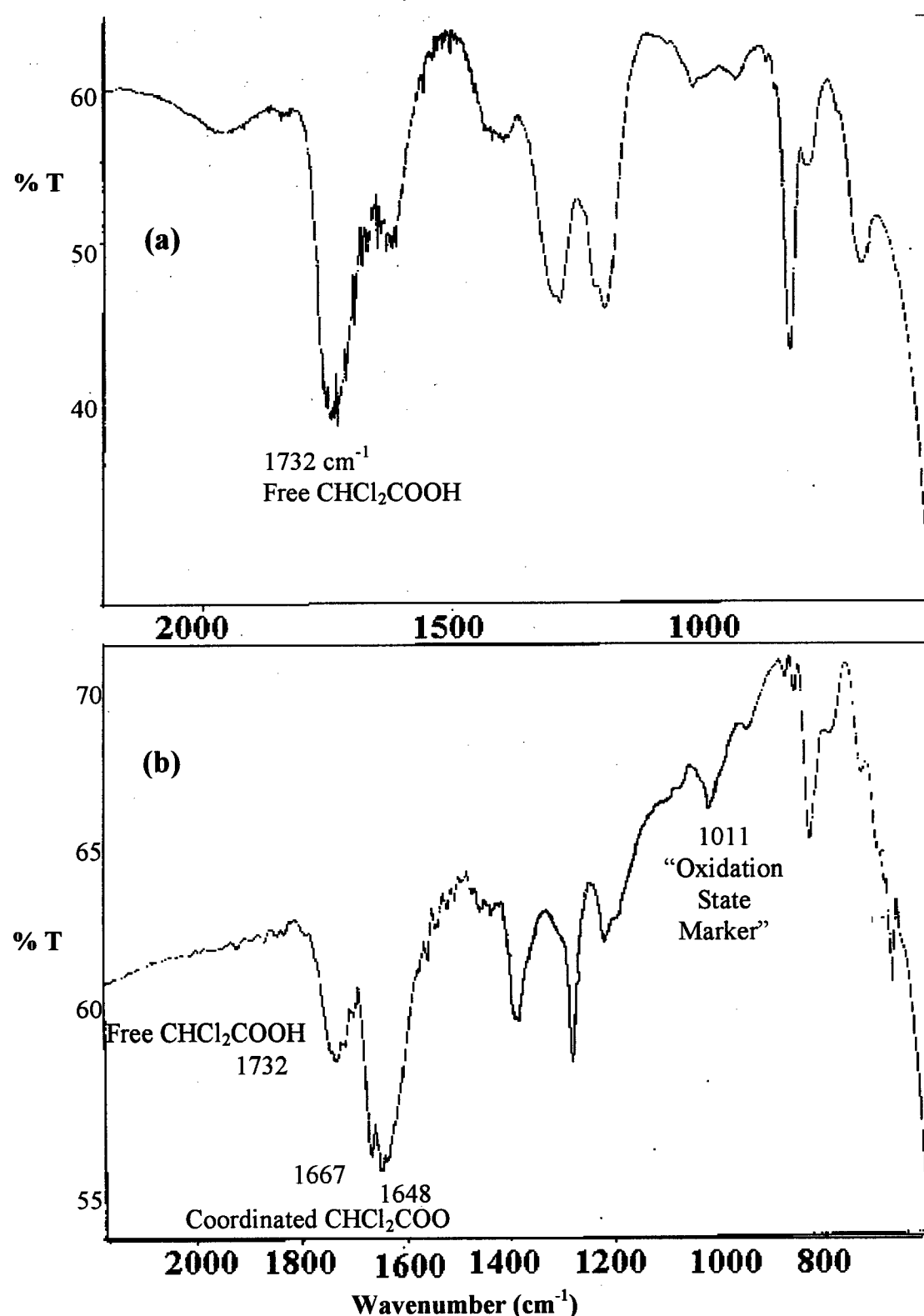


Figure 6.10. Infrared spectra of (a) free CHCl_2COOH and (b) $\text{Ru}^{\text{IV}}(\text{TMP})(\text{CHCl}_2\text{COO})_2$ (6), obtained as Nujol mulls in KBr plates.

two ν_{CO} absorptions is lower than that of the free acetate, and η^2 -bidendate if the difference is larger.⁹ $\text{Ru}(\text{CH}_3\text{COO})_2(\text{CO})_2(\text{PPh}_3)_2$, with η^1 -acetate ligands, has ν_{CO} absorptions at 1613 and 1315 cm^{-1} , corresponding to a difference of 289 cm^{-1} ; $\text{RuCl}(\text{CH}_3\text{COO})(\text{CO})(\text{PPh}_3)_2$, with one η^2 -acetate, has ν_{CO} absorptions at 1507 and 1465 cm^{-1} , corresponding to a difference of 42 cm^{-1} .⁹ Hence, a large difference between the two ν_{CO} absorptions relative to that of the free acetate is indicative of η^1 -monodentate binding mode for the acetate, and vice versa. Consideration of the steric constraints presented by the TMP ligand and the expected six-coordinate Ru(IV) centre in (5) and (6) imply the presence of η^1 -acetates; however, the IR data for (5) and (6) suggest η^2 -acetates, as differences between the ν_{CO} absorptions (main peak and shoulder) are 39 and 19 cm^{-1} , respectively. Nevertheless, an η^2 -binding mode would require both complexes to contain the unlikely, eight-coordinate ruthenium centres.

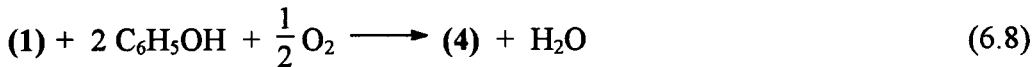
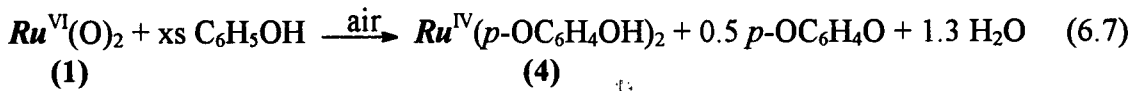
The solution magnetic susceptibility, MS, IR, ^1H and ^{19}F -NMR data all support the formulation of (5) as $\text{Ru}^{\text{IV}}(\text{TMP})(\text{CF}_3\text{COO})_2$. The elemental analysis of (5) gives agreeable values for H and N (Section 6.2); however, the extremely low C content, which cannot be explained, is not consistent with solvated acid, solvent or water, or the presence of axial ligands other than CF_3COO . The poor elemental analysis is likely due to decomposition of (5) when the excess acid and solvent are removed with heat. Nonetheless, all the spectroscopic data point to the formulation of $\text{Ru}^{\text{IV}}(\text{TMP})(\text{X})_2$ ($\text{X} = \text{CF}_3\text{COO}$ and CHCl_2COO) for the Ru-porphyrin products from the reactions between (1) and HX acids.

6.4 Oxidation of Phenol by Ru^{VI}(TMP)(O)₂

6.4.1 Stoichiometric Oxidation of Phenol

The stoichiometric and catalytic oxidations of phosphines (Chapter 3) and alcohols (Chapter 4) have been discussed, and a key step in both systems is believed to involve the disproportionation of Ru^{IV}(TMP)(O) to Ru^{VI}(TMP)(O)₂ (**1**) and Ru^{II}(TMP). Also the reaction of Ru^{IV}(TMP)(O) and H₂O to give Ru^{IV}(TMP)(OH)₂ (herein referred to as the reaction involving the “conversion to a bis(hydroxo) species”), followed by alcohol metathesis to form Ru^{IV}(TMP)(OR)₂ species, is implicated from the reaction conditions required for the catalyzed O₂-oxidation of alcohols (Chapter 4). That Ru^{IV}(TMP)(O) prefers to react via disproportionation or conversion to a bis(hydroxo) species, rather than acting as an O-atom transfer agent is suggested in both the phosphine and alcohol systems; therefore, the initially proposed phenol oxidation mechanism (Eqs. 6.2 to 6.4)³ was re-examined in this thesis work. In fact, experimental results now disfavour the successive two-step oxidation mechanism presented in Eqs. 6.2 to 6.4.

Previous work in this laboratory showed that the reaction between (**1**) and phenol under 1 atm air gives 1 equivalent of a paramagnetic Ru^{IV}(TMP) species, tentatively formulated from ¹H-NMR data as Ru^{IV}(TMP)(*p*-OC₆H₄OH)₂ (**4**), 0.5 equivalent of *p*-benzoquinone and 1.3 equivalents of H₂O [Eq. 6.7, *Ru* = Ru(TMP)],³ however, the expected reaction stoichiometry according to the proposed mechanism (Eqs. 6.2 to 6.4) is shown in Eq. 6.8.



The successive two-step oxidation mechanism (Eqs. 6.2 to 6.4) can account for the formation of the suggested Ru-porphyrin product (**4**), but cannot adequately explain the formation of the *p*-benzoquinone. Moreover, the data from the present thesis work, particularly the mass spectrum of (**4**) (Figure 6.11), show it to contain axial OC₆H₅, rather than *p*-OC₆H₄OH, ligands, and thus (**4**) is more favourably formulated as

Ru^{IV}(TMP)(OC₆H₅)₂. In addition, the metathesis reaction between Ru^{IV}(TMP)(O*i*Pr)₂ and phenol (50-fold excess) in benzene-*d*₆ under 1 atm Ar gives a product with an *in situ* ¹H-NMR spectrum identical to that obtained for isolated (**4**).[†] A small amount of product assignable to Ru^{IV}(TMP)(*p*-OC₆H₄OH)₂ is formed from the metathesis reaction between *p*-hydroquinone (1.5 x 10⁻³ M) and Ru^{IV}(TMP)(O*i*Pr)₂ (1 x 10⁻³ M) in benzene-*d*₆; the ¹H-chemical shifts (β -pyrrole-H, -34.7; *o*-Me, 2.99; *p*-Me, 3.04; *m*-H, 7.55; axial ligand, 14.4, -21.6, -23.8) (Figure 6.12) of the new compound are distinctively different from those of (**4**).[‡] Hence, (**4**) is now considered to be Ru^{IV}(TMP)(OC₆H₅)₂. Of note, the preliminary work carried out in this laboratory^{3a} included the attempted purification of (**4**) by column chromatography, and the isolated compound gave elemental analysis data (C, 74.55; H, 5.63; N, 5.11; O, 5.40) which agreed with those calculated for Ru^{IV}(TMP)(*p*-OC₆H₄OH)₂ (C₆₈H₆₂N₄RuO₄; C, 74.22; H, 5.67; N, 5.09; O, 5.82); those calculated for Ru^{IV}(TMP)(OC₆H₅)₂ (C₆₈H₆₂N₄RuO₂) are: C, 76.45; H, 5.85; N, 5.24; O, 3.00.

[†] ¹H-NMR data for (**4**) in benzene-*d*₆: β -pyrrole-H, -30.5; *m*-H, 7.60; *o*-Me, 2.90; *p*-Me, 3.00; axial ligand, 49.7, -68.2, -71.9 (Chapter 4, Table 4.1).

[‡] Of note, almost no *p*-hydroquinone is detected (Fig. 6.12), but some *p*-benzoquinone and (**1**) can be seen. *p*-Hydroquinone is likely oxidized by (**1**), which can be reformed from the reaction of Ru^{IV}(TMP)(O*i*Pr)₂ with H₂O (Chapter 4). Although the metathesis reaction is not complete, the ¹H-signals assignable to Ru^{IV}(TMP)(*p*-OC₆H₄OH)₂ clearly show that (**4**) is not the bis(hydroquinoxo) species.

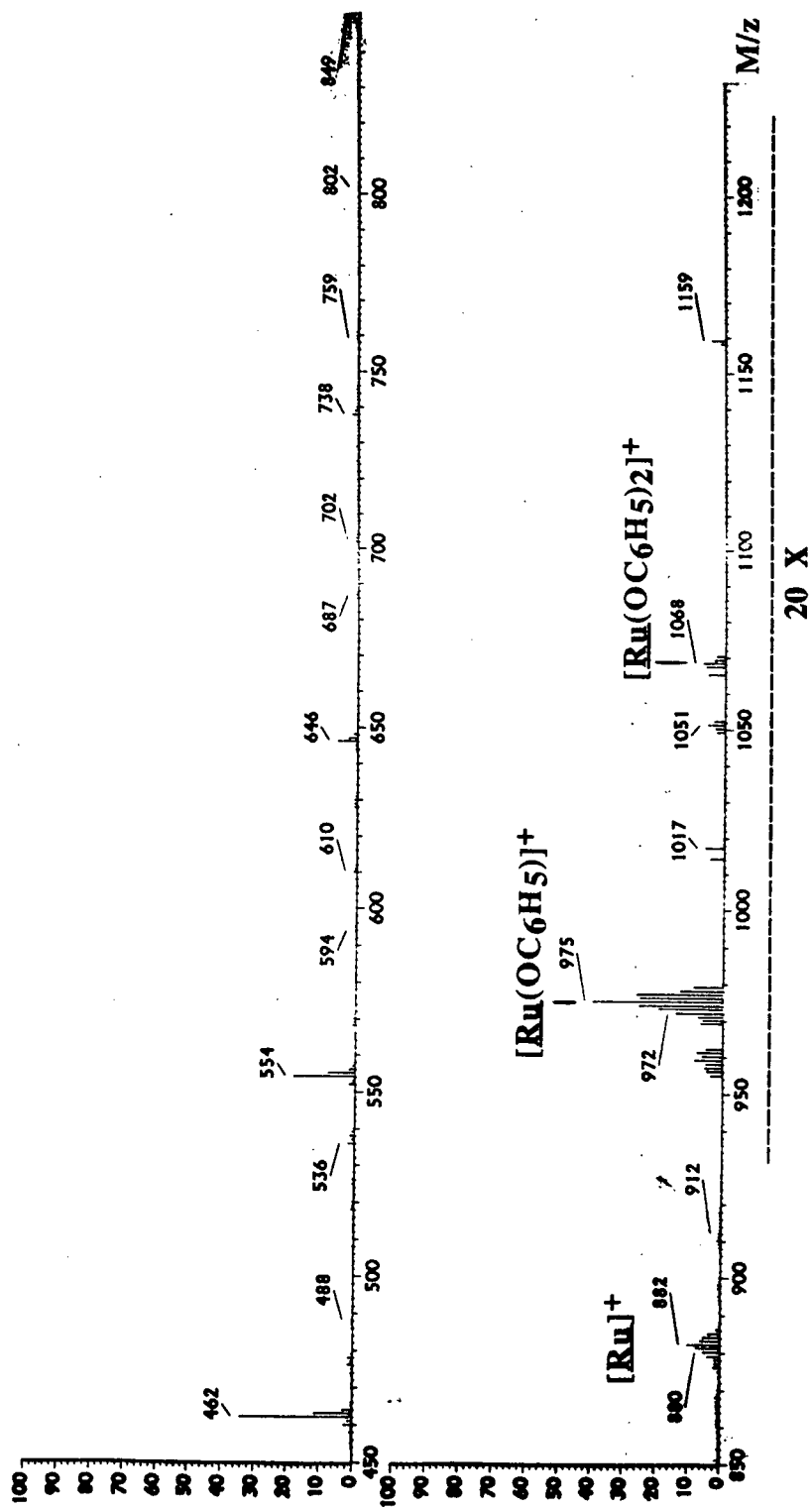


Figure 6.11. Mass spectrum (EI ionization) of $\text{Ru}^{\text{IV}}(\text{TMP})(\text{OC}_6\text{H}_5)_2$, (4). (4) was prepared from the reaction between $\text{Ru}^{\text{VI}}(\text{TMP})(\text{O})_2$ and excess phenol in benzene, followed by removal of solvent and excess phenol under vacuum. (Phenol sublimes under vacuum at room temperature.)

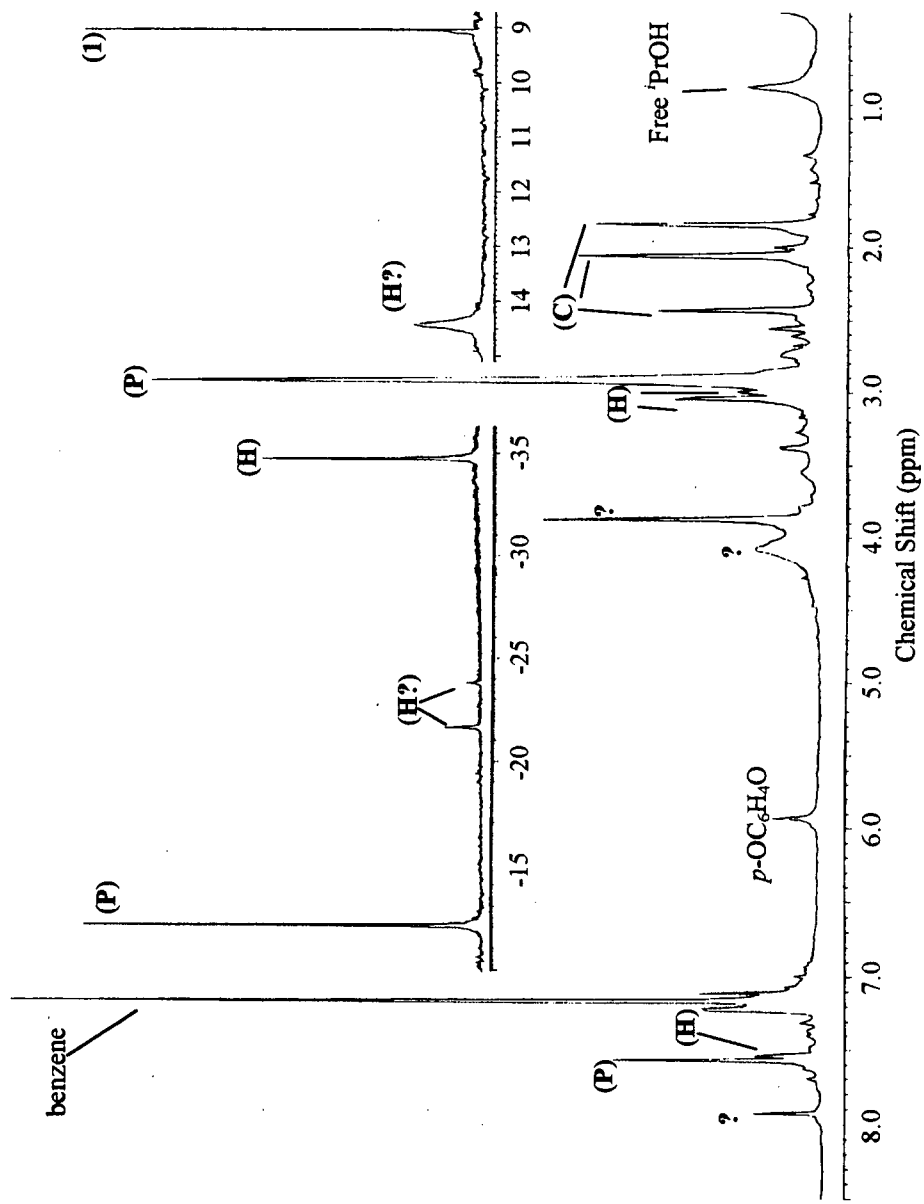
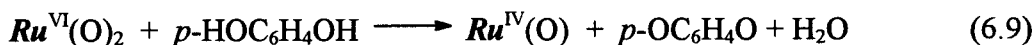


Figure 6.12. ^1H -NMR spectrum (400 MHz) for the reaction between *p*-hydroquinone and $\text{Ru}^{\text{IV}}(\text{TMP})(\text{O}'\text{Pr})_2$ (**P**) (see Chapter 4, Table 4.1) in benzene- d_6 at $\sim 25^\circ\text{C}$ under 1 atm Ar. (1) = $\text{Ru}^{\text{VI}}(\text{TMP})(\text{O})_2$; (**H**) = $\text{Ru}^{\text{IV}}(\text{TMP})(\text{O}'\text{Pr})_2$; (**C**) = $\text{Ru}^{\text{VI}}(\text{TMP})(\text{CO})$ (β -pyrrole-H at 8.8 ppm observed, but not shown in the above spectrum). The insets show the expand upfield (2x) and downfield (8x) regions.

In the present thesis work, attempts to purify (**4**) by the reported column chromatography procedure^{3a} were unsuccessful in removing the *p*-benzoquinone product, and hence, elemental analysis was not obtained for (**4**); however, the ¹H-NMR data, the metathesis reaction and the mass spectral data all suggest (**4**) to be the bis(phenoxy) complex. The good elemental analysis determined for the supposed Ru^{IV}(TMP)(*p*-OC₆H₄OH)₂, particularly the oxygen content, was probably fortuitous, and might have resulted from *p*-benzoquinone impurity; the compound could have been Ru^{IV}(TMP)(OC₆H₅)₂•2H₂O, which would give an elemental analysis (C₆₈H₆₆N₄RuO₄; C, 73.96; H, 6.02; N, 5.07; O, 5.79) equally agreeable with that reported earlier.^{3a} The phenol oxidation mechanism needs to be reconsidered to account for the formation of the bis(phenoxy) species (**4**), as well as the production of *p*-benzoquinone.

The observed *p*-benzoquinone is undoubtedly formed via the oxidation of *p*-hydroquinone, which is initially produced from the oxidation of phenol by (**1**) via reaction 6.2. That (**1**) oxidizes, in fact catalytically under O₂, *p*-hydroquinone to *p*-benzoquinone in benzene is demonstrated in separate experiments. Under 1 atm O₂ with [p-hydroquinone] = 1.5 x 10⁻³ M and [(1)] = 5.5 x 10⁻⁵ M, 8 equivalents of *p*-benzoquinone were produced in 20 min (0.4 turnover min⁻¹). Under 1 atm O₂ with [p-hydroquinone] = 1.5 x 10⁻³ M and [(1)] = 5.5 x 10⁻⁶ M, 200 equivalents of *p*-benzoquinone were produced when the benzene solution was analyzed by GC after 22 h. Of note, no noticeable continuation of the catalysis was observed in the solution after 22 h, possibly due to the deactivation or decomposition of (**1**) via some unknown pathway. Species (**1**) clearly catalyzed the O₂-oxidation of *p*-hydroquinone, as no

p-benzoquinone was formed in the absence of (1) under corresponding conditions. The O₂-oxidation of *p*-hydroquinone catalyzed by (1) is likely initiated by the reaction represented in Eq. 6.9 [*Ru* = Ru(TMP)], and Ru^{IV}(TMP)(O) can then regenerate (1) via disproportionation (Chapters 3 and 4).



The reaction between (1) and *p*-hydroquinone (~ 1:2 ratio) under 1 atm air at room temperature was monitored by ¹H-NMR spectroscopy, and after approximately 2 min, the spectrum showed that mainly (1) was present (Figure 6.13). Ru^{IV}(TMP)(O) and a Ru(II) species, possibly Ru^{II}(TMP)(*p*-HOC₆H₄OH)₂ (~ 10%),[†] can also be detected. At this time no free *p*-hydroquinone was present in the benzene-*d*₆ solution, implying that the oxidation of hydroquinone by (1) is rapid; furthermore, the ~ 90% reconversion to (1) suggests that the disproportionation of Ru^{IV}(TMP)(O) [and the aerobic oxidation of the Ru(II) species to (1)] is also fast (Chapter 3). No special precautions were taken to dry the benzene-*d*₆ solvent, and as such the H₂O stoichiometry in Eq. 6.9 cannot be determined, although 1 equivalent of H₂O is expected to be present by mass balance. The mechanism for the stoichiometric oxidation of *p*-hydroquinone by (1) cannot be determined from the current preliminary data; a hydride transfer mechanism analogous to that suggested for the alcohol oxidation (Chapter 4) is plausible, although two successive one-electron transfer/deprotonation steps can equally apply.

[†] A β -pyrrole-H signal at 8.5 ppm shows that a Ru^{II}(TMP) species is present in solution; however, the ¹H-NMR data (Ref. 3a) for a Ru^{II}(TMP) species proposed as the bis(*p*-HOC₆H₄OH) complex are different: β -pyrrole-H, 8.64; *o*-Me, 2.50; *p*-Me, 1.70. As only the β -pyrrole signal at 8.5 ppm can be clearly observed, and the other signals are presumably buried beneath those of (1), the identity of the Ru^{II}(TMP) species is unclear. After 10 min, only (1) and *p*-benzoquinone are present.

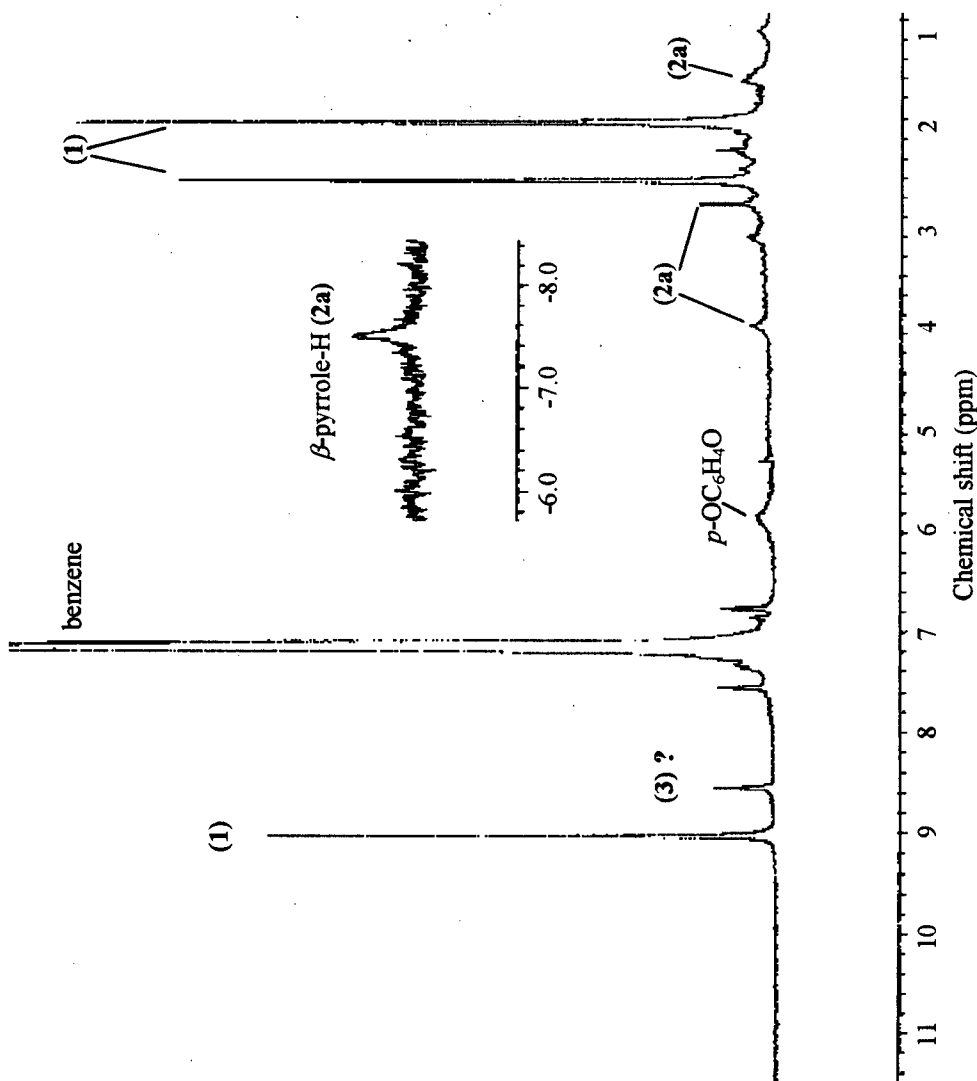


Figure 6.13. ^1H -NMR spectrum (200 MHz) acquired after 2 min for the reaction between $\text{Ru}^{\text{V}}(\text{TMP})(\text{O})_2$ (1) ($\sim 8 \times 10^{-4}$ M) and p -hydroquinone (1.5×10^{-3} M) in benzene- d_6 under 1 atm air. Inset shows the upfield region (4x). (2a) = $\text{Ru}^{\text{IV}}(\text{TMP})(\text{O})$; (3)? = $\text{Ru}^{\text{II}}(\text{TMP})(p\text{-HOC}_6\text{H}_4\text{OH})_2$ (see text).

The production of 0.5 equivalent of *p*-benzoquinone, which cannot be explained by the scheme in Eqs. 6.2 to 6.4, provides a key insight into the phenol oxidation mechanism. The *p*-benzoquinone was observed by both $^1\text{H-NMR}$ spectroscopy^{3a} and in this thesis work by gas chromatography experiments ($[(1)] = 2.0 \times 10^{-3} \text{ M}$ and [phenol] = 5 and 8-fold excesses in the respective studies). Attempts to detect the intermediate *p*-hydroquinone by GC analysis were unsuccessful. The $t_{1/2}$ value for the reaction between phenol and (1) under NMR experimental conditions ($\sim 10^{-2} \text{ M}$ and 10^{-3} M , respectively) is approximately 16 min (estimated from $k_{\text{obs}} = 0.069 \text{ M}^{-1}\text{s}^{-1} \times 0.01 \text{ M} = 0.00069 \text{ s}^{-1}$),³ while the $t_{1/2}$ value for the reaction between *p*-hydroquinone ($\sim 10^{-3} \text{ M}$) and (1) is approximately 0.1 min (a rough estimate of $t_{1/2}$ of $\sim 0.08 \text{ min}$ is made using $5 t_{1/2} = 1 \text{ turnover} = 0.4 \text{ min}$). That no *p*-hydroquinone is detected by GC is certainly a consequence of the faster reaction of (1) with *p*-hydroquinone than with phenol, and any *p*-hydroquinone produced from the initial oxidation of phenol will be oxidized at a faster rate by any species (1) that remains in solution. In essence (1), a 2-electron oxidant, oxidizes phenol to *p*-benzoquinone via the *p*-hydroquinone intermediate, which is a 4-electron process; this explains the formation of 0.5 equivalent of *p*-benzoquinone for every equivalent of (1).

A proposed mechanism for the oxidation of phenol involving the $\text{Ru}^{\text{IV}}(\text{TMP})(\text{O})/\text{Ru}^{\text{IV}}(\text{TMP})(\text{OH})_2$ interconversion, the chemistry of which is consistent within that of the Ru(TMP)/alcohol systems (Chapter 4), is outlined in Figure 6.14;

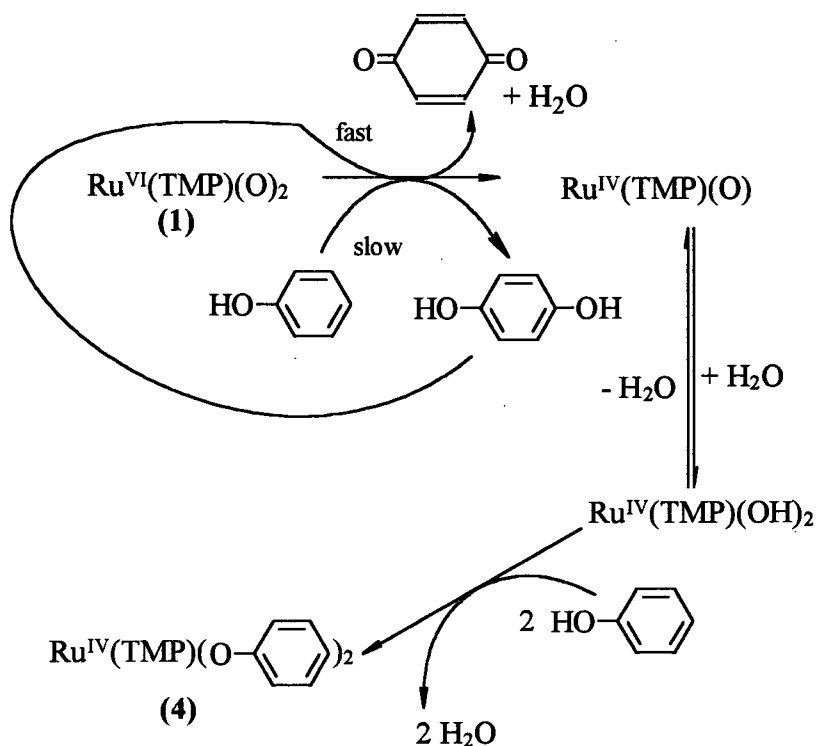
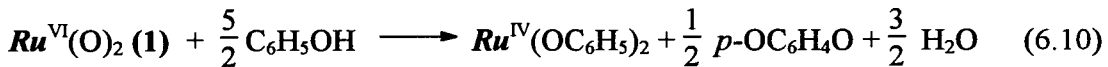


Figure 6.14. Phenol oxidation mechanism based on the reversible interconversion of $\text{Ru}^{\text{IV}}(\text{TMP})(\text{O})$ to a bis(hydroxo) species and phenol metathesis reactions. The reaction of (1) and phenol produces *p*-hydroquinone, which is further oxidized to *p*-benzoquinone at a faster rate compared to the rate of the phenol oxidation. Disproportionation of $\text{Ru}^{\text{IV}}(\text{TMP})(\text{O})$ to (1) and $\text{Ru}^{\text{II}}(\text{TMP})$ is a competing pathway, and under anaerobic conditions, some $\text{Ru}(\text{II})$ -species can be detected (see text).

according to the scheme, the overall reaction should produce 0.5 equivalent of *p*-benzoquinone and 1.5 equivalents of H₂O [Eq. 6.10; *Ru* = Ru(TMP)]. The stoichiometry of reaction 6.10 closely accounts for the experimentally observed 0.5 quinone and 1.3 H₂O.³



A Ru-porphyrin species formulated from ¹H-NMR data as

Ru^{II}(TMP)(*p*-HOC₆H₄OH)₂ (3) has been observed in the reaction between (1) and excess phenol under anaerobic conditions;^{3a} however, (3) only accounted for ~ 40% of the reaction products, with the other ~60% being (4). The large percentage of (4) was explained within the successive two-step oxidation mechanism (Eqs. 6.2 to 6.4), with trace O₂ being the cause for the formation of (4).^{3a} This is now considered unlikely considering that the concentration of (1) was 4 x 10⁻³ M,^{3a} and even with only one freeze-pump-thaw cycle the system should not have contained enough dissolved O₂ to give rise to the large amount of observed (4). Furthermore, the fact that (4) is the bis(phenoxo) complex, not the bis(*p*-hydroquinoxo) complex as proposed initially, invalidates the above “trace O₂” explanation. The reaction of (1) and phenol under anaerobic conditions was repeated in this thesis work, and the formation of (4) was always observed in excess of 90%, with (3) accounting for < 10% of the inorganic products.

That (4) is produced even in the absence of O₂ is inconsistent with the formerly suggested mechanism (Eqs. 6.2 to 6.4). The production of (4) via the bis(hydroxo) species, within the present mechanism (Figure 6.14), is expected to occur if H₂O is present, and to inhibit the conversion to the bis(hydroxo) species is impossible, as the

oxidation reaction produces H₂O. Even under initially dry conditions, the conversion to the bis(hydroxo) species can occur once some H₂O forms, and subsequently (**4**) is produced via the metathesis reaction with Ru^{IV}(TMP)(OH)₂. Under anaerobic conditions, the disproportionation of 2 Ru^{IV}(TMP)(O) to (**1**) and Ru^{II}(TMP), followed by ligation of *p*-hydroquinone and/or phenol to the Ru(II) centre provides a plausible explanation to account for the formation of the Ru(II) species (**3**). As the disproportionation pathway accounts for < 10% of the loss of Ru^{IV}(TMP)(O) (see above), its contribution to the reformation of (**1**) is insignificant; therefore, disproportionation is not considered to be one of the main reactions followed by the kinetics monitored for the loss of (**1**) (see Section 6.4.2)

6.4.2 Kinetic Studies

When (**1**) (4×10^{-3} M) reacted with phenol (2×10^{-2} M) in benzene-*d*₆ under 1 atm air or O₂, no other intermediates were observed in the ¹H-NMR spectrum of the solution en route to the product (**4**).^{3a} The kinetic data in the present thesis work for the stoichiometric oxidation of phenol by (**1**) under 1 atm air at various temperatures are shown in Figure 6.15. The reaction is first-order in (**1**), as demonstrated by a linear semilog plot (inset of Figure 6.2); this first-order dependence is also confirmed, as the same k_{obs} values are obtained with varying amounts of initial (**1**) at the same [phenol] value of 0.0381 M (see Figure 6.16 and Appendix F). The kinetic data are independent of O₂ partial pressure, as kinetics obtained under 1 atm O₂ or air were identical. Also, purging the solutions with N₂ for 10 min did not affect the kinetics (Appendix F).

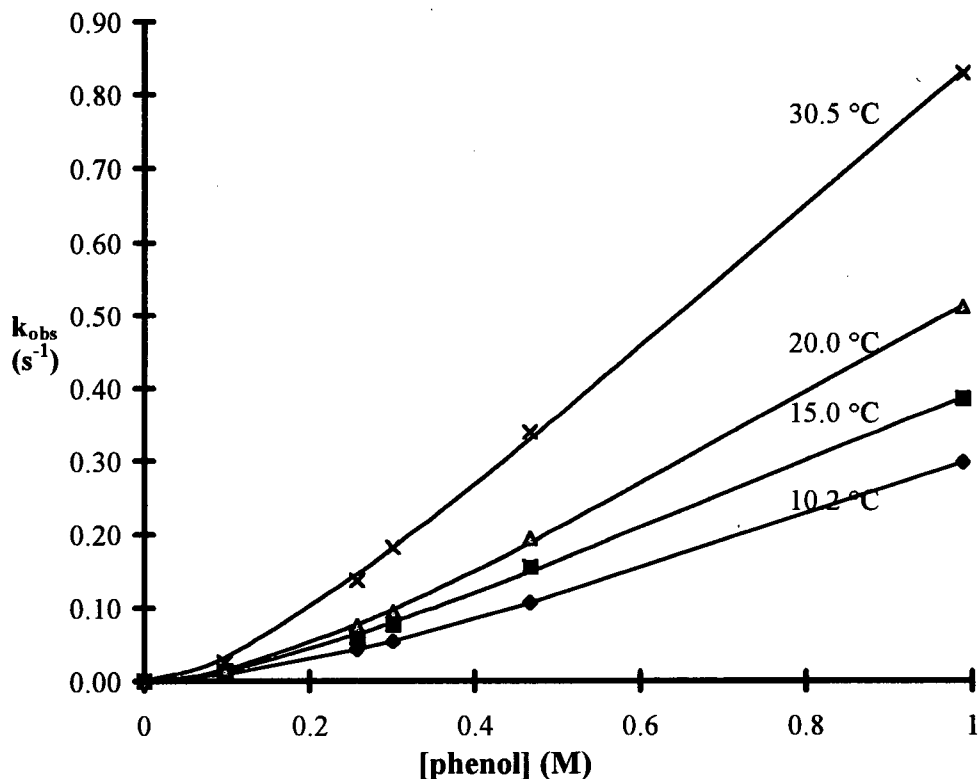


Figure 6.15. Plots of k_{obs} versus [phenol] for the oxidation of phenol by $\text{Ru}^{\text{VI}}(\text{TMP})(\text{O})_2$ (**1**) in benzene under 1 atm air at various temperatures. $[(\mathbf{1})] \sim 10^{-6}$ M. k_{obs} values are tabulated in Appendix F. Kinetic data were obtained on a stopped-flow spectrophotometer.

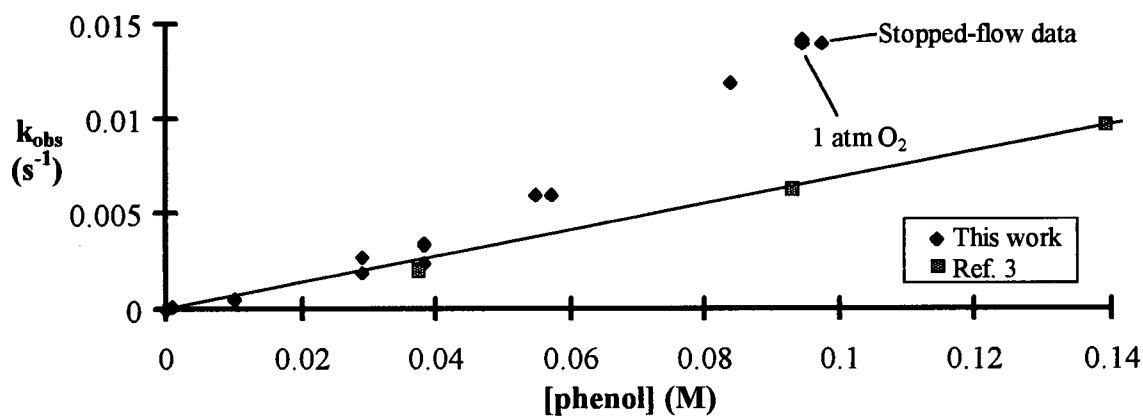


Figure 6.16. Plot of k_{obs} versus [phenol] for the oxidation of phenol by $\text{Ru}^{\text{VI}}(\text{TMP})(\text{O})_2$ in benzene at 20.0 °C under 1 atm air, except for the point labelled “1 atm O₂”. $[(\mathbf{1})] \sim 10^{-6}$ M. The raw data are listed in Appendix F. Kinetic data were obtained on the HP 8452A Diode-Array instrument, except for the point indicated as “Stopped-flow data”.

The non-linearity in the plots of k_{obs} versus [phenol] can be seen readily, illustrating a non-first-order dependence in phenol. Earlier preliminary work in this laboratory was carried out at a lower [phenol] region (up to 0.14 M) and less data were obtained.³ The kinetic experiments were repeated in this thesis work at the lower [phenol] region (see Figure 6.16), and while the k_{obs} values obtained at [phenol] = 0.0381 M agreed reasonably well with that obtained in the preliminary work, the other data from the earlier work clearly do not agree with those obtained in the present studies. This reason for this non-agreement is not known, but only the new curved-dependence data will be considered in the following discussion.

The $\log(k_{\text{obs}})$ versus $\log[\text{phenol}]$ plots are linear with slopes averaging 1.51 ± 0.09 (Figure 6.17), which suggest a 3/2 order dependence in phenol. A log-log plot is generally somewhat misleading, as a reaction with k_{obs} going from 1st- to 2nd-order kinetics with increasing added reagent (cf. Figure 6.15) might exhibit an average apparent order of 3/2; however, the plot for the data at 20 °C (Figure 6.17) is linear over 2 orders of magnitude of [phenol] values. The linearity of a log-log plot for a 1st- to 2nd-order dependence system is unlikely to extend over such a large concentration range (0.01 to 1.0 M), and hence the k_{obs} expression may indeed take the form $k_{\text{obs}} = A \cdot [\text{phenol}]^{3/2}$ (see Table 6.3). The curvature in the k_{obs} versus [phenol] plots could possibly be ascribed to “solvent effects”, as the [phenol] corresponds to ~ 10% mole fraction for the case of the highest concentration used; however, the curvature is considered to be real as the non-linearity starts at [phenol] values as low as ~ 0.04 M for the data at 20 °C.

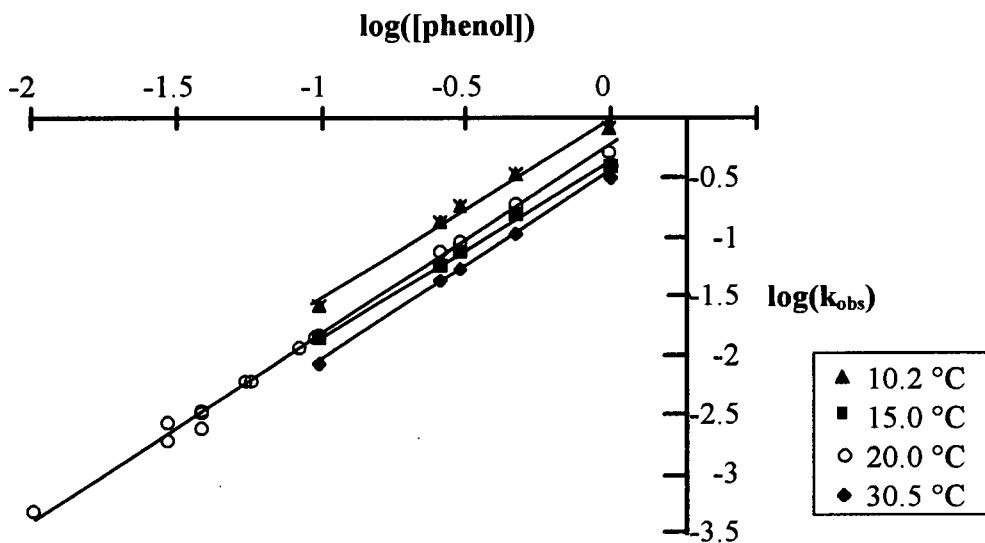


Figure 6.17. Log(k_{obs}) versus log[phenol] plot for the oxidation of phenol at various temperatures. The average of the slopes are 1.51 ± 0.09 .

Table 6.3. Values for the parameter A for the oxidation of phenol by (1), derived from the expression $k_{\text{obs}} = A \cdot [\text{phenol}]^{3/2}$. The activation energy, ΔE^\ddagger , is also calculated from the values of A from the Arrhenius plot (Figure 6.18).

Temperature	A ($M^{-3/2}s^{-1}$)
10.2 °C	0.362 ± 0.03
15.0 °C	0.425 ± 0.03
20.0 °C	0.583 ± 0.04
30.5 °C	0.98 ± 0.07
$\Delta E^\ddagger = 39 \pm 2 \text{ kJ mol}^{-1}$	
precollision factor ^a = $(5.1 \pm 0.3) \times 10^6 \text{ s}^{-1}$	

^a Calculated at every temperature and then averaged.

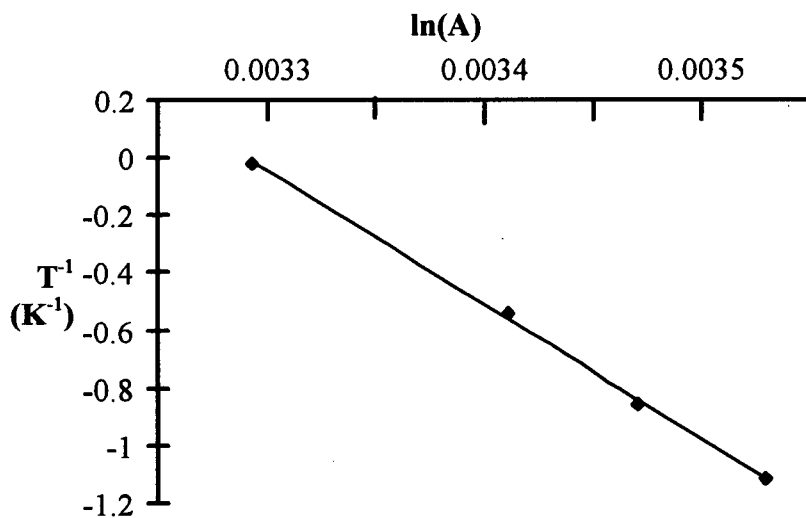
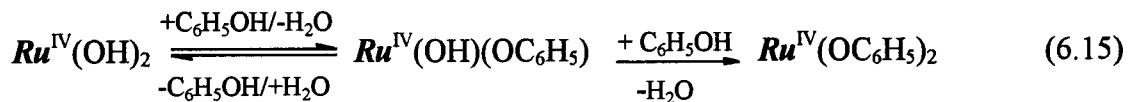
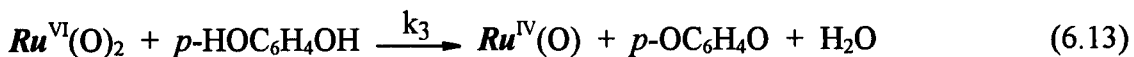
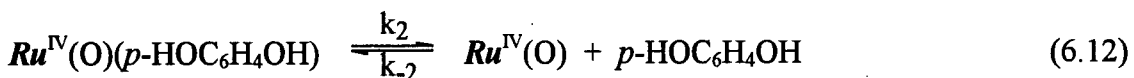
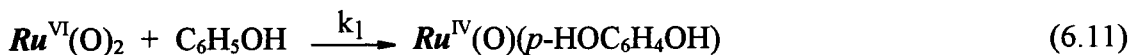


Figure 6.18. Arrhenius plot, $\ln(A)$ versus T^{-1} , for the parameter A for the reaction between (1) and phenol. The values for A are listed in Table 6.3.

According to the mechanism proposed in Figure 6.14, the following reaction pathways [Eqs. 6.11 to 6.15; $Ru= Ru(TMP)$] are expected to play a role in the rate law for the phenol oxidation reaction.



The [(1)] values were $\sim 10^{-3}$ M in $^1\text{H-NMR}$ and GC studies (see earlier, Section 6.4.1), and the oxidation by (1) of the *p*-hydroquinone formed ($\sim 10^{-3}$ M) was shown to be

faster than that of phenol ($\sim 10^{-2}$ M). In the kinetic studies, the [(1)] values were three orders of magnitude lower ($\sim 10^{-6}$ M), while [phenol] values were higher (0.01 to 1 M); therefore, the rate of oxidation of the *p*-hydroquinone formed ($\sim 10^{-6}$ M) might not have been faster than that of phenol. In addition, the reversible coordination and recoordination reactions of *p*-hydroquinone (Eq. 6.12) may contribute to the overall rate law, as similar reactions with OPPh_3 are found to be significant within the phosphine systems (Chapter 3). Clearly, more work is necessary to arrive at a rate law which can accommodate the experimental data, namely the curvature in the k_{obs} versus [phenol] plots.

The Arrhenius plot (Figure 6.18) for the parameter A gives an activation energy, ΔE^\ddagger , of 39 ± 2 kJ mol⁻¹ and a precollision factor of $(5.1 \pm 0.3) \times 10^6$ s⁻¹. The parameter A is presumably comprised of various rate constants and equilibrium constants for the reaction pathways (Eqs. 6.11 to 6.15), but they are still useful for indicating the general ease of the phenol oxidation reaction. The ΔE^\ddagger value is similar to the ΔH^\ddagger value of 45 kJ mol⁻¹ (which corresponds to $\Delta E^\ddagger \sim 48$ kJ mol⁻¹) for the ¹PrOH oxidation by (1) (Chapter 4), implying perhaps that cleavage of the aromatic C-H bond requires approximately the same energy as that for the α -C-H bond in ¹PrOH.

6.5 O₂-Oxidation of *N,N*-Dimethylaniline Catalyzed by Ru^{VI}(TMP)(O)₂

Following the oxidation of phenol, other mono-substituted aromatics (*N,N*-dimethylaniline, methoxybenzene, toluene, chlorobenzene, bromobenzene and nitrobenzene) were tested as potential substrates. Only *N,N*-dimethylaniline, which contains the electron releasing NMe₂ group, was oxidized by (1). Under 1 atm air the

oxidation of *N,N*-dimethylaniline is catalytic, producing a hydroxy-*N,N*-dimethylaniline, as shown by GC-MS analysis (Appendix G), and the oxidation presumably occurs at the para position based on analogy with the phenol system (Section 6.4.1). Figure 6.19 shows the proposed scheme for the oxidation reaction.

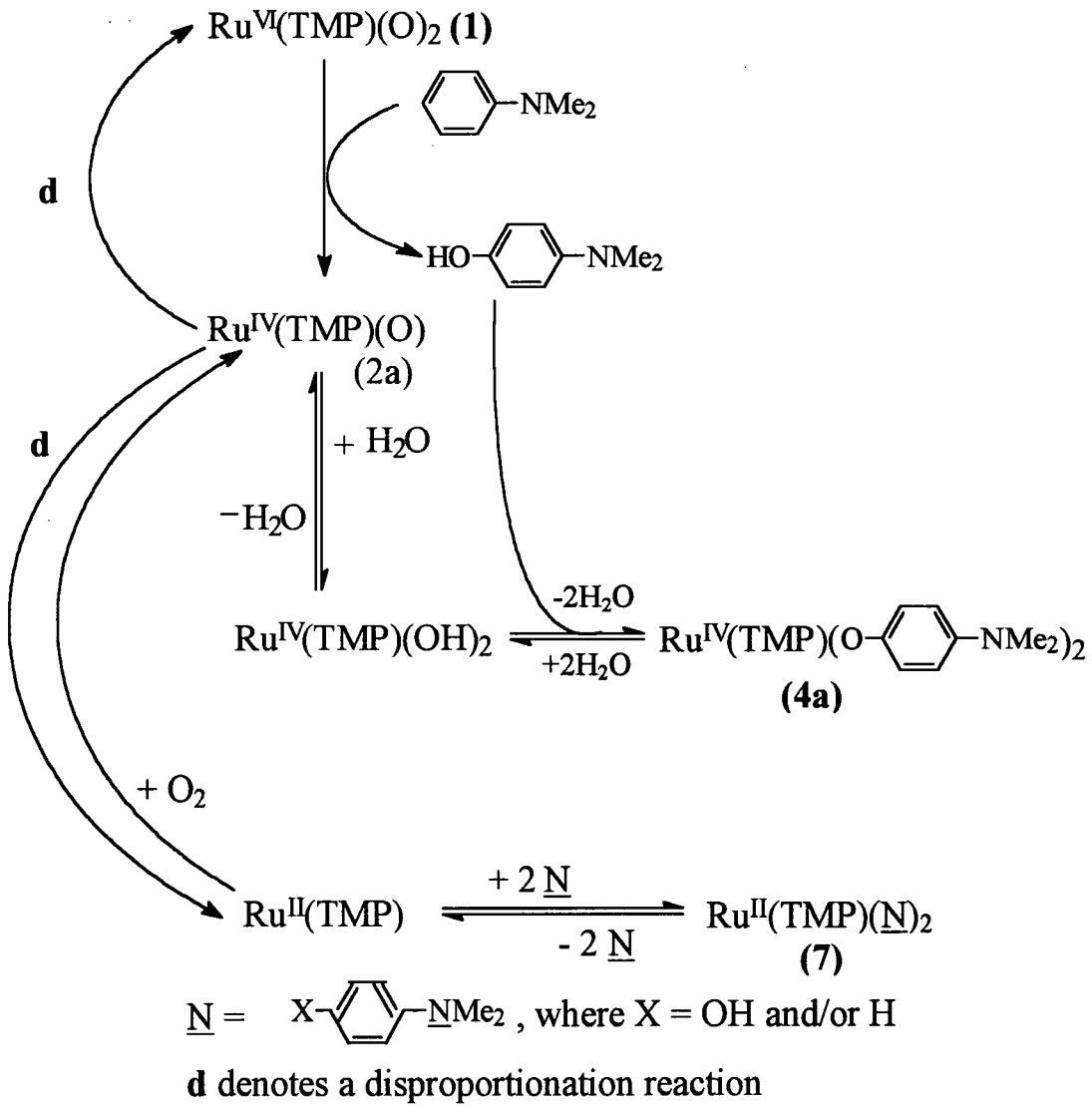


Figure 6.19. Proposed scheme for the oxidation of *N,N*-dimethylaniline catalyzed by $\text{Ru}^{\text{VI}}(\text{TMP})(\text{O})_2$ (1) under 1 atm air. Trace H_2O was present, as the benzene- d_6 was not dried; in any case H_2O is generated during formation of (4a) from (1).

Figure 6.20 shows the $^1\text{H-NMR}$ spectra recorded on monitoring the reaction between (1) and *N,N*-dimethylaniline (1:4) in benzene- d_6 under 1 atm air. After 1 min, $\text{Ru}^{\text{IV}}(\text{TMP})(\text{O})$ was not detected, but ^1H -resonances for the TMP ligand characteristic of those within a bis(alkoxo)-Ru(IV) species, (4a), were seen (*o*-Me, 2.99; *p*-Me, 2.90; *m*-H 7.60; β -pyrrole-H, -22 ppm) (see Chapter 4, Table 4.1), and these are assigned to $\text{Ru}^{\text{IV}}(\text{TMP})(p\text{-OC}_6\text{H}_4\text{NMe}_2)_2$. Of note, the axial *p*-OC₆H₄NMe₂ ligand protons within (4a) are not detected by $^1\text{H-NMR}$ spectroscopy, while those of the OC₆H₅ ligands within the analogous complex (4) (Table 4.1) are clearly detectable. The reason for the non-detection of the *p*-OC₆H₄NMe₂ ligands is not substantiated; however, one factor for the non-detection of the alkoxo ligand protons by $^1\text{H-NMR}$ spectroscopy can be the rapid exchange of the alkoxo ligands with excess alcohol in solution (Section 4.3.1). The amount of species (4a) increases over time (Figure 6.20) and, unlike in the reaction between (1) and phenol, $^1\text{H-NMR}$ signals corresponding to Ru(II) species (7) and a Ru(TMP)(CO) species (D) were observed as well after 30 min. After a total of 60 min, the benzene- d_6 solvent was removed under vacuum, and the solid residue was analyzed by mass spectrometry (Figure 6.3).

Species (7) is thought to be a mixture of $\text{Ru}^{\text{II}}(\text{TMP})(p\text{-NMe}_2\text{C}_6\text{H}_4\text{X})_2$ species (where X = H or OH). The mass spectral data in Figure 6.3 suggest that Ru(TMP) species containing either one NMe₂C₆H₅ or one *p*-NMe₂C₆H₄OH ligand are present, with mass peaks at 1003 and 1019 amu, respectively. In solution, (7) is likely a six-coordinate, bis(amine)ruthenium(II) species, rather than the five-coordinate complex suggested from the mass spectra. The sixth ligand is perhaps labile and readily dissociates when (7) is

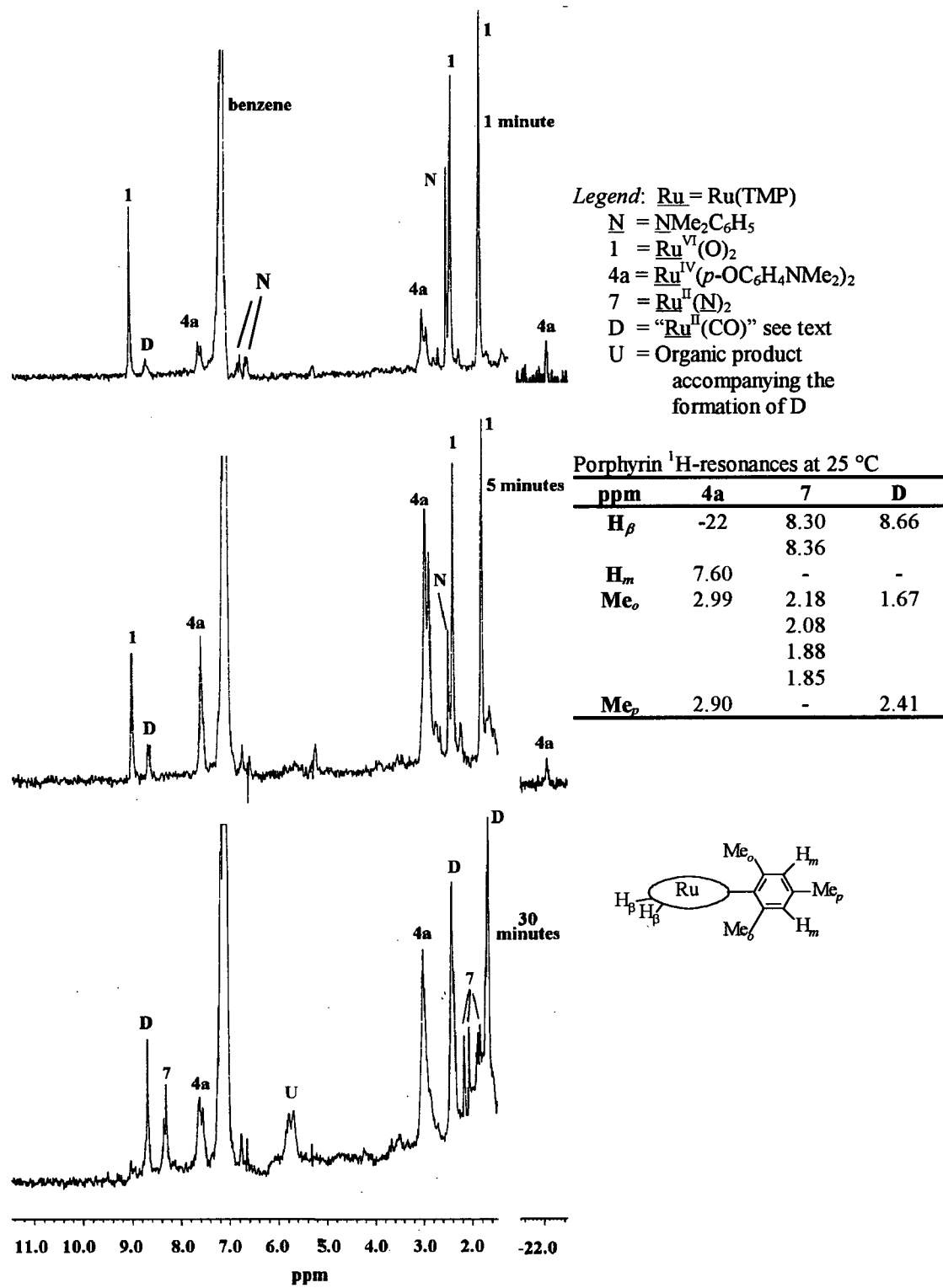


Figure 6.20. ^1H -NMR (200 MHz) spectra for the reaction “ $\text{Ru}^{\text{VI}}(\text{TMP})(\text{O})_2 + 4 \text{N},\text{N}$ -dimethylaniline” in benzene- d_6 at 25 °C under 1 atm air. $[(1)] = 2.0 \times 10^{-3}$ M.

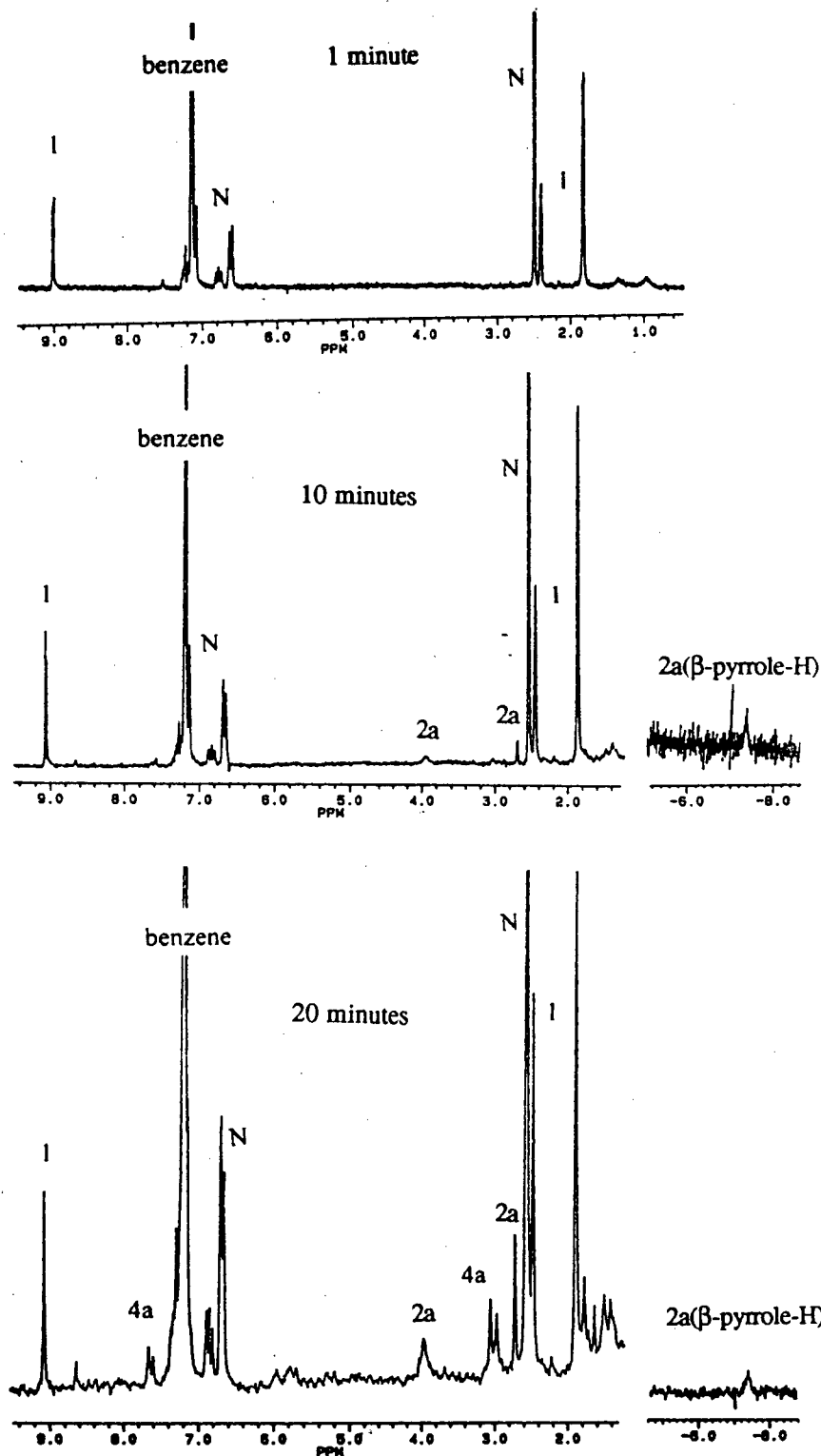


Figure 6.21. ^1H -NMR (200 MHz) spectra monitoring the reaction " $\text{Ru}^{\text{VI}}(\text{TMP})(\text{O})_2 + 10 \text{ } N,N\text{-dimethylaniline}$ " in benzene- d_6 at 25 °C under 1 atm argon. $[(\text{I})] = 1.0 \times 10^{-3}$ M. Refer to the legend in Fig. 6.20 for the identities of the observed Ru(TMP) species. 2a = $\text{Ru}^{\text{IV}}(\text{TMP})(\text{O})$.

ionized by the fast atom bombardment ionization method in the MS experiment. In a separate experiment, Ru^{II}(TMP)(MeCN)₂ was added to a benzene-*d*₆ solution containing excess *N,N*-dimethylaniline (aniline:Ru = 10:1), and ¹H-resonances corresponding to a new Ru(II) species were assumed to be those of Ru^{II}(TMP)(NMe₂C₆H₅)₂ (β -pyrrole-H, 8.34; *o*-Me, 2.05; *p*-Me, 2.45 ppm; axial ligand protons were not observed, presumably due to rapid exchange of the ligands with free *N,N*-dimethylaniline); the data support the suggestion of (7) (β -pyrrole-H, ~8.3 ppm; see Figure 6.20) as species containing coordinated NMe₂C₆H₅ and/or *p*-NMe₂C₆H₄OH ligands. The ¹H-NMR data for (7) in Figure 6.20 (at 30 min) show more than one set of *o*-Me ¹H-resonances, which can result from three different coordination environments about the Ru(II) centre where two dimethylaniline, one hydroxy-dimethylaniline and one dimethylaniline, and two hydroxy-dimethylaniline, ligands are present, respectively.

The solid residue that had been subjected to mass analysis was also analyzed by IR spectroscopy, and a band at 1942 cm⁻¹ is assignable to a Ru^{II}(TMP)(CO) species (D) (ν_{CO} = 1943 cm⁻¹, Chapter 2); however, the ¹H-NMR signals assignable to (D) in Figure 6.20 do not correspond well (except for the β -pyrrole ¹H-signal) to those of Ru^{II}(TMP)(CO) itself (β -pyrrole-H, 8.79; *o*-Me, 2.20, 1.83; *p*-Me, 2.48 ppm; Chapter 2). Nonetheless, the mass spectrum (Figure 6.3) of the solid sample, which also contains (D), shows a mass peak centred around 912 amu, consistent with the presence of a Ru^{II}(TMP)(CO) species (MW = 910 g mol⁻¹). Accompanying the formation of (D) is an organic product (U), which exhibits ¹H-NMR signals in the 5.5 to 6 ppm region (Figure 6.20). The identities of (D) and (U) are not known.

Of note, the reaction between (1) and *N,N*-dimethylaniline under 1 atm Ar, unlike the reaction under 1 atm air, produced some Ru^{IV}(TMP)(O) after 10 min; Ru^{IV}(TMP)(*p*-OC₆H₄NMe₂)₂ (**4a**) was not observed at this time, and was only seen after about 20 min (Figure 6.21). Also, the ¹H-resonance at 8.66 ppm attributable to the β -pyrrole-H of the TMP ligand within (**D**) was observed after 20 min. Unlike the reaction under 1 atm air, the reaction under Ar, after ~ 40 min, showed decomposition of the Ru-porphyrin species in the benzene-*d*₆ solution, as suggested by the disappearance of the characteristic TMP ¹H-NMR signals for all the species in solution. The natures of the Ru^{II}(TMP)(CO) formation and Ru(TMP) decomposition reactions are not known.

The ¹H-NMR spectra (Figure 6.21) for the reaction under Ar showed that Ru^{IV}(TMP)(O) was first detected, followed by (**4a**). For the reaction under air (Figure 6.20), ¹H-resonances corresponding to (**7**) appear after those for (**4a**). This chronological order in which the Ru-porphyrin species are detected supports the mechanism presented in Figure 6.19. Of note, the formation of the Ru(II) species (**7**) (Figure 6.20) provides a potential pathway for regenerating Ru^{VI}(TMP)(O)₂ under air or O₂, the criterion being that the axial aniline ligands are labile. Indeed, the oxidation of NMe₂C₆H₅ to *p*-NMe₂C₆H₄OH by (1) is catalytic in air, although only marginally with less than 10 total turnovers (Table 6.4). Of note, the oxidation of phenol to *p*-hydroquinone by (1) is not catalytic, as the product Ru^{IV}(TMP)(OC₆H₅)₂ (**4**) does not regenerate (1) under air in wet benzene.

Table 6.4. Aerobic oxidation of *N,N*-dimethylaniline catalyzed by Ru^{VI}(TMP)(O)₂ (**1**) under 1 atm air in benzene.

Reaction Conditions	Time (hours)	% conversion to <i>p</i> -hydroxy- <i>N,N</i> -dimethylaniline ^b [total turnovers]
24 °C [(1)] = 3.3 × 10 ⁻³ M [aniline] = 0.0158 M H ₂ O added ^a	28.5	47% [2.5]
	29.0	33% [3.1]
	29.0	19.7% [2.1]
50 °C [(1)] = 7.4 × 10 ⁻⁴ M [aniline] = 0.0316 M H ₂ O added ^a	18.0	12.7% [5.4]
	18.5	8.4% [9.1]
	36.5	8.8% [9.4]
[(1)] = 7.4 × 10 ⁻⁴ M [aniline] = 0.0631 M H ₂ O added ^a	18.5	8.6% [7.3]
	18.5	4.9% [8.4]

^a 50 µL H₂O was added to 0.50 mL benzene solutions, otherwise benzene (HPLC grade) was used directly.

^b An hydroxy-*N,N*-dimethylaniline is suggested from GCMS analysis (Appendix G), and incorporation of the O-atom at the para position is based on analogy with the phenol system (see text).

6.6 Conclusions

A reaction between Ru^{VI}(TMP)(O)₂ (**1**) and strong organic acids (CF₃COOH, CHCl₂COOH) was discovered and the Ru products are bis(acetato)ruthenium(IV) type species. Such reactions are of interest because acids have been observed to enhance the reactivity within systems used for the stoichiometric and catalytic hydroxylation of alkanes.^{1,2} The oxidation product from the reaction between (**1**) and HX, when identified, will reveal the nature of the reaction.

The preliminary study conducted earlier in this laboratory on the oxidation of phenol³ by (**1**) was re-examined in this thesis. A new mechanism is proposed consistent with the oxidation chemistry of (**1**) discovered within the phosphine and alcohol systems (Chapters 3 and 4); Ru^{IV}(TMP)(O) is no longer considered to be an active oxidant. Rather, a Ru^{IV}(TMP)(O)/Ru^{IV}(TMP)(OH)₂ interconversion, and disproportionation of 2 equivalents of Ru^{IV}(TMP)(O) to Ru^{II}(TMP) and Ru^{VI}(TMP)(O)₂, are considered to be the significant reaction pathways for Ru^{IV}(TMP)(O). Kinetic studies for the phenol system reveal a non-first-order (between first and second) dependence on the phenol, which cannot be satisfactorily accommodated within the formerly successive two-step oxidation³ or the current single O-atom oxidation and Ru^{IV}(TMP)(O)/Ru^{IV}(TMP)(OH)₂ interconversion mechanisms. Preliminary work on the oxidation of *N,N*-dimethylaniline suggests the process to be similar to the phenol oxidation. GC-MS analysis suggests the product from the oxidation reaction to be a hydroxy-*N,N*-dimethylaniline; a larger scale reaction should be carried out so that the organic product could be isolated and its identity confirmed. Unlike the phenol system, the *N,N*-dimethylaniline system is catalytic (< 10

total turnovers) under 1 atm air in benzene; however, the catalytic activity of (1) is lost, involving decomposition of Ru(TMP) species and formation of a Ru^{II}(TMP)(CO) species, of which the natures are unknown at this time.

References

- 1 T.-C. Lau and C.-K. Mak, *J. Chem. Soc., Chem. Commun.*, 766 (1993); 943 (1995).
- 2 a) H. Otake, T. Higuchi and M. Hirobe, *Heterocycles*, **40**, 867 (1995).
b) H. Otake, T. Higuchi and M. Hirobe, *J. Am. Chem. Soc.*, **114**, 10660 (1992).
- 3 a) N. Rajapakse, Ph.D. Dissertation, University of British Columbia, 1990.
b) N. Rajapakse, B. R. James and D. Dolphin, *Stud. Surf. Sci. Catal.*, **55**, 109 (1990).
- 4 a) C. Sishta, Ph.D. Dissertation, University of British Columbia, 1990.
b) C. S. Alexander, Ph.D. Dissertation, University of British Columbia, 1995.
- 5 J. T. Groves and K.-H. Ahn, *Inorg. Chem.*, **26**, 3833 (1987).
- 6 a) W. H. Leung and C.-M. Che, *J. Am. Chem. Soc.*, **111**, 8812 (1989).
b) W.-H. Leung, C.-M. Che, C.-H. Yeung and C.-K. Poon, *Polyhedron*, **12**, 2331 (1993).
c) J.-S. Huang, C.-M. Che and C.-K. Poon, *J. Chem. Soc., Chem. Commun.*, 161 (1992).
- 7 a) D. F. Evans, *J. Chem. Soc.*, 2003 (1959).
b) D. H. Live and S. I. Chan, *Anal. Chem.*, **42**, 791 (1970).
- 8 G. N. La Mar and F. A. Walker, in *The Porphyrins*, ed. D. Dolphin, Volume 4, Academic Press, New York, Chapter 2, 1979.
- 9 K. Nakamoto, *Infrared and Raman Spectra of Inorganic and Coordination Compounds*, 3rd Ed., John Wiley and Sons, Toronto, 1978, p. 232.

Chapter 7

**Conclusion
and
Recommendations for Future Work**

7.1 General Conclusions

The stoichiometric and catalytic O₂-oxidations of a variety of organic substrates (phosphines, alcohols, alkenes and alkanes) effected by *trans*-Ru^{VI}(porp)(O)₂ species (porp = TMP, TDCPP and TDCPP-Cl₈)[†] were presented in the preceding chapters. The preparation of the Ru(TDCPP-Cl₈) species was a collaborative joint effort with Xie from Dolphin's group.

The kinetic data for the oxidation of EAr₃ substrates (E = P, As, Sb) by Ru^{VI}(TMP)(O)₂ (**1**) in benzene reveal a characteristic two-phase reaction, with the faster stage occurring on a timescale ~ 10⁻² s and the slower ~ 10¹ s. The faster reaction is considered to be an O-atom transfer involving the electrophilic attack of a Ru=O moiety of (**1**) on the lone pair of electrons on the E-atom, to form initially

Ru^{IV}(TMP)(O)(OEAr₃). A plot of ΔH₁[‡] (but not log $\frac{k_X}{k_H}$) for the O-atom transfer versus the Hammett factor σ was close to linear, suggesting that a more electron-withdrawing para substituent gives a more favourable, lower value ΔH₁[‡]. The ΔS₁[‡] values for the O-atom transfer reactions correlate with the substrate molecular masses, with bulkier substrates giving more favourable, less negative ΔS₁[‡] values, an indication that the O-atom transfers occur via strong Ru=O vibrational coupling. The slower stage of the reaction of (**1**) with EAr₃ is thought to involve the dissociation of OEAr₃ from Ru^{IV}(TMP)(O)(OEAr₃) to form Ru^{IV}(TMP)(O), which then disproportionates to (**1**) and Ru^{II}(TMP); EAr₃ readily coordinates to the latter species to form the 5-coordinate

[†] TMP, TDCPP and TDCPP-Cl₈ = dianions of *meso*-tetramesityl, *meso*-tetra(2,6-dichlorophenyl) porphyrins and *meso*-tetra(2,6-dichlorophenyl)-β-octachloroporphyrin, respectively.

Ru^{II}(TMP)(EAr₃) product. The oxidation of EAr₃ becomes catalytic under air or O₂, and preliminary data show that the catalysis is slow compared to the stoichiometric reaction; approximately 1 turnover h⁻¹ is obtained for the PPh₃ system at ambient conditions.

The paramagnetic Ru(IV) species formed from the reaction of (1) with ^tPrOH was formulated as Ru^{IV}(TMP)(OH)₂ in previous preliminary work in this laboratory; it is now reformulated as Ru^{IV}(TMP)(O^tPr)₂ from crystallographic and spectroscopic studies in the present thesis work. The oxidation of the alcohol is proposed to involve an initial cleavage of the α -C-H with transfer of a hydride to a Ru=O moiety. The oxidation of ^tPrOH to acetone by (1), under air in wet benzene, is catalytic, and (1) can also oxidize benzyl alcohol to benzaldehyde (without further oxidation to benzoic acid); in a benzene/3.0 M aq. KOH 2-phase system, 2000 equivalents of benzaldehyde are produced in ~ 13 d at 50 °C. Species (1) can also oxidize Ph₃CH to Ph₃COH catalytically under air. Ru^{VI}(TDCPP)(O)₂ is slightly more reactive and can also oxidize adamantane to 1-adamantanol, although both systems give only a few total turnovers. That these dioxo complexes use solely O₂ as the oxidant for these alkane systems demonstrates some remarkable chemistry.

For the first time, Ru(TDCPP-Cl₈) species are prepared and used as catalyst precursors for the O₂-oxidation of alcohols, alkenes and alkanes. The oxidation of benzyl alcohol catalyzed by Ru^{VI}(TDCPP-Cl₈)(O)₂ is about as effective as that by (1) under corresponding conditions, and the mechanism is presumably the same. The oxidations of neat cyclohexene, *cis*-cyclooctene and methylcyclohexane operate via free-radical

pathways to give turnovers of $\sim 10^5$, probably based on hydroperoxide formation and decomposition mediated by Ru(TDCPP-Cl₈) species.

The reactions of (1) with HX acids (X = Cl, CF₃COO, CHCl₂COO) are found to give Ru^{IV}(TMP)(X)₂ products, as established by NMR and IR spectroscopies and mass spectrometry. The bis(acetato)ruthenium(IV) species are similar to the paramagnetic bis(halo)ruthenium(IV) complexes that have been characterized previously in this laboratory.

The stoichiometric oxidation of phenol by (1) in benzene was proposed from previous preliminary work in this laboratory to form Ru^{IV}(TMP)(*p*-OC₆H₄OH)₂. The present data favour the formulation of the Ru(IV) product as Ru^{IV}(TMP)(OC₆H₅)₂; furthermore, the reaction mechanism is proposed to involve a Ru^{IV}(TMP)(O)/Ru^{IV}(TMP)(OH)₂ interconversion, followed by phenol metathesis with the bis(hydroxo) species. The Ru^{IV}(TMP)(O) intermediate is not considered to be an active oxidant; the species either undergoes the disproportionation or interconversion pathways (see above). Species (1), under air, also catalytically oxidizes *N,N*-dimethylaniline, presumably to *p*-HOC₆H₄NMe₂ (see Section 7.2); however, less than 10 total turnovers are obtained in 1 d.

7.2 Recommendations for Future Work

A wide area of O₂-oxidation chemistry mediated by Ru(porp) species was opened up in this thesis work. The potential of these Ru-porphyrin species, particularly the TDCPP-Cl₈ type, as O₂-oxidation catalysts has yet to be determined. The O₂-oxidation of

a wider variety of substrates (alkenes and alkanes) catalyzed by the Ru(TDCPP-Cl₈) species deserves greater study to establish the scope of the usage of such metalloporphyrins.

The following experiments are suggested as starting points in answering some questions raised in Chapter 6. Although the reaction of (1) with HX acids undoubtedly gives Ru^{IV}(TMP)(X)₂ species, the reaction mechanism is not understood; furthermore, the product from the HX species is not known. Stoichiometric titration studies are obviously needed to elucidate the nature of these reactions.

The scheme proposed in Chapter 6 for the oxidation of phenol by (1) is consistent with the experimental observations, as well as with the chemistry of Ru(TMP) species within the phosphine and alcohol systems; however, the mechanism does not accommodate satisfactorily the observed kinetic data, which show a non-first-order (~ 1.5) dependence on phenol. An initial step would be to acquire more kinetic data over lower [phenol] values ($< 10^{-2}$ M) to determine whether the non-first-order dependence is valid over a greater concentration range.

The GCMS data show that the O-atom is incorporated into the substrate during the oxidation of *N,N*-dimethylaniline by (1); the product is presumably *p*-HOC₆H₄NMe₂, and that the oxidation occurs at the para position is based on analogy with the phenol system. More direct identification of the oxidation product is necessary, and a larger scale reaction, followed by product separation, would be one way to confirm that *p*-HOC₆H₄NMe₂ is formed.

Appendix A. Kinetic Data for the Oxidation of EAr₃.

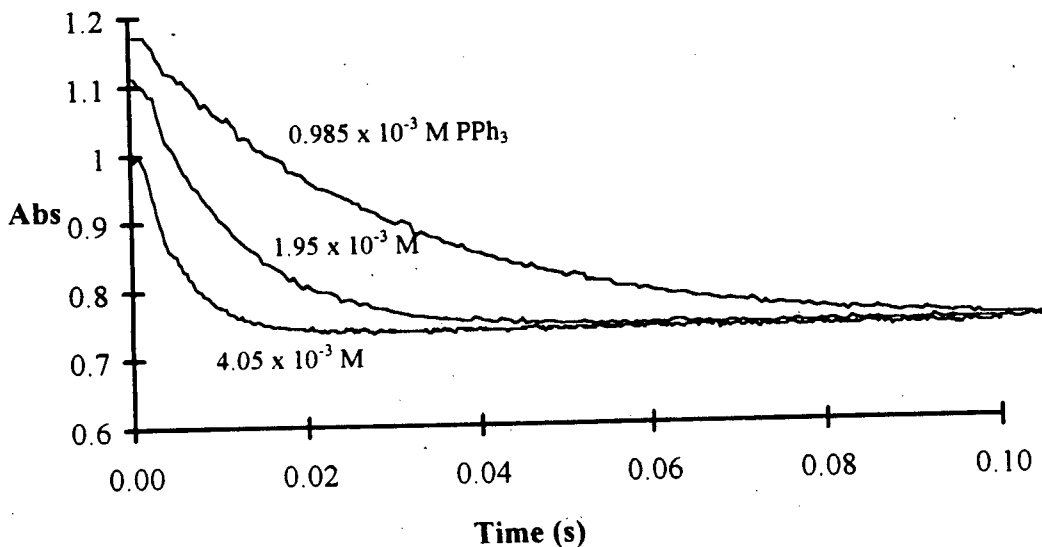


Figure A.1. Absorbance-time traces monitored at 422 nm by stopped-flow spectrophotometry for the reaction of Ru^{VI}(TMP)(O)₂ ($4.2 \times 10^{-6} \text{ M}$ in benzene) and PPh₃.

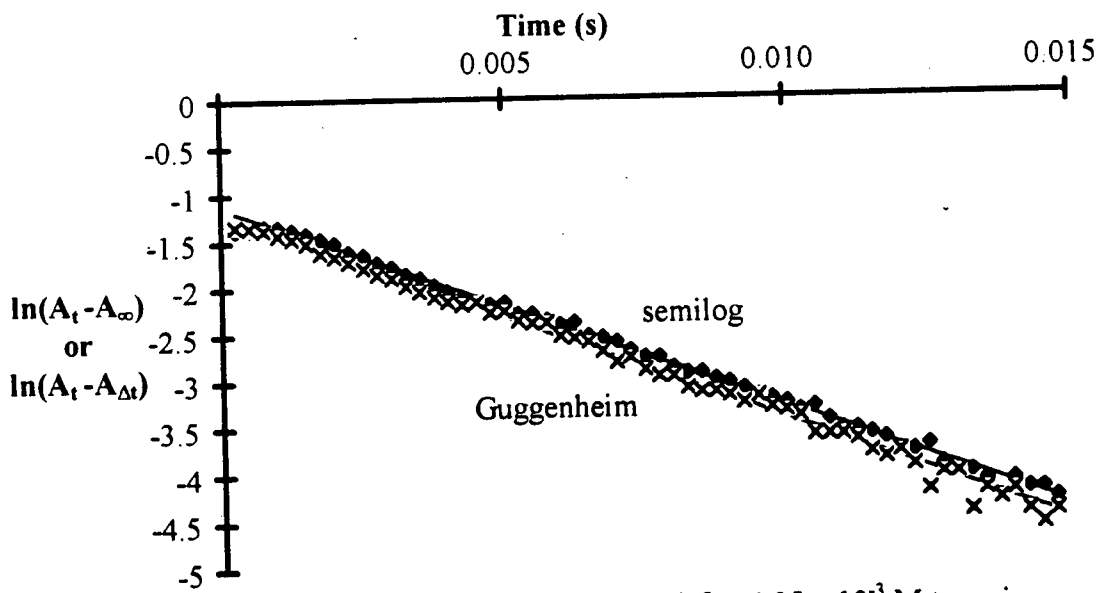


Figure A.2. Semilog and Guggenheim plots for $[\text{PPh}_3] = 4.05 \times 10^{-3} \text{ M}$ trace in Figure A.1 above, where A_t = absorbance at time t , A_∞ = final absorbance, and $\Delta t = 0.0075 \text{ s}$. Slope = $k_{\text{obs}} = 216 \pm 1.7$, 220 ± 1.7 and 227 ± 2 by semilog, Guggenheim and curve-fitting analyses, respectively.

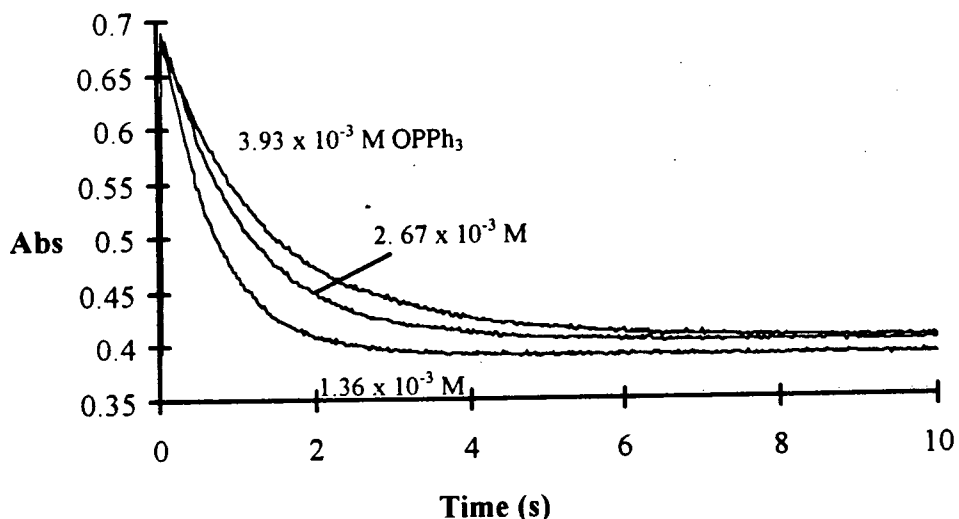


Figure A.3. Absorbance-time traces monitored at 430 nm by stopped-flow spectrophotometry for the loss of the intermediate $\text{Ru}^{\text{VI}}(\text{TMP})(\text{O})(\text{OPPh}_3)$ via further reaction with PPh_3 ($3.9 \times 10^{-3} \text{ M}$) (initial $[\text{Ru}^{\text{VI}}(\text{TMP})(\text{O})_2] = 4.2 \times 10^{-6} \text{ M}$ in benzene).

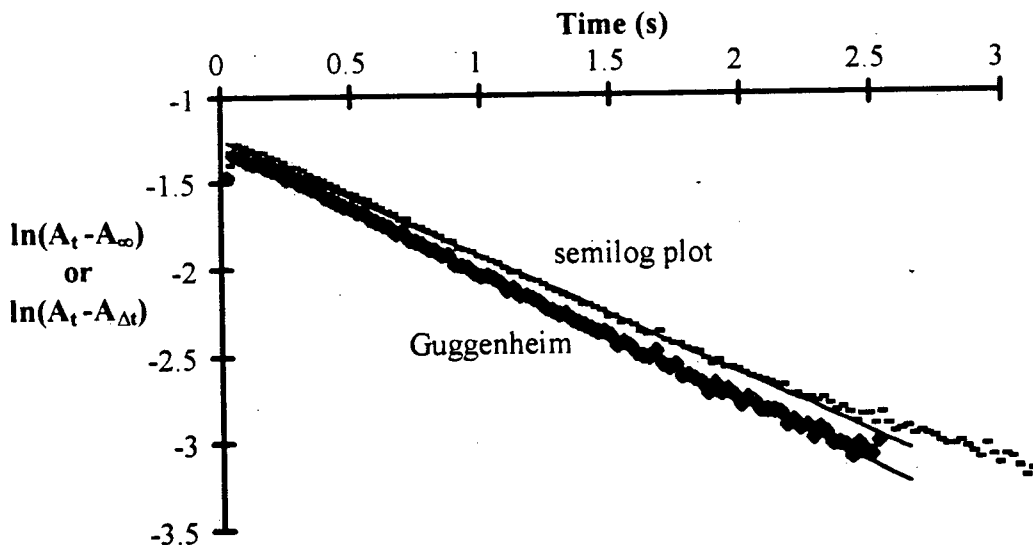


Figure A.4. Semilog and Guggenheim plots for $[\text{PPh}_3] = 3.83 \times 10^{-3} \text{ M}$, $[\text{OPPh}_3] = 3.93 \times 10^{-3} \text{ M}$ trace in Figure A.3 above. A_t = absorbance at time t , A_∞ = final absorbance, and $\Delta t = 1.0 \text{ s}$. Slope = $k'_{\text{obs}} = 0.686 \pm 0.01$, 0.739 ± 0.01 and 0.713 ± 0.008 by semilog, Guggenheim and curve-fitting analyses, respectively.

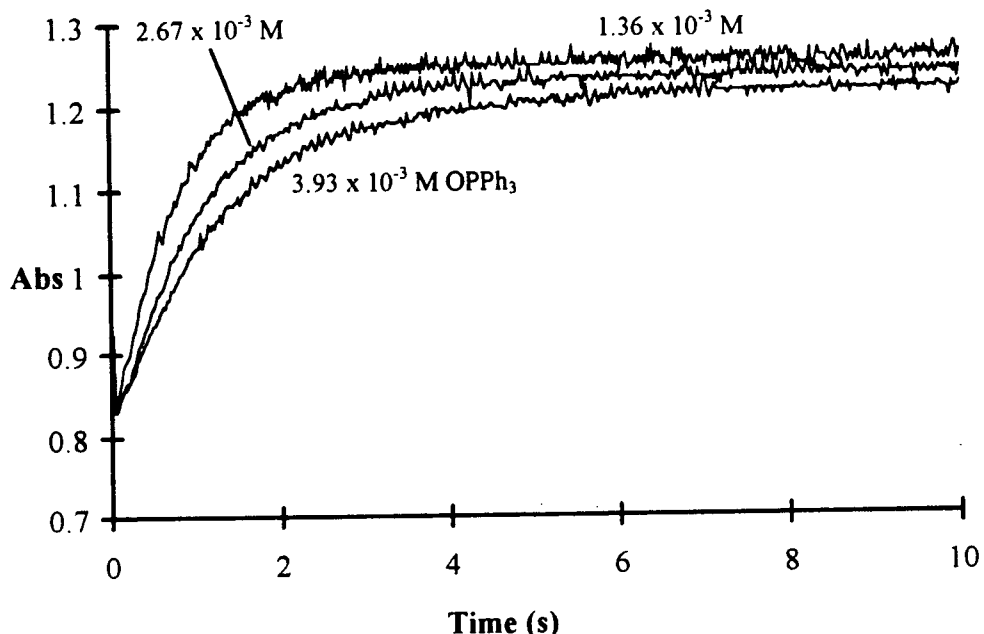


Figure A.5. Absorbance-time traces monitored at 412 nm by stopped-flow spectrophotometry for the accumulation of the product $\text{Ru}^{\text{II}}(\text{TMP})(\text{PPh}_3)$ (initial $[\text{Ru}^{\text{VI}}(\text{TMP})(\text{O})_2] = 4.2 \times 10^{-6}$ M in benzene). $[\text{PPh}_3] = 3.9 \times 10^{-3}$ M.

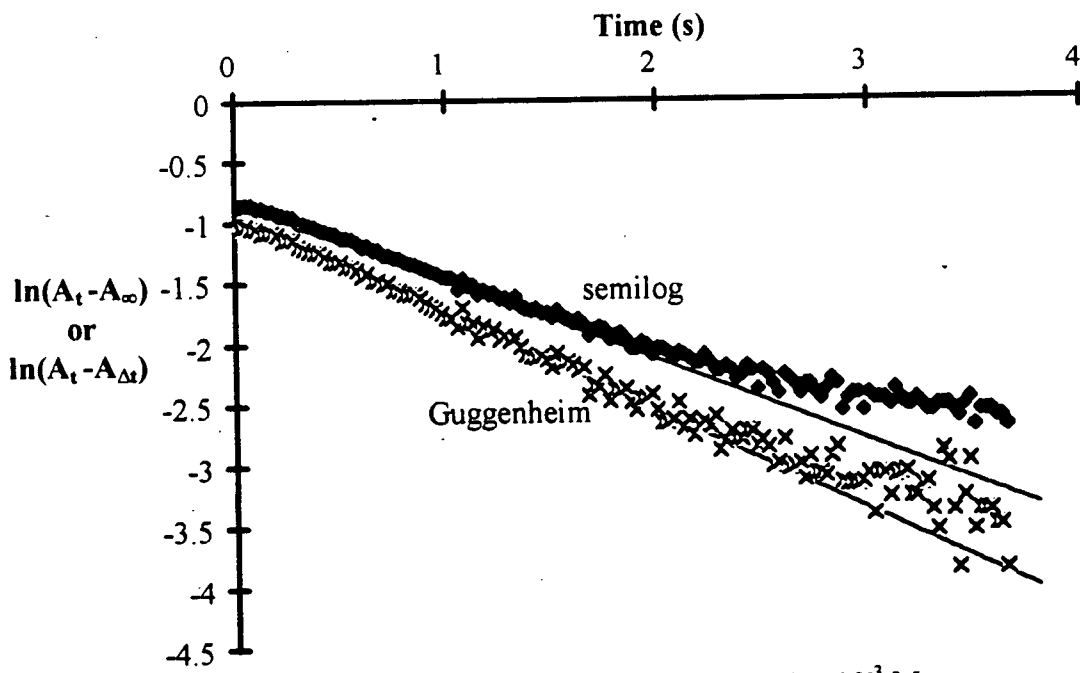


Figure A.6. Semilog and Guggenheim plots for $[\text{PPh}_3] = 3.83 \times 10^{-3}$ M, $[\text{OPPh}_3] = 3.93 \times 10^{-3}$ M trace in Figure A.5 above. A_t = absorbance at time t , A_∞ = final absorbance, and $\Delta t = 1.0$ s. Slope = $k'_{\text{obs}} = 0.693 \pm 0.011$, 0.809 ± 0.02 and 0.748 ± 0.009 by semilog, Guggenheim and curve-fitting analyses, respectively.

Table A.1.1. Pseudo-1st-order rate constants for the oxidation of PPh_3 by $\text{Ru}^{\text{V}}(\text{TMP})(\text{O})_2$ (1).

[1]	[PPh_3] (10^{-3} M)	[OPPh_3] (10^{-3} M)	k_{obs} (s^{-1}) ^a (O-atom transfer)	k'_{obs} (s^{-1}) ^b (Slower 2nd reaction)
10.1 °C				
	0.985	4.05	35.2 ± 0.2	0.101 ± 0.002 [0.0961]
	1.00	2.75	38.3 ± 0.3	0.186 ± 0.003 [0.183]
4.2×10^{-6} M	1.01	1.40	36.1 ± 0.2	0.274 ± 0.004 [0.274]
	1.04	-	37.2 ± 0.2	-
	1.95	4.01	69.7 ± 0.5	0.298 ± 0.005 [0.286]
	1.99	2.72	76.4 ± 0.5	0.389 ± 0.6 [0.352]
	2.03	1.39	74.7 ± 0.6	0.613 ± 0.009 [0.571]
	2.07	-	74.5 ± 0.6	-
	2.90	3.97	109 ± 1	0.374 ± 0.007
	2.95	2.70	116 ± 1	0.575 ± 0.009
	3.01	1.37	137 ± 1	0.712 ± 0.01
	3.07	-	137 ± 1	-
	3.83	3.93	153 ± 1.4	0.495 ± 0.008
	3.90	2.67	156 ± 1.5	0.662 ± 0.009
	3.97	1.36	158 ± 1.5	1.17 ± 0.03
	4.05	-	148 ± 1.4	-
20.0 °C				
1.59×10^{-6} M	0.0501	-	2.90 ± 0.02	-
	0.0501	1.43	2.83 ± 0.02	-
	0.119	-	6.23 ± 0.03	-
			6.35 ± 0.05	-
	0.169		9.35 ± 0.6	-
			10.44 ± 0.8	-
4.2×10^{-6} M	0.985	4.05	52.0 ± 0.4	0.142 ± 0.004
	1.00	2.75	-	0.242 ± 0.005
	1.01	1.40	-	0.340 ± 0.005
	1.04	-	-	-
	1.95	4.01	86 ± 0.7	0.320 ± 0.005
	1.99	2.72	-	0.438 ± 0.007
	2.03	1.39	-	0.752 ± 0.008
	2.07	-	103 ± 1	-
	2.90	3.97	-	0.493 ± 0.007
	2.95	2.70	-	0.685 ± 0.009
	3.01	1.37	180 ± 1.5	1.10 ± 0.02
	3.07	-	161 ± 1.2	-
	3.83	3.93	227 ± 2	0.713 ± 0.008
	3.90	2.67	229 ± 2	0.937 ± 0.009
	3.97	1.36	245 ± 2	1.27 ± 0.02
	4.05	-	227 ± 2	-

Table A.1.1 continued..

[(1)]	[PPh₃] (10 ⁻³ M)	[OPPb₃] (10 ⁻³ M)	k_{obs} (s⁻¹)^a (O-atom transfer)	k'_{obs} (s⁻¹)^b (Slower 2nd reaction)
30.7 °C 4.2 x 10 ⁻⁶ M	0.985	4.05	62.6 ± 0.5	0.179 ± 0.003
	1.00	2.75	80.5 ± 0.9	0.337 ± 0.005
	1.01	1.40	74.6 ± 0.7	0.475 ± 0.008
	1.04	-	71.9 ± 0.7	-
	1.95	4.01	143 ± 1	0.498 ± 0.006
	1.99	2.72	147 ± 1	0.642 ± 0.007
	2.03	1.39	144 ± 1	0.946 ± 0.01
	2.07	-	144 ± 1	-
	2.90	3.97	218 ± 2	0.808 ± 0.01
	2.95	2.70	223 ± 2	0.935 ± 0.02
	3.01	1.37	217 ± 2	1.33 ± 0.02
	3.07	-	207 ± 2	-
	3.83	3.93	274 ± 2	1.18 ± 0.03
	3.90	2.67	286 ± 3	1.31 ± 0.03
40.2 °C 4.2 x 10 ⁻⁶ M	3.97	1.36	273 ± 3	1.88 ± 0.04
	4.05	-	-	-
	0.985	4.05	94.7 ± 0.8	0.207 ± 0.006
	1.00	2.75	102 ± 1	0.367 ± 0.008
	1.01	1.40	98.0 ± 0.9	0.470 ± 0.008
	1.04	-	-	-
	1.95	4.01	182 ± 2	0.549 ± 0.009
	1.99	2.72	187 ± 2	0.682 ± 0.01
	2.03	1.39	181 ± 2	0.847 ± 0.01
	2.07	-	-	-
	2.90	3.97	268 ± 2	0.892 ± 0.02
	2.95	2.70	280 ± 3	1.04 ± 0.02
	3.01	1.37	275 ± 2	1.42 ± 0.03
	3.07	-	-	-
4.05	3.83	3.93	-	1.14 ± 0.02
	3.90	2.67	-	1.28 ± 0.02
	3.97	1.36	380 ± 4	1.67 ± 0.03
	4.05	-	-	-

^a Monitored at 422 nm for the loss of (1).^b Monitored at 430 nm for the loss of Ru^{IV}(TMP)(O)(OPPh₃). Values in [] were obtained at 412 nm for the appearance of the product Ru^{II}(TMP)(PPh₃).

Table A.1.2. Pseudo-1st-order rate constants for the oxidation of PPh_3 by $\text{Ru}^{\text{VI}}(\text{TMP})(\text{O})_2$ (1). Saturation kinetics study.

	$[\text{PPh}_3]^a$ (M)	$k'_{\text{obs}} (\text{s}^{-1})^b$ (Slower 2nd reaction)
11.2 °C	0.0184	14.97 ± 0.5
		15.13 ± 0.4
		15.13 ± 0.5
	0.0323	18.56 ± 0.4
		16.97 ± 0.4
		16.93 ± 0.3
	0.0462	17.64 ± 0.2
		16.58 ± 0.2
20.5 °C	0.0114	10.09 ± 0.4
	0.0323	15.42 ± 0.5
	0.0462	17.25 ± 0.6
		17.43 ± 0.7
30.1 °C	0.0184	15.21 ± 0.3
		16.94 ± 0.4
		16.97 ± 0.4
	0.0323	22.37 ± 0.3
		22.81 ± 0.4
		23.46 ± 0.4
	0.0462	27.4 ± 0.5
		28.79 ± 0.7
		28.79 ± 0.6
40.1 °C	0.0162	16.86 ± 0.6
		17.98 ± 0.4
		17.0 ± 0.5
	0.0323	32.32 ± 0.6
		29.77 ± 0.4
		31.9 ± 0.8
	0.0462	35.5 ± 0.6
		35.63 ± 0.8

^a $[\text{OPPh}_3] = 1.3 \times 10^{-5}$ M in all the runs. $[(1)] = 2 \times 10^{-6}$ M.

^b Monitored at 412 nm for the appearance of the product $\text{Ru}^{\text{II}}(\text{TMP})(\text{PPh}_3)$.

Table A.2. Pseudo-1st-order rate constants for the oxidation of $P(p\text{-MeO-C}_6\text{H}_4)_3$ (L) by $\text{Ru}^{\text{VI}}(\text{TMP})(\text{O})_2$ (1).

[1] (M)	[L] (10 ⁻⁴ M)	[OPPh ₃] (10 ⁻³ M)	k _{obs} (s ⁻¹) ^a (O-atom transfer)	k' _{obs} (s ⁻¹) ^b (Slower 2nd reaction)
10.1 °C	1.07	-	8.60 ± 0.07 8.62 ± 0.07 8.65 ± 0.07	-
2.5 × 10 ⁻⁶ M	2.12	-	16.8 ± 0.15 16.9 ± 0.15 16.9 ± 0.2	-
	4.21	-	33.7 ± 0.3 33.6 ± 0.4 33.2 ± 0.3	-
	8.25	-	67.8 ± 0.6 68.3 ± 0.6 66.8 ± 0.7	-
	1.16	2.90	-	0.0248 ± 0.0005
	1.18	1.48	-	0.0365 ± 0.0007
	2.30	2.89	-	0.0503 ± 0.001
	2.35	1.47	-	0.0770 ± 0.001
	3.44	2.88	-	0.0749 ± 0.002
	3.50	1.47	-	0.113 ± 0.003
20.4 °C	1.07	-	12.2 ± 0.1 12.7 ± 0.1 12.6 ± 0.1	-
	2.12	-	22.9 ± 0.2 22.8 ± 0.2 22.8 ± 0.2	-
	4.21	-	45.3 ± 0.4 45.4 ± 0.4 45.8 ± 0.4	-
	8.25	-	89.2 ± 0.9 89.0 ± 0.9 91.1 ± 1	-
	1.16	2.90	-	0.0391 ± 0.0008
	1.18	1.48	-	0.0625 ± 0.001
	2.30	2.89	-	0.0732 ± 0.002
	2.35	1.47	-	0.108 ± 0.003
	3.44	2.88	-	0.101 ± 0.003
	3.50	1.47	-	0.164 ± 0.005

Table A.2 continued...

[(1)]	[(L)] (10^{-4} M)	[OPPh₃] (10^{-3} M)	k_{obs} (s ⁻¹) ^a (O-atom transfer)	k'_{obs} (s ⁻¹) ^b (Slower 2nd reaction)
30.1 °C	1.07	-	17.3 ± 0.2	-
			17.0 ± 0.2	-
			17.4 ± 0.2	-
	2.5 × 10 ⁻⁶ M	-	30.3 ± 0.4	-
			30.4 ± 0.5	-
			31.0 ± 0.4	-
			45.3 ± 0.6	-
	4.21	-	45.4 ± 0.7	-
			45.8 ± 0.6	-
			89.2 ± 1	-
39.9 °C	8.25	-	89.0 ± 1	-
			91.1 ± 1	-
			-	0.0549 ± 0.0009
			-	0.0773 ± 0.001
			-	0.0988 ± 0.002
			-	0.140 ± 0.003
	3.44	2.88	-	0.142 ± 0.003
			-	0.202 ± 0.004
			-	-
			-	-
39.9 °C	1.07	-	23.3 ± 0.3	-
			21.9 ± 0.4	-
			21.7 ± 0.3	-
	2.12	-	38.8 ± 0.4	-
			40.3 ± 0.6	-
			38.5 ± 0.5	-
			78.7 ± 0.9	-
	4.21	-	78.8 ± 0.7	-
			78.5 ± 0.8	-
			160 ± 1.4	-
39.9 °C	8.25	-	160 ± 1.7	-
			159 ± 1.5	-
			-	-
	3.50	2.90	-	0.0728 ± 0.001
			-	0.0961 ± 0.001
			-	0.129 ± 0.002
			-	0.177 ± 0.003
			-	0.194 ± 0.004
			-	0.270 ± 0.006

^a Monitored at 422 nm for the loss of (**1**).^b Monitored at 430 nm for the loss of Ru^{IV}(TMP)(O)(OPPh₃).

Table A.3. Pseudo-1st-order rate constants for the oxidation of $\text{P}(p\text{-Me-C}_6\text{H}_4)_3$ (L) by $\text{Ru}^{\text{VI}}(\text{TMP})(\text{O})_2$ (1).

[1]	[L] (10^{-4} M)	[OPPh ₃] (10^{-3} M)	k_{obs} (s ⁻¹) ^a (O-atom transfer)	k'_{obs} (s ⁻¹) ^b (Slower 2nd reaction)
10.1 °C	2.05	-	8.25 ± 0.09 8.52 ± 0.1 8.22 ± 0.08	-
2.5 x 10 ⁻⁶ M	4.08	-	17.1 ± 0.2 17.2 ± 0.2 17.2 ± 0.2	-
	8.08	-	35.3 ± 0.3 35.3 ± 0.3 34.1 ± 0.4	-
	12.0	-	53.8 ± 0.6 53.0 ± 0.5 53.0 ± 0.6	-
10.3 °C	1.02	4.89	-	0.00906 ± 0.0001
	1.04	2.49	-	0.0154 ± 0.0003
	1.52	4.88	-	0.0133 ± 0.0002
	1.55	2.49	-	0.0245 ± 0.0003
	2.53	4.86	-	0.0250 ± 0.0004
	2.58	2.48	-	0.0404 ± 0.0006
20.4 °C	2.05	-	12.3 ± 0.1 12.2 ± 0.1 12.2 ± 0.14	-
	4.08	-	24.2 ± 0.3 24.1 ± 0.3 24.6 ± 0.2	-
	8.08	-	47.7 ± 0.5 49.7 ± 0.5 48.1 ± 0.4	-
	12.0	-	71.7 ± 0.9 72.4 ± 0.7 70.7 ± 0.9	-
	1.02	4.89	-	0.0152 ± 0.0002
	1.04	2.49	-	0.0249 ± 0.0004
	1.52	4.88	-	0.0202 ± 0.0003
	1.55	2.49	-	0.0343 ± 0.0005
	2.53	4.86	-	0.0339 ± 0.0005
	2.58	2.48	-	0.0631 ± 0.0008

Table A.3 continued...

[(1)]	[(L)] (10^{-4} M)	[OPPh₃] (10^{-3} M)	k_{obs} (s ⁻¹) (O-atom transfer)	k'_{obs} (s ⁻¹) (Slower 2nd reaction)
30.1 °C	2.5 × 10 ⁻⁶ M	2.05	-	16.2 ± 0.2 16.3 ± 0.2 16.4 ± 0.16
		4.08	-	32.2 ± 0.5 31.8 ± 0.4
		8.08	-	32.0 ± 0.5 66.2 ± 0.8 65.1 ± 0.9
		12.0	-	66.0 ± 0.8 93.2 ± 1 95.7 ± 1
	30.0 °C		99.8 ± 1	-
		1.02	4.89	-
		1.04	2.49	-
		1.52	4.88	-
		1.55	2.49	-
		2.53	4.86	-
39.9 °C	2.5 × 10 ⁻⁶ M	2.05	-	0.0185 ± 0.0003
		4.08	-	0.0322 ± 0.0005
		8.08	-	0.0254 ± 0.0004
		12.0	-	0.0433 ± 0.0007
		1.04	2.49	0.0447 ± 0.0005
		1.55	2.49	0.0718 ± 0.0009
		2.58	2.48	-
	30.0 °C	2.05	-	21.4 ± 0.3
		4.08	-	22.1 ± 0.3 21.6 ± 0.35
		8.08	-	38.3 ± 0.5 37.3 ± 0.45
		12.0	-	39.3 ± 0.5 81.9 ± 0.8
		1.04	2.49	81.7 ± 0.9
		1.55	2.49	81.0 ± 1
		2.58	2.48	130 ± 1.5
		1.02	4.89	129 ± 1.7
		1.52	4.88	126 ± 2
		2.53	4.86	-
	39.9 °C			0.0384 ± 0.0004
				0.0510 ± 0.0006
				0.0862 ± 0.0009
				0.0228 ± 0.0003
				0.0300 ± 0.0004
				0.0547 ± 0.0007

^a Monitored at 422 nm for the loss of (1).^b Monitored at 430 nm for the loss of Ru^{IV}(TMP)(O)(OPPh₃).

Table A.4. Pseudo-1st-order rate constants for the oxidation of $P(p\text{-F-C}_6\text{H}_4)_3$ (**L**) by $\text{Ru}^{\text{VI}}(\text{TMP})(\text{O})_2$ (**1**).

[1]	[L] (10^{-4} M)	[OPPh ₃] (10^{-3} M)	k_{obs} (s ⁻¹) (O-atom transfer)	k'_{obs} (s ⁻¹) (Slower 2nd reaction)
9.9 °C 1.7×10^{-6} M	0.609	-	4.84 ± 0.03	-
	1.21	-	10.6 ± 0.07	-
	2.40	-	18.5 ± 0.1	-
	4.71	-	36.2 ± 0.2	-
10.3 °C	1.57	2.72	-	0.0396 ± 0.0004
	1.60	1.38	-	0.0808 ± 0.002
	2.34	2.70	-	0.0592 ± 0.0006
	2.39	1.38	-	0.100 ± 0.001
	3.11	2.69	-	0.0783 ± 0.0007
	3.17	1.37	-	0.143 ± 0.001
20.4 °C	0.609	-	6.96 ± 0.05	-
	1.21	-	13.3 ± 0.1	-
	2.40	-	26.0 ± 0.2	-
	4.71	-	49.8 ± 0.4	-
	1.57	2.72	-	0.0596 ± 0.0006
	1.60	1.38	-	0.104 ± 0.001
	2.34	2.70	-	0.0873 ± 0.0007
	2.39	1.38	-	0.141 ± 0.002
	3.11	2.69	-	0.124 ± 0.001
	3.17	1.37	-	0.187 ± 0.002
	0.609	-	9.26 ± 0.08	-
	1.21	-	17.6 ± 0.1	-
30.1 °C	2.40	-	33.3 ± 0.2	-
	4.71	-	65.0 ± 0.5	-
	1.57	2.72	-	0.0788 ± 0.0008
	1.60	1.38	-	0.134 ± 0.001
	2.34	2.70	-	0.128 ± 0.001
	2.39	1.38	-	0.185 ± 0.002
	3.11	2.69	-	0.152 ± 0.001
	3.17	1.37	-	0.243 ± 0.002
	0.609	-	12.3 ± 0.09	-
	1.21	-	23.3 ± 0.2	-
	2.40	-	44.0 ± 0.4	-
	4.71	-	81.4 ± 0.7	-
39.9 °C	1.57	2.72	-	0.0914 ± 0.0008
	1.60	1.38	-	0.145 ± 0.001
	2.34	2.70	-	0.135 ± 0.001
	2.39	1.38	-	0.203 ± 0.002
	3.11	2.69	-	0.173 ± 0.002
	3.17	1.37	-	0.272 ± 0.003

^a Monitored at 422 nm for the loss of (**1**).

^b Monitored at 430 nm for the loss of $\text{Ru}^{\text{IV}}(\text{TMP})(\text{O})(\text{OPPh}_3)$.

Table A.5. Pseudo-1st-order rate constants for the oxidation of $P(p\text{-Cl-C}_6\text{H}_4)_3$ (L) by $\text{Ru}^{\text{VI}}(\text{TMP})(\text{O})_2$ (1).

[1]	[L] (10^{-4} M)	[OPPh ₃] (10^{-3} M)	k_{obs} (s ⁻¹) ^a (O-atom transfer)	k'_{obs} (s ⁻¹) ^b (Slower 2nd reaction)
9.8 °C	1.00	-	9.72 ± 0.05	-
			9.90 ± 0.04	-
			9.44 ± 0.05	-
2.5 x 10 ⁻⁶ M	1.98	-	17.8 ± 0.1	-
			18.0 ± 0.1	-
			17.9 ± 0.1	-
	2.94	-	27.0 ± 0.2	-
			26.9 ± 0.2	-
			27.1 ± 0.2	-
10.3 °C	4.81	-	44.2 ± 0.3	-
			43.4 ± 0.4	-
			43.0 ± 0.4	-
			-	0.0277 ± 0.0003
20.2 °C	1.25	3.59	-	0.0457 ± 0.0005
			-	0.0427 ± 0.0005
			-	0.0625 ± 0.0007
	1.98	1.83	-	0.0492 ± 0.0006
			-	0.0998 ± 0.001
			-	-
20.3 °C	2.94	-	15.8 ± 0.1	-
			14.8 ± 0.1	-
			15.0 ± 0.1	-
	4.81	-	26.1 ± 0.2	-
			26.0 ± 0.3	-
			24.8 ± 0.2	-
20.3 °C	1.25	3.59	36.5 ± 0.4	-
			37.1 ± 0.3	-
			37.4 ± 0.4	-
	1.98	1.83	61.5 ± 0.5	-
			61.5 ± 0.6	-
			60.0 ± 0.6	-
20.3 °C	2.94	-	-	0.0429 ± 0.0005
			-	0.0680 ± 0.0008
			-	0.0542 ± 0.0006
	4.81	-	-	0.0899 ± 0.001
			-	0.0770 ± 0.0009
			-	0.121 ± 0.002

Table A.5 continued..

[(1)]	[(L)] (10^{-4} M)	[OPPh₃] (10^{-3} M)	k_{obs} (s ⁻¹) ^a (O-atom transfer)	k'_{obs} (s ⁻¹) ^b (Slower 2nd reaction)
30.4 °C	1.00	-	18.2 ± 0.1	
			18.3 ± 0.2	
			17.9 ± 0.2	
	1.98	-	34.4 ± 0.3	
			34.4 ± 0.4	
			34.0 ± 0.4	
	2.94	-	50.5 ± 0.6	
			49.2 ± 0.5	
			48.1 ± 0.5	
	4.81	-	79.4 ± 0.7	
			82.5 ± 0.8	
			78.4 ± 0.8	
30.0 °C	1.25	3.59	-	0.0562 ± 0.0007
	1.27	1.83	-	0.0888 ± 0.001
	1.86	3.57	-	0.0812 ± 0.0009
	1.90	1.82	-	0.115 ± 0.001
	2.47	3.55	-	0.107 ± 0.001
	2.52	1.81	-	0.172 ± 0.002
39.9°C	1.00	-	23.9 ± 0.3	
			24.5 ± 0.2	
			24.7 ± 0.2	
	1.98	-	43.8 ± 0.4	
			43.3 ± 0.5	
			43.3 ± 0.4	
	2.94	-	66.8 ± 0.6	
			68.6 ± 0.6	
			64.3 ± 0.7	
	4.81	-	105 ± 1	
			106 ± 1	
			106 ± 1	
40.0 °C	1.25	3.59	-	0.0715 ± 0.001
	1.27	1.83	-	0.112 ± 0.002
	1.86	3.57	-	0.109 ± 0.002
	1.90	1.82	-	0.147 ± 0.003
	2.47	3.55	-	0.137 ± 0.002
	2.52	1.81	-	0.186 ± 0.003

^a Monitored at 422 nm for the loss of (1).^b Monitored at 430 nm for the loss of Ru^{IV}(TMP)(O)(OPPh₃).

Table A.6. Pseudo-1st-order rate constants for the oxidation of $P(p\text{-CF}_3\text{-C}_6\text{H}_4)_3$ (**L**) by $\text{Ru}^{\text{V}}(\text{TMP})(\text{O})_2$ (**1**).

[1]	[L] (10^{-4} M)	[OPPh ₃] (10^{-3} M)	k_{obs} (s ⁻¹) (O-atom transfer)	k'_{obs} (s ⁻¹) ^b (Slower 2nd reaction)
10.1 °C 4.4×10^{-6} M	1.33	4.11	9.05 ± 0.04	0.0194 ± 0.0003
	1.35	2.10	9.24 ± 0.04	0.0299 ± 0.0005
	1.98	4.10	12.6 ± 0.05	0.0354 ± 0.0004
	2.02	2.09	13.5 ± 0.06	0.0513 ± 0.0006
	2.63	4.07	17.7 ± 0.1	0.0464 ± 0.0005
	2.68	2.08	16.6 ± 0.1	0.0670 ± 0.0009
20.3 °C	1.33	4.11	12.9 ± 0.1	0.0310 ± 0.0005
	1.35	2.10	13.4 ± 0.1	0.0501 ± 0.0006
	1.98	4.10	19.4 ± 0.1	0.0512 ± 0.0007
	2.02	2.09	17.2 ± 0.1	0.0707 ± 0.0007
	2.63	4.07	25.1 ± 0.2	0.0675 ± 0.0008
	2.68	2.08	24.8 ± 0.2	0.119 ± 0.001
30.0 °C	1.33	4.11	17.1 ± 0.1	0.0543 ± 0.0006
	1.35	2.10	17.6 ± 0.1	0.0732 ± 0.0007
	1.98	4.10	27.0 ± 0.3	0.0795 ± 0.0009
	2.02	2.09	25.8 ± 0.2	0.102 ± 0.001
	2.63	4.07	34.6 ± 0.3	0.105 ± 0.001
	2.68	2.08	34.3 ± 0.4	0.140 ± 0.0016
39.9 °C	1.33	4.11	23.9 ± 0.2	0.0764 ± 0.001
	1.35	2.10	24.0 ± 0.2	0.0997 ± 0.001
	1.98	4.10	34.4 ± 0.3	0.114 ± 0.001
	2.02	2.09	33.8 ± 0.4	0.148 ± 0.0013
	2.63	4.07	44.0 ± 0.4	0.150 ± 0.0017
	2.68	2.08	42.9 ± 0.3	0.191 ± 0.002

^a Monitored at 422 nm for the loss of (**1**).

^b Monitored at 430 nm for the loss of $\text{Ru}^{\text{IV}}(\text{TMP})(\text{O})(\text{OPPh}_3)$.

Table A.7. Pseudo-1st-order rate constants for the oxidation of $[P(2\text{-pyridyl})_3](PPh_3)(Cl)_2Ru(L)$ by $Ru^{VI}(TMP)(O)_2(1)$.

[1)]	[L)] (10^{-5} M)	k_{obs} (s^{-1}) ^a	
		(O-atom transfer)	
10.4 °C 1.5×10^{-6} M	2.19	0.205 ± 0.005	0.248 ± 0.006
	4.38	0.513 ± 0.01	0.508 ± 0.009
	6.58	0.664 ± 0.01	0.665 ± 0.01
	8.77	0.886 ± 0.012	0.925 ± 0.014
	11.0	1.04 ± 0.02	1.05 ± 0.016
20.3 °C	2.19	0.383 ± 0.008	0.403 ± 0.009
	4.38	0.677 ± 0.01	0.687 ± 0.01
	6.58	0.982 ± 0.02	0.984 ± 0.02
	8.77	1.27 ± 0.02	1.26 ± 0.02
	11.0	1.55 ± 0.03	1.52 ± 0.03
30.0 °C	2.19	0.571 ± 0.01	0.576 ± 0.009
	4.38	0.960 ± 0.013	0.940 ± 0.01
	6.58	1.35 ± 0.02	1.31 ± 0.03
	8.77	1.77 ± 0.04	2.02 ± 0.04
	11.0	2.31 ± 0.05	2.19 ± 0.04
39.9 °C	2.19	0.828 ± 0.01	0.826 ± 0.01
	4.38	1.36 ± 0.02	1.39 ± 0.03
	6.58	1.96 ± 0.04	2.03 ± 0.04
	8.77	2.62 ± 0.05	2.66 ± 0.05
	11.0	3.22 ± 0.06	3.28 ± 0.08

^a Monitored at 422 nm for the loss of (1).

Table A.8. Pseudo-1st-order rate constants for the oxidation of AsPh₃ and SbPh₃, (L), by Ru^{VI}(TMP)(O)₂ (1).

[1)]	[AsPh ₃] (10 ⁻³ M)	k _{obs} (s ⁻¹) ^a (O-atom transfer)
9.9 °C 2.3 x 10 ⁻⁶ M	1.48	0.928 ± 0.008
	2.91	1.75 ± 0.01
	4.36	2.68 ± 0.01
	5.61	3.29 ± 0.016
19.8 °C	1.48	1.30 ± 0.01
	2.91	2.60 ± 0.01
	4.36	4.10 ± 0.022
	5.61	5.32 ± 0.03
	75.0	69.0 ± 0.4
30.1 °C	1.48	2.21 ± 0.01
	2.91	4.07 ± 0.02
	4.36	6.55 ± 0.05
	5.61	8.19 ± 0.04
39.9 °C	1.48	3.06 ± 0.02
	2.91	6.02 ± 0.07
	4.36	9.06 ± 0.06
	5.61	12.1 ± 0.1
		1.06 ± 0.01
		1.78 ± 0.006
		2.69 ± 0.014
		3.49 ± 0.02
		-
		2.75 ± 0.017
		4.10 ± 0.015
		5.43 ± 0.03
		66.4 ± 0.5
		-
		2.21 ± 0.02
		4.06 ± 0.02
		6.13 ± 0.04
		8.26 ± 0.03
		2.33 ± 0.01
		4.35 ± 0.03
		6.47 ± 0.03
		8.54 ± 0.06
		-
		3.20 ± 0.02
		6.21 ± 0.03
		9.08 ± 0.08
		2.99 ± 0.02
		6.24 ± 0.04
		9.54 ± 0.09
		11.9 ± 0.1
[1)]	[SbPh ₃] (10 ⁻⁴ M)	k _{obs} (s ⁻¹) ^b (O-atom transfer)
9.7 °C 3.0 x 10 ⁻⁶ M	1.14	423 ± 10
	2.19	647 ± 30
	3.17	820 ± 40
	4.08	1216 ± 100
14.5 °C	1.14	445 ± 30
	2.19	673 ± 50
	3.17	872 ± 70
	4.08	1300 ± 120
20.3 °C	1.14	464 ± 40
	2.19	700 ± 60
	3.17	933 ± 85
	4.08	1410 ± 130
25.4 °C	1.14	-
	2.19	713 ± 60
	3.17	1080 ± 100
	4.08	1570 ± 150

^a Monitored at 422 nm for the loss of (1).

^b Monitored at 430 nm for the appearance of Ru^{IV}(TMP)(O)(OSbPh₃).

Appendix B. Mathematical Derivation for the Equation Reflecting the Observed 1st-Order Absorbance-Time Changes in the Oxidation of PPh_3 by $\text{Ru}^{\text{VI}}(\text{TMP})(\text{O})_2$

B.1 O-atom Transfer (Faster Kinetic Phase)

The O-atom transfer is a simple (1) $\xrightarrow{k_{\text{obs}}}$ (2) reaction. If the reaction follows first-order kinetic behaviour, the absorbance contributions due to (1) and (2) are the following: $a = a_0 \exp(-k_{\text{obs}}t)$; $b = b_\infty - b_\infty \exp(-k_{\text{obs}}t)$, where a_0 = initial absorbance of (1), b_∞ = final absorbance due to complete formation of (2), k_{obs} = pseudo-1st-order rate constant and t = time. Thus the absorbance observed at any time, t , is $\text{Abs} = a + b = (a_0 - b_\infty) \exp(-k_{\text{obs}}t) + b_\infty$. A semilog plot of $\ln(\text{Abs} - b_\infty)$ versus t should give a straight line with slope $= -k_{\text{obs}}$ in the case where $a_0 > b_\infty$. When $a_0 < b_\infty$ the absorbances are rising, and $\ln |\text{Abs} - b_\infty|$ should be used instead.

B.2. Dissociation of OL Followed by Disproportionation (Slower Kinetic Phase)

The following mechanism was proposed in Chapter 3.



Only (2) and (5) were observed in $^1\text{H-NMR}$ studies during this stage of the reaction [(1) has been completely consumed in the faster O-atom transfer reaction]. The observed rate expression is represented by Eq. B.5.

$$\frac{d[(2)]}{dt} = k_2[(2)] - k_2[\text{OL}][(3)] - k_1[\text{L}][(1)] = \frac{d[(5)]}{dt} = k_4[\text{L}][(4)] \quad (\text{B.5})$$

$[(1)] = [(4)] = K_3^{1/2}[(3)]$, as the only source of (1) is via the disproportionation reaction, Eq. B.2. Upon substitution of (1) and (4) by $K_3^{1/2}[(3)]$ into Eq. B.5, we obtain Eqs. B.6, B.7 and B.8.

$$k_2[(2)] - k_2[\text{OL}][(3)] - k_1K_3^{1/2}[\text{L}][(3)] - k_4K_3^{1/2}[\text{L}][(3)] = 0 \quad (\text{B.6})$$

$$[(3)] = \frac{k_2}{k_2[\text{OL}] + k_1K_3^{1/2}[\text{L}] + k_4K_3^{1/2}[\text{L}]} [(2)] \quad (\text{B.7})$$

$$[(1)] = \frac{k_2K_3^{1/2}}{k_2[\text{OL}] + k_1K_3^{1/2}[\text{L}] + k_4K_3^{1/2}[\text{L}]} [(2)] \quad (\text{B.8})$$

Thus, the rate expression (Eq. B.5) becomes Eq. B.9.

$$\begin{aligned} \frac{d[(2)]}{dt} &= -k_2[(2)] + \frac{k_2k_2[\text{OL}]}{k_2[\text{OL}] + k_1K_3^{1/2}[\text{L}] + k_4K_3^{1/2}[\text{L}]} [(2)] + \\ &\quad \frac{k_1k_2K_3^{1/2}[\text{L}]}{k_2[\text{OL}] + k_1K_3^{1/2}[\text{L}] + k_4K_3^{1/2}[\text{L}]} [(2)] = -k'_{\text{obs}}[(2)], \text{ where} \end{aligned} \quad (\text{B.9})$$

$k'_{\text{obs}} = \frac{k_2k_4K_3^{1/2}[\text{L}]}{k_2[\text{OL}] + (k_1+k_4)K_3^{1/2}[\text{L}]}$ in the presence of excess [L] and [OL]. As only (2) and (5) are present in any significant quantities, the relationship between the observed rate and absorbance changes follows the same derivation as in the previous section.

Appendix C. Oxidation of Alcohols and Alkanes by Ru^{VI}(TMP)(O)₂

C.1 Kinetic Data for the Stoichiometric Oxidation of Alcohols under 1 atm Ar.

Table C.1.1. [PrOH] = 0.0435 M in benzene-*d*₆. [Ru^{VI}(TMP)(O)₂] = 4.0 × 10⁻⁴ M.
Temperature = 18.2 °C.

Time (s)	Integration of <i>p</i> - and <i>o</i> -Me groups of Ru ^{IV} (TMP)(O'Pr) ₂ (Arbitrary Units)	Integration of <i>p</i> -Me of Ru ^{VI} (TMP)(O) ₂ (Arbitrary Units)
0	0	100
2115	82.2	208.2
3825	80.8	138.0
5395	49.9	60.7
8955	55.0	57.1
11130	91.2	88.4
14280	90.0	64.7
18075	126.8	73.5
21315	120.6	47.6
25350	135.4	46.8
28360	73.2	23.4

$$k_{\text{obs}} = 2.0 \times 10^{-5} \text{ s}^{-1}$$

Table C.1.2. [PrOH] = 0.0568 M in benzene-*d*₆. [Ru^{VI}(TMP)(O)₂] = 4.0 × 10⁻⁴ M.
Temperature = 18.2 °C.

Time (s)	Integration of <i>p</i> - and <i>o</i> -Me groups of Ru ^{IV} (TMP)(O'Pr) ₂ (Arbitrary Units)	Integration of <i>p</i> -Me of Ru ^{VI} (TMP)(O) ₂ (Arbitrary Units)
0	0	100
1340	12.9	109.8
3600	14.2	79.76
4620	23.9	76.0
8380	30.4	54.56
11785	46.2	62.7
14700	50.4	56.3
17575	44.3	35.6
68610	200	17

$$k_{\text{obs}} = 1.9 \times 10^{-5} \text{ s}^{-1}$$

Table C.1.3. [ⁱPrOH] = 0.131 M in benzene-*d*₆. [Ru^{VI}(TMP)(O)₂] = 4.0 × 10⁻⁴ M.
Temperature = 18.2 °C.

Time (s)	Integration of <i>p</i> - and <i>o</i> -Me groups of Ru ^{IV} (TMP)(O ⁱ Pr) ₂ (Arbitrary Units)	Integration of <i>p</i> -Me of Ru ^{VI} (TMP)(O) ₂ (Arbitrary Units)
0	0	100
1805	65.1	163.4
3560	93.6	200.4
5025	67.4	87.3
8640	91.6	64.6
10860	130.9	96.5
13980	107.2	58.2
17925	131.1	58.6
21120	128.4	41.1
25110	136.9	40.2
$k_{obs} = 4.2 \times 10^{-5} \text{ s}^{-1}$		

Table C.1.4. [ⁱPrOH] = 0.174 M in benzene-*d*₆. [Ru^{VI}(TMP)(O)₂] = 3.8 × 10⁻⁴ M.
Temperature = 18.2 °C.

Time (s)	Integration of <i>p</i> - and <i>o</i> -Me groups of Ru ^{IV} (TMP)(O ⁱ Pr) ₂ (Arbitrary Units)	Integration of <i>p</i> -Me of Ru ^{VI} (TMP)(O) ₂ (Arbitrary Units)
0	0	10
930	3.9	7.95
1795	6.0	9.0
$k_{obs} = 8.0 \times 10^{-5} \text{ s}^{-1}$		

Table C.1.5. [ⁱPrOH] = 0.435 M in benzene-*d*₆. [Ru^{VI}(TMP)(O)₂] = 3.8 × 10⁻⁴ M.
Temperature = 18.2 °C.

Time (s)	Integration of <i>p</i> - and <i>o</i> -Me groups of Ru ^{IV} (TMP)(O ⁱ Pr) ₂ (Arbitrary Units)	Integration of <i>p</i> -Me of Ru ^{VI} (TMP)(O) ₂ (Arbitrary Units)
0	0	10
540	2.45	5.2
1200	3.1	5.1
2340	7.0	6.3
3540	7.7	4.55
$k_{obs} = 1.2 \times 10^{-4} \text{ s}^{-1}$		

Table C.1.6. [*i*PrOH] = 0.435 M in benzene-*d*₆. [Ru^{VII}(TMP)(O)₂] = 5.2 × 10⁻⁴ M.
Temperature = 18.2 °C.

Time (s)	Integration of <i>para</i> and <i>ortho</i> -Me's of Ru ^{IV} (TMP)(O <i>i</i> Pr) ₂ (Arbitrary Units)	Integration of <i>para</i> -Me of Ru ^{VII} (TMP)(O) ₂ (Arbitrary Units)
0	0	10
600	3.6	6.15
1260	5.1	5.9
2280	7.4	6.5
3240	8.2	6.3
5280	51	36
$k_{obs} = 1.2 \times 10^{-4} \text{ s}^{-1}$		

Table C.1.7. [*i*PrOH] = 0.871 M in benzene-*d*₆. [Ru^{VII}(TMP)(O)₂] = 5.2 × 10⁻⁴ M.
Temperature = 18.2 °C.

Time (s)	Integration of <i>p</i> - and <i>o</i> -Me groups of Ru ^{IV} (TMP)(O <i>i</i> Pr) ₂ (Arbitrary Units)	Integration of <i>p</i> -Me of Ru ^{VII} (TMP)(O) ₂ (Arbitrary Units)
0	0	10
900	1.35	5.15
1800	1.3	5.25
2700	4.72	2.25
3600	3.2	6.3
4500	5.15	5.6
$k_{obs} = 1.37 \times 10^{-4} \text{ s}^{-1}$		

Table C.1.8. [*i*PrOH] = 0.161 M in benzene-*d*₆. [Ru^{VII}(TMP)(O)₂] = 4.0 × 10⁻⁴ M.
Temperature = 28.5 °C.

Time (s)	Integration of <i>p</i> - and <i>o</i> -Me groups of Ru ^{IV} (TMP)(O <i>i</i> Pr) ₂ (Arbitrary Units)	Integration of <i>p</i> -Me of Ru ^{VII} (TMP)(O) ₂ (Arbitrary Units)
0	0	10
540	4.1	8.1
1155	4.1	6.0
1750	7.1	7.0
2910	7.7	6.1
4230	11.0	7.0
$k_{obs} = 1.20 \times 10^{-4} \text{ s}^{-1}$		

Table C.1.9. [ⁱPrOH] = 0.174 M in benzene-*d*₆. [Ru^{VI}(TMP)(O)₂] = 4.0 × 10⁻⁴ M.
Temperature = 35.5 °C.

Time (s)	Integration of <i>p</i> - and <i>o</i> -Me groups of Ru ^{IV} (TMP)(O <i>i</i> Pr) ₂ (Arbitrary Units)	Integration of <i>p</i> -Me of Ru ^{VI} (TMP)(O) ₂ (Arbitrary Units)
0	0	10
850	1.75	4.2
1320	3.8	4.3
1920	4.3	5.0
3440	5.3	5.0
4320	5.4	3.8
$k_{obs} = 1.82 \times 10^{-4} \text{ s}^{-1}$		

Table C.1.10. [ⁱPrOH] = 0.218 M in benzene-*d*₆. [Ru^{VI}(TMP)(O)₂] = 4.0 × 10⁻⁴ M.
Temperature = 18.2 °C.

Time (s)	Mole Fraction of Ru ^{VI} (TMP)(O) ₂ ^a
0	1
750	0.912
2485	0.832
4285	0.698
$k_{obs} = 8.0 \times 10^{-5} \text{ s}^{-1}$	

^a The data presented are now tabulated as mole fractions of Ru^{VI}(TMP)(O)₂,

$X = \text{Integration}_{p\text{-Me(Ru(VI))}} / [\text{Integration}_{p\text{-Me(Ru(VI))}} + \frac{1}{3} \text{ Integration}_{p,o\text{-Me(Ru(IV))}}]$. The data from Table C.1.1 - 1.9 were converted to mole fractions to derive k_{obs} (see Chapter 4).

Table C.1.11. [ⁱPrOH] = 0.218 M in benzene-*d*₆. [Ru^{VI}(TMP)(O)₂] = 2.0 × 10⁻⁴ M.
Temperature = 18.2 °C.

Time (s)	Mole Fraction of Ru ^{VI} (TMP)(O) ₂
0	1
1040	0.922
2660	0.846
4200	0.80
$k_{obs} = 7.8 \times 10^{-5} \text{ s}^{-1}$	

Table C.1.12. [¹PrOH] = 0.218 M in benzene-*d*₆. [Ru^{VI}(TMP)(O)₂] = 4.0 × 10⁻⁴ M.
Temperature = 18.2 °C.

Time (s)	Mole Fraction of Ru ^{VI} (TMP)(O) ₂
0	1
4665	0.584
6005	0.586
7555	0.495
	k _{obs} = 9.2 × 10 ⁻⁵ s ⁻¹

Table C.1.13. [¹PrOD-*d*₈] = 1.74 M in benzene-*d*₆. [Ru^{VI}(TMP)(O)₂] = 4.0 × 10⁻⁴ M.
Temperature = 18.0 °C.

Time (s)	Mole Fraction of Ru ^{VI} (TMP)(O) ₂
0	1
780	0.89
1680	0.806
2580	0.7865
3480	0.77
4380	0.741
	k _{obs} = 1.3 × 10 ⁻⁴ s ⁻¹

Table C.1.14. [¹PrOD-*d*₈] = 0.327 M in benzene-*d*₆. [Ru^{VI}(TMP)(O)₂] = 4.0 × 10⁻⁴ M.
Temperature = 18.0 °C.

Time (s)	Mole Fraction of Ru ^{VI} (TMP)(O) ₂
0	1
720	0.87
1320	0.865
2280	0.84
2940	0.81
4800	0.763
	k _{obs} = 6.66 × 10 ⁻⁵ s ⁻¹

Table C.1.15. [$^3\text{PrOD}-d_8$] = 0.131 M in benzene- d_6 . [$\text{Ru}^{VI}(\text{TMP})(\text{O})_2$] = 4.0×10^{-4} M. Temperature = 18.0 °C.

Time (s)	Mole Fraction of $\text{Ru}^{VI}(\text{TMP})(\text{O})_2$
0	1
600	0.935
1200	0.922
1800	0.933
3000	0.911
4920	0.878
	$k_{obs} = 3.1 \times 10^{-5} \text{ s}^{-1}$

Table C.1.16. [$^3\text{PrOH}$] = 0.0408 M in benzene- d_6 . [KOH] = 4×10^{-6} M. [$\text{Ru}^{VI}(\text{TMP})(\text{O})_2$] = 4.0×10^{-4} M. Temperature = 18.2 °C.

Time (s)	Mole Fraction of $\text{Ru}^{VI}(\text{TMP})(\text{O})_2$
0	1
600	0.818
1530	0.813
2550	0.733
4530	0.614
8250	0.56
	$k_{obs} = 9.0 \times 10^{-5} \text{ s}^{-1}$

Table C.1.17. [$^3\text{PrOH}$] = 0.0408 M in benzene- d_6 . [KOH] = 2×10^{-5} M. [$\text{Ru}^{VI}(\text{TMP})(\text{O})_2$] = 4.0×10^{-4} M. Temperature = 18.2 °C.

Time (s)	Mole Fraction of $\text{Ru}^{VI}(\text{TMP})(\text{O})_2$
0	1
210	0.889
810	0.793
2910	0.699
3510	0.700
4410	0.594
	$k_{obs} = 1.2 \times 10^{-4} \text{ s}^{-1}$

Table C.1.18. [$^{t}\text{PrOH}$] = 0.0816 M in benzene- d_6 . [KOH] = 4×10^{-6} M.
 $[\text{Ru}^{\text{VI}}(\text{TMP})(\text{O})_2]$ = 4.0×10^{-4} M. Temperature = 18.2 °C.

Time (s)	Mole Fraction of $\text{Ru}^{\text{VI}}(\text{TMP})(\text{O})_2$
0	1
900	0.90
2820	0.75
6600	0.60
	$k_{\text{obs}} = 1.1 \times 10^{-4} \text{ s}^{-1}$

Table C.1.19. [$^{t}\text{PrOH}$] = 0.130 M in benzene- d_6 . [KO'Bu] = 1.2×10^{-4} M.
 $[\text{Ru}^{\text{VI}}(\text{TMP})(\text{O})_2]$ = 2.0×10^{-4} M. Temperature = 18.2 °C.

Time (s)	Mole Fraction of $\text{Ru}^{\text{VI}}(\text{TMP})(\text{O})_2$
0	1
150	0.90
450	0.75
750	0.68
	$k_{\text{obs}} = 5.4 \times 10^{-4} \text{ s}^{-1}$

Table C.1.20. [$^{t}\text{PrOH}$] = 0.130 M in benzene- d_6 . [KO'Bu] = 1.6×10^{-3} M.
 $[\text{Ru}^{\text{VI}}(\text{TMP})(\text{O})_2]$ = 4.0×10^{-4} M. Temperature = 18.2 °C.

Time (s)	Mole Fraction of $\text{Ru}^{\text{VI}}(\text{TMP})(\text{O})_2$
0	1
360	0.133
	$k_{\text{obs}} = 5.6 \times 10^{-3} \text{ s}^{-1}$

Table C.1.21. [¹PrOH] = 0.130 M in benzene-*d*₆. [¹BuOH] = 0.177 M.
 $[\text{Ru}^{\text{VI}}(\text{TMP})(\text{O})_2] = 4.0 \times 10^{-4}$ M. Temperature = 18.2 °C.

Time (s)	Mole Fraction of $\text{Ru}^{\text{VI}}(\text{TMP})(\text{O})_2$
0	1
810	0.99
2850	0.97
5010	0.95
	$k_{\text{obs}} = 9.2 \times 10^{-6} \text{ s}^{-1}$

Table C.1.22. [¹PrOH] = 0.130 M in benzene-*d*₆. [¹BuOH] = 0.530 M.
 $[\text{Ru}^{\text{VI}}(\text{TMP})(\text{O})_2] = 4.0 \times 10^{-4}$ M. Temperature = 18.2 °C.

Time (s)	Mole Fraction of $\text{Ru}^{\text{VI}}(\text{TMP})(\text{O})_2$
0	1
2520	0.99
4500	0.98
10000	0.96
	$k_{\text{obs}} = 3.6 \times 10^{-6} \text{ s}^{-1}$

Table C.1.23. [Benzyl alcohol] = 0.193 M in benzene-*d*₆.
 $[\text{Ru}^{\text{VI}}(\text{TMP})(\text{O})_2] = 2.0 \times 10^{-4}$ M. Temperature = 18.0 °C.

Time (s)	Mole Fraction of $\text{Ru}^{\text{VI}}(\text{TMP})(\text{O})_2$
0	1
510	0.717
1290	0.555
2010	0.335
2610	0.299
3630	0.154
	$k_{\text{obs}} = 5.06 \times 10^{-4} \text{ s}^{-1}$

Table C.1.24. [Benzyl alcohol] = 0.129 M in benzene-*d*₆.
 $[\text{Ru}^{\text{VI}}(\text{TMP})(\text{O})_2] = 3.0 \times 10^{-4}$ M. Temperature = 18.0 °C.

Time (s)	Mole Fraction of $\text{Ru}^{\text{VI}}(\text{TMP})(\text{O})_2$
0	1
300	0.852
900	0.719
1800	0.509
2460	0.432
3000	0.359
	$k_{\text{obs}} = 3.57 \times 10^{-4} \text{ s}^{-1}$

Table C.1.25. [Benzyl alcohol] = 0.0966 M in benzene-*d*₆.
 $[\text{Ru}^{\text{VI}}(\text{TMP})(\text{O})_2] = 3.0 \times 10^{-4}$ M. Temperature = 18.2 °C.

Time (s)	Mole Fraction of $\text{Ru}^{\text{VI}}(\text{TMP})(\text{O})_2$
0	1
720	0.856
1320	0.726
2100	0.609
2700	0.575
3480	0.434
	$k_{\text{obs}} = 2.28 \times 10^{-4} \text{ s}^{-1}$

Table C.1.26. [Benzyl alcohol] = 0.193 M in benzene-*d*₆.
 $[\text{Ru}^{\text{VI}}(\text{TMP})(\text{O})_2] = 3.0 \times 10^{-4}$ M. Temperature = 29.5 °C.

Time (s)	Mole Fraction of $\text{Ru}^{\text{VI}}(\text{TMP})(\text{O})_2$
0	1
300	0.613
600	0.451
900	0.275
1200	0.15
	$k_{\text{obs}} = 1.47 \times 10^{-4} \text{ s}^{-1}$

Table C.1.27. [Benzyl alcohol] = 0.0966 M in benzene- d_6 .
 $[\text{Ru}^{\text{VI}}(\text{TMP})(\text{O})_2] = 3.0 \times 10^{-4}$ M. Temperature = 29.5 °C.

Time (s)	Mole Fraction of $\text{Ru}^{\text{VI}}(\text{TMP})(\text{O})_2$
0	1
300	0.768
720	0.616
1200	0.401
1620	0.425
2100	0.274
	$k_{\text{obs}} = 7.41 \times 10^{-4} \text{ s}^{-1}$

Table C.1.28. [Benzyl alcohol] = 0.161 M in benzene- d_6 .
 $[\text{Ru}^{\text{VI}}(\text{TMP})(\text{O})_2] = 3.0 \times 10^{-4}$ M. Temperature = 34.5 °C.

Time (s)	Mole Fraction of $\text{Ru}^{\text{VI}}(\text{TMP})(\text{O})_2$
0	1
270	0.486
615	0.277
900	0.164
	$k_{\text{obs}} = 2.26 \times 10^{-3} \text{ s}^{-1}$

Table C.1.29. [Benzyl alcohol] = 0.0966 M in benzene- d_6 .
 $[\text{Ru}^{\text{VI}}(\text{TMP})(\text{O})_2] = 3.0 \times 10^{-4}$ M. Temperature = 34.5 °C.

Time (s)	Mole Fraction of $\text{Ru}^{\text{VI}}(\text{TMP})(\text{O})_2$
0	1
360	0.545
720	0.427
990	0.410
1260	0.286
	$k_{\text{obs}} = 1.37 \times 10^{-3} \text{ s}^{-1}$

Table C.1.30. [Benzyl alcohol] = 0.0322 M in benzene-*d*₆.
 $[\text{Ru}^{\text{VI}}(\text{TMP})(\text{O})_2] = 3.0 \times 10^{-4}$ M. Temperature = 34.5 °C.

Time (s)	Mole Fraction of $\text{Ru}^{\text{VI}}(\text{TMP})(\text{O})_2$
0	1
300	0.811
600	0.626
900	0.516
1200	0.40
	$k_{\text{obs}} = 7.52 \times 10^{-4} \text{ s}^{-1}$

**C.2 Data for the Catalytic Oxidation of Alcohols in Benzene at 50 °C
under 1 Atm Air.**

Table C2.1. [Benzyl alcohol] = 0.121 M; [Ru^{VII}(TMP)(O)₂] = 2.56 × 10⁻⁵ M
30 μL 3.0 M aqueous KOH. Blank benzyl alcohol contains 0.174%
benzaldehyde.

Time (h)	Amount of Benzaldehyde (Arbitrary Units) ^a	Amount of Benzyl alcohol (Arbitrary Units) ^a
17.25	2466 2146	128990 84690
41.75	8935 5250	282790 113400
67.5	10358 10012	219070 179380
91.5	5580 6148	81365 84881
115.5	8372 12503	103440 154090
141	6663 5085	76489 58019
166	5423 6097	62989 65081
191.5	2340 2698	22020 26863
234.5	4674 4832	44081 44437
259	1894 2519	17512 25095

^a Second set of values in correspond to data from a second GC run for the same sample.

Table C2.2. [Benzyl alcohol] = 0.242 M; $[\text{Ru}^{\text{VI}}(\text{TMP})(\text{O})_2] = 2.56 \times 10^{-5}$ M
 30 μL 3.0 M aqueous KOH. Blank benzyl alcohol contains 0.174% benzaldehyde.

Time (h)	Amount of Benzaldehyde (Arbitrary Units) ^a	Amount of Benzyl alcohol (Arbitrary Units) ^a
17.25	5210	220470
	5318	221710
41.75	10570	275790
	11035	273770
67.75	22708	424950
	7206	130280
91.75	12923	188880
	6204	83797
116	29382	392590
	23962	323130
141.5	11163	129500
	11865	136620
166.25	15965	166030
	13078	139400
191.5	6943	65093
	8241	78154
234.5	2908	24787
	2453	21542

^a See footnote *a* for Table C.2.1.

Table C2.3. [Benzyl alcohol] = 0.483 M; $[\text{Ru}^{\text{VI}}(\text{TMP})(\text{O})_2] = 2.56 \times 10^{-5}$ M
 30 μL 3.0 M aqueous KOH. Blank benzyl alcohol contains 0.174% benzaldehyde.

Time (h)	Amount of Benzaldehyde (Arbitrary Units) ^a	Amount of Benzyl alcohol (Arbitrary Units) ^a
17.75	6356 7991	468220 605370
41.75	17669 16266	727430 693480
67.75	13809 16923	387560 500590
91.75	23066 24948	499500 568720
116.5	40029 16708	722480 311130
141.5	20428 21472	311660 332190
166.5	20531 5493	281680 77760
191.75	3120 2847	39047 35490
234.75	5127 5061	54642 54414
259.5	3589 4308	37622 47706
283.15	4032 2878	40980 27753
307.75	12039 10812	105910 96041
334	8293 7894	74321 67489

^a See footnote *a* for Table C.2.1.

Table C2.4. [Benzyl alcohol] = 0.878 M; $[\text{Ru}^{\text{VI}}(\text{TMP})(\text{O})_2] = 2.56 \times 10^{-5}$ M
 30 μL 3.0 M aqueous KOH. Blank benzyl alcohol contains 0.174% benzaldehyde.

Time (h)	Amount of Benzaldehyde (Arbitrary Units) ^a	Amount of Benzyl alcohol (Arbitrary Units) ^a
18	7986 6211	991370 869580
41.75	13053 15489	970480 1156000
67.75	11232 11727	582850 719600
91.75	22805 22861	1012100 1031700
116.75	17076 18004	652320 724730
141.75	26168 14971	842020 470820
166.5	5424 2499	150490 71781
192	3136 2056	76891 55694
235	3558 3171	77071 70126
259.75	4462 4819	88628 99322
283.5	2827 3038	53784 55869
308	12391 13183	214570 231900
334	10445	190150

^a See footnote *a* for Table C.2.1.

C.3 Data for the Catalytic Oxidation of Alkanes in Benzene at 24 °C under 1 Atm Air.

Table C.3.1. $[Ph_3CH] = 2.89 \times 10^{-3}$ M; $[Ru^{VI}(TMP)(O)_2] = 1.2 \times 10^{-4}$ M

Time (h)	Percentage conversion of Ph_3CH to Ph_3COH (%)
0	0
20	1.51
45	2.07
93	3.33
118.5	3.98
142	4.30
166.5	5.12
191	5.22
215.5	6.29
244	6.68
262	6.96
287.5	6.87
360	7.88
410	8.80
505	9.86
1150	13.93

Table C.3.2. $[Adamantane] = 6.28 \times 10^{-3}$ M; $[Ru^{VI}(TDCPP)(O)_2] = 2.39 \times 10^{-4}$ M

Time (h)	Percentage conversion of adamantane to 1-adamantanol (%)
0	0
19.5	0.44
43.5	1.13
67.25	2.11
93	3.42
117	4.30
145.5	4.38
166.5	4.96
189	5.37
213	6.20
262	6.48
312	8.82
407	10.21

Table C.3.3. $[Ph_3CH] = 4.64 \times 10^{-3} M$, $[Ru^{VI}(TDCPP)(O)_2] = 2.39 \times 10^{-4} M$

Time (h)	Percentage conversion of Ph_3CH to Ph_3COH (%)
0	0
20	2.21
44	3.57
68	6.09
93	7.74
117	9.38
146	11.31
164	12.33
190	14.25
212.5	15.57
261	18.43
312	23.92
407.5	31.36
481.5	38.56
1150	67.01

Appendix D Supplementary Data for the Crystallographic Structures of $\text{Ru}^{\text{IV}}(\text{TMP})(\text{OR})_2$

D.1 $\text{Ru}^{\text{IV}}(\text{TMP})(\text{O}^i\text{Pr})_2$

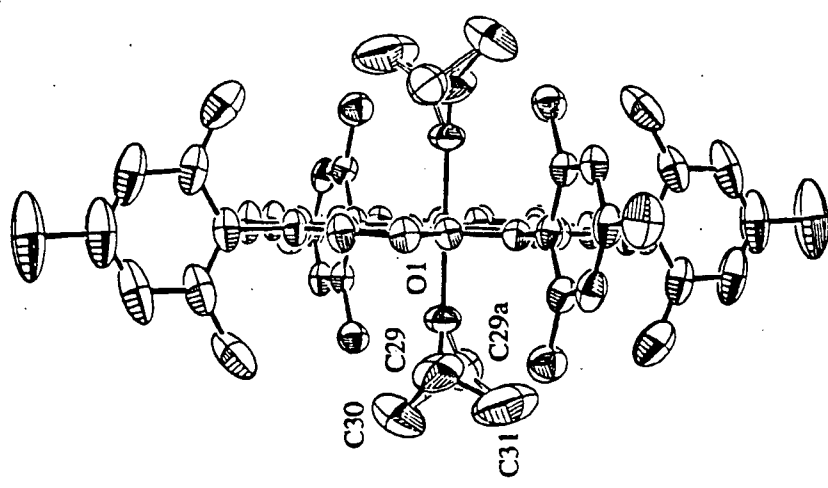


Figure D.1.1 ORTEP Plot showing sideway view along the porphyrin plane of $\text{Ru}^{\text{IV}}(\text{TMP})(\text{O}^i\text{Pr})_2$.

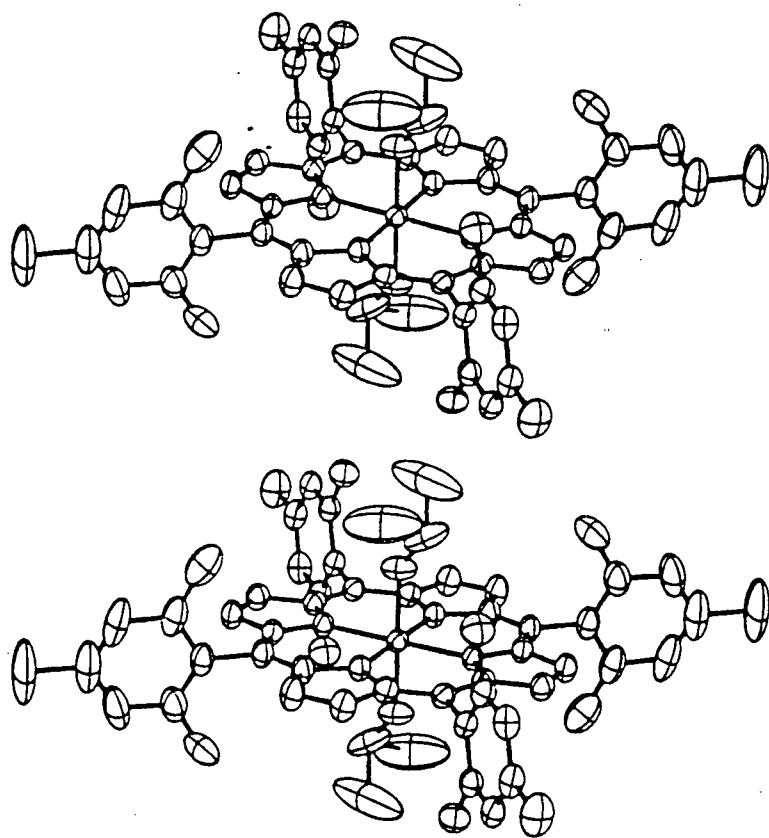


Figure D.1.2 Stereoview of $\text{Ru}^{\text{IV}}(\text{TMP})(\text{O}^i\text{Pr})_2$.

Table D.1.1. Experimental Details.**A. Crystal Data**

Empirical Formula	C ₆₂ H ₆₆ N ₄ O ₂ Ru
Formula Weight	1000.30
Crystal Color, Habit	black, irregular
Crystal Dimensions	0.15 x 0.25 x 0.32 mm
Crystal System	tetragonal
Lattice Type	I-centered
No. of Reflections Used for Unit Cell Determination (2θ range)	25 (35.7 - 53.8°)
Omega Scan Peak Width at Half-height	0.380
Lattice Parameters	a = 27.967(1) Å c = 1.4.274(2) Å V = 11164(1) Å ³
Space Group	I4 ₁ /a (#88)
Z value	8
D _{calc}	1.190 g cm ⁻³
F ₀₀₀	4208
μ(CuKa)	26.13 cm ⁻¹

B. Intensity Measurements

Diffractometer	Rigaku AFC6S
Radiation	CuKα (λ = 1.54178 Å) graphite monochromated
Take-off Angle	6.0°
Detector Aperture	6.0 mm horizontal 6.0 mm vertical
Crystal to Detector Distance	285 mm
Temperature	21.0 °C
Scan Type	ω-2θ

Scan Rate	16.0°/min (in ω) (up to 9 scans)
Scan Width	$(0.89 + 0.20 \tan \theta)^\circ$
$2\theta_{\max}$	155.5°
No. of Reflections Measured	Total: 5676 Unique: 5448 ($R_{\text{int}} = 0.020$)
Corrections	Lorentz-polarization Absorption (trans. factors: 0.779 - 1.000) Secondary Extinction (coefficient: $3.2(4) \times 10^{-8}$)

C. Structure Solution and Refinement

Structure Solution	Patterson Methods (DIRDIF92 PATTY)
Refinement	Full-matrix least-squares
Function Minimized	$\sum \omega (F_o - F_c)^2$
Least Squares Weights	$1/\sigma^2(F_o) = 4F_o^2/\sigma^2(F_o^2)$
p-factor	0.000
Anomalous Dispersion	All non-hydrogen atoms
No. Observations ($I > 3.00\sigma(I)$)	3417
No. Variables	318
Reflection/Parameter Ratio	10.75
Residuals: R ; R_w	0.043; 0.044
Goodness of Fit Indicator	2.34
Max Shift/Error in Final Cycle	0.001
Maximum peak in Final Diff. Map	$0.42 \text{ e} \cdot \text{\AA}^{-3}$
Minimum peak in Final Diff. Map	$-0.32 \text{ e} \cdot \text{\AA}^{-3}$

Table D.1.2. Atomic Coordinates and B_{eq} .

atom	x	y	z	B_{eq}	occ.
Ru(1)	0.2500	0.2500	0.2500	3.80(1)	0.50
O(1)	0.1975(1)	0.2814(1)	0.3064(3)	6.9(1)	
N(1)	0.2059(1)	0.1987(1)	0.1968(2)	4.17(8)	
N(2)	0.2604(1)	0.2096(1)	0.3663(2)	4.09(8)	
C(1)	0.1827(2)	0.1999(2)	0.1111(3)	5.0(1)	
C(2)	0.1562(2)	0.1562(2)	0.0999(4)	6.1(1)	
C(3)	0.1636(2)	0.1295(2)	0.1765(4)	5.8(1)	
C(4)	0.1951(1)	0.1559(1)	0.2375(3)	4.4(1)	
C(5)	0.2113(1)	0.1399(1)	0.3245(3)	4.3(1)	
C(6)	0.2416(1)	0.1650(1)	0.3831(3)	4.3(1)	
C(7)	0.2583(2)	0.1486(1)	0.4722(3)	4.8(1)	
C(8)	0.2868(2)	0.1827(2)	0.5084(3)	5.1(1)	
C(9)	0.2885(2)	0.2214(1)	0.4424(3)	4.5(1)	
C(10)	0.3148(2)	0.2634(2)	0.4530(3)	5.0(1)	
C(11)	0.1980(2)	0.0900(1)	0.3557(3)	4.3(1)	
C(12)	0.2266(2)	0.0519(2)	0.3280(3)	4.5(1)	
C(13)	0.2153(2)	0.0063(2)	0.3581(3)	5.0(1)	
C(14)	0.1774(2)	-0.0023(2)	0.4170(4)	5.4(1)	
C(15)	0.1498(2)	0.0356(2)	0.4442(3)	5.6(1)	
C(16)	0.1590(2)	0.0824(2)	0.4140(3)	4.9(1)	
C(17)	0.2699(2)	0.0595(2)	0.2669(4)	6.0(1)	
C(18)	0.1662(2)	-0.0526(2)	0.4491(4)	8.2(2)	
C(19)	0.1274(2)	0.1225(2)	0.4442(4)	7.2(2)	
C(20)	0.3419(2)	0.2679(2)	0.5447(4)	5.9(1)	
C(21)	0.3895(3)	0.2531(2)	0.5497(5)	7.5(2)	
C(22)	0.4117(3)	0.2558(3)	0.6377(6)	10.1(2)	
C(23)	0.3895(4)	0.2710(3)	0.7152(6)	11.6(3)	
C(24)	0.3433(4)	0.2850(2)	0.7088(5)	10.9(3)	
C(25)	0.3186(3)	0.2837(2)	0.6227(5)	8.2(2)	
C(26)	0.4152(2)	0.2345(3)	0.4670(6)	10.6(3)	
C(27)	0.4153(4)	0.2732(3)	0.8103(6)	18.6(4)	
C(28)	0.2672(3)	0.2988(3)	0.6198(5)	11.7(3)	
C(29)	0.1679(4)	0.2763(4)	0.379(1)	11.6(4)	0.70
C(29a)	0.158(1)	0.2972(9)	0.309(2)	9.0(6)	0.30
C(30)	0.1602(4)	0.3300(5)	0.4065(9)	25.0(6)	
C(31)	0.1191(3)	0.2644(4)	0.333(1)	22.1(5)	

$$B_{eq} = \frac{8}{3}\pi^2[U_{11}(aa^*)^2 + U_{22}(bb^*)^2 + U_{33}(cc^*)^2 + 2U_{12}aa^*bb^*\cos\gamma + 2U_{13}aa^*cc^*\cos\beta + 2U_{23}bb^*cc^*\cos\alpha]$$

Table D.1.3. Bond Lengths (Å).^a

<u>atom</u>	<u>atom</u>	<u>distance</u>	<u>atom</u>	<u>atom</u>	<u>distance</u>
Ru(1)	O(1)	1.892(3)	Ru(1)	N(1)	2.038(3)
Ru(1)	N(2)	2.029(3)	O(1)	C(29)	1.34(1)
O(1)	C(29a)	1.18(3)	N(1)	C(1)	1.385(5)
N(1)	C(4)	1.366(5)	N(2)	C(6)	1.375(5)
N(2)	C(9)	1.380(5)	C(1)	C(2)	1.437(6)
C(1)	C(10)*	1.377(6)	C(2)	C(3)	1.341(6)
C(3)	C(4)	1.441(5)	C(4)	C(5)	1.396(5)
C(5)	C(6)	1.384(5)	C(5)	C(11)	1.511(5)
C(6)	C(7)	1.431(5)	C(7)	C(8)	1.346(6)
C(8)	C(9)	1.436(6)	C(9)	C(10)	1.394(6)
C(10)	C(20)	1.517(6)	C(11)	C(12)	1.389(5)
C(11)	C(16)	1.387(6)	C(12)	C(13)	1.384(5)
C(12)	C(17)	1.508(6)	C(13)	C(14)	1.373(6)
C(14)	C(15)	1.368(6)	C(14)	C(18)	1.511(6)
C(15)	C(16)	1.401(6)	C(16)	C(19)	1.493(6)
C(20)	C(21)	1.396(8)	C(20)	C(25)	1.364(8)
C(21)	C(22)	1.403(8)	C(21)	C(26)	1.476(9)
C(22)	C(23)	1.34(1)	C(23)	C(24)	1.35(1)
C(23)	C(27)	1.539(g)	C(24)	C(25)	1.410(8)
C(25)	C(28)	1.499(g)	C(29)	C(30)	1.56(1)
C(29)	C(31)	1.55(2)	C(29a)	C(30)	1.66(3)
C(29a)	C(31)	1.47(3)			

^aHere and elsewhere in D.1, * refers to symmetry operation: 1/2-x, 1/2-y, 1/2-z.

Table D.1.4. Bond Angles (°).

<u>atom</u>	<u>atom</u>	<u>atom</u>	<u>angle</u>	<u>atom</u>	<u>atom</u>	<u>atom</u>	<u>angle</u>
O(1)	Ru(1)	O(1)*	180.0	O(1)	Ru(1)	N(1)	91.0(1)
O(1)	Ru(1)	N(1)*	89.0(1)	O(1)	Ru(1)	N(2)	91.2(2)
O(1)	Ru(1)	N(2)*	88.8(2)	N(1)	Ru(1)	N(1)*	180.0
N(1)	Ru(1)	N(2)	90.0(1)	N(1)	Ru(1)	N(2)*	90.0(1)
N(2)	Ru(1)	N(2)*	180.0	Ru(1)	O(1)	C(29)	139.7(5)
Ru(1)	O(1)	C(29a)	155(1)	Ru(1)	N(1)	C(1)	126.6(3)
Ru(1)	N(1)	C(4)	126.4(3)	C(1)	N(1)	C(4)	107.0(3)
Ru(1)	N(2)	C(6)	126.3(3)	Ru(I)	N(2)	C(9)	126.4(3)
C(6)	N(2)	C(9)	107.2(3)	N(1)	C(1)	C(2)	108.7(4)
N(1)	C(1)	C(10)*	125.4(4)	C(2)	C(1)	C(10)*	125.9(4)
C(1)	C(2)	C(3)	107.6(4)	C(2)	C(3)	C(4)	107.6(4)
N(1)	C(4)	C(3)	109.1(4)	N(1)	C(4)	C(5)	126.0(4)
C(3)	C(4)	C(5)	124.9(4)	C(4)	C(5)	C(6)	125.0(4)
C(4)	C(5)	C(11)	118.6(4)	C(6)	C(5)	C(11)	116.3(4)
N(2)	C(6)	C(5)	126.2(4)	N(2)	C(6)	C(7)	108.8(4)
C(5)	C(6)	C(7)	125.0(4)	C(6)	C(7)	C(8)	107.8(4)
C(7)	C(8)	C(9)	107.5(4)	N(2)	C(9)	C(8)	108.6(4)
N(2)	C(9)	C(10)	125.9(4)	C(8)	C(9)	C(10)	125.6(4)
C(1)*	C(10)	C(9)	125.7(4)	C(1)*	C(10)	C(20)	119.0(4)
C(9)	C(10)	C(20)	115.3(4)	C(5)	C(11)	C(12)	118.8(4)
C(5)	C(11)	C(16)	120.8(4)	C(12)	C(11)	C(16)	120.3(4)
C(11)	C(12)	C(13)	119.1(4)	C(11)	C(12)	C(17)	121.4(4)
C(13)	C(12)	C(17)	119.5(4)	C(12)	C(13)	C(14)	121.9(4)
C(13)	C(14)	C(15)	118.3(4)	C(13)	C(14)	C(18)	120.5(5)
C(15)	C(14)	C(18)	121.2(5)	C(14)	C(15)	C(16)	122.1(5)
C(11)	C(16)	C(15)	118.3(4)	C(11)	C(16)	C(19)	121.6(4)
C(15)	C(16)	C(19)	120.2(5)	C(10)	C(20)	C(21)	119.7(6)
C(10)	C(20)	C(25)	119.6(5)	C(21)	C(20)	C(25)	120.6(6)
C(20)	C(21)	C(22)	117.0(7)	C(20)	C(21)	C(26)	121.8(6)
C(22)	C(21)	C(26)	121.2(7)	C(21)	C(22)	C(23)	123.4(8)
C(22)	C(23)	C(24)	118.7(8)	C(22)	C(23)	C(27)	121(1)
C(24)	C(23)	C(27)	119(1)	C(23)	C(24)	C(25)	121.2(9)
C(20)	C(25)	C(24)	119.1(7)	C(20)	C(25)	C(28)	121.7(6)
C(24)	C(25)	C(28)	119.1(8)	O(1)	C(29)	C(30)	100(1)
O(1)	C(29)	C(31)	103(1)	C(30)	C(29)	C(31)	101.0(8)
O(1)	C(29a)	C(30)	101(1)	O(1)	C(29a)	C(31)	117(2)
C(30)	C(29a)	C(31)	100(1)				

Table D.1.5. Least-Square Planes.

Plane number 1		Plane number 2		Plane number 3	
Atoms defining plane	Distance	Atoms defining plane	Distance	Atoms defining plane	Distance
N(1)	-0.008(3)	N(1)	-0.003(3)	N(2)	-0.001(3)
N(2)	-0.005(3)	C(1)	0.005(5)	C(6)	0.002(4)
C(1)	0.006(5)	C(2)	-0.002(5)	C(7)	-0.001(4)
C(2)	0.007(5)	C(3)	-0.003(5)	C(8)	0.000(5)
C(3)	0.004(5)	C(4)	0.004(4)	C(9)	0.001(4)
C(4)	0.002(4)	Additional Atoms		Additional Atoms	
C(5)	-0.002(4)	Ru(1)	0.039	Ru(l)	0.031
C(6)	0.001(4)	C(5)	0.005	C(5)	-0.004
C(7)	0.002(4)	C(10)*	0.005	C(10)	0.022
C(8)	-0.001(5)	Plane number 4		Plane number 7	
C(9)	-0.003(4)	Atoms defining plane	Distance	Atoms defining plane	Distance
C(10)	0.014(5)	N(1)	-0.001(3)	C(20)	0.001(4)
Additional Atoms		N(2)	0.000(3)	C(21)	-0.004(5)
Ru(l)	0.022	C(4)	0.004(4)	C(22)	0.005(7)
O(1)	-1.867	C(5)	-0.003(4)	C(23)	-0.001(8)
C(11)	0.097	C(6)	0.002(4)	C(24)	-0.003(7)
C(20)	-0.021	Additional Atoms		C(25)	0.001(6)
Plane number 6		Ru(1)	0.034	Additional atoms	
Atoms defining plane	Distance	Ru(1)		C(10)	-0.084
C(11)	-0.001(4)	Ru(1)		C(26)	-0.041
C(12)	0.008(4)	Ru(1)		C(27)	0.004
C(13)	-0.011(4)	Ru(1)		C(28)	-0.025
C(14)	0.003(4)	Plane number 5		Atoms defining plane	
C(15)	0.006(5)	Atoms defining plane	Distance	N(1)*	0.023(4)
C(16)	-0.006(4)	N(2)	-0.002(3)	C(1)*	-0.002(3)
Additional Atoms		C(9)	0.003(4)	C(9)	0.003(4)
C(5)	0.054	C(10)	0.000(5)	C(10)	0.000(5)
C(17)	0.053	Additional Atoms		Atoms defining plane	
C(18)	-0.007	Ru(1)	Distance	Ru(1)	-0.008
C(19)	-0.029	Ru(1)		Atoms defining plane	

Table D.1.5. Least-Square Planes (continued).

plane	mean deviation	χ^2
1	0.0046	22.5
2	0.0032	3.0
3	0.0010	0.4
4	0.0019	1.6
5	0.0019	1.3
6	0.0059	13.8
7	0.0025	1.2

Dihedral angles between planes (°)

plane	1	2	3	4	5	6
2	0.35					
3	0.18	0.33				
4	0.22	0.36	0.04			
5	1.13	1.25	1.31	1.35		
6	86.94	86.63	86.95	86.97	86.74	
7	94.15	93.97	93.97	93.93	95.22	81.61

Table D.1.6. Non-bonded Contacts out to 3.60 Å.

atom	atom	distance	ADC	atom	atom	distance	ADC
C(7)	C(14)	3.511(6)	4	C(7)	C(15)	3.530(6)	4
C(8)	C(15)	3.515(6)	4	C(13)	C(17)	3.552(7)	4
C(7)	H(2)	2.89	4	C(13)	H(3)	2.78	44411
C(13)	H(9)	2.94	4	C(14)	H(3)	2.68	44411
C(14)	H(5)	2.87	4	C(15)	H(4)	2.93	44411
C(15)	H(3)	2.96	44411	C(16)	H(4)	2.98	44411
H(1)	H(34)	2.50	45507	H(2)	H(7)	2.56	44411
H(4)	H(15)	2.55	4	H(6)	H(24)	2.36	45067

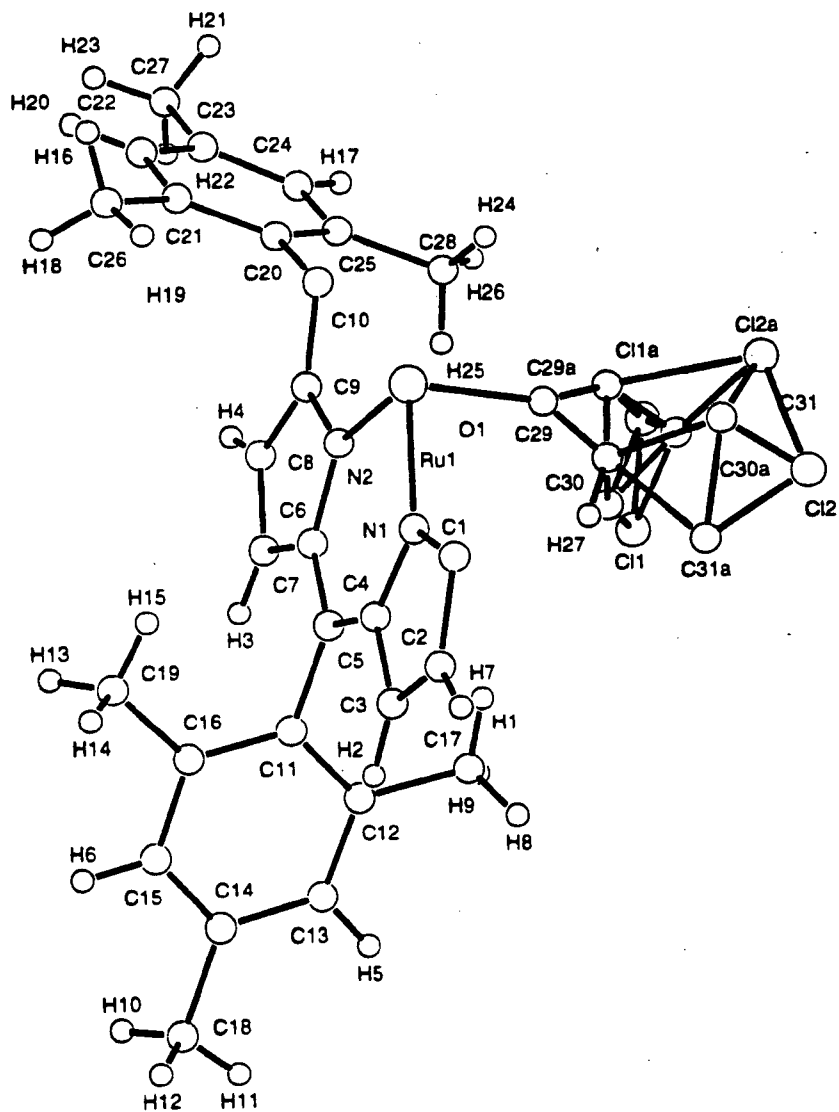
D.2. $\text{Ru}^{\text{IV}}(\text{TMP})(\text{OCH}(\text{CH}_2\text{Cl})_2)_2$ 

Figure D.2.1. PLUTO Plot for the partial structure of $\text{Ru}^{\text{IV}}(\text{TMP})(\text{OCH}(\text{CH}_2\text{Cl})_2)_2$.

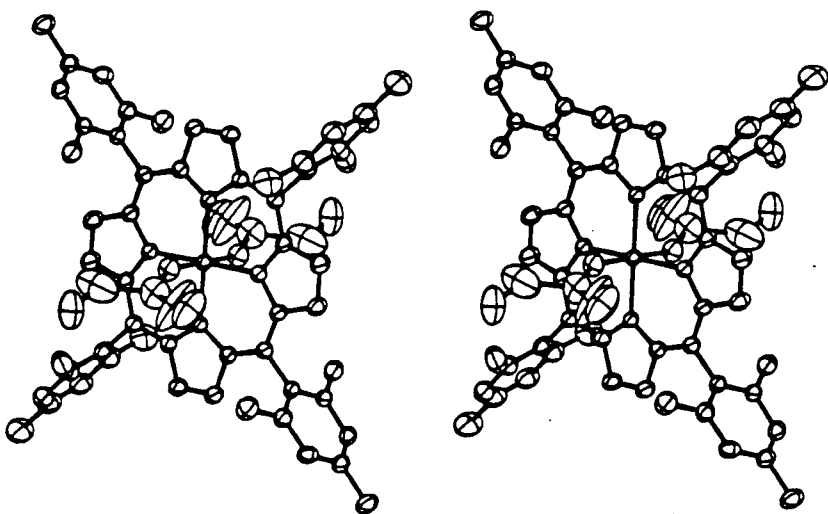


Figure D.2.2. Stereoview of Ru^{IV}(TMP)(OCH(CH₂Cl)₂)₂.

Table D.2.1. Experimental Details.**A. Crystal Data**

Empirical Formula	C ₆₂ H ₆₂ Cl ₄ O ₂ N ₄ Ru
Formula Weight	1138.08
Crystal Color, Habit	dark-brown prism, prism
Crystal Dimensions	0.40 x 0.40 x 0.40 mm
Crystal System	tetragonal
Lattice Type	I-centered
No. of Reflections Used for Unit Cell Determination (2θ range)	25 (20.1 - 27.1°)
Omega Scan Peak Width at Half-height	0.39°
Lattice Parameters	a = 29.334(2) Å c = 13.517(6) Å V = 11630(4) Å ³
Space Group	I4 ₁ /a (#88)
Z value	8
D _{calc}	1.300 g cm ⁻³
F ₀₀₀	4720.00
μ(MoKα)	4.98 cm ⁻¹

B. Intensity Measurements

Diffractometer	Rigaku AFC6S
Radiation	MoKα ($\lambda = 0.71069 \text{ \AA}$) graphite monochromated Take-off Angle 6.0°
Detector Aperture	6.0 mm horizontal 6.0 mm vertical
Crystal to Detector Distance	285 mm
Temperature	21.0 °C
Scan Type	ω-2θ

Scan Rate	$16.0^\circ \text{ min}^{-1}$ (in ω) (up to 9 scans)
Scan Width	$(1.37 + 0.35 \tan \theta)^\circ$
$2\theta_{\max}$	55.1°
No. of Reflections Measured	Total: 7249 Unique: 6984 ($R_{\text{int}} = 0.034$)
Corrections	Lorentz-polarization Absorption (trans. factors: 0.933 - 1.000)

C. Structure Solution and Refinement

Structure Solution	Patterson Methods (DIRDIF92 PATTY)
Refinement	Full-matrix least-squares
Function Minimized	$\sum \omega(F_o - F_c)^2$
Least Squares Weights	$1/\sigma^2(F_o) = 4F_o^2/\sigma^2(F_o^2)$
p-factor	0.008
Anomalous Dispersion	All non-hydrogen atoms
No. Observations ($I > 3.00\sigma(I)$)	2421
No. Variables	376
Reflection/Parameter Ratio	6.44
Residuals: R ; R_w	0.051; 0.046
Goodness of Fit Indicator	2.62
Max Shift/Error in Final Cycle	0.03
Maximum peak in Final Diff. Map	$0.75 \text{ e}^- \text{\AA}^{-3}$
Minimum peak in Final Diff. Map	$-0.41 \text{ e}^- \text{\AA}^{-3}$

Table D.2.2. Atomic Coordinates and B_{eq} .

atom	x	y	z	B_{eq}	occ.
Ru(1)	0.2500	0.2500	0.7500	5.02(2)	0.50
Cl(1)	0.4133(3)	0.2522(2)	0.6392(8)	21.4(3)	0.68
Cl(1a)	0.4034(9)	0.2128(7)	0.703(1)	20.0(7)	0.32
Cl(2)	0.3415(2)	0.1637(2)	0.4757(6)	17.6(3)	0.68
Cl(2a)	0.3487(6)	0.1449(6)	0.601(2)	21.3(8)	0.32
O(1)	0.2998(2)	0.2206(2)	0.6859(5)	8.6(2)	
N(1)	0.2386(2)	0.2897(2)	0.6296(3)	5.4(1)	
N(2)	0.2923(2)	0.2990(2)	0.8060(4)	5.7(1)	
C(1)	0.2109(2)	0.2795(2)	0.5500(5)	6.0(2)	
C(2)	0.2109(2)	0.3170(2)	0.4832(5)	7.1(2)	
C(3)	0.2386(2)	0.3492(2)	0.5210(5)	7.1(2)	
C(4)	0.2559(2)	0.3323(2)	0.6140(5)	5.6(2)	
C(5)	0.2856(2)	0.3563(2)	0.6740(5)	5.6(2)	
C(6)	0.3021(2)	0.3403(2)	0.7635(5)	5.8(2)	
C(7)	0.3327(2)	0.3646(2)	0.8278(6)	7.4(2)	
C(8)	0.3397(3)	0.3382(3)	0.9081(6)	8.1(2)	
C(9)	0.3146(2)	0.2969(2)	0.8957(5)	6.1(2)	
C(10)	0.3133(2)	0.2611(2)	0.9626(5)	6.3(2)	
C(11)	0.2993(2)	0.4035(2)	0.6412(5)	5.3(2)	
C(12)	0.3365(3)	0.4096(2)	0.5783(5)	6.3(2)	
C(13)	0.3463(2)	0.4538(3)	0.5462(5)	6.6(2)	
C(14)	0.3210(3)	0.4909(2)	0.5762(6)	6.5(2)	
C(15)	0.2848(3)	0.4836(2)	0.6379(5)	6.4(2)	
C(16)	0.2734(2)	0.4400(2)	0.6724(5)	5.5(2)	
C(17)	0.3655(3)	0.3704(3)	0.5446(6)	9.1(3)	
C(18)	0.3324(3)	0.5384(2)	0.5401(6)	9.3(2)	
C(19)	0.2330(3)	0.4350(2)	0.7382(6)	7.9(2)	
C(20)	0.3397(4)	0.2654(2)	1.0588(7)	7.1(3)	
C(21)	0.3181(4)	0.2820(3)	1.1419(7)	8.3(3)	
C(22)	0.3428(4)	0.2843(3)	1.2306(7)	10.4(3)	
C(23)	0.3864(-D)	0.2710(4)	1.2347(9)	10.7(4)	
C(24)	0.4080(3)	0.2554(3)	1.1540(10)	9.9(3)	
C(25)	0.383 i-(4)	0.2521(3)	1.0622(8)	9.5(3)	
C(26)	0.2689(4)	0.2966(3)	1.1396(7)	12.9(4)	
C(27)	0.4151(4)	0.2750(3)	1.3306(8)	16.3(4)	
C(28)	0.4085(3)	0.2338(4)	0.9746(9)	12.7(4)	
C(29)	0.3269(9)	0.222(1)	0.623(3)	13.8(10)	0.68
C(29a)	0.340(2)	0.202(2)	0.689(3)	11(1)	0.32
C(30)	0.366(1)	0.2439(9)	0.628(4)	30(1)	0.68
C(30a)	0.375(2)	0.201(3)	0.638(5)	20(2)	0.32
C(31)	0.318(1)	0.171(1)	0.556(3)	25(1)	0.68
C(31a)	0.334(2)	0.216(2)	0.496(7)	29(3)	0.32

$$B_{eq} = \frac{8}{3}\pi^2 [U_{11}(aa^*)^2 + U_{22}(bb^*)^2 + U_{33}(cc^*)^2 + 2U_{12}aa^*bb^*\cos\gamma + 2U_{13}aa^*cc^*\cos\beta + 2U_{23}bb^*cc^*\cos\alpha]$$

Table D.2.3. Bond Lengths (Å).

<u>atom</u>	<u>atom</u>	<u>distance</u>	<u>atom</u>	<u>atom</u>	<u>distance</u>
Ru(1)	O(1)	1.905(6)	Ru(1)	N(1)	2.029(4)
Ru(1)	N(2)	2.042(5)	Cl(1)	C(30)	1.42(4)
Cl(1)	C(30a)	1.87(8)	Cl(1a)	C(30)	1.75(5)
Cl(1a)	C(30a)	1.25(4)	Cl(2)	C(31)	1.30(3)
Cl(2)	C(31a)	1.58(5)	Cl(2a)	C(30a)	1.89(7)
O(1)	C(29a)	1.29(5)	O(1)	C(29)	1.16(3)
N(1)	C(1)	1.381(7)	N(1)	C(4)	1.365(7)
N(2)	C(6)	1.373(7)	N(2)	C(9)	1.379(7)
C(1)	C(2)	1.425(8)	C(1)	C(10)*	1.394(8)
C(2)	C(3)	1.346(8)	C(3)	C(4)	1.445(8)
C(4)	C(5)	1.383(8)	C(5)	C(6)	1.384(8)
C(5)	C(11)	1.509(8)	C(6)	C(7)	1.439(8)
C(7)	C(8)	1.350(8)	C(8)	C(9)	1.427(8)
C(9)	C(10)	1.387(8)	C(10)	C(20)	1.519(9)
C(11)	C(12)	1.393(8)	C(11)	C(16)	1.378(8)
C(12)	C(13)	1.397(8)	C(12)	C(17)	1.501(9)
C(13)	C(14)	1.379(9)	C(14)	C(15)	1.366(9)
C(14)	C(18)	1.513(9)	C(15)	C(16)	1.399(8)
C(16)	C(19)	1.491(8)	C(20)	C(21)	1.38(1)
C(20)	C(25)	1.35(1)	C(21)	C(22)	1.40(1)
C(21)	C(26)	1.51(1)	C(22)	C(23)	1.34(1)
C(23)	C(24)	1.34(1)	C(23)	C(27)	1.55(1)
C(24)	C(25)	1.44(1)	C(25)	C(28)	1.49(1)
C(29a)	C(30)	1.66(5)	C(29a)	C(30a)	1.25(7)
C(29)	C(30)	1.31(4)	C(29)	C(30a)	1.57(4)
C(29)	C(31)	1.77(5)	C(29)	C(31a)	1.74(9)

Here and elsewhere in D.2, * Denotes symmetry operation: 1/2-x, 1/2-y, 3/2-z.

Table D.2.4. Bond Angles (°).

atom	atom	atom	angle	atom	atom	atom	angle
O(1)	Ru(1)	O(1)*	180.0	O(1)	Ru(1)	N(1)	91.2(2)
O(1)	Ru(1)	N(1)*	88.8(2)	O(1)	Ru(1)	N(2)	91.2(2)
O(1)	Ru(1)	N(2)*	88.8(2)	N(1)	Ru(1)	N(1)*	180.0
N(1)	Ru(1)	N(2)	89.7(2)	N(1)	Ru(1)	N(2)*	90.3(2)
N(2)	Ru(1)	N(2)*	180.0	Ru(1)	O(1)	C(29a)	150(2)
Ru(1)	O(1)	C(29)	146(1)	Ru(1)	N(1)	C(1)	126.7(4)
Ru(1)	N(1)	C(4)	125.9(4)	C(1)	N(1)	C(4)	107.4(5)
Ru(1)	N(2)	C(6)	126.4(4)	Ru(1)	N(2)	C(9)	125.7(4)
C(6)	N(2)	C(9)	107.9(5)	N(1)	C(1)	C(2)	109.0(6)
N(1)	C(1)	C(10)*	125.4(6)	C(2)	C(1)	C(10)*	125.6(6)
C(1)	C(2)	C(3)	107.6(6)	C(2)	C(3)	C(4)	107.5(6)
N(1)	C(4)	C(3)	108.5(6)	N(1)	C(4)	C(5)	127.7(6)
C(3)	C(4)	C(5)	123.8(6)	C(4)	C(5)	C(6)	124.0(6)
C(4)	C(5)	C(11)	117.7(6)	C(6)	C(5)	C(11)	118.3(6)
N(2)	C(6)	C(5)	126.3(6)	N(2)	C(6)	C(7)	108.4(6)
C(5)	C(6)	C(7)	125.3(6)	C(6)	C(7)	C(8)	107.2(6)
C(7)	C(S)	C(9)	108.3(6)	N(2)	C(9)	C(8)	108.1(6)
N(2)	C(9)	C(10)	126.4(6)	C(8)	C(9)	C(10)	125.4(6)
C(1)*	C(10)	C(9)	125.4(6)	C(1)*	C(10)	C(20)	115.8(6)
C(9)	C(10)	C(20)	118.7(6)	C(5)	C(11)	C(12)	120.4(6)
C(5)	C(11)	C(16)	118.4(6)	C(12)	C(11)	C(16)	121.2(6)
C(11)	C(12)	C(13)	118.0(7)	C(11)	C(12)	C(17)	122.0(7)
C(13)	C(12)	C(17)	119.9(7)	C(12)	C(13)	C(14)	122.0(7)
C(13)	C(14)	C(15)	118.2(7)	C(13)	C(14)	C(18)	120.8(8)
C(15)	C(14)	C(18)	121.0(8)	C(14)	C(15)	C(16)	122.2(7)
C(11)	C(16)	C(15)	118.4(6)	C(11)	C(16)	C(19)	122.9(6)
C(15)	C(16)	C(19)	118.7(7)	C(10)	C(20)	C(21)	119.5(8)
C(10)	C(20)	C(25)	119.5(9)	C(21)	C(20)	C(25)	121.0(9)
C(20)	C(21)	C(22)	118.4(9)	C(20)	C(21)	C(26)	121.6(8)
C(22)	C(21)	C(26)	119(1)	C(21)	C(22)	C(23)	121(1)
C(22)	C(23)	C(24)	121(1)	C(22)	C(23)	C(27)	122(1)
C(24)	C(23)	C(27)	116(1)	C(23)	C(24)	C(25)	119(1)
C(20)	C(25)	C(24)	119(1)	C(20)	C(25)	C(28)	123.0(10)
C(24)	C(25)	C(28)	117(1)	O(1)	C(29a)	C(30a)	139(5)
O(1)	C(29)	C(30)	125(3)	O(1)	C(29)	C(30a)	120(4)
O(1)	C(29)	C(31)	104(2)	O(1)	C(29)	C(31a)	142(3)
C(30)	C(29)	C(31)	124(2)	Cl(1)	C(30)	C(29a)	121(4)
Cl(1)	C(30)	C(29)	160(3)	Cl(1a)	C(30)	C(29)	109(3)
Cl(1)	C(30a)	C(29a)	117(4)	Cl(1)	C(30a)	C(29)	102(4)
Cl(1a)	C(30a)	C(29a)	98(5)	Cl(1a)	C(30a)	C(29)	124(4)
Cl(2)	C(31)	C(29)	119(3)	Cl(2a)	C(31)	C(29)	98(3)
Cl(2)	C(31a)	C(29)	106(4)				

Table D.2.5. Least-Square Planes.

Plane number 1		Plane number 2	
Atoms defining plane	Distance	Atoms defining plane	Distance
Ru(1)	0.004	N(1)	0.000(5)
N(1)	0.019	C(1)	0.003(7)
N(2)	0.022	C(2)	-0.005(7)
C(1)	0.012	C(3)	0.005(7)
C(2)	-0.022	C(4)	-0.002(6)
C(3)	-0.019	Additional Atoms	Distance
C(4)	-0.003	Ru(1)	-0.053
C(5)	0.005	C(5)	0.005
C(6)	0.013	C(10)	-0.113
C(7)	0.011	Plane number 3	
C(8)	-0.013	Atoms defining plane	Distance
C(9)	-0.008	N(2)	0.005(5)
C(10)	-0.022	C(6)	-0.009(6)
Additional Atoms	Distance	C(7)	0.007(7)
O(1)	1.906	C(8)	-0.002(8)
C(29a)	3.025	C(9)	-0.005(7)
C(29)	2.901	Additional Atoms	Distance
C(30)	3.501	Ru(1)	-0.033
C(30a)	4.182	C(5)	-0.035
C(31)	3.750	C(10)	-0.009
C(31a)	3.928		
H(27)	2.560		

Plane number 4		Plane number 5		Plane number 6		Plane number 7	
Atoms defining plane	Distance	Atoms defining plane	Distance	Atoms defining plane	Distance	Atoms defining plane	Distance
Ru(1)	-0.010	Ru(1)	-0.007	C(11)	-0.003(6)	C(20)	-0.002(7)
N(1)	0.013	N(1)*	-0.003	C(12)	0.003(6)	C(21)	0.004(8)
N(2)	0.007	N(2)	0.013	C(13)	-0.004(7)	C(22)	-0.001(9)
C(4)	-0.007	C(1)*	0.012	C(14)	0.003(6)	C(23)	-0.01(1)
C(5)	-0.003	C(9)	-0.007	C(15)	-0.004(6)	C(24)	0.007(9)
C(6)	0.000	C(10)	-0.009	C(16)	0.004(6)	C(25)	-0.002(8)
Additional atoms	Distance	Additional atoms	Distance	Additional atoms	Distance	Additional atoms	Distance
C(5)	-0.002	C(5)	-0.027	C(5)	-0.069	C(10)	-0.043
C(10)	-0.048	C(10)	-0.009	C(17)	0.014	C(26)	-0.010
				C(18)	-0.006	C(27)	0.048
				C(19)	-0.028	C(28)	-0.014

Table D.2.5. Least-Square Planes (continued).**Summary**

<u>plane</u>	<u>mean deviation</u>	χ^2
1	0.0135	0.0
2	0.0029	1.1
3	0.0056	4.2
4	0.0067	0.0
5	0.0084	0.0
6	0.0034	1.6
7	0.0036	1.1

Dihedral angles between planes

<u>plane</u>	<u>1</u>	<u>2</u>	<u>3</u>	<u>4</u>	<u>5</u>	<u>6</u>
2	1.09					
3	0.83	1.72				
4	0.22	0.92	1.04			
5	0.55	1.63	0.52	0.76		
6	87.11	87.60	86.28	87.30	86.72	
7	92.84	91.93	92.87	92.75	93.19	83.87

Table D.2.6. Non-bonded Contacts out to 3.60 Å.

<u>atom</u>	<u>atom</u>	<u>distance</u>	<u>ADC</u>	<u>atom</u>	<u>atom</u>	<u>distance</u>	<u>ADC</u>
Cl(1a)	C(24)	3.44(2)	54616	C(2)	C(13)	3.592(9)	45412
C(3)	C(14)	3.524(9)	45412	C(3)	C(13)	3.581(9)	45412
Cl(1)	H(26)	2.96	45615	Cl(1)	H(17)	3.03	45615
Cl(1a)	H(4)	3.24	54616	Cl(2a)	H(4)	3.15	54616
C(13)	H(2)	2.99	3	C(14)	H(2)	2.67	3
C(14)	H(6)	2.90	45412	C(15)	H(13)	2.82	45412
C(15)	H(2)	2.91	3	C(27)	H(21)	2.90	45715
H(5)	H(18)	2.55	55403	H(6)	H(13)	2.38	45412
H(11)	H(18)	2.26	55403	H(20)	H(20)	2.38	55713
H(21)	H(22)	2.09	54716				

Appendix E. Oxidation of Alcohols, Alkenes and Alkanes by Ru(TDCPP-Cl₈) Species.

E.1. Oxidation of benzyl alcohol at 50 °C under 1 atm air.

Table E.1. [Ru^{VII}(TDCPP-Cl₈)(O)₂] = 3.5 × 10⁻⁵ M
[benzyl alcohol] = 0.290 M [benzyl alcohol] = 0.580 M

Time (h)	Conversion to benzaldehyde (%)	Time (h)	Conversion to benzaldehyde (%)
0	0	0	0
24	1.06	24	0.627
47.5	2.28	47.5	1.74
74.25	3.95	74.25	2.60
92.5	4.31	92.5	3.33
116.5	5.85	116.5	3.71
140.5	6.08	140.5	4.34
244	7.36	166.5	4.90
289.5	7.90	188	4.72
360	8.65	216.5	5.20
412	9.74	294	5.66
		263	5.74
		313	6.29
		384	6.90

[422 nm species] = 1.9 × 10⁻⁵ M
[benzyl alcohol] = 0.0242 M 0.121 M 0.242 M 0.483 M

Time (h)	Conversion to benzaldehyde (%)	Time (h)	Conversion to benzaldehyde (%)
0	0	0	0
24	2.7733	1.9161	0.86
49.5	4.8985	2.81385	1.53
101	6.7525	4.4155	2.61
119.75	7.5445	5.1305	2.99
144.25	8.377	5.634	3.22
168.75	7.9495	6.169	3.56
		169	2.54
		194	3.90
		219	2.85
		242.5	4.15
		288.75	3.06
		312	4.62
		337	3.49
		360.5	5.04
			3.97
			5.38
			3.95
			5.74
			4.50
			5.80
			4.52

E.2. Oxidation of Alkenes under 1 Atm O₂.

Table E.2.1. Oxidation of cyclohexene at 35 °C.
 $[Ru^{II}(TDCPP-Cl_8)(CO)] = 3.1 \times 10^{-5}$ M.

Substance present ^a	Blank 23 h at 35 °C (arbitrary units)	Ru ^{II} (TDCPP-Cl ₈)(CO) heated for 23 h (arbitrary units)
cyclohexene ^b	16098000	200640
cyclohexene-oxide	2427	3755
cyclohexene-2-ol	31695	47629
cyclohexene-2-one	46473	45773
cyclohexene-peroxides	638	1089
dimers	4604	7414

^a See Section E.4 later for the identification of the substances present by GCMS analysis.

^b The 20% loss due to evaporation has NOT been taken into account in this reported value; i.e. the amount of cyclohexene is increased by 20% prior to the calculation of percentage conversion (see Chapter 5).

Table E.2.2. Oxidation of *cis*-cyclooctene at 93 °C.
 $[Ru^{VI}(TDCPP-Cl_8)(O_2)] = 5.0 \times 10^{-5}$ M. Values in parentheses are those for the blank cyclooctene system at 110 °C heated for 23 h.

TIME (h)	8	26 {23}	32	55
Amount of cyclooctene (Arbitrary units)	601640	185130 {2517200; 1697400} ^a	279330	26106
Amount of epoxide	73218	112940 {232670; 166060}	226300	50896
Amount of other products ^b	14661	16954 {102897; 49390}	40074	13165

^a Two sets of data are given, which correspond to 2 GC runs of the same sample.

^b See Section E.5 later for the identification of the other products by GCMS analysis.

E.3. Oxidation of Alkanes.

Table E.3.1. Oxidation of methylcyclohexane under 1 atm O₂.
 Ru^{II}(TDCPP-Cl₈)(CO) (1); Ru^{VI}(TDCPP-Cl₈)(O)₂ (2).

Substance present ^a	Blank 24 h at 100 °C	[1] = 3.1x10 ⁻⁵ M 20 h at 93 °C	[2] = 1.1x10 ⁻⁵ M 17.5 h at 93 °C	[2] = 3.1x10 ⁻⁵ M 22.5 h at 100 °C
methylcyclohexane ^b	6460500	3206100	1324900	347380
	19985	88347	16673	17588
	9044	21819	5428	2821
	1643	15232	3257	2761
	3000	36750	7010	7368
	1353	14679	2945	2846
	5900	12142	3357	5104
C ₇ H ₁₄ O ₃ Mixture of ring-opened acids and/or peroxides	0	27272	8451	9441

^a See Section E.6 later for the identification of the substances present by GCMS analysis.

^b The 20% loss due to evaporation has NOT been taken into account in this reported value; i.e. the amount of methylcyclohexane is increased by 20% prior to the calculation of percentage conversion (see Chapter 5).

Table E.3.2. Oxidation of Ph₃CH catalyzed by Ru^{VI}(TDCPP-Cl₈)(O)₂ at 24 °C under 1 atm air in benzene. [Ru^{VI}(TDCPP-Cl₈)(O)₂] = 3.1 x 10⁻⁴ M; [Ph₃CH] = 0.0223 M.

Time (h)	Turnovers per mole of initial porphyrin
0	0
26	0.895
45.5	1.21
75.5	1.42
96	1.56
148.5	1.69
484	3.07

E.4. GCMS Data for the Cyclohexene Oxidation.

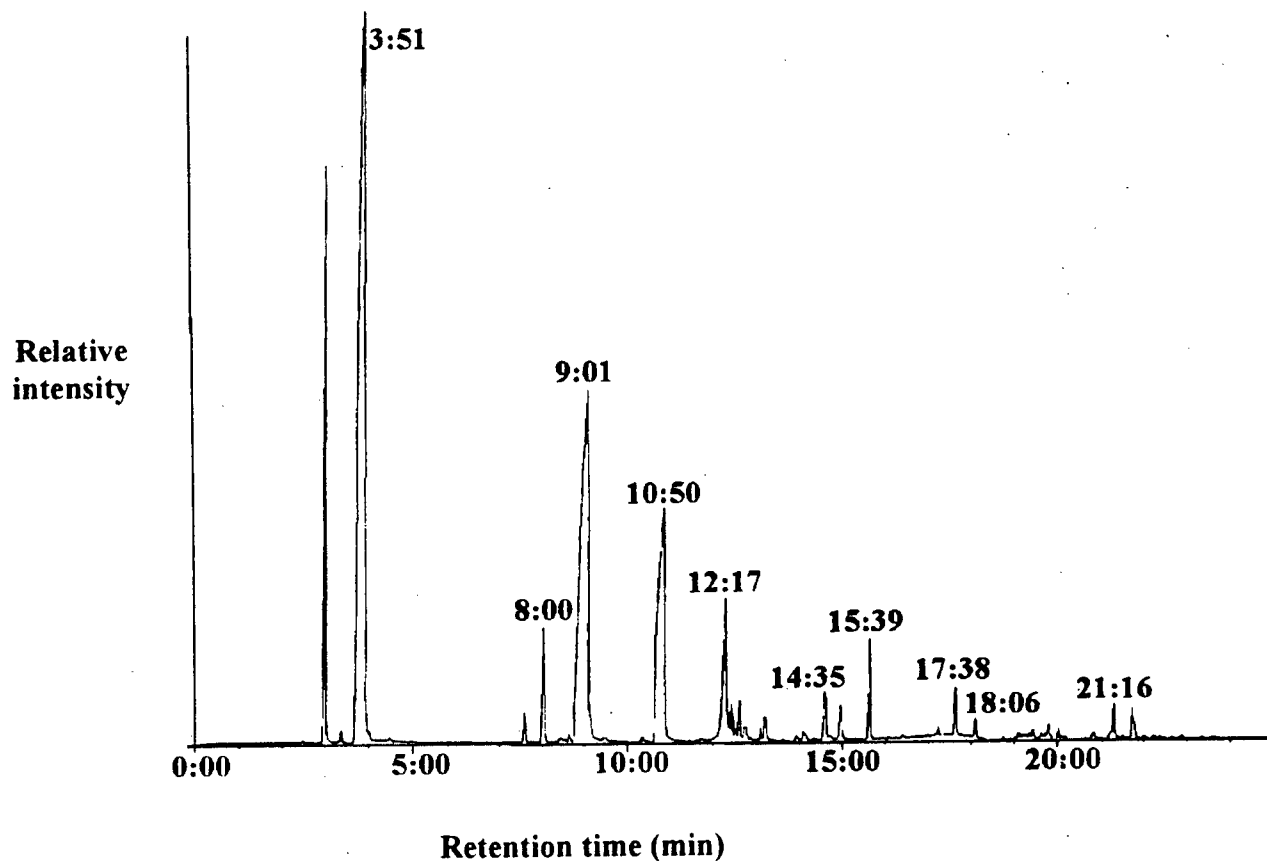


Figure E.4.1.. GC trace for the run in Table E.2.2 for the oxidation of cyclohexene.

Table E.4.1. Retention times and identity of substances from the GCMS analysis.

Retention Time (min)	Substance	Retention Time (min)	Substance
3:51	cyclohexene	14:35	cyclohexene-peroxide
8:00	cyclohexene-oxide	15:39	Dimeric product
9:01	cyclohexene-2-ol	17:38	DIMER
10:50	cyclohexene-2-one	18:06	DIMER
12:17	cyclohexene-3-one	21:16	DIMER

Figure E.4.2. Low Resolution Mass Spectra for the various products indicated in Figure E.4.1.

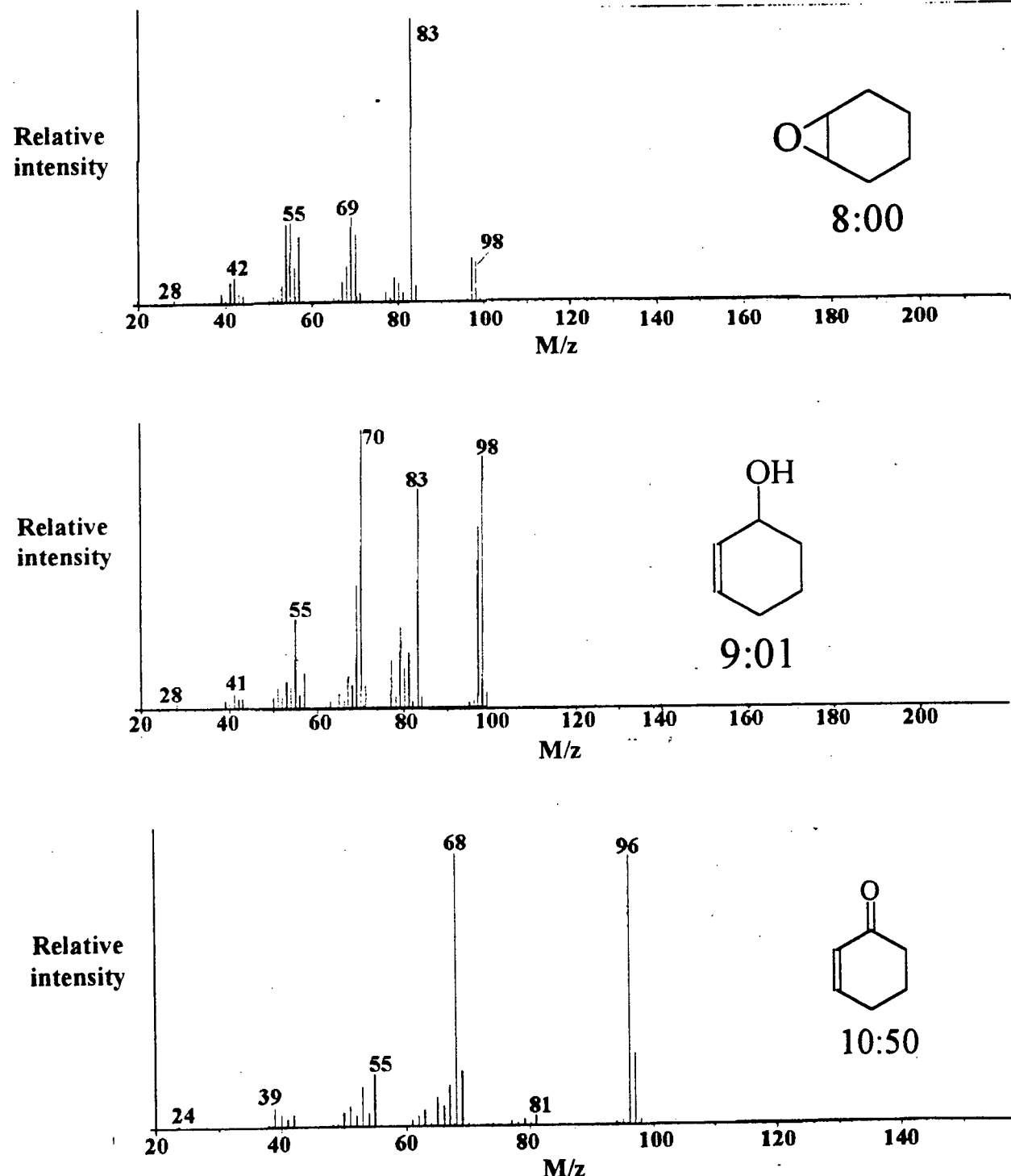


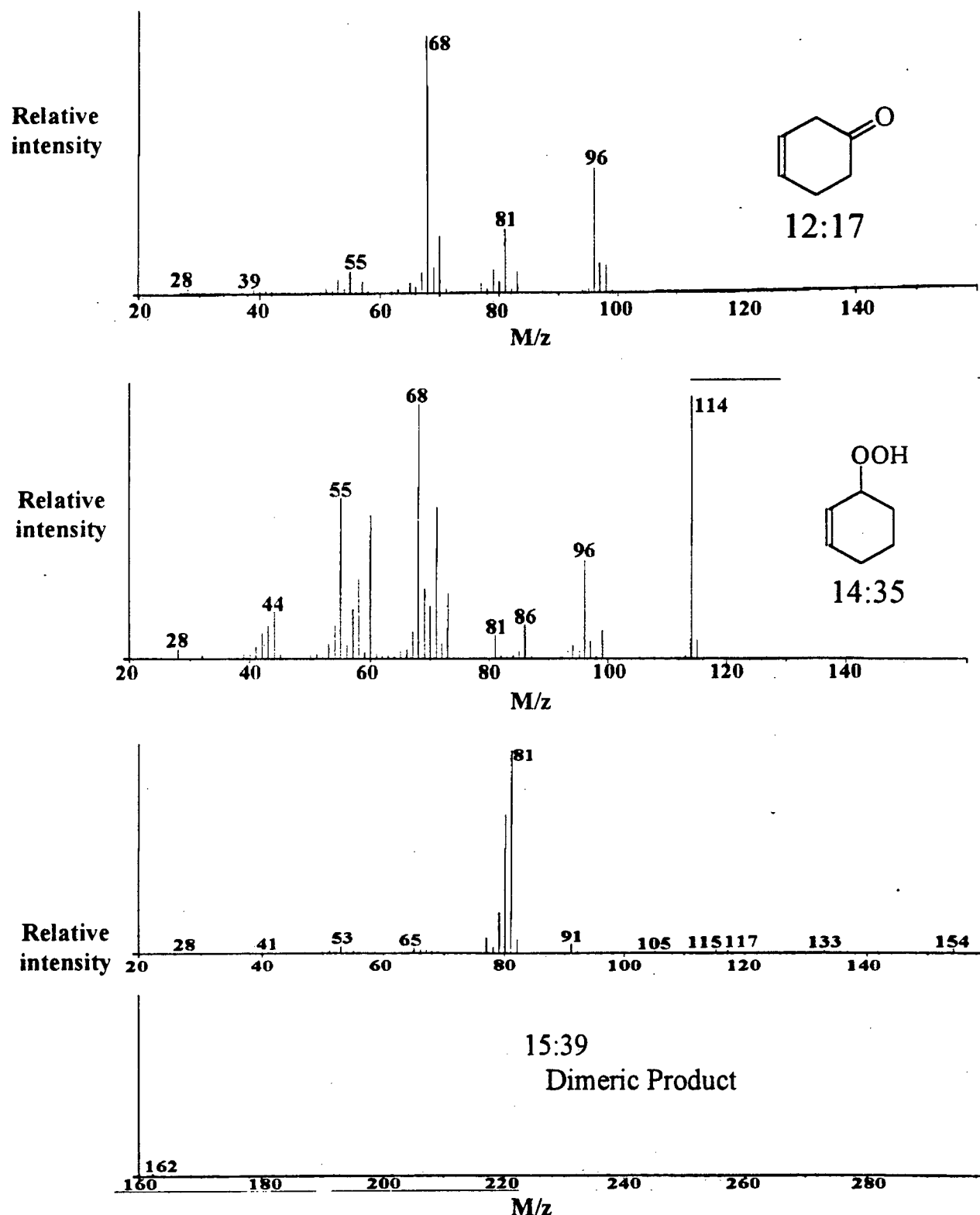
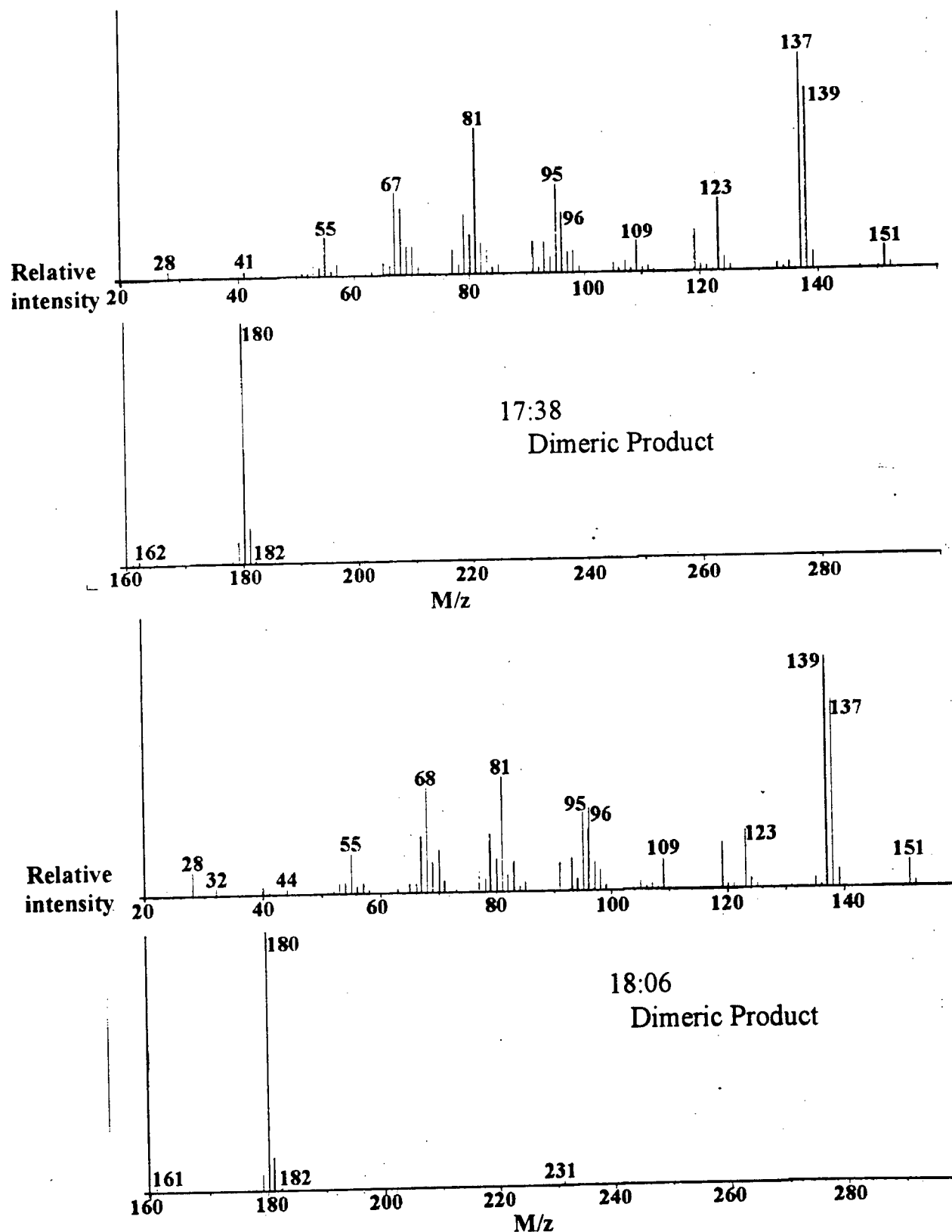
Figure E.4.2. *continued...*

Figure E.4.2. *continued...*

E.5. GCMS Data for the Cyclooctene Oxidation.

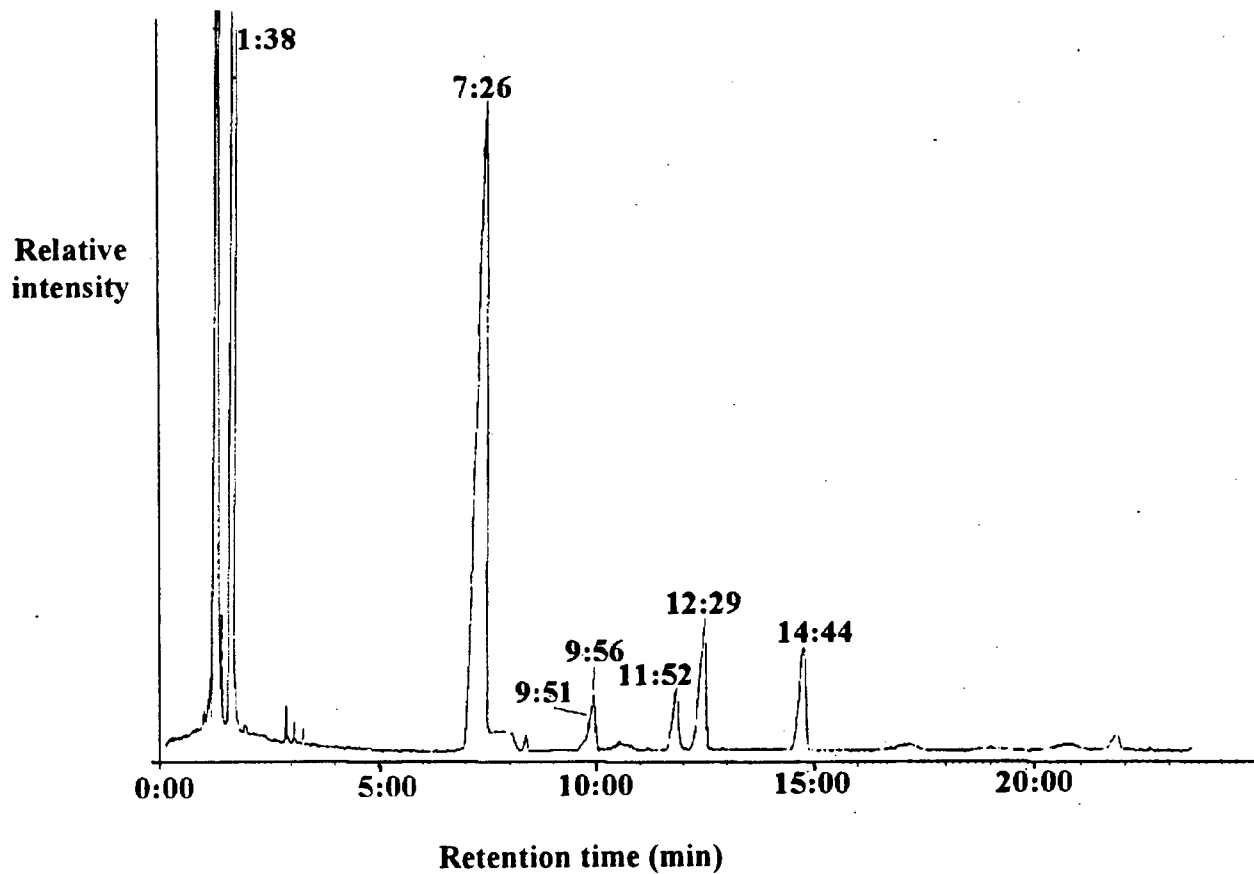
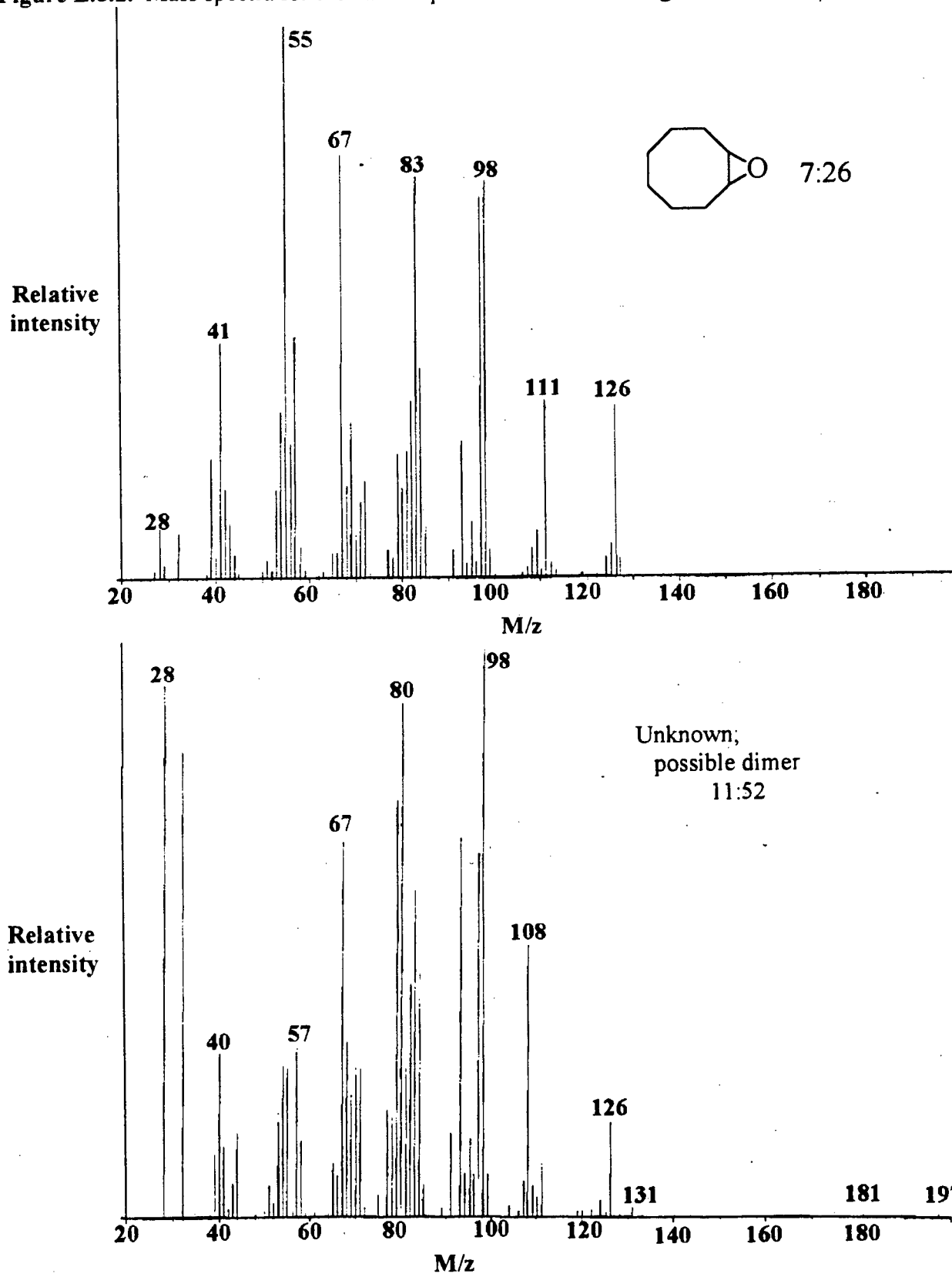
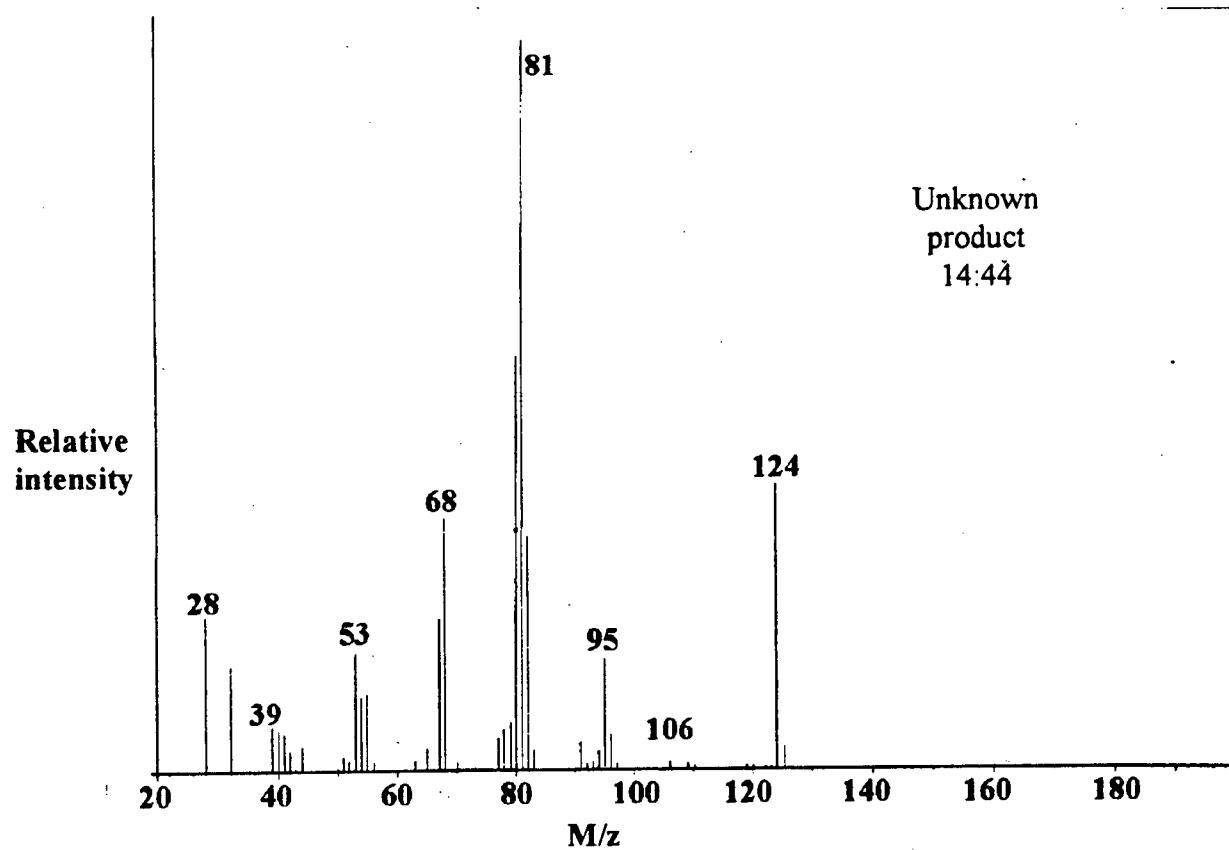
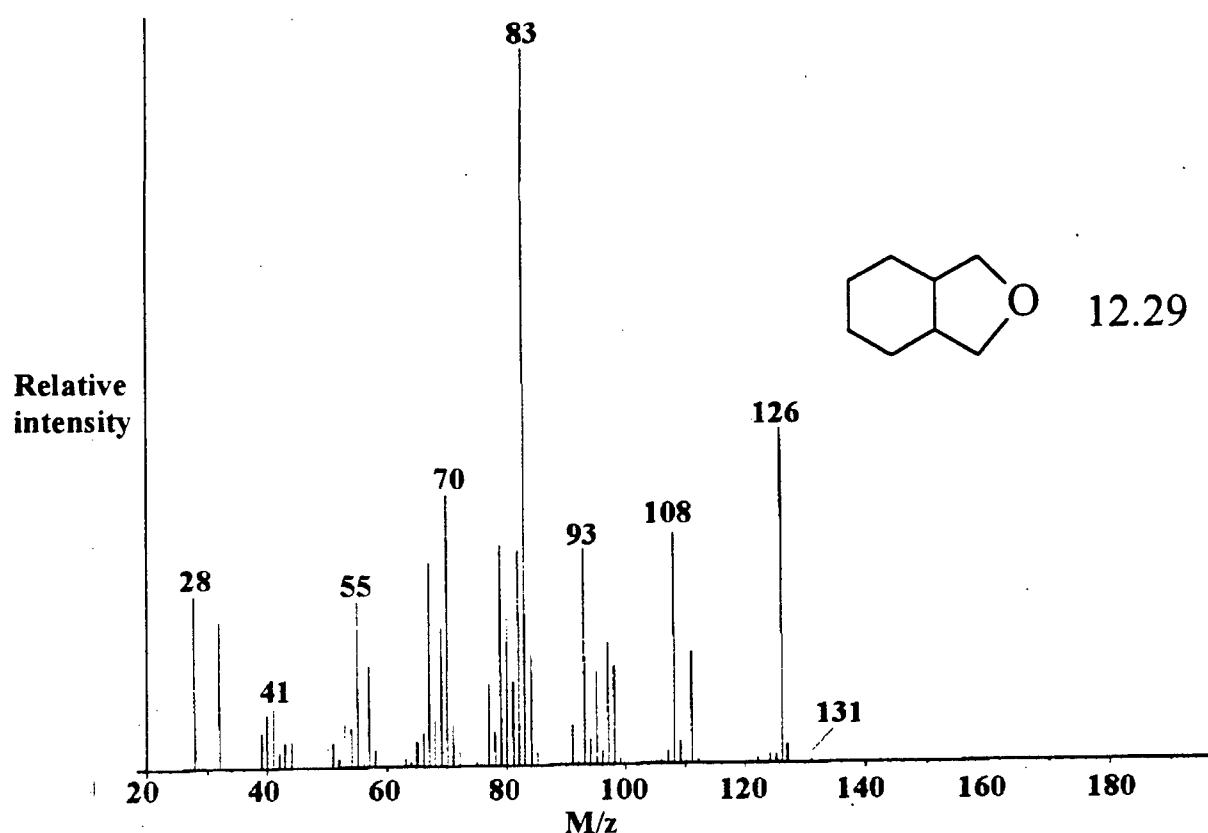


Figure E.5.1. GC trace for the run in Table E.2.1 for the oxidation of cyclooctene.

Table E.5.1. Retention times and identity of substances from the GCMS analysis.

Retention Time (min)	Substance	Retention Time (min)	Substance
1:38	cyclooctene	11:52	unknown, possible dimer
7:26	cyclooctene-oxide	12:29	<i>cis</i> -7-oxabicyclo[4.3.0]-nonane
9:51	unknown	14:44	unknown
9:56	unknown		

Figure E.5.2. Mass spectra for the various products indicated in Figure E.5.1.



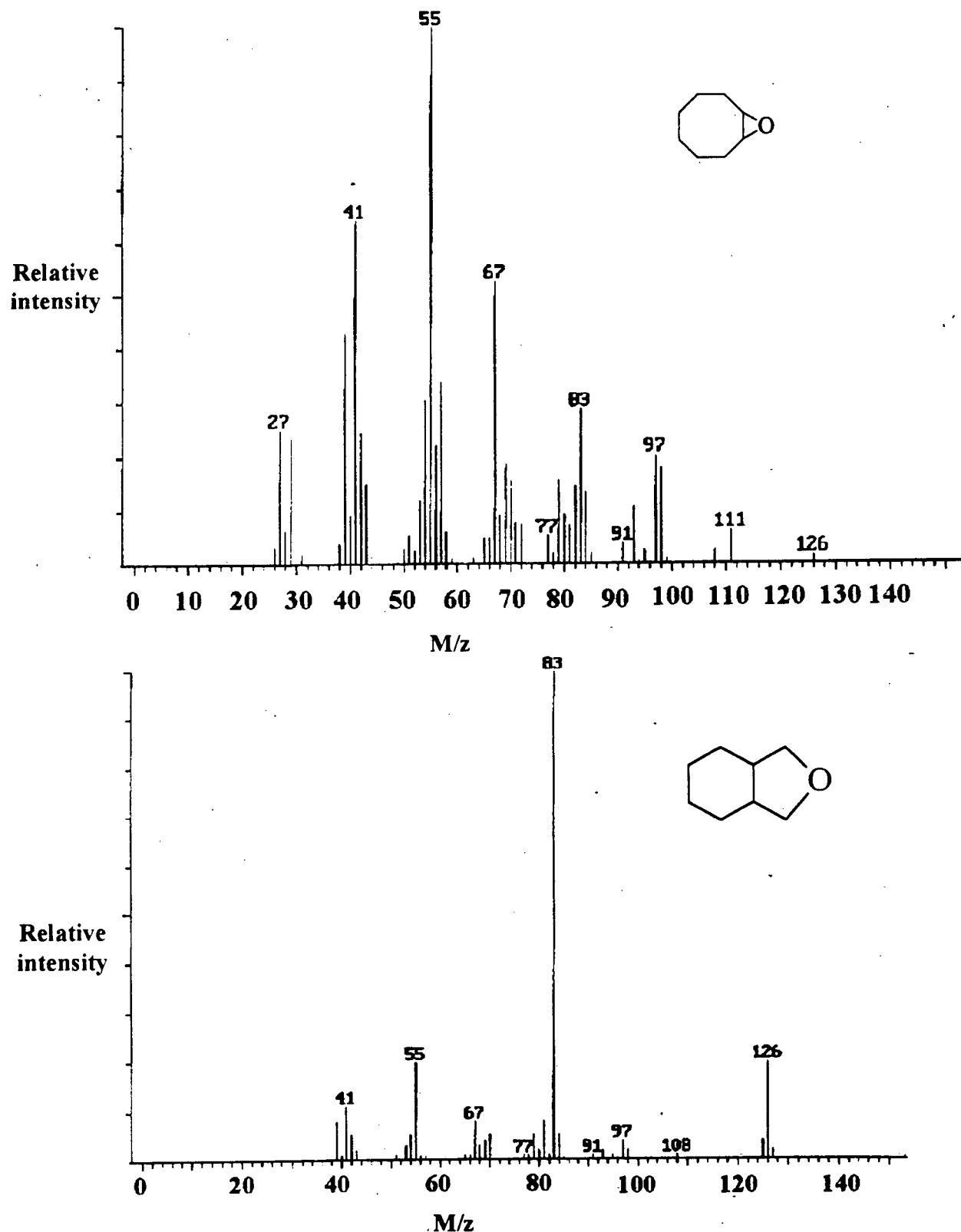


Figure E.5.3. Known fragmentation patterns for cyclooctene-oxide and *cis*-7-oxabicyclo[4.3.0]-nonane.

E.6. GCMS Data for the Methylcyclohexane Oxidation.

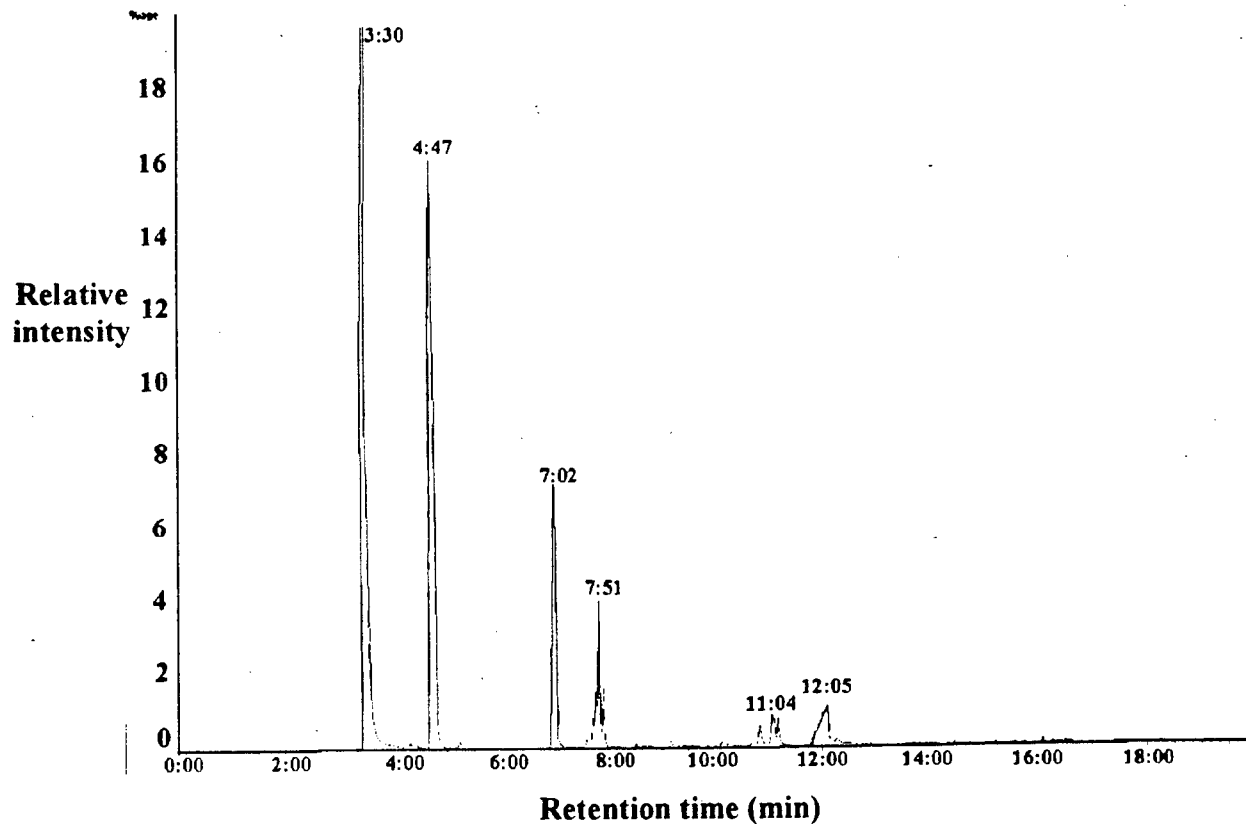


Figure E.6.1. GC trace for the run in Table E.3.1 for the oxidation of methylcyclohexane.

Table E.6.1. Retention times and identity of substances from the GCMS analysis.

Retention Time (min)	Substance	Retention Time (min)	Substance
4:47	methylcyclohexane	7:47 ^a	(2,3 and 4)-methylcyclohexanone
		7:51	
		7:55 ^a	
7:02	1-methylcyclohexanol	10:30	
		11:04	1-ol-(2,3 and 4)-ones
		11:11	
7:36 ^a	(2,3 and 4)-methylcyclohexanol	12:05	Peroxide and/or acid
7:43 ^a			

^a These retention times were not shown on the above chromatogram due to the lack of space.

Figure E.6.2. Low resolution mass spectra for the various products indicated in Figure E.6.1.

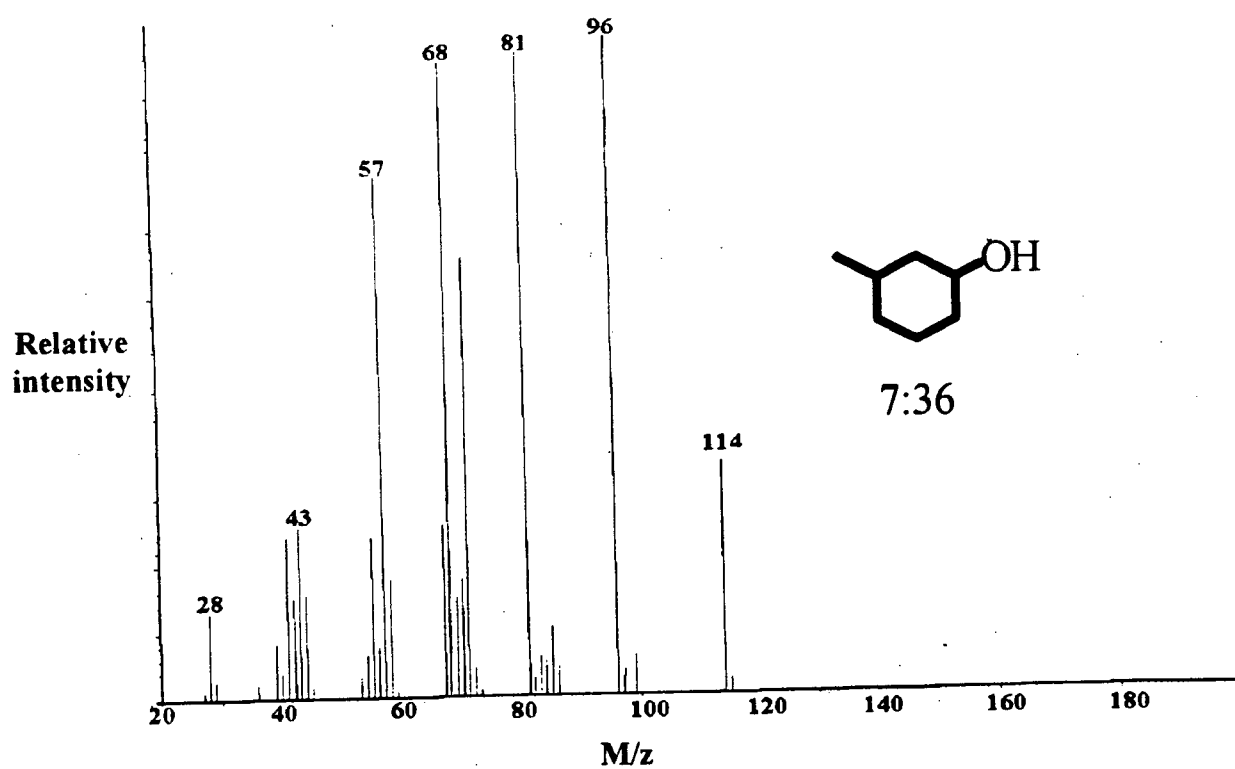
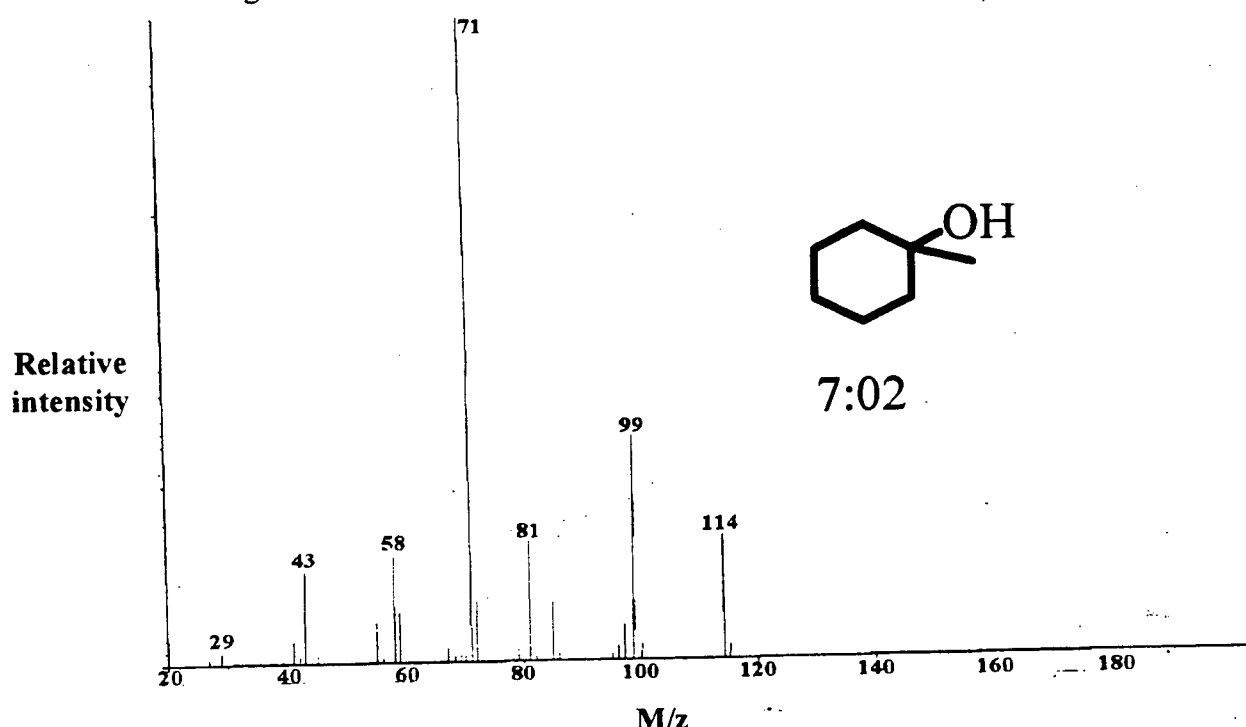


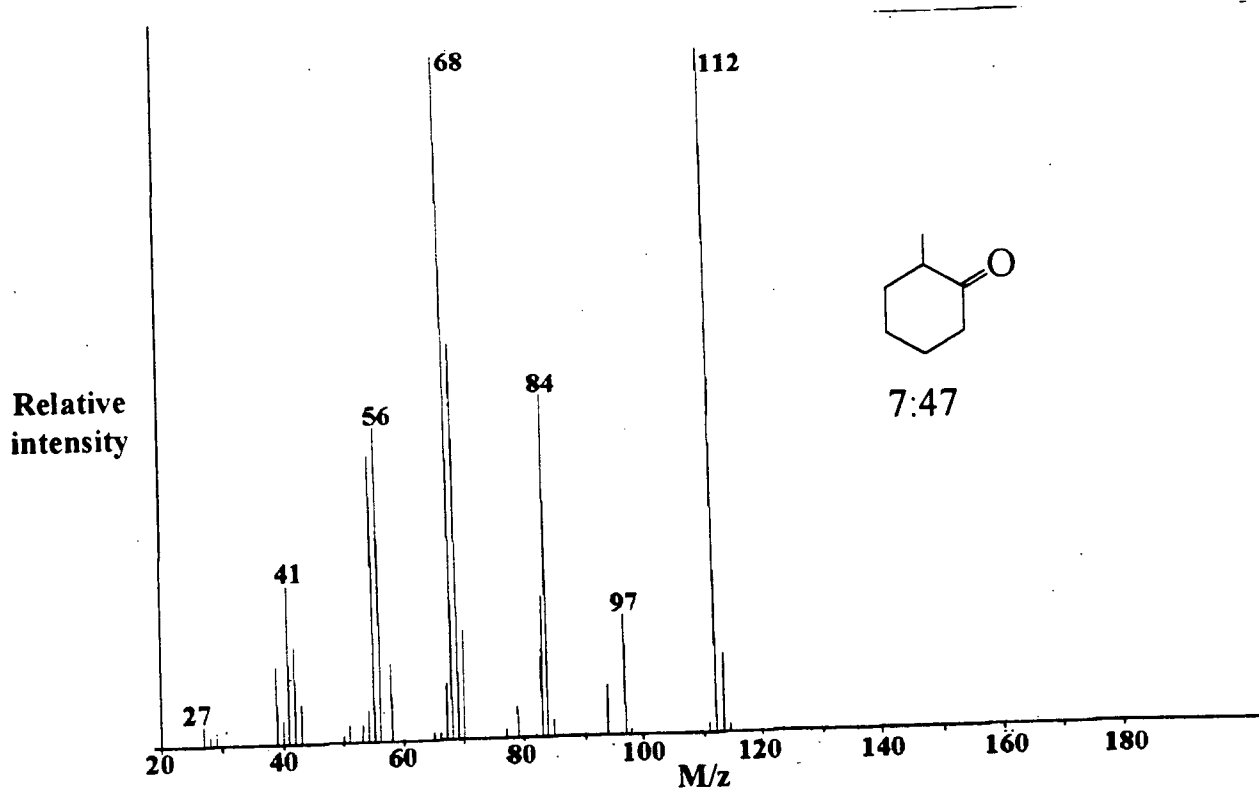
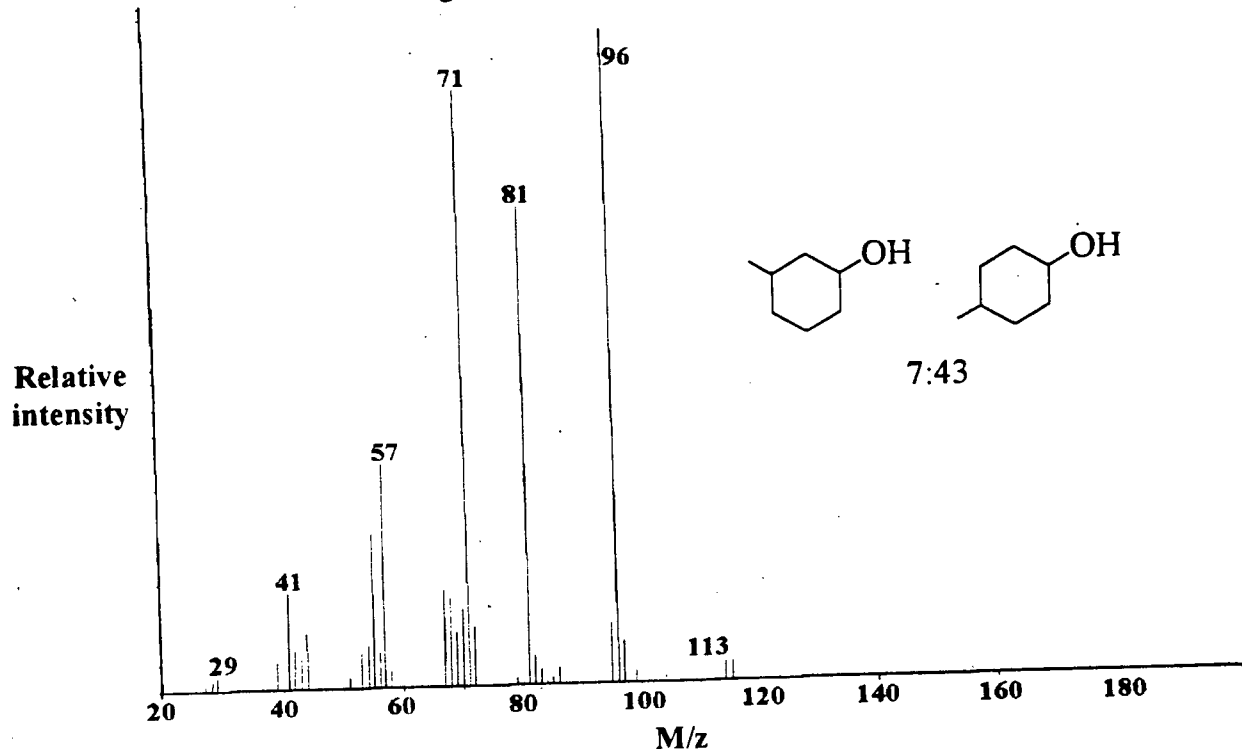
Figure E.6.2. *continued..*

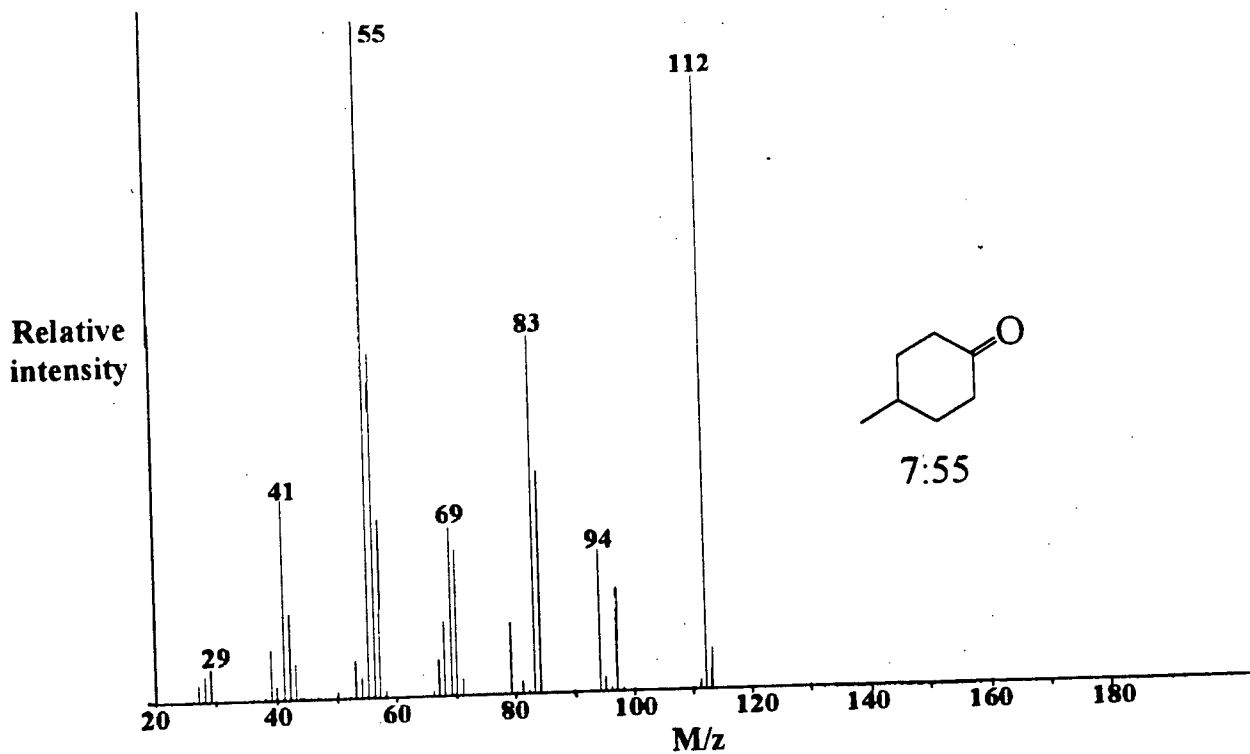
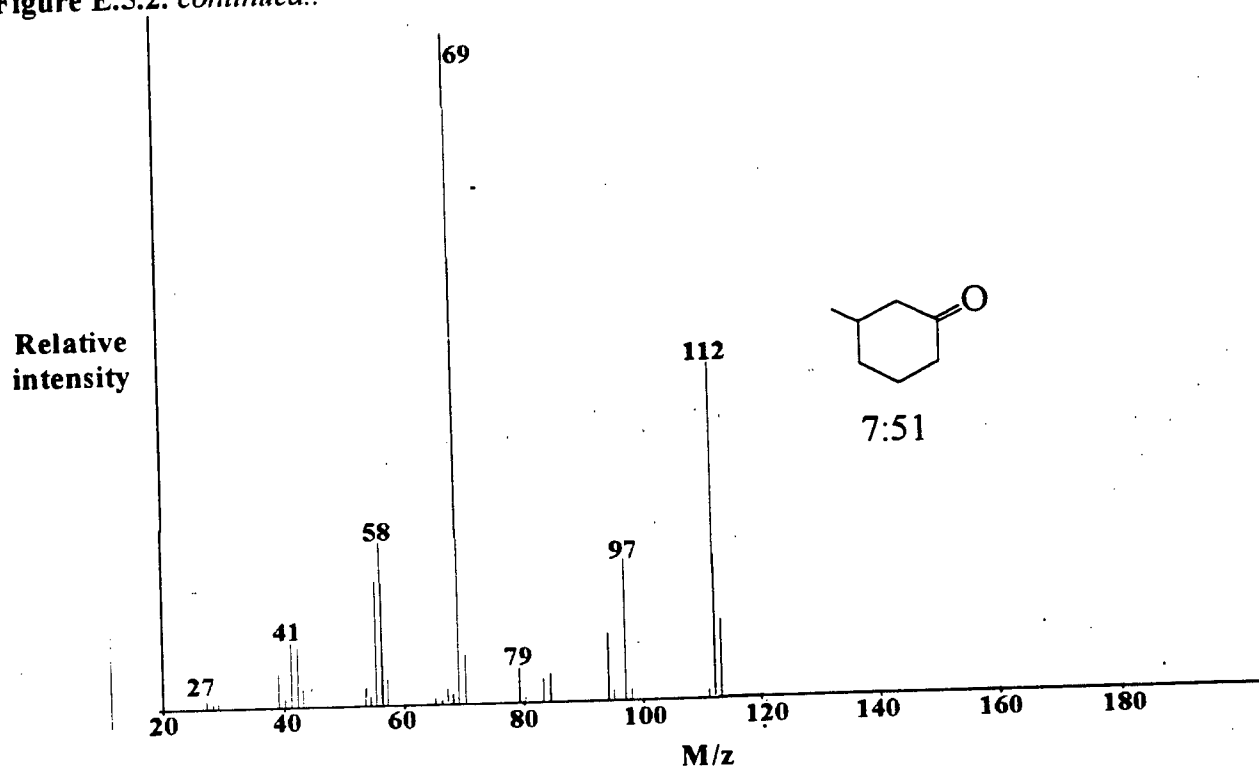
Figure E.5.2. *continued..*

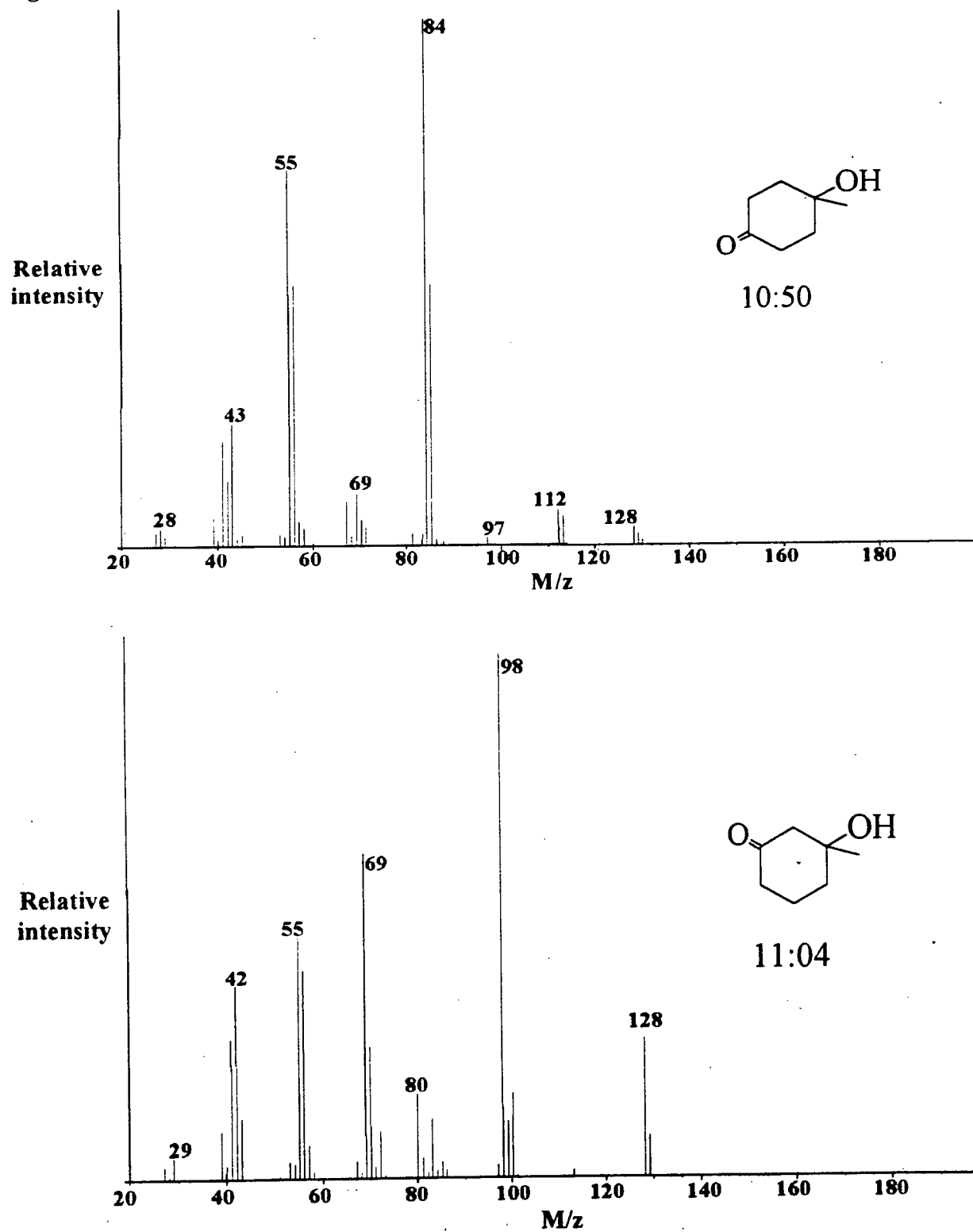
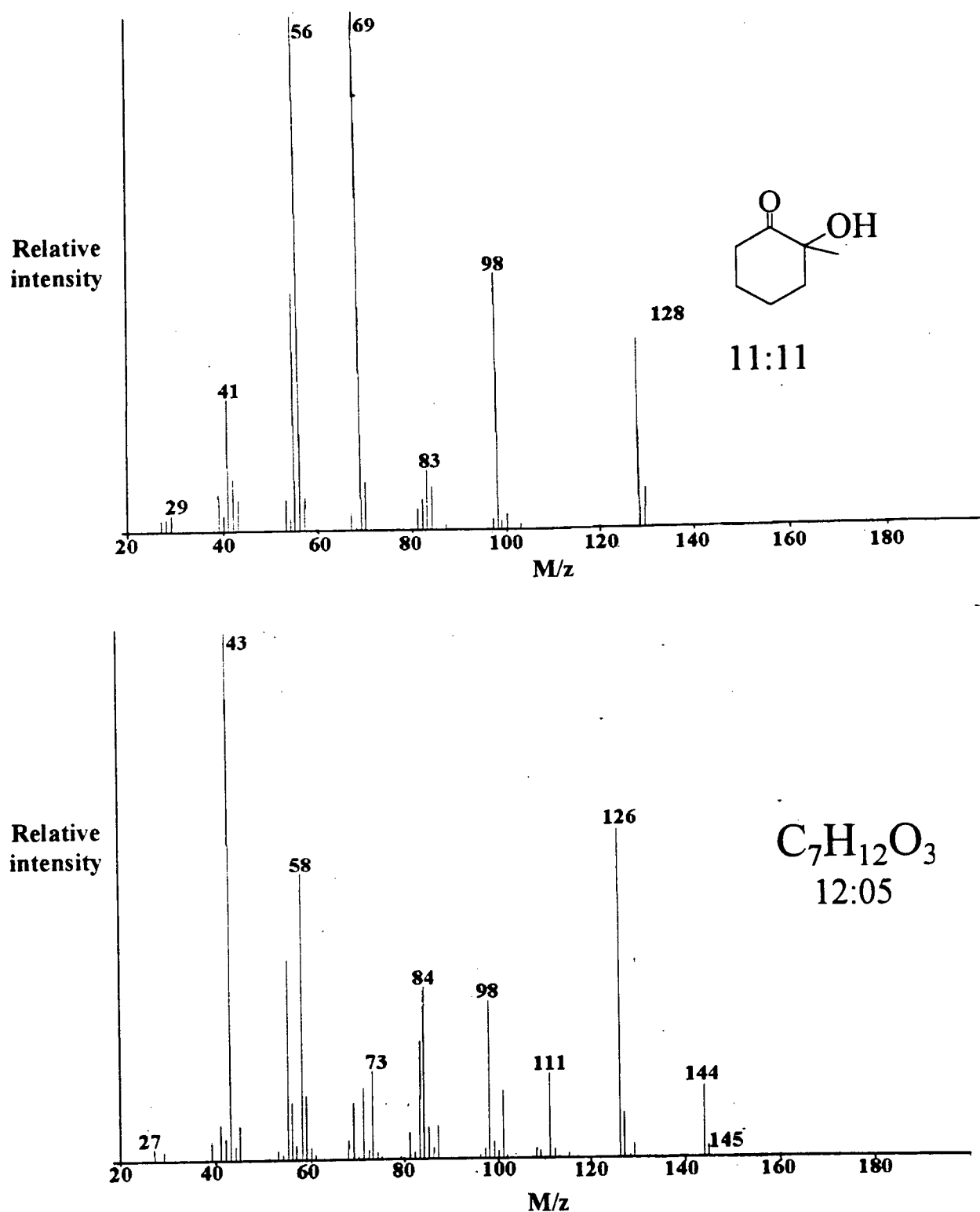
Figure E.5.2. *continued..*

Figure E.5.2. *continued..*

Appendix F. Kinetics Data for the Oxidation of Phenol by Ru^{VI}(TMP)(O)₂.

Table F.1. Pseudo-first-order rate constants, k_{obs} , for the oxidation of phenol by Ru^{VI}(TMP)(O)₂ (1) (5.0×10^{-6} M) in benzene under 1 atm air, unless indicated otherwise. Data acquired on stopped-flow instrument.

[phenol] (M)	283.4 K	288.2 K	293.2 K	303.6 K
k _{obs} (s ⁻¹) (errors < 5% from linear regression of semilog plots)				
0.0973	8.66×10^{-3}	1.40×10^{-2}	1.45×10^{-2}	2.58×10^{-2}
0.257	4.30×10^{-2}	5.95×10^{-2}	7.50×10^{-2} (7.25×10^{-2}) ^a (7.67×10^{-2}) ^b	1.37×10^{-1}
0.301	5.36×10^{-2}	7.70×10^{-2}	9.40×10^{-2}	1.82×10^{-1}
0.467	1.07×10^{-1}	1.56×10^{-1}	1.93×10^{-1}	3.40×10^{-1}
0.989	2.98×10^{-1}	3.86×10^{-1}	5.12×10^{-1}	8.30×10^{-1}

^a Solutions purged with N₂ for 10 min.

^b [(1)] = 3.0×10^{-6} M.

Table F.2. Absorbance-time data for the oxidation of phenol by Ru^{VI}(TMP)(O)₂ (1) in benzene under 1 atm air at 293.2 K, unless indicated otherwise.

[(1)] = 4.5×10^{-6} M [phenol] = 0.0102 M		[(1)] = 5.2×10^{-7} M [phenol] = 0.0292 M		[(1)] = 5.2×10^{-6} M [phenol] = 0.0292 M	
Time (s)	Absorbance ^a	Time (s)	Absorbance ^a	Time (s)	Absorbance ^a
30	1.195	20	0.139	20	1.408
750	1.070	140	0.120	140	1.360
1470	0.932	260	0.103	260	1.286
2190	0.811	380	0.093	380	1.195
2910	0.721	500	0.084	500	1.108
3630	0.656	620	0.079	620	1.027
4350	0.609	740	0.074	740	0.959
5070	0.577	860	0.071	860	0.904
5790	0.554	980	0.069	980	0.862
6510	0.539	1100	0.067	1100	0.828
7230	0.527	1220	0.066	1220	0.801
∞	0.50	∞	0.062	∞	0.70
$k_{\text{obs}} = 4.8 \times 10^{-4} \text{ s}^{-1}$		$k_{\text{obs}} = 2.7 \times 10^{-3} \text{ s}^{-1}$		$k_{\text{obs}} = 2.0 \times 10^{-3} \text{ s}^{-1}$	

^a Absorbance at 422 nm, monitored for the loss of (1).

Table F.2. *continued.*

$[(1)] = 4.0 \times 10^{-6} \text{ M}$ $[\text{phenol}] = 0.0381 \text{ M}$		$[(1)] = 2.5 \times 10^{-6} \text{ M}$ $[\text{phenol}] = 0.0381 \text{ M}$		$[(1)] = 1.0 \times 10^{-5} \text{ M}$ $[\text{phenol}] = 0.0381 \text{ M}$ (monitored at 518 nm)	
Time (s)	Absorbance ^a	Time (s)	Absorbance ^a	Time (s)	Absorbance
20	1.099	20	0.630	20	0.236
80	1.006	140	0.510	140	0.220
140	0.920	260	0.425	260	0.209
200	0.844	380	0.367	380	0.201
260	0.777	500	0.325	500	0.197
320	0.719	620	0.298	620	0.193
380	0.670	740	0.280	740	0.191
440	0.629	860	0.267	860	0.190
∞	0.42	980	0.260	980	0.189
		1100	0.255	1100	0.189
		1220	0.251	∞	0.185
		∞	0.24		
$k_{\text{obs}} = 2.85 \times 10^{-3} \text{ s}^{-1}$		$k_{\text{obs}} = 3.15 \times 10^{-3} \text{ s}^{-1}$		$k_{\text{obs}} = 3.43 \times 10^{-3} \text{ s}^{-1}$	
$[(1)] = 3.6 \times 10^{-6} \text{ M}$ $[\text{phenol}] = 0.0547 \text{ M}$		$[(1)] = 3.8 \times 10^{-6} \text{ M}$ $[\text{phenol}] = 0.0381 \text{ M}$		$[(1)] = 4.7 \times 10^{-6} \text{ M}$ $[\text{phenol}] = 0.0381 \text{ M}$	
Time (s)	Absorbance ^a	Time (s)	Absorbance ^a	Time (s)	Absorbance ^a
20	0.909	20	0.980	10	1.219
140	0.668	140	0.693	100	0.880
260	0.537	260	0.531	190	0.691
380	0.468	380	0.450	280	0.615
500	0.435	500	0.410	370	0.588
620	0.418	620	0.390	460	0.579
740	0.411	740	0.380	550	0.576
860	0.408	860	0.376	640	0.576
980	0.406	980	0.374	730	0.577
1100	0.406	1100	0.374	∞	0.575
∞	0.40	1220	0.373		
		∞	0.37		
$k_{\text{obs}} = 6.03 \times 10^{-3} \text{ s}^{-1}$		$k_{\text{obs}} = 6.0 \times 10^{-3} \text{ s}^{-1}$		$k_{\text{obs}} = 1.19 \times 10^{-2} \text{ s}^{-1}$	

^a Absorbance at 422 nm, monitored for the loss of (1).

Table F.2. continued.

$[(1)] = 4 \times 10^{-6} \text{ M}$ $[\text{phenol}] = 0.0943 \text{ M}$		$[(1)] = 5 \times 10^{-6} \text{ M}$ $[\text{phenol}] = 0.0943 \text{ M}$ 1 atm O ₂		$[(1)] = 5 \times 10^{-6} \text{ M}$ $[\text{phenol}] = 0.0943 \text{ M}$ 1 atm N ₂	
Time (s)	Absorbance ^a	Time (s)	Absorbance ^a	Time (s)	Absorbance ^a
10	1.341	10	1.404	10	1.395
50	1.128	58	1.230	58	1.058
90	0.935	106	1.034	106	0.858
130	0.815	154	0.913	154	0.755
170	0.745	202	0.846	202	0.693
210	0.705	250	0.812	250	0.665
250	0.684	298	0.795	298	0.654
290	0.671	346	0.787	346	0.648
330	0.665	394	0.783	394	0.645
610	0.659	442	0.781	442	0.641
∞	0.65	490	0.780	490	0.641
		∞	0.78	∞	0.64
$k_{\text{obs}} = 1.41 \times 10^{-1} \text{ s}^{-1}$		$k_{\text{obs}} = 1.40 \times 10^{-1} \text{ s}^{-1}$		$k_{\text{obs}} = 1.41 \times 10^{-1} \text{ s}^{-1}$	

^a Absorbance at 422 nm, monitored for the loss of (1).

Appendix G. Oxidation of *N,N*-dimethylaniline by Ru^{VI}(TMP)(O)₂ in benzene.

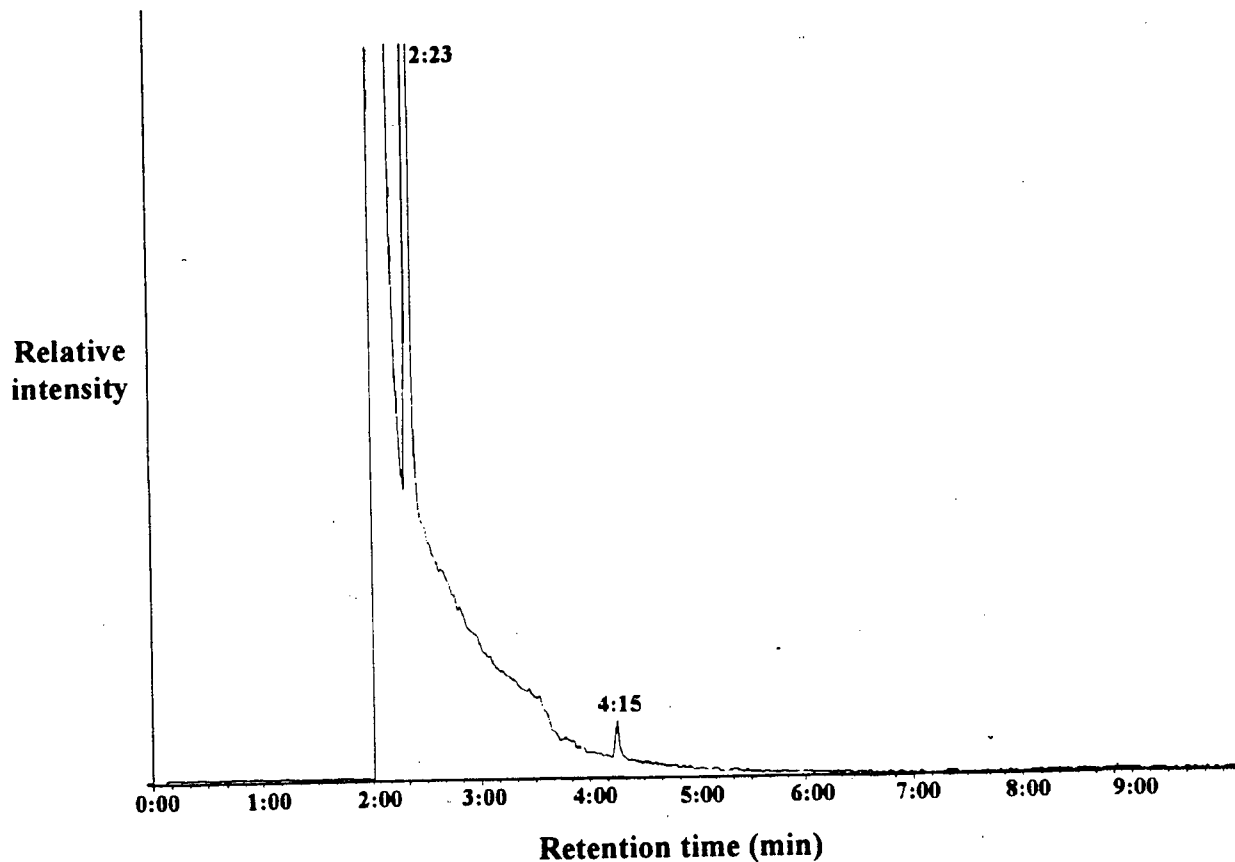


Figure G.1. GC trace of a benzene solution containing Ru^{VI}(TMP)(O)₂ with *N,N*-dimethylaniline added. The sample with analytes corresponding to the retention times of 2:23 and 4:15 minutes were subjected to MS analysis (Figures G.2 and 3).

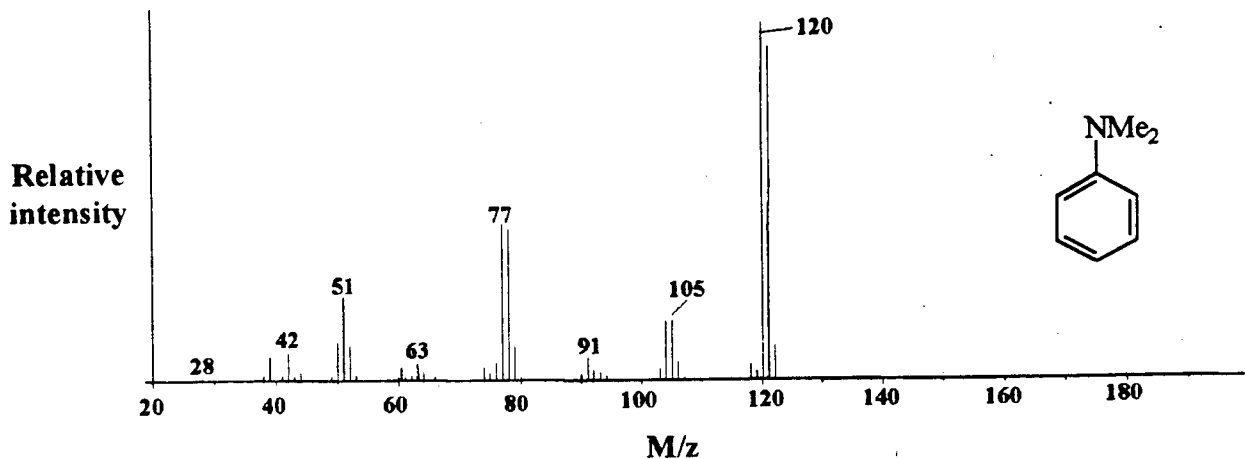


Figure G.2. Mass spectrum of analyte at 2:23 in the GC trace in Figure G.1.

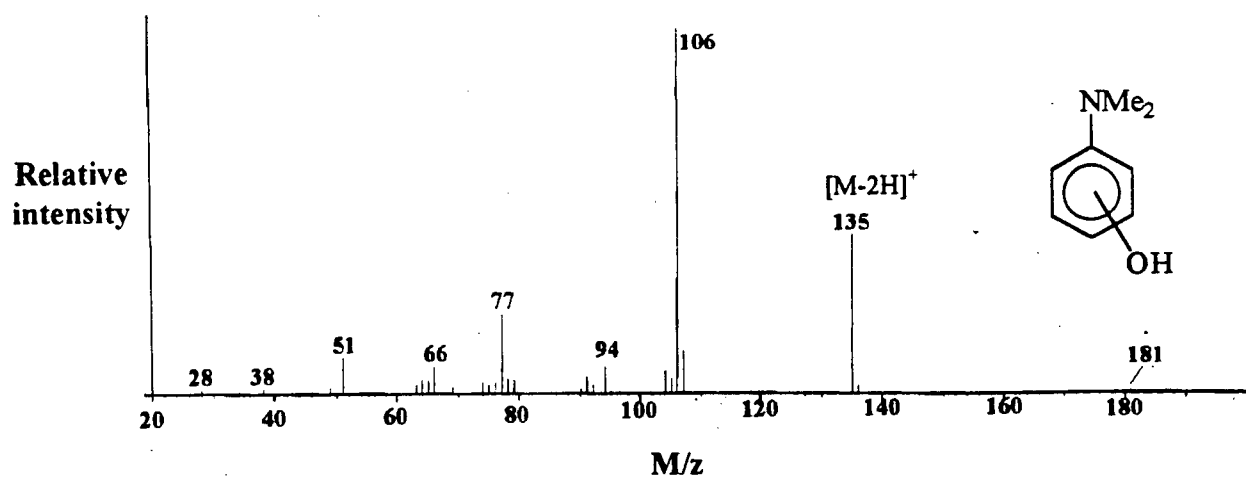


Figure G.3. Mass spectrum of analyte at 4:15 in the GC trace in Figure G.1.